

ESSENTIAL ROLES OF CONVERGENCE AND EXTENSION GASTRULATION
MOVEMENTS IN ZEBRAFISH SOMITE DEVELOPMENT

By

Chunyue Yin

Dissertation

Submitted to the Faculty of the
Graduate School of Vanderbilt University
in partial fulfillment of the requirements for
the degree of

DOCTOR OF PHILOSOPHY

in

Biological Sciences

May, 2007

Nashville, Tennessee

Approved:

Professor Todd R. Graham

Professor Lilianna Solnica-Krezel

Professor Christopher V.E. Wright

Professor Bruce Appel

Professor Chin Chiang

ACKNOWLEDGEMENTS

Many people have been a part of my graduate education, as friends, teachers, and colleagues. Dr. Lilianna Solnica-Krezel, first and foremost, has been all of these. Lila, you are the best advisor and teacher I could have wished for. Thank you for saying “you sure can do it” to me when I hesitate, and caring about every step I take to develop as a scientist. I appreciate your tremendous support, guidance, and enthusiasm over the years. I feel really lucky to have been your student.

I feel spoiled for being surrounded by knowledgeable and friendly colleagues who help me daily. I would like to thank all the former and current members of the L. S-K lab, who have provided more support than I could have asked for. I am grateful for having had the opportunity to work with Dr. Florence Marlow, who showed me the zebrafish embryo for the first time and brought me the wonderful experience as a rotation student. Thank you for continuously being my best friend and sending me those warm emails when I was down. Also, I would like to thank Dr. Jacek Topczewski for offering me his brilliant ideas, Dr. Jason Jesson for teaching me molecular biology, Dr. Thomas Wilm for scientific and political discussions. Thanks to Dr. Adi Inbal, Dr. Terry Van Ray, and Dr. Seok-Hyung Kim for scientific discussions, technical suggestions, career advices and critical comments on my writing. I would especially like to express my appreciation of Dr. Diane Sepich and Dr. Fang Lin. Diane, thank you for the time-lapse tricks, great massage therapy, and your patience in answering my crazy questions. Fang, thank you for being my big sister and providing me useful advice both inside and outside of lab. Thank you to my fellow graduate students, Jennifer Panizzi, Christina Speirs, Xinxin Zeng, Dan

Carlin, and Yong Cha for all the support, great conversations and laughs. Thanks to Josh Clanton, Amy Bradshaw, Jared Ruddick, and Heidi Beck for taking good care of the fish.

This work would not have been possible without the help from my collaborators. Many thanks to Dr. Jonathan Gitlin, Dr. Stephen Johnson and Bryce Mendelsohn at Washington University, for their outstanding efforts in developing the copper story. Thanks to Dr. Emmanuel Farge and Philippe-Alexandre Pouille at Institut Curie in France. Working with them has been a great example to me of positive scientific interactions. My special thank to Dr. Maria Kiskowski in the Department of Mathematics for teaching me computational modeling. I feel so lucky to have someone like you to help me explore the new field of research.

I sincerely thank my thesis committee, Dr. Todd Graham, Dr. Bruce Appel, Dr. Chin Chiang, and Dr. Christopher Wright. I really appreciate your advice, support and enthusiasm. I also want to thank my department, the Developmental Biology program and zebrafish community at Vanderbilt University for providing such a great collaborative environment.

There are also many people whose guidance and encouragement have helped me get through those critical moments. Thanks to Dr. Mark Cooper, Dr. Clarissa Henry and all the professors I met during the Embryology course at MBL. Thank you for showing me how to do good science.

Finally, I would like to give my special thank to my parents back in China, for giving me every opportunity to fulfill my dream and enduring my absence. Your support and encouragement through the years has helped me more than you know. I hope that I will make you proud.

TABLE OF CONTENTS

	Page
ACKNOWLEDGEMENTS.....	ii
LIST OF FIGURES.....	viii
LIST OF TABLES	xi
LIST OF ABBREVIATIONS.....	xii
 Chapter	
I. INTRODUCTION.....	1
Zebrafish as a model system for studying vertebrate gastrulation movements.	2
Fate map of the zebrafish gastrula	3
Gastrulation movements construct the vertebrate body plan	7
Distinct cellular behaviors underlie region-specific gastrulation movements ..	9
Molecular regulation of C&E gastrulation movements	15
Non-canonical Wnt signaling controls C&E gastrulation movements	19
Somite differentiation in zebrafish.....	22
Genetic screens for genes regulating zebrafish early development.....	27
Goals, findings and hypotheses resulting from this work	31
 II. CONVERGENCE AND EXTENSION MOVEMENTS MEDIATE THE SPECIFICATION AND FATE MAINTENANCE OF ZEBRAFISH SLOW MUSCLE PRECURSORS	 35
Summary.....	35
Introduction	36
Results	40
Simultaneous loss of Kny and Tri function impairs slow muscle development.....	40
Reduced numbers of prospective adaxial cells are specified in <i>kny;tri</i> double mutants.....	48
The prospective adaxial cell population in <i>kny;tri</i> double mutants is defective in C&E movements at late gastrulation.....	56
The lateral prospective adaxial cells in the double mutants fail to maintain their identity during segmentation	58
Perturbed Hh signaling is not responsible for the defects in adaxial cell fate maintenance in <i>kny;tri</i> double mutants	65
Cell autonomy of Kny and Tri during adaxial cell specification and	

	C&E movements	66
	Discussion.....	72
	C&E movements regulate the size of the contact between the inducing and responding tissues during adaxial cell specification	73
	Medial convergence of prospective adaxial cells is crucial for their continuous reception of short range Hh signal and fate maintenance....	76
	Non-canonical Wnt/PCP pathway in adaxial cell specification and C&E movements of the paraxial mesoderm	78
	Experimental Procedures.....	80
	Zebrafish maintenance, embryo generation, and staging	80
	In situ hybridization, immunohistochemistry, and cell proliferation assay	80
	Microinjections	81
	Time-lapse recording and analysis.....	81
	Cell lineage tracing/uncaging analysis	82
	Transplantation experiments.....	82
III.	COOPERATION OF POLARIZED CELL INTERCALATIONS DRIVES CONVERGENCE AND EXTENSION OF PRESOMITIC MESODERM DURING ZEBRAFISH GASTRULATION.....	84
	Summary.....	84
	Results and Discussion.....	85
	Experimental Procedures.....	116
	Zebrafish maintenance, embryo generation, and staging	116
	RNA microinjections.....	116
	Time-lapse recording and analysis.....	116
	Confocal imaging	117
	PIV analyses.....	118
	Computational modeling of the cell intercalation behaviors	118
	Supplementary information	119
	Computational modeling of the cell intercalation behaviors during C&E.....	119
IV.	CONVERGENCE AND EXTENSION MOVEMENTS AFFECT DYNAMIC NOTOCHORD-SOMITE INTERACTIONS ESSENTIAL FOR ZEBRAFISH SLOW MUSCLE MORPHOGENESIS.....	125
	Summary.....	125
	Introduction	126
	Results	129
	Lateral migration of the slow muscles is compromised in <i>kny;tri</i> double mutants	129
	The <i>kny;tri</i> adaxial cells fail to undergo cell shape changes prior to lateral migration	134
	The morphogenetic defects of the <i>kny;tri</i> adaxial cells are cell	

non-autonomous.....	139
Close apposition of the somitic boundaries is not responsible for the adaxial cell morphogenesis defects in <i>kny;tri</i> double mutants.....	140
The <i>kny;tri</i> double mutant adaxial cells exhibit prolonged contacts with the notochord.....	146
An intact notochord is not required for normal slow muscle morphogenesis	150
Abnormal notochord properties impede the adaxial cell rotation in <i>kny;tri</i> double mutants.....	151
Discussion.....	156
The adaxial cells undergo dramatic cell shape changes preceding lateral migration	158
Abnormal notochord properties impede the adaxial cell shape changes in <i>kny;tri</i> double mutants.....	159
Fn and the adaxial cell shape changes.....	162
Slow muscle migration in <i>kny;tri</i> double mutants	163
Experimental Procedures.....	165
Zebrafish maintenance, embryo generation, and staging	165
In situ hybridization and immunohistochemistry.....	165
Microinjections	167
Transplantation and shield ablation experiments.....	167

V. ATP7A DETERMINES A HIERARCHY OF COPPER METABOLISM DURING EMBRYOGENESIS ESSENTIAL FOR NOTOCHORD DEVELOPMENT.....	168
Summary.....	168
Introduction	169
Results	171
Small molecules allow the specific manipulation of copper during development.....	171
Copper deficiency phenocopies <i>calamity</i> ^{vu69}	182
The expression pattern of zebrafish <i>atp7a</i> correlates with observed phenotypes	187
Rescue of <i>calamity</i> with human ATP7A and assessment of cell autonomy	187
Gene dosage of zebrafish <i>atp7a</i> determines the sensitivity to copper deprivation.....	190
Discussion.....	197
Experimental Procedures.....	201
Zebrafish maintenance and analysis.....	201
Pharmacologic compounds	202
Immunohistochemistry and in situ hybridization.....	202
Alcian blue staining.....	203
Dianisidine staining	203
Tyrosinase assay.....	204

	Calamity sequence analysis	204
	Cloning of zebrafish <i>atp7a</i>	205
	Morpholino and mRNA injection	205
	Transplantation.....	206
VI.	OVERVIEW AND FUTURE DIRECTIONS.....	207
	Diverse cellular behaviors underlie regional C&E movements	209
	Molecular regulation of region-specific C&E movements	214
	Non-canonical Wnt signaling defines polarized cell intercalations during C&E.....	217
	Establishment of ML cell polarity by non-canonical Wnt signaling during C&E.....	222
	Roles of C&E movements in zebrafish slow muscle development	228
	Modifier screen to identify genes essential for early embryogenesis	233
	Potential interactions between copper and glypican during embryogenesis.	238
	REFERENCES.....	246

LIST OF FIGURES

Figure	Page
1.1 Gastrulation movements shape the zebrafish embryo	5
1.2 Cell behaviors employed in gastrulation movements.....	11
1.3 Spatial and temporal pattern of C&E gastrulation movements.....	13
1.4 Molecular regulation of C&E gastrulation movements.....	17
1.5 Somite differentiation in zebrafish	25
1.6 Genetic screen to identify modifiers of the <i>kny</i> ^{m818} mutant phenotype	30
2.1 Loss of Kny and Tri function impairs zebrafish slow muscle development.....	43
2.2 Fast muscle development in <i>kny;tri</i> double mutants	44
2.3 The somite morphology and slow muscle development in the non-canonical Wnt/PCP mutants	47
2.4 C&E movements define the number of prospective adaxial cells specified during gastrulation.....	52
2.5 Numbers of <i>myoD</i> -expressing cells along the mediolateral dimension at 95% epiboly and the tailbud stages	54
2.6 C&E movements of the prospective adaxial cell population during late gastrulation.....	60
2.7 The prospective adaxial cells in <i>kny;tri</i> double mutants fail to maintain their identity during early segmentation	63
2.8 The range of Hh signaling in the PSM declines during early segmentation.....	68
2.9 Cell autonomy of Kny and Tri in adaxial cell specification and convergence movements of the PSM.....	71
2.10 A model for C&E movements mediating the specification and maintenance of adaxial cell fate.....	75
3.1 Patterns of C&E movements in the dorsal mesoderm.....	88

3.2 C&E movements of the axial mesoderm and medial PSM.....	90
3.3 C&E movements of the medial PSM entail multiple cell intercalations	95
3.4 Computational modeling predicts the contributions of individual cell intercalations to C&E	101
3.5 The amount of GFP-Pk and GFP-Xdsh expressed has no detectable effect on the mediolateral polarity of the labeled cells	106
3.6 Subcellular localization of GFP-Pk during C&E	108
3.7 Subcellular localization of GFP-Xdsh in the axial mesoderm during C&E	111
3.8 Subcellular localization of GFP-Xdsh in the medial PSM at the tailbud stage	113
4.1 <i>kny;tri</i> double mutants are defective in slow muscle migration	132
4.2 Quantification of the shape changes of adaxial cells prior to lateral migration.....	136
4.3 The <i>kny;tri</i> adaxial cells fail to undergo proper shape changes before lateral migration	138
4.4 <i>Kny</i> and <i>Tri</i> act in cell non-autonomous fashion during slow muscle morphogenesis.....	142
4.5 Somitic boundaries are not required for the shape changes or lateral migration of the adaxial cells	145
4.6 The adaxial cells in <i>kny;tri</i> double mutants keep prolonged contact with the notochord	149
4.7 The presence of an intact notochord is not essential for slow muscle morphogenesis.....	152
4.8 Abnormal notochord properties impede the shape changes of adaxial cells	155
5.1 Schematic of the small-molecule screen for drugs perturbing copper metabolism ..	173
5.2 Copper-deficient embryos display a pleiotropic phenotype	179
5.3 Small-molecule effects are rapid, saturable, and dose and time dependent.....	181
5.4 The zebrafish <i>calamity</i> ^{<i>vu69</i>} is defective in the zebrafish ortholog of the Menkes disease gene and is phenocopied by copper deficiency	184

5.5 Alignment of amino acid sequences of human and zebrafish <i>atp7a</i>	186
5.6 Expression pattern of <i>atp7a</i> via in situ hybridization.....	189
5.7 Rescue of <i>cal</i> with human ATP7A and transplantation experiments.....	192
5.8 Interaction of <i>atp7a</i> dosage and developmental copper deficiency	195
5.9 <i>atp7a</i> morpholino causes abnormal splicing of the zebrafish <i>atp7a</i> transcript.....	197
6.1 Four distinct domains of C&E movements in the zebrafish gastrula and the underlying cell movement behaviors.....	210
6.2 Non-canonical Wnt signaling regulates diverse cellular behaviors that underlie C&E movements	213
6.3 Polarized protrusive activities in cells undergoing C&E.....	219
6.4 Non-canonical Wnt signaling regulates the polarized orientation of cell intercalations during C&E	224
6.5 <i>vu66</i> mutation impairs C&E and enhances <i>kny</i> ^{m818} mutant phenotype	235
6.6 <i>calamity</i> (<i>cal</i> ^{vu69}) mutation genetically interacts with <i>kny</i> ^{vu68} mutation	239
6.7 Treatments of WT embryos with neocuproine phenocopy the <i>cal</i> ^{vu69} defects and enhance the <i>cal</i> ^{vu69} and <i>kny</i> mutant phenotypes	242
6.8 Glypican1 recycling in cell cultural and the involvement of copper.....	244

LIST OF TABLES

Table	Page
2.1 Numbers of slow muscle fibers and adaxial cells per somite	49
2.2 Shape, size, and orientation of the prospective adaxial cells during late gastrulation.....	55
4.1 Introducing WT notochord cells suppressed the rotation defect of the <i>kny;tri</i> double mutant adaxial cells.....	157
5.1 Small molecules utilized for copper homeostasis screen.....	175
5.2 Small molecules perturbing copper homeostasis	176

LIST OF ABBREVIATIONS

μg	microgram
μm	micrometer
μM	micromole/liter
Am	Axial mesoderm
Ap	Animal pole
AP	anteroposterior
Bmp	Bone morphogenetic protein
bp	base pair
C&E	Convergence and Extension
<i>cal</i>	<i>calamity</i>
cM	centimorgan
<i>cyc</i>	<i>cyclops</i>
Daam1	Dishevelled associated activator of morphogenesis
Dg	Diego
dpf	days post fertilization
Dsh	Dishevelled
DV	Dorsoventral
ECM	Extracellular matrix
FGF	Fibroblast growth factor
EMT	epithelial-mesenchymal transition
ENU	N-ethyl N-nitrosourea

Ep	Epidermis
Fb	Forebrain
<i>flh</i>	<i>floating head</i>
Fmi	Flamingo
Fn	Fibronectin
<i>fss</i>	<i>fused somite</i>
Fz	Frizzled
G protein	Guanine nucleotide exchange protein
GFP	Green fluorescent protein
GPCR	G protein coupled receptor
GTPase	guanosine triphosphatase
Has2	Hyaluronan sythizing enzyme 2
Hb	Hindbrain
Hg	Hatching gland
Hh	Hedgehog
Hhip	Hedgehog interacting protein
hpf	hours post fertilization
JAK	Janus kinases
JNK	Jun N-terminal kinase
<i>kny</i>	<i>knypek/glypican4</i>
L	Leucine
LWR	Length-to-width ratio
Mb	midbrain

MBT	Mid-blastrula transition
memRFP	membrane-localized red fluorescent protein
ML	Mediolateral
MMP	matrix metalloproteinase
MO	Morpholino Oligonucleotides
NC	Notochord
NCEZ	no convergence no extension zone
Ne	Neural ectoderm
NeoC	Neocuproine
ng	nanogram
Nne	Non-neural ectoderm
NO	nitric oxid
HS	heparan sulfate
NT	Neural tube
<i>ntl</i>	<i>no tail</i>
<i>papc</i>	<i>paraxial protocadherin</i>
<i>oep</i>	<i>one-eyed pinhead</i>
P	Proline
PBS	phosphate buffered saline
PCP	Planar cell polarity
PDZ	Postsynaptic density, Disc-large, ZO1
pg	picogram
PGE ₂	prostaglandin E ₂

PIV	Particle image velocimetry
Pk	Prickle
PKC	Protein kinase C
Pp	Prechordal plate
<i>ppt</i>	<i>pipetail</i>
PSM	Presomitic mesoderm
<i>ptc1</i>	<i>patched 1</i>
PTU	phenylthiourea
RNA	ribonucleic acid
Rok	Rho kinase
Sc	Spinal Cord
<i>slb</i>	<i>silberblick</i>
<i>smbpc</i>	<i>slow muscle binding protein c</i>
SNO	S-nitrosylation
So	Somite
<i>sqt</i>	<i>squint</i>
Stat3	Signal transducer and activator of transcription 3
<i>stbm</i>	<i>strabismus</i>
TB	Tailbud
TGN	trans-Golgi network
Tm	Tail mesoderm
<i>tri</i>	<i>trilobite</i>
Vg	Vegetal pole

Wnt5	Wingless, Int-1 5
Wnt11	Wingless, Int-1 11
WT	Wild-type
Y	Tyrosine
Ysl	Yok syncytial layer

CHAPTER I

INTRODUCTION

Gastrulation is a crucial phase in early vertebrate embryogenesis, during which the basic body plan of the mature organism is established. Prior to gastrulation, the vertebrate embryo is a simple blastula that consists of numerous blastomeres. The first sign of gastrulation is the formation of the Spemann-Mangold organizer, which is located at the dorsal aspect of the blastopore and serves as the signaling center that specifies and patterns the three germ layers - ectoderm, mesoderm and endoderm (Spemann, 1938). During gastrulation, cells engage into massive morphogenetic movements to various destinations, acquire new neighbors, and adopt distinct cell fates in response to local cell-cell signaling (Stern, 2004). These highly coordinated inductive events and cell movements transform an initially unstructured group of blastomeres into a multilayered embryo with defined dorsoventral (DV) and anteroposterior (AP) axes by the end of gastrulation.

Vertebrate gastrulation involves four evolutionarily conserved morphogenetic movements: epiboly, internalization, convergence and extension (Figure 1.1) (Keller et al., 2003; Solnica-Krezel, 2005). Internalization movements bring the presumptive mesoderm and endoderm cells from the outer layer of the gastrula to a position underneath the future ectoderm. Epiboly movements spread and thin the embryonic tissues during gastrulation. Convergence and extension (C&E) movements simultaneously narrow the germ layers mediolaterally and elongate the embryo from

head to tail. Whereas detailed descriptions of gastrulation movements have been generated by using microscopic imaging techniques in embryos or tissue explants of various vertebrate species (Keller et al., 2003; Solnica-Krezel, 2005; Stern, 2004), surprisingly little is known about the molecular and cellular mechanisms driving and directing these movements.

The morphogenetic movements that shape the embryo and the inductive events that specify different cell fates are the key components of vertebrate gastrulation. Disruption of gastrulation movements is often accompanied by severe early patterning defects. For instance, classic experiments by Holtfreter in 1930s first showed that exogastrulation results in the failure of neural induction in urodeles (Holtfreter, 1933). In fish and mouse, mutations inactivating members of the Nodal family of Transforming growth factor- β (TGF β) signaling impair internalization movements during gastrulation. In Nodal-deficient embryos, the prospective mesodermal and endodermal cells do not express the proper marker genes, but instead assume the neuroectoderm or tail fates (Carmany-Rampey and Schier, 2001; Conlon et al., 1991; Conlon et al., 1994; Feldman et al., 2000; Feldman et al., 1998; Zhou et al., 1993). Due to the pleiotropic phenotype of the gastrulation mutants, it is difficult to determine the relative influence of defective movements on cell fate specification and morphogenetic events during later development.

Zebrafish as a model system for studying vertebrate gastrulation movements

In the past 10 years, the teleost zebrafish *Danio rerio* has emerged as a powerful model system for investigation of vertebrate development (Driever et al., 1996; Driever et al., 1994). The rapid external development, optical transparency and accessibility of the

zebrafish embryo are particularly useful for studying cell movements *in vivo*. Adult zebrafish are easy to raise with a short generation time of three months. A mating fish pair can generate hundreds of eggs at weekly intervals. Because of their small size, zebrafish can be economically and efficiently maintained in large numbers. These features make zebrafish amenable to large-scale forward genetic screens. Two classes of zebrafish mutations that interfere with morphogenetic processes of gastrulation have been recovered from previous mutagenesis screens (Hammerschmidt et al., 1996a; Kimmel et al., 1989; Mullins et al., 1996; Solnica-Krezel et al., 1996). One class disrupts morphogenesis as a consequence of abnormal patterning, while the second class specifically disrupts C&E or epiboly gastrulation movements. For example, the C&E mutant embryos exhibit a shortened body but normal tissue patterning during gastrulation (Myers et al., 2002b), presenting a powerful genetic tool with which to investigate the roles of C&E gastrulation movements in subsequent cell fate specification and later embryogenesis.

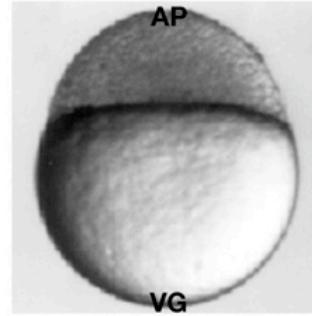
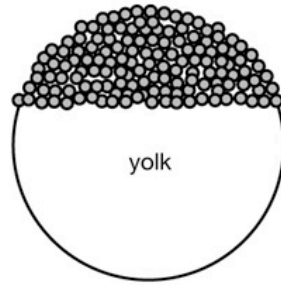
Fate map of the zebrafish gastrula

During the first three hours of development, the zebrafish embryo undergoes rapid synchronous cell divisions to form a mound of blastomeres atop a large syncytial yolk cell (Fig. 1.1 A) (Kimmel et al., 1995). Maternally-contributed transcripts and proteins govern the development during cleavage stages. Zygotic transcription starts at the mid-blastula transition (MBT), which occurs at the 512/1024-cell stage (3 hours post fertilization; hpf) (Kane and Kimmel, 1993).

Figure 1.1. Gastrulation movements shape the zebrafish embryo. Before gastrulation initiates, the zebrafish embryo contains a mound of blastomeres atop a large syncytial yolk cell (A). (B) Fate map of the zebrafish embryo at early gastrula stage. Germ layers are arranged along the animal-vegetal axis, whereas the different mesodermal and ectodermal fates are arranged along the dorso-ventral axis. (C) During gastrulation, epiboly movements (red arrow) spread the blastoderm and the yolk syncytial layer towards the vegetal pole. Internalization movements bring the mesendodermal cells underneath the ectoderm to form the three germ layers (green arrow). Convergence (blue arrow) and extension (yellow arrow) movements simultaneously narrow and lengthen the embryonic axes, resulting in a narrow and elongated embryo with three germ layers by the end of gastrulation (D). Abbreviations: AP, animal pole; VG, vegetal pole; nne, non-neural ectoderm; ne, neural ectoderm; tm, tail mesoderm; psm, presomitic mesoderm; am, axial mesoderm; ysl, yolk syncytial layer; V, ventral; D, dorsal; fb, forebrain; mb, midbrain; hb, hindbrain; sc, spinal cord; hg, hatching gland; pp, prechordal plate; nc, notochord; ep, epidermis; A, anterior; P, posterior.

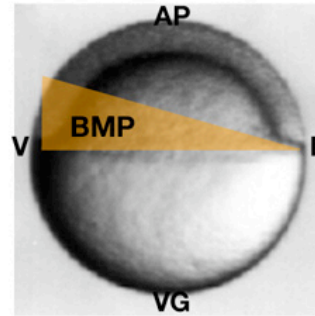
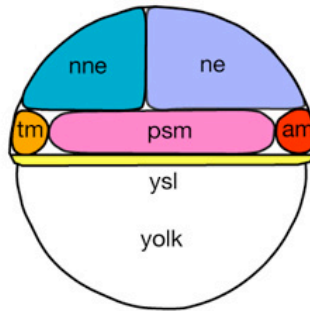
A

Sphere
(4 hpf)



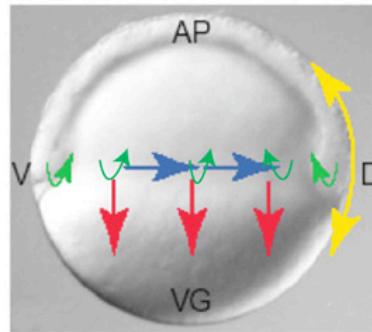
B





50% epiboly
(5.25 hpf)



C

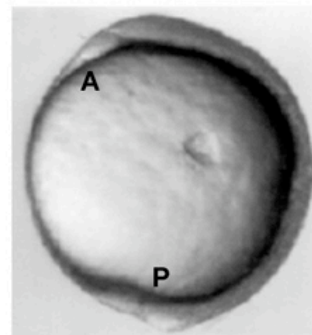
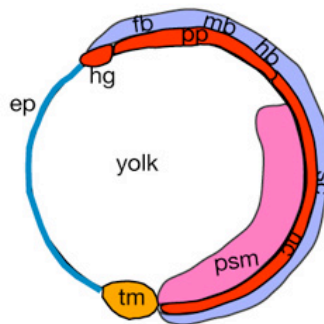
Shield
(6 hpf)



-  Epiboly
-  Internalization
-  Convergence
-  Extension

D

Tailbud
(10 hpf)



In zebrafish, the initial DV asymmetry is established during cleavage stages when the embryo still exhibits a radially symmetric morphology (Schier and Talbot, 2005). The earliest sign of the DV polarity is the asymmetric distribution of the maternal transcripts of *squint* at the 4-cell stage (1 hpf) (Gore et al., 2005). *squint* encodes a Nodal-related morphogen that induces mesendodermal gene expression in a concentration-dependent manner and acts directly at a distance (Chen and Schier, 2001). At the 4-cell stage, maternal *squint* transcripts are localized to two blastomeres of the 4-cell embryo, predicting the presumptive dorsal side (Gore et al., 2005).

At the 128-cell stage (2 ¼ hpf), the maternal β -catenin protein starts to accumulate in the nuclei of the dorsal marginal cells to induce the formation of the Spemann-Mangold organizer (Schneider et al., 1996; Solnica-Krezel, 1999). Soon after MBT, β -catenin activates the expression of many zygotic genes in the organizer region (Schier and Talbot, 2005). Zygotic *squint* expression induces the mesendodermal fates at the dorsal margin (Dougan et al., 2003). The expression of *bozozok*, *chordin*, *dickkopfl*, and members of the Fibroblast growth factor (FGF) family triggers the dorsal fates by inhibiting the activation of ventralizing and posteriorizing signals at the dorsal side, including the Bone morphogenetic proteins (Bmps) of the TGF β superfamily and canonical Wnt ligands (Fekany-Lee et al., 2000; Furthauer et al., 2004; Hashimoto et al., 2000; Schneider et al., 1996; Schulte-Merker et al., 1997; Solnica-Krezel et al., 1995). As a consequence, a ventral-dorsal gradient of Bmp activity is established at the onset of gastrulation (Hammerschmidt et al., 1996b), and cells acquire different fates depending on their positions in the gastrula (Kimmel et al., 1990) (Figure 1.1B). In the fate map of early zebrafish gastrula, precursors for different germ layers are arranged along the

animal-vegetal axis, with ectoderm located animally, mesoderm more marginally, and endoderm intermingled with mesoderm at the margin (Kimmel et al., 1990) (Figure 1.1B). Precursors for different mesodermal cell types are arranged along the DV gastrula axis (Kimmel et al., 1990). Cells located most dorsally, at the low Bmp activity, give rise to the notochord and the anterior prechordal mesoderm. More laterally located cells that receive intermediate levels of Bmp signaling are designated to form trunk somites and heart. Ventral cells that contain the highest Bmp activity form the ventro-posterior embryonic structures, including the tail somite, blood and pronephric ducts (Agathon et al., 2003). Notably, due to the complex cell movements during gastrulation, the DV arrangement of the tissue precursors in the gastrula fate-map does not correspond exactly to the DV positions of these tissues at later stages (Harland, 2004). One such example is that the posterior notochord and posterior somites are close together in the tail mesoderm, but their precursors occupy at the opposite ends of the DV axis at the onset of gastrulation (Kanki and Ho, 1997). For simplicity, in describing gastrulating zebrafish embryos, I refer to the Spemann-Mangold organizer region as “dorsal” and to the region most distal to the organizer as “ventral”.

Gastrulation movements construct the vertebrate body plan

Based on the early gastrula fate map defined in part by early patterning signals, gastrulation movements reorganize the blastoderm into the basic vertebrate body plan. The morphogenesis of zebrafish presomitic mesoderm (PSM) provides an example of how gastrulation movements shape and position organ rudiments. In zebrafish, the trunk somites are derived from the PSM located at the dorsal-lateral blastoderm margin at the

beginning of gastrulation (Kimmel et al., 1990). As gastrulation proceeds, epiboly movements spread the PSM vegetally over the yolk mass and internalization movements place it underneath the ectoderm (Figure 1.1C). Upon internalization, the PSM undergoes C&E movements that narrow its width along the mediolateral (ML) axis and bring it near the axial mesoderm (convergence), while elongating it in the AP dimension (extension) (Kimmel et al., 1995; Henry et al., 2000; Schoenwolf and Smith, 2000; Solnica-Krezel, 2005) (Figure 1.1C). By the end of gastrulation, the PSM forms anteroposteriorly-elongated territories flanking the axial mesoderm and initiates segmentation (Figure 1.1D) (Stickney et al., 2000).

Consistent with the critical roles of gastrulation movements in the PSM morphogenesis, perturbation of these movements often leads to defects in somite formation. For example, zebrafish *spadetail* mutants, in which the T-box transcription factor Tbx16 is inactivated, exhibit a deficiency of the trunk somites (Griffin et al., 1998). Cell tracing analyses showed that the PSM in *spadetail* mutants does not converge towards the dorsal midline during gastrulation. Instead, cells that normally form the trunk somites migrate vegetally and accumulate in the tailbud (Ho and Kane, 1990). In other mutants with impaired C&E movements, the somites are mediolaterally broadened and anteroposteriorly shortened (Hammerschmidt et al., 1996a; Henry et al., 2000; Solnica-Krezel et al., 1996). These studies shed light on the roles of gastrulation movements in zebrafish somite development.

Distinct cellular behaviors underlie region-specific gastrulation movements

The remarkable tissue morphogenesis during gastrulation is achieved through coordinated movements of individual cells. However, we only have limited knowledge of the cellular behaviors underlying the different types of gastrulation movements. In zebrafish as well as in the frog *X. laevis*, epiboly movements are driven mainly by radial intercalation, whereby cells intercalate between cells in a different layer to generate fewer layers of greater area (Figure 1.2) (Keller, 1980; Warga and Kimmel, 1990). The internalization movements in zebrafish are driven by the “synchronized ingression” behavior. Mesendodermal cells move in a coherent sheet towards the blastoderm margin, where they lose coherence with their neighbors and ingress individually or in groups (Adams, 2004; D'Amico and Cooper, 2001).

Upon internalization, all three germ layers undergo C&E movements in a distinct spatial and temporal pattern (Figure 1.3). Spatially, three distinct C&E movement domains have been recognized along the DV dimension of the zebrafish gastrula (Figure 1.3A) (Myers et al., 2002a; Myers et al., 2002b). First, at the most ventral region, also known as the “no convergence no extension zone”, mesodermal cells do not participate in C&E movements, but rather migrate along the yolk into the tailbud region (Myers et al., 2002b). Second, in the lateral domain, C&E movements of the lateral mesoderm are initially slow, and then accelerate as cells migrate closer to the dorsal midline. The dorsal convergence of lateral mesodermal cells is driven by directed migration without frequent cell rearrangements (Figure 1.2) (Jessen et al., 2002; Myers et al., 2002b). Finally, in the dorsal region, the axial mesoderm undergoes strong extension and limited convergence by ML intercalation, the rearrangement of cells along the ML axis causing the tissue to

Figure 1.2. Cell behaviors employed in gastrulation movements. During epiboly movements, radial intercalation in which cells intercalate with the cells in the more superficial or deeper layer leads to the spreading and thinning of the blastoderm. Convergence and extension movements can be produced by several cell behaviors in a region-specific manner. The convergence and extension of the dorsal mesoderm are achieved by the combination of anteroposteriorly oriented cell division, anteriorly directed cell migration, and mediolateral intercalation. In the lateral mesoderm, cells converge towards the midline mainly by directed migration.

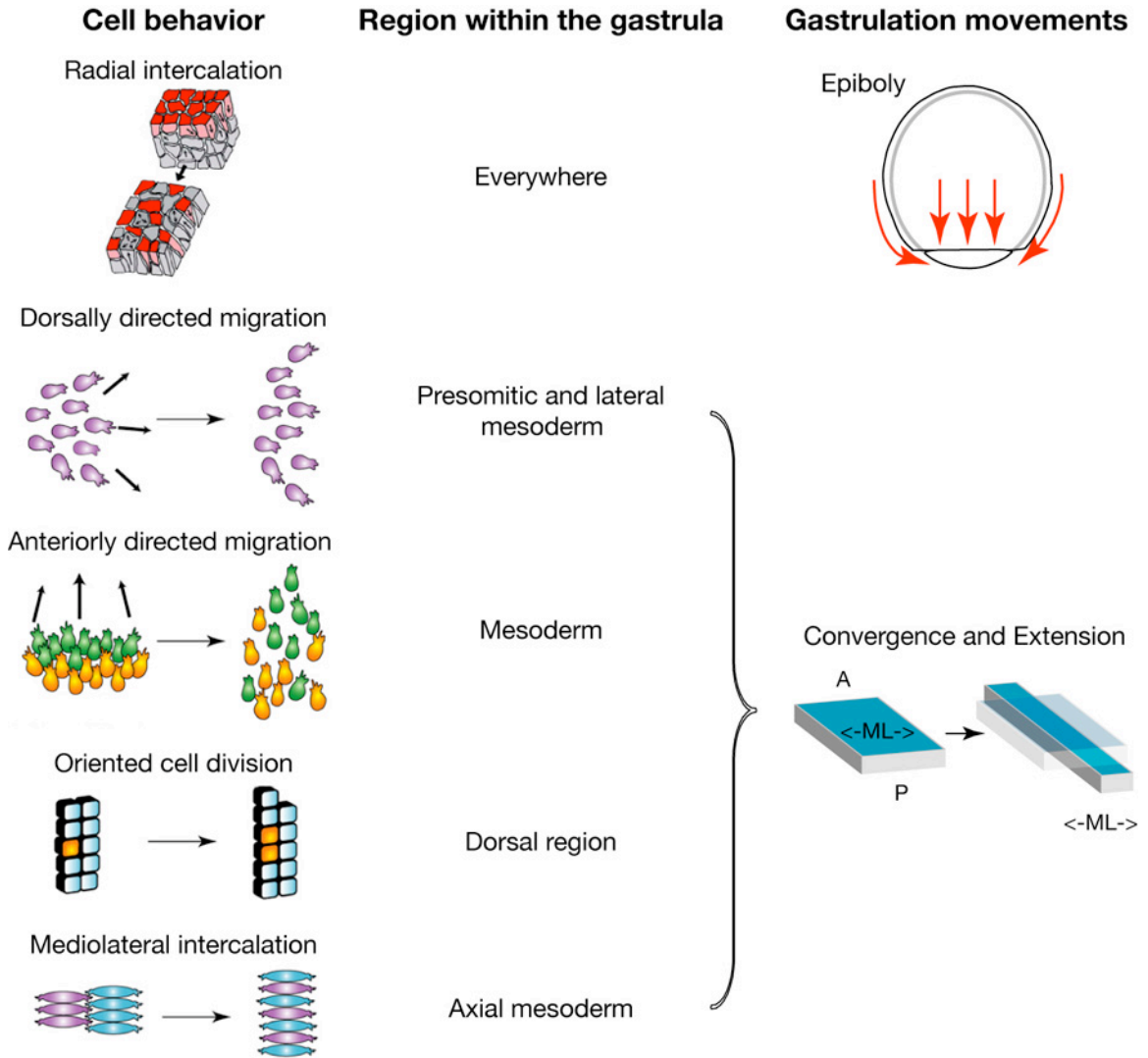
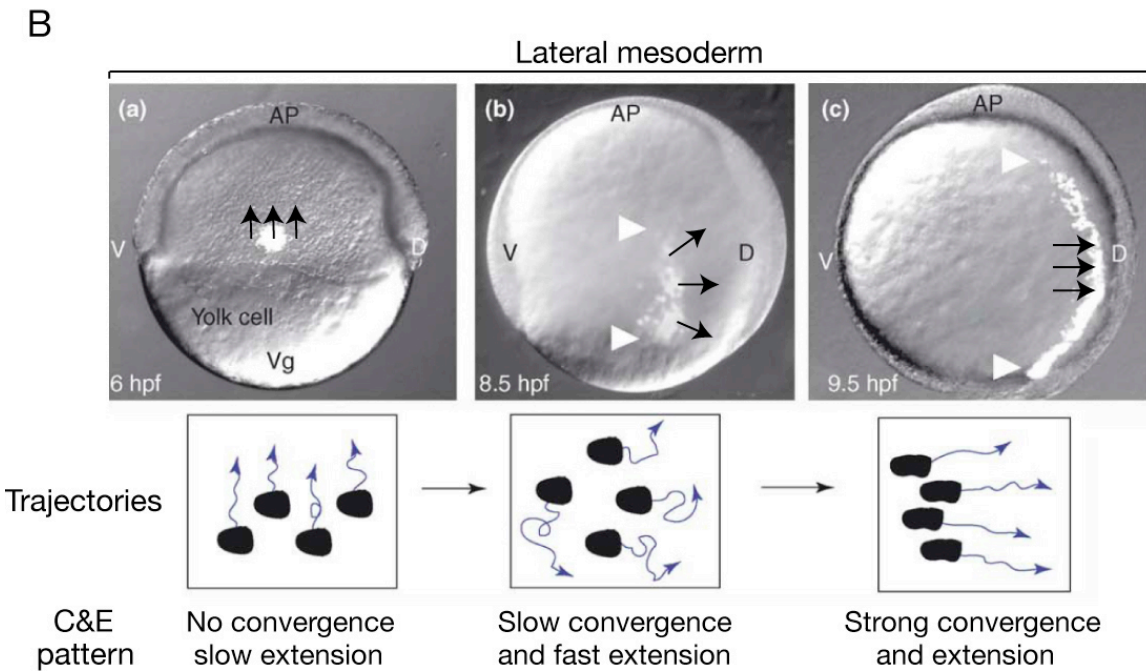
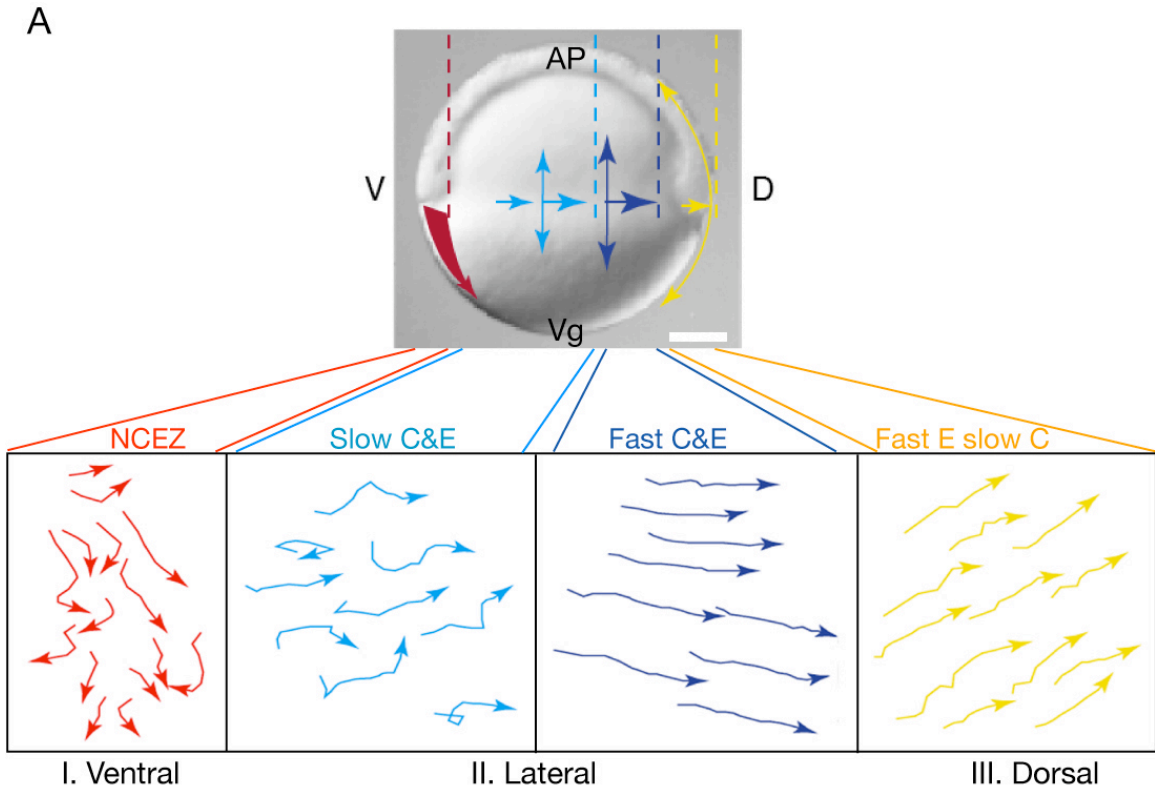


Figure 1.3. Spatial and temporal pattern of C&E gastrulation movements. (B) Distinct domains of C&E movements along the dorsoventral axis. Mesodermal cells within the “no convergence no extension zone” (NCEZ, red) migrate vegetally without any dorsal bias. In the lateral domain, mesodermal cells undergo C&E movements at increasing speeds as they migrate close to the dorsal midline (light and dark blue). To achieve effective C&E movements, the lateral mesodermal cells need to become mediolaterally oriented and elongated. In the most dorsal region where the axial mesoderm is located (yellow), strong extension is accompanied with slow convergence. AP, animal pole; Vg, vegetal pole; D, dorsal; V, ventral. Modified from Myers et al., Trends in genetics, 2002. (A) C&E movements of a small cell population within the lateral mesoderm throughout gastrulation. The population is labeled by photoactivation of fluorescein-caged dye at the onset of gastrulation. Modified from Solnica-Krezel, Curr Opin Genet Dev 2006.



narrow mediolaterally and lengthen along the AP axis (Figure 1.2) (Glickman et al., 2003; Keller and Tibbetts, 1989). Furthermore, the dorsal cells divide preferentially along the AP dimension, providing an additional mechanism that underlies the strong extension of the dorsal tissue (Figure 1.2) (Gong et al., 2004). Interestingly, in the dorsal region of the embryo, the axial mesoderm and adjacent PSM exhibit similar convergence rates, but the extension rate is three-fold higher in the axial mesoderm than in the PSM (Glickman et al., 2003). Similar observation has been reported in *X. laevis* (Keller et al., 2003; Wilson and Keller, 1991; Wilson et al., 1989). However, it is not clear what movement behaviors of the presomitic cells account for the different C&E rates between the axial and presomitic mesoderm.

In addition to the spatial differences, the C&E rates of the same tissue may change in the course of gastrulation and involve distinct cellular behaviors (Sepich et al., 2005). Cells in the dorsal axial mesoderm initially migrate away from the margin by directed migration, contributing to tissue extension (Figure 1.2) (Solnica-Krezel, 2006). Between mid-gastrulation (7.5 hpf) and early segmentation stages, the axial mesodermal cells engage in ML intercalation, driving both convergence and extension (Figure 1.2) (Glickman et al., 2003). The C&E of the lateral mesoderm is also driven by a stereotyped sequence of cellular behaviors (Figure 1.3B). During early gastrulation (6 hpf – 7.5 hpf), cells in the lateral mesoderm migrate towards the animal pole with little dorsal bias, resulting in extension but not convergence of the tissue (Sepich et al., 2005). Convergence of the lateral domain initiates at mid-gastrulation, whereby cells migrate dorsally along complex trajectories with their direction biased either animally or vegetally according to their positions along the animal-vegetal axis. This fanning of cell

trajectories leads to slow C&E movements (Jessen et al., 2002; Sepich et al., 2005). During late gastrulation, when cells become more dorsally located, they adopt mediolaterally-elongated morphology and converge towards the midline along straighter trajectories and at higher speeds (Figure 1.3B) (Myers et al., 2002a; Myers et al., 2002b).

Molecular regulation of C&E gastrulation movements

The dynamic spatial and temporal pattern of C&E gastrulation movements and the involvement of distinct cell behaviors reflect the complexity of the underlying molecular mechanisms (Figure 1.4). The ventral-dorsal gradient of Bmp activity specifies different cell fates in the zebrafish gastrula (Figure 1.1B) (Kishimoto et al., 1997; Neave et al., 1997; Schier and Talbot, 2005). Inactivation of Bmp ligands, their receptors, as well as other transducers of the signaling cascade results in dorsalized embryos, which exhibit an elongated morphology at the end of gastrulation and later lose the ventral tail structures (Hammerschmidt et al., 1996a; Hammerschmidt et al., 1996b; Myers et al., 2002a; Solnica-Krezel et al., 1996). These defects result from reduced Bmp activity and consequent ectopic C&E of the ventral cells at the expense of vegetal migration to the tailbud (Myers et al., 2002a). Conversely, ventralized mutants that are defective in the function of Bmp antagonists, such as Chordin, exhibit a round morphology at the end of gastrulation, due to decreased C&E movements (Hammerschmidt and Mullins, 2002; Hammerschmidt et al., 1996b). Reduction of C&E movements in ventralized mutants is correlated with dorsally expanded Bmp activity (Myers et al., 2002a). These findings have led to a model in which the ventral-dorsal gradient of Bmp activity coordinates patterning of cell fates and C&E movements along the DV gastrula axis. High Bmp

activity levels in the ventral region inhibit C&E movements, specifying the “no convergence no extension zone”. In the lateral domain, the decreasing of Bmp activity is correlated with an increase in the rates of C&E driven by directed migration. The low Bmp activity near the dorsal region promotes strong extension with limited convergence driven by ML intercalation (Myers et al., 2002a).

Recent studies have characterized several pathways and molecules that either provide directional cues or regulate the efficiency of C&E movements. In the lateral mesoderm of the zebrafish gastrula, dorsal convergence initiates at mid-gastrulation and occurs at increasing speeds as cells migrate closer to the dorsal midline (Figure 1.3B) (Sepich et al., 2005). The initial slow directed migration of lateral mesoderm cells is reminiscent of the chemotactic cell movements. Computational modeling analyses predicted the presence of chemoattractant cues that emanate from the dorsal midline to guide the direction of convergence movements (Sepich et al., 2005). Work in the chick demonstrated that different FGFs in the primitive streak (blastopore) and the embryo midline serve as chemorepellents or chemoattractants to regulate the movements of the internalized mesoderm away from the blastopore or later its convergence towards the midline, respectively (Yang et al., 2002b). Similar roles of FGF signaling have not been reported during zebrafish C&E. Instead, the guiding cues in zebrafish gastrula are likely to be controlled by JAK/Stat3 signaling downstream of β -catenin (Yamashita et al., 2002). Ubiquitously expressed Stat3 is activated on the dorsal side of the blastula shortly after MBT (Yamashita et al., 2002). In Stat3-depleted embryos, the initiation of dorsal convergence in the lateral mesoderm is delayed (Sepich et al., 2005), and the directed cell migration is reduced (Yamashita et al., 2002). The requirement for Stat3 signaling in the

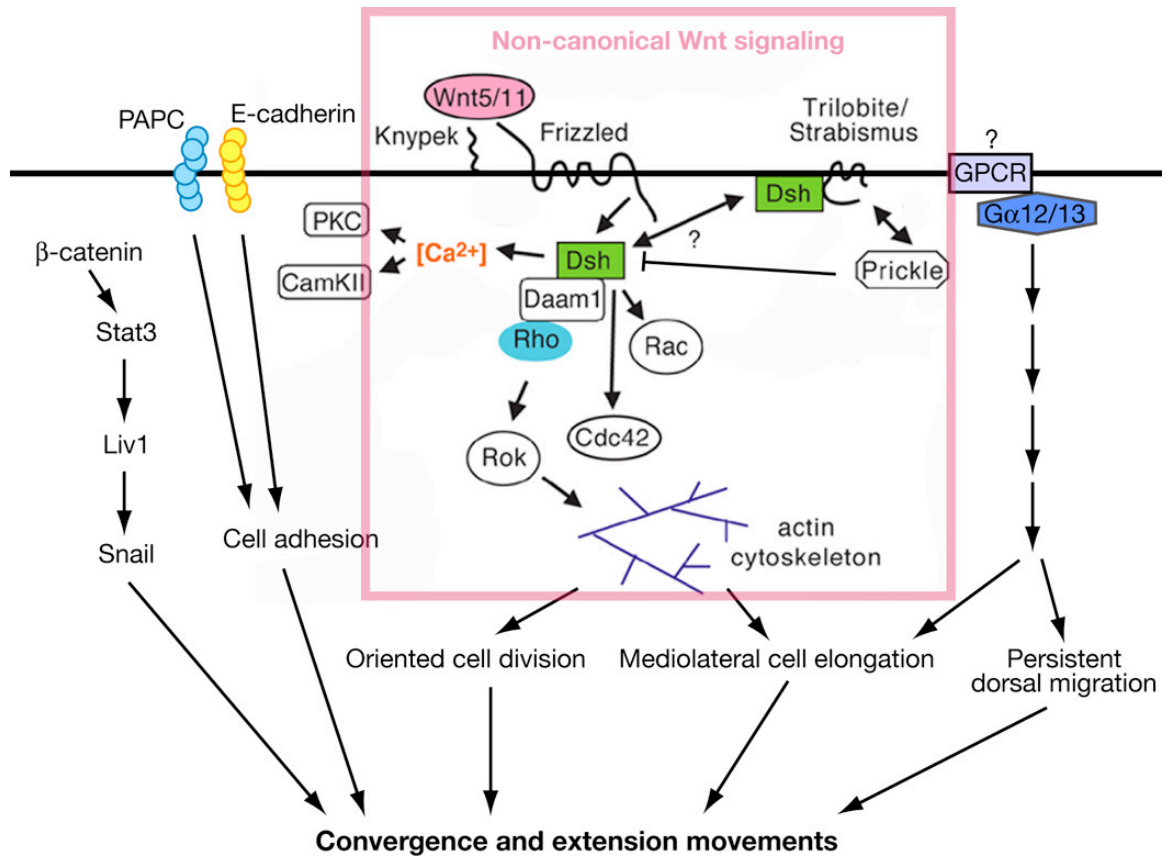


Figure 1.4. Molecular regulation of C&E gastrulation movements

convergence of lateral cells is cell non-autonomous, supporting the notion that Stat3-activated signals in the dorsal midline define the directionality of convergence movements (Yamashita et al., 2002). Several other molecules and pathways have also been implicated in regulating the directed migration of lateral cells, including G α 12/13 (Lin et al., 2005), Hyaluronan (Bakkers et al., 2004), and the COX-1-Ptges-EP4 pathway (Cha et al., 2006) (Figure 1.4).

As the lateral mesodermal cells migrate closer to the dorsal midline, they become highly elongated mediolaterally, form cellular protrusions along the ML axis, and converge at fast speeds along straight trajectories (Jessen et al., 2002; Myers et al., 2002b). This fast C&E phase is controlled by non-canonical Wnt signaling (Jessen et al., 2002; Myers et al., 2002b; Topczewski et al., 2001), a vertebrate equivalent of the *D. melanogaster* planar cell polarity (PCP) pathway that polarizes cells within the plane of tissue (See below) (Adler, 2002; Klein and Mlodzik, 2005).

The cell behaviors underlying the C&E of adjacent mesoderm can be strikingly different. Whereas the lateral mesodermal cells converge towards the midline without frequent neighbor exchanges (Myers et al., 2002b), C&E of the dorsal axial mesoderm is driven mainly by ML cell intercalations (Glickman et al., 2003). ML intercalation of the axial mesodermal cells and directed migration of the lateral cells share some common molecular regulators, including non-canonical Wnt signaling and G α 12/13 signal transducers (Lin et al., 2005; Myers et al., 2002b). In addition, ML intercalation of the axial cells is dependent on the function of a T-box transcription factor No tail/Brachyury. In frog, Xbrachyury functions as a switch between cell migration in the anterior-most axial mesoderm and convergent extension in the trunk axial mesoderm by inhibiting cell

migration (Kwan and Kirschner, 2003). Similarly, in zebrafish *no tail* mutants, ML intercalation initiates in the axial mesoderm but cannot be completed, resulting in the severe disruption of convergence movements, but not extension (Glickman et al., 2003). To function properly, ML intercalation must be oriented parallel to the ML axis, and transverse to the AP axis. A recent work demonstrated that in the *X.laevis* chordamesoderm, graded activin-like signaling that establishes AP polarity acts in parallel or upstream of non-canonical Wnt pathway to regulate the orientation of ML intercalation (Ninomiya et al., 2004). Whether a similar mechanism contributes to the C&E of the dorsal mesoderm in zebrafish remains to be investigated.

Non-canonical Wnt signaling controls C&E gastrulation movements

In both zebrafish and frog, non-canonical Wnt signaling serves as the key regulator of C&E movements by mediating the ML elongation and alignment of the mesodermal and ectodermal cells, as well as the stability and polarized orientation of the cellular protrusions essential for C&E (Keller, 2005; Myers et al., 2002b; Tada et al., 2002). Non-canonical Wnt signaling is activated upon the binding of Wnt ligands Wnt5 and Wnt11 to the transmembrane receptor Frizzled7 (Fz7), which requires the extracellular heparan sulfate proteoglycan Knypek/Glypican4 (Kny). Activated Fz7 recruits the docking protein Dishevelled (Dsh) to the cell membrane and the signal acts through small guanosine triphosphatases (GTPases), including Cdc42, Rac and Rho, to regulate cytoskeleton rearrangements (Figure 1.4) (Klein and Mlodzik, 2005; Leptin, 2005; Myers et al., 2002b). The transduction of non-canonical Wnt signaling relies on the co-factors of the pathway, including the transmembrane PDZ domain binding protein

Trilobite/Strabismus/Van Gogh-like 2 (Tri) (Jessen et al., 2002; Park and Moon, 2002), the cytoplasmic protein Prickle (Pk) (Carreira-Barbosa et al., 2003; Veeman et al., 2003b), the ankyrin-repeat protein Diego (Dg) (Moeller et al., 2006), and the serpentine cadherin domain containing receptor Flamingo (Fmi) (Figure 1.4) (Formstone and Mason, 2005). Both gain- and loss-of-function manipulations of non-canonical Wnt components impair C&E without affecting cell fate (Carreira-Barbosa et al., 2003; Heisenberg et al., 2000; Jessen et al., 2002; Kilian et al., 2003; Sokol, 1996; Topczewski et al., 2001; Wallingford et al., 2000), indicating that a balance of non-canonical Wnt signaling is essential for normal C&E movements.

How non-canonical Wnt signaling promotes C&E is not fully understood. The existing data argue for a permissive rather than an instructive role for this pathway in C&E. In zebrafish *kny* and *tri* mutants, dorsal convergence of the lateral mesoderm initiates normally, indicating that the dorsal chemoattractant cues guiding the direction of C&E is independent of non-canonical Wnt signaling (Sepich et al., 2005). Furthermore, ubiquitously expressed non-canonical Wnt components can rescue the non-canonical Wnt mutant phenotype (Heisenberg et al., 2000; Kilian et al., 2003; Marlow et al., 2002; Topczewski et al., 2001), supporting the notion that directionality of polarity is mediated by a different signal and non-canonical Wnt signaling is required for the mesodermal cells to interpret the polarity signal and undergo effective C&E movements (Sepich et al., 2005; Solnica-Krezel, 2006). Recent studies suggest a role for non-canonical Wnt signaling in modulating cell adhesion (Ulrich et al., 2005; Ungar et al., 1995; Witzel et al., 2006), providing a possible mechanism by which non-canonical Wnts regulate polarized cell behaviors during C&E.

It has been well documented that non-canonical Wnt signaling regulates ML cell polarity essential for the cell movement behaviors underlying C&E, including directed migration, anteroposteriorly oriented cell division, and ML intercalation (Gong et al., 2004; Jessen et al., 2002; Kilian et al., 2003; Marlow et al., 2002; Topczewski et al., 2001; Wallingford et al., 2000). However, it is still unclear how the ML cell polarity is established. In fly, components of the PCP pathway are localized asymmetrically in the cell (Adler, 2002; Klein and Mlodzik, 2005). In the fly wing epithelium, each cell develops a distally pointing actin-based hair and PCP signaling is required in these cells for direct regulation of the cytoskeletal organization (Adler, 2002). The PCP components, including Dsh, Fz, Pk, and Strabismus (Stbm), are initially distributed uniformly on the apical cell membrane. Upon activation of the PCP pathway, Fz and Dsh become asymmetrically localized to the distal cell membrane. Meanwhile Pk and Stbm become enriched proximally to suppress Fz and Dsh on the proximal side, thereby facilitating the accumulation of Fz and Dsh on the distal side (Adler, 2002; Jenny et al., 2003; Klein and Mlodzik, 2005; Mlodzik, 2002). Dsh was reported to be expressed at the ML cell edges in the intercalating cells in the *X. laevis* dorsal marginal zone explants (Kinoshita et al., 2003). Pk has been shown to be localized at the anterior cell edges in the Ascidian notochord (Jiang et al., 2005), and in the zebrafish notochord and neural tube cells during somitogenesis (Ciruna et al., 2006), respectively. However, localization of non-canonical Wnt components has not been well studied during vertebrate gastrulation and the molecular mechanisms by which non-canonical Wnt signaling acts remain poorly understood.

Somite differentiation in zebrafish

Shortly after the C&E movements position the PSM next to the dorsal midline at the end of gastrulation, the first pair of somites forms (Stickney et al., 2000). In zebrafish, additional somites are generated at 30 min intervals in an anterior to posterior wave until a total of about 30 somite pairs formed alongside the notochord at 24 hpf (Kimmel et al., 1995).

Segmented somites give rise to the vertebrae and muscle of the trunk and tail (Pourquie, 2001). Zebrafish somite is predominantly myotome, with sclerotome a relatively minor component (Stickney et al., 2000) (Figure 1.5). Recent studies suggest that dermomyotome exists in the zebrafish somite as a layer of somitic cells expressing *pax3* and *pax7* genes, external to the newly formed myotome (Devoto et al., 2006). During somitogenesis, the sclerotome precursors initially form as a cluster of cells on the ventromedial surface of the somite, and migrate dorsally to encircle the notochord and neural tube (Figure 1.5) (Morin-Kensicki and Eisen, 1997). The myotome consists of two classes of muscle fibers: slow muscle fibers, which are mononucleate and reside at the lateral surface of the myotome; and fast muscle fibers, which are polynucleate and constitute the medial portion of the myotome (Figure 1.5) (Devoto et al., 1996). The fast muscles are derived from the lateral somitic cells that are located in the lateral portion of the somite (Coutelle et al., 2001; Weinberg et al., 1996). The slow muscles originate from the adaxial cells, which are specified as two patches of presomitic cells adjacent to the axial mesoderm during mid-gastrulation (Coutelle et al., 2001; Thisse et al., 1993; Weinberg et al., 1996). They can be recognized by their distinct cuboidal morphology, notochord-adjacent positions, and early expression of the myogenic factors MyoD and

Myf5 (Coutelle et al., 2001; Devoto et al., 1996; Weinberg et al., 1996). Concurrent with the specification of adaxial cells during gastrulation, the axial and presomitic mesoderm undergoes marked C&E movements (Glickman et al., 2003; Henry et al., 2000; Myers et al., 2002b; Warga and Kimmel, 1990). Whether C&E gastrulation movements have an influence on the adaxial cell fate remains to be investigated.

During somitogenesis, the adaxial cells undergo dramatic morphological changes to form a single stack of anteroposteriorly-elongated cells flanking the notochord (van Eeden et al., 1996). The majority of the adaxial cells migrate laterally throughout the somite and differentiate into a monolayer of slow muscle fibers at the myotome surface (Figure 1.5) (Devoto et al., 1996). Some adaxial cells do not migrate, but remain close to the notochord, where they differentiate as so-called “muscle pioneers” that express the Engrailed proteins (Hatta et al., 1991). The lateral migration of slow muscle cells also initiates a medial-to-lateral wave of fast muscle differentiation and morphogenesis (Henry and Amacher, 2004).

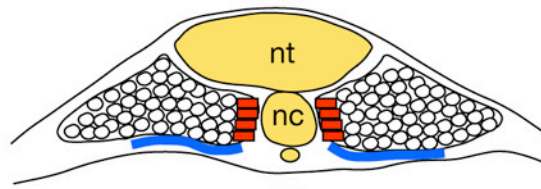
Several studies have established that different levels of Hedgehog (Hh) signaling emanating from the axial mesoderm produce different cell types in the zebrafish myotome (Figure 1.5). High levels of Hh signal induce Engrailed-expressing muscle pioneers and a small subset of fast muscle fibers, the Engrailed-expressing medial fast fibers (Wolff et al., 2003). Slightly lower levels of Hh signal induce the slow muscle fibers that migrate to the myotome surface. Finally, the lateral somitic cells that receive low levels of Hh are designated to become fast muscles (Blagden et al., 1997; Coutelle et al., 2001; Hirsinger et al., 2004; Wolff et al., 2003).

The specification of myotomal cell types is also controlled by the time at which

Figure 1.5. Somite differentiation in zebrafish. (A-B) Schematic transverse-section through the anterior trunk region of the zebrafish embryo. At the 8-somite stage (A), the slow muscle precursors, the adaxial cells (red), occupy a monolayer next to the notochord and receive the highest level of Hedgehog signal (purple). The lateral somitic cells (white) that receive low level of Hedgehog are designated to become fast muscle. The sclerotome precursors (blue) are localized ventral to the somite at the 8-somite stage. During somitogenesis, majority of the slow muscle cells (red) migrate laterally through the somite. At 24 hpf (B), they form a monolayer at the myotome surface whereas fast muscles (white) remain deep. Some slow muscle cells do not migrate and continuously receive high level of Hedgehog. These so-called muscle pioneers and the notochord-adjacent fast muscle cells (pink) strongly express Engrailed proteins. The sclerotomal cells (blue) migrate dorsally during somitogenesis to encircle the spinal cord and notochord. Abbreviations: nt, neural tube; nc, notochord; Hh, Hedgehog.

A

8-somite
(13 hpf)



Dorsal

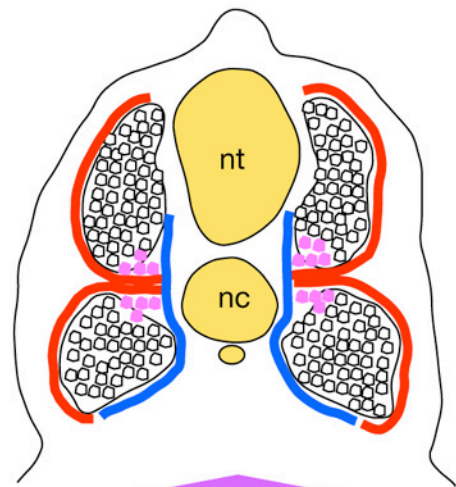


Ventral



B

24 hpf



Hh

cells receive the Hh signal (Wolff et al., 2003). Early exposure of somitic cells to Hh signal is restricted to the adaxial cells that lie immediately next to the dorsal midline. The gradient of Hh activity within the adaxial cell population is essential for the separation of the precursors of muscle pioneers and migrating slow muscles (Wolff et al., 2003). It is only after the lateral migration of the slow muscle cells that a subset of lateral somitic cells becomes exposed to the Hh signal; by this time, they are irreversibly committed to the fast lineage and give rise to the medial fast muscles (Wolff et al., 2003).

Whereas the molecular mechanisms specifying the slow muscle fate are well documented, there is little understanding of how the slow muscle morphogenesis is controlled. Although Hh signal derived from the notochord is critical for the specification and differentiation of slow muscle cells, mutant analyses argue against a role of Hh in the shape change or lateral migration of these cells (Barresi et al., 2000; Baxendale et al., 2004; Nakano et al., 2004; Roy et al., 2001). A previous report demonstrated that the migration of slow muscle cells follows a dynamic wave of *m-* and *n-cadherin* co-expression moving mediolaterally through the developing somite (Cortes et al., 2003). The large extracellular polysaccharide Hyaluronan and its synthesizing enzymes are also required for the normal slow muscle migration (Bakkers et al., 2004). Aside from these studies, our understanding of the cellular and molecular regulation of zebrafish slow muscle morphogenesis remains incomplete.

Genetic screens for genes regulating zebrafish early development

To obtain a full picture of the molecular and cellular basis of gastrulation movements, one needs to identify the genes involved and determine the hierarchy of their

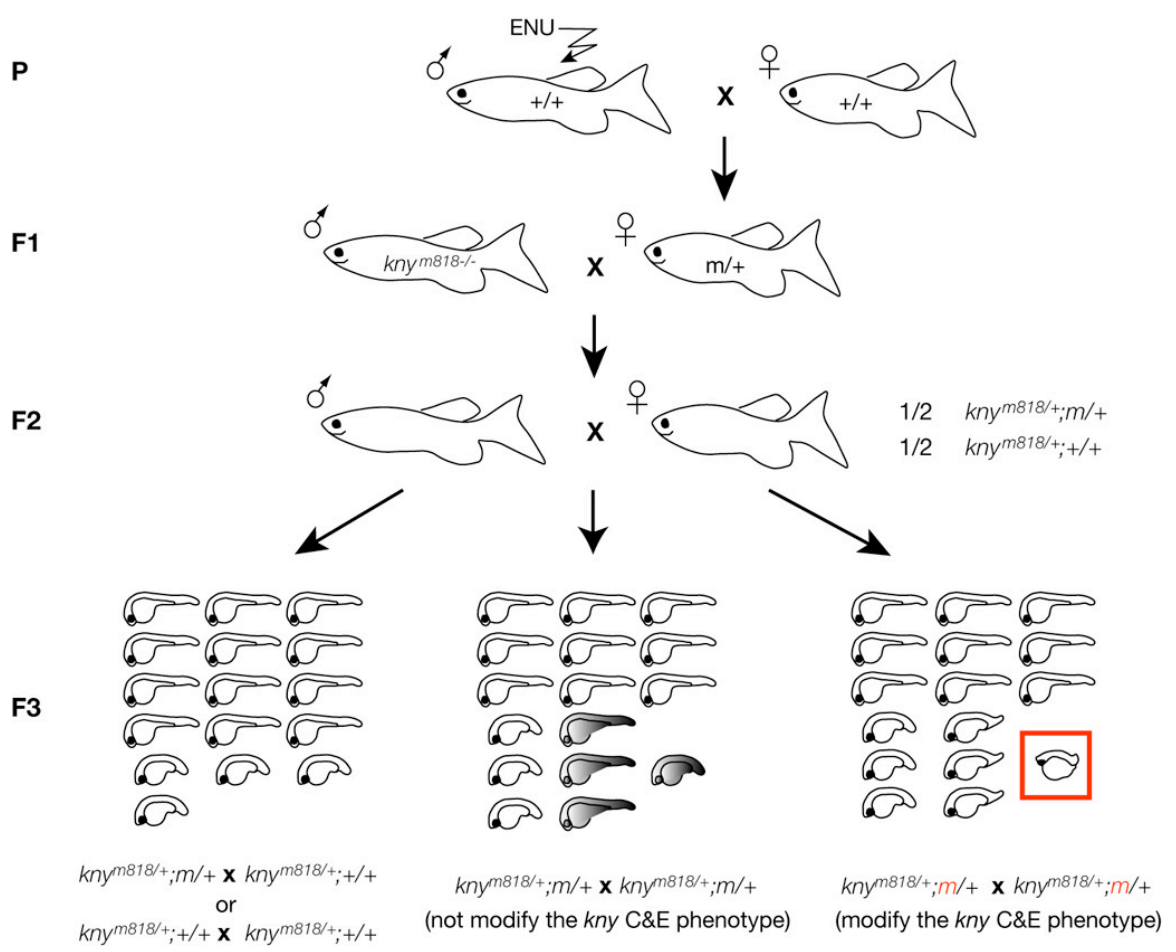
action. One main advantage of using zebrafish as a model system to study embryonic development is its accessibility to genetic manipulations. Zebrafish can be efficiently mutated by a variety of chemical, biological, and radiological means (Amsterdam et al., 1997; Davidson et al., 2003; Driever et al., 1996; Grunwald and Streisinger, 1992; Mullins et al., 1994; Solnica-Krezel et al., 1994). The short generation time, small size, inexpensive maintenance, and high fecundity also make zebrafish amenable to large-scale genetic screens. Several forward genetic screens have been conducted in zebrafish and the mutants isolated from these screens have already significantly contributed to our understanding of early vertebrate development and organogenesis (Driever et al., 1996; Haffter et al., 1996).

In the standard three-generation genetic screens, wild-type (WT) males are mutagenized with *N*-ethyl *N*-nitrosourea (ENU) to induce point mutations in spermatogonial cells (Driever et al., 1996). The mutagenized males are crossed with WT females to generate F1 founder fish, each heterozygous for a set of unique mutations. F1 fish are outcrossed to WT and half of the resulting F2 siblings carry the mutation(s). These F2 fish are intercrossed, in turn, to obtain homozygous offsprings (Driever et al., 1996). If the mutation is recessive, 1/4 of the embryos in the crosses of two F2 heterozygote parents are expected to display a phenotype. Traditional genetic screens isolated mutants by looking for morphogenetic defects in early development (Driever et al., 1996). The drawback of this screening strategy is that it may miss mutations causing subtle phenotypes. Recent screens have included *in situ* hybridization or immunohistochemistry so that changes in the expression of a particular marker gene can be scored (Kazakova et al., 2006; Kudoh et al., 2001; Kuhlman and Eisen, 2006). The

generation of GFP-reporter lines in zebrafish allows looking at marker gene expression in live embryos, thus has significantly simplified the screening procedures (Linney and Udvardia, 2004; Udvardia and Linney, 2003). Once a mutant animal is identified, the underlying molecular lesion will be cloned and the gene is further studied through functional analyses.

In the large-scale genetic screens completed in 1996, several mutations affecting gastrulation movements were found (Hammerschmidt et al., 1996a; Solnica-Krezel et al., 1996). However, in the subsequent screens, new alleles of these identified mutant loci rather than mutations in new loci were isolated (Weidinger et al., 1999). It is possible that the remaining genes, even though they are involved in gastrulation movements, are functionally redundant so that mutating one of these genes will not produce a detectable phenotype. In addition, maternal protein contribution might allow zygotic mutants in many loci to progress through early cleavages and gastrulation. An effective strategy for identifying such genes is to screen for modifiers in a sensitized genetic background. One of the zebrafish C&E mutants, homozygotes of the hypomorphic *kny*^{m818} allele, can be rescued by injecting synthetic WT *kny* RNA and the homozygous adults are viable and fertile. We thus conducted a pilot screen for recessive mutations that exacerbate the gastrulation defects of the *kny*^{m818} allele (Figure 1.6). We followed the standard three-generation screen strategy, except that in the F1 generation, the founder fish were crossed to *kny*^{m818} homozygotes. Consequently, all F2 fish were heterozygous for *kny*^{m818} and half of them carried the newly induced mutation(s). We then intercrossed F2 siblings and screened the resulting progeny for recessive mutations in addition to *kny*^{m818}. For recessive mutations not linked to the *kny* locus, 1/16 of the F3 embryos should represent

Figure 1.6. Genetic screen to identify modifiers of the *kny*^{m818} mutant phenotype. Males mutagenized with ENU were mated to wild-type females. Each F1 progeny that carried a distinct mutation **m** were crossed to *kny*^{m818} homozygote fish. All F2 progeny were heterozygous for *kny*^{m818} and half of them also carried the mutation **m**. Embryos were collected from the matings between the F2 fish. Without additional mutations, ¼ of the embryos would exhibit the *kny*^{m818} mutant phenotype. If both parents were heterozygous for **m** and **m** modified the *kny* mutant phenotype, fewer (suppressor) or more (enhancer) than ¼ of the embryos would show *kny*^{m818}-like phenotypes.



double mutants of *kny*^{m818} and this new mutation. The enhancer mutants were identified based on the morphological phenotypes, such as length and width of the embryonic body axes, cyclopia, and jaw abnormalities (Topczewski et al, 2001). Previous work from our laboratory has identified the *tri*^{m209} mutation as a semidominant enhancer of cyclopia and the *no tail*^{b195} mutation as a recessive enhancer of the defective posterior development in *kny*^{m119} mutants in AB genetic background (Marlow et al., 2004; Marlow et al., 1998).

Goals, findings and hypotheses resulting from this work

This work has investigated the roles of C&E gastrulation movements in multiple aspects of zebrafish somite development, including somite formation, and the specification and morphogenesis of somitic derivatives. During gastrulation, C&E movements shape and position the PSM alongside the nascent axial mesoderm (Myers et al., 2002b; Stickney et al., 2000). In *kny;tri* non-canonical Wnt mutants, C&E of the PSM is compromised, culminating in the formation of mediolaterally broadened and anteroposteriorly shortened somites (Henry et al., 2000). To elucidate the cellular behaviors driving the morphogenesis of PSM during gastrulation, I performed time-lapse analyses on both WT and *kny;tri* double mutant embryos. Combining *in vivo* and *in silico* approaches, I demonstrated that the PSM C&E is achieved by the cooperation of polarized planar and radial cell intercalations that preferentially separate anterior and posterior neighbors in a cell layer. In *kny;tri* double mutants, the frequency of cell intercalations is altered and the AP bias in radial intercalation is lost. Polarized radial intercalation represents a novel cellular behavior that promotes tissue extension and is the first example of non-canonical Wnt signaling polarizing cell movements between

different cell layers. I also showed that during the C&E of zebrafish dorsal mesoderm, the non-canonical Wnt signaling component Pk is asymmetrically localized at the anterior cell edge, whereas Dsh is enriched at the posterior edge. The anterior localization of Pk and posterior localization of Dsh in the dorsal mesoderm of zebrafish gastrula are reminiscent of the proximal distribution of Pk and distal distribution of Dsh in the fly wing (Adler, 2002; Klein and Mlodzik, 2005), suggesting that the molecular mechanisms by which non-canonical Wnt/PCP pathway regulates cell polarity are evolutionarily conserved. In *kny*, *tri* individual mutants and *kny;tri* double mutants, the asymmetric localization of Pk and Dsh is compromised. Based on these observations, I propose that AP polarity cues act upstream of non-canonical Wnt signaling to regulate differential cell properties along the AP and ML surfaces of the dorsal mesodermal cells. This, in turn, defines the anteroposteriorly-biased orientation of cell intercalations during C&E.

To determine whether C&E movements influence somite patterning and morphogenesis, I investigated the development of somitic derivatives in WT and *kny;tri* double mutant embryos. By applying cell tracing analyses and genetic manipulations, I demonstrated that C&E mediates the specification and fate maintenance of zebrafish slow muscle precursors, the adaxial cells. During gastrulation, C&E affects the number of prospective adaxial cells specified by defining the AP dimension of the interface between the inducing axial and responding presomitic tissues. Convergence of the prospective adaxial cells towards the notochord is essential for their fate maintenance during early segmentation, when the range of Hh signaling decreases in the paraxial mesoderm. These

studies underscore the significance of precise coordination between cell movements and inductive tissue interactions during cell fate specification.

During somitogenesis, the adaxial cells dramatically change shapes and migrate laterally to form a monolayer of slow muscle fibers at the myotome surface (Devoto et al., 1996). Using confocal imaging techniques and embryonic manipulations, I revealed novel cellular behaviors and tissue interactions during zebrafish slow muscle morphogenesis. In *kny;tri* double mutants, impaired C&E disrupts differentiation and morphogenesis of the notochord, which in turn impedes the adaxial cell shape changes and interferes with their lateral migration. This study provides an example of C&E movements ensuring proper differentiation of organ rudiments, which is necessary for tissue interactions during later development.

Finally, to identify additional genes involved in zebrafish C&E and early embryogenesis, I conducted a genetic screen for enhancers of the *kny*^{m818} mutant defects. I screened 100 F2 families and identified several mutations that interact with the *kny*^{m818} allele during gastrulation, indicating that this is an effective strategy towards finding new regulators of C&E. In parallel, I participated in a standard three-generation screen and isolated a mutation *calamity*^{yu69}, which is genetically linked to the *kny* locus and affects pigmentation and notochord development. Combining forward and chemical genetic approaches, we determined that *calamity*^{yu69} inactivates a zebrafish homolog of the human Menkes *atp7a* gene, which is critical for copper homeostasis in humans. Genetic mosaic analyses indicate that in contrast to previous hypotheses, the *atp7a* gene acts cell-autonomously in melanocytes to ensure the normal function of cuproenzymes producing melanin. These data reveal unexpected roles of copper during early embryogenesis and

suggest that suboptimal copper metabolism may contribute to birth defects. Identification of the *calamity*^{vu69} mutant establishes a novel vertebrate model for studying the human Menkes disease and copper metabolism. As *calamity*^{vu69} mutation exacerbates the *kny* mutant phenotype, it also affords a new tool to study interactions between copper and glypicans.

Taken together, my studies bring new insights into our understanding of the molecular and cellular basis underlying C&E gastrulation movements, and the roles of C&E movements in cell fate specification and late tissue morphogenesis.

CHAPTER II

CONVERGENCE AND EXTENSION MOVEMENTS MEDIATE THE SPECIFICATION AND FATE MAINTENANCE OF ZEBRAFISH SLOW MUSCLE PRECURSORS

This paper is in press under the same title in *Developmental Biology*, 2007.

Chunyue Yin and Lilianna Solnica-Krezel

Department of Biological Sciences, Vanderbilt University, Nashville, Tennessee

Summary

During vertebrate gastrulation, concurrent inductive events and cell movements fashion the body plan. Convergence and extension (C&E) gastrulation movements narrow the vertebrate embryonic body mediolaterally while elongating it rostrocaudally. Segmented somites are shaped and positioned by C&E alongside the notochord and differentiate into skeleton, fast and slow muscles during somitogenesis. In zebrafish, simultaneous inactivation of non-canonical Wnt signaling components *Knypek* and *Trilobite* strongly impairs C&E gastrulation movements. Here we show that *knypek;trilobite* double mutants exhibit a severe deficit in slow muscles and their precursor, adaxial cells, revealing essential roles of C&E movements in adaxial cell development. Adaxial cells become distinguishable in the presomitic mesoderm during late gastrulation by their expression of myogenic factors and axial-adjacent position. Using cell tracing analyses and genetic manipulations, we demonstrate that C&E

movements regulate the number of prospective adaxial cells specified during gastrulation by determining the size of the interface between the inductive axial and target presomitic tissues. During segmentation, when the range of Hedgehog signaling from the axial tissue declines, tight apposition of prospective adaxial cells to the notochord, which is achieved by convergence movements, is necessary for their continuous Hedgehog reception and fate maintenance. We provide direct evidence to show that the deficiency of adaxial cells in *knypek; trilobite* double mutants is due to impaired C&E movements, rather than an alteration in Hedgehog signal and its reception, or a cell-autonomous requirement for Knypek and Trilobite in adaxial cell development. Our results underscore the significance of precise coordination between cell movements and inductive tissue interactions during cell fate specification.

Keywords: Non-canonical Wnt; Knypek; Trilobite; Adaxial cell; Gastrulation; Hedgehog.

Introduction

The basic vertebrate body plan is established during gastrulation by a set of highly conserved morphogenetic movements, including epiboly, internalization, convergence and extension (C&E) (Keller et al., 2003; Solnica-Krezel, 2005; Warga and Kimmel, 1990). One intriguing aspect of developmental biology is to understand the connection between the morphogenetic processes of gastrulation that shape the embryo and the inductive tissue interactions that specify different cell fates. However, impaired gastrulation movements are often accompanied by early patterning defects, making it

difficult to determine the consequences of defective movements on cell fate specification (Kimmel et al., 1989; Myers et al., 2002a).

Large-scale genetic screens in zebrafish isolated a group of mutations disrupting C&E gastrulation movements that narrow the forming embryonic tissues mediolaterally and lengthen them anteroposteriorly (Hammerschmidt et al., 1996; Myers et al., 2002b; Solnica-Krezel et al., 1996). The C&E mutants exhibit a shortened body but normal tissue patterning during gastrulation (Myers et al., 2002b), presenting a powerful genetic tool with which to investigate the roles of gastrulation movements in subsequent cell fate specification. Molecular analyses revealed that many of the C&E mutations inactivate components of non-canonical Wnt signaling, a vertebrate equivalent of the *D. melanogaster* planar cell polarity (PCP) pathway that polarizes cells within the plane of epithelium (Adler, 2002; Klein and Mlodzik, 2005). During vertebrate gastrulation, non-canonical Wnt signaling directs the mediolateral (ML) cell elongation critical for cell behaviors underlying C&E (Jessen et al., 2002; Myers et al., 2002b; Wallingford et al., 2000). *knypek(kny)* and *trilobite(tri)* encode two components of non-canonical Wnt signaling, a heparan sulfate proteoglycan of the glypican family (Topczewski et al., 2001), and a transmembrane protein homologous to *D. melanogaster strabismus/van gogh* and mammalian *van gogh-like 2* (Jessen and Solnica-Krezel, 2004; Jessen et al., 2002), respectively. *kny* and *tri* genes act both cell-autonomously and non-autonomously to regulate the ML elongation of mesodermal cells during C&E (Jessen et al., 2002; Topczewski and LSK, unpublished). Compared to *kny* and *tri* individual mutants, *kny;tri* double mutants show additive C&E defects (Henry et al., 2000; Marlow et al., 1998).

Despite detailed analyses of the C&E movements in these mutants, the effect of these defective gastrulation movements on cell fate specification is less understood.

Segmented somites form alongside the notochord following gastrulation and serve as a scaffold to guide further elaboration of the vertebrate body plan (Brennan et al., 2002; Pourquie, 2001). In zebrafish, trunk somites are derived from the presomitic mesoderm (PSM) that is located at the dorsolateral blastoderm margin, the blastopore equivalent of zebrafish gastrula (Kimmel et al., 1990; Stickney et al., 2000). Upon internalization, the PSM undergoes C&E movements to form anteroposteriorly elongated territories flanking the axial mesoderm (Myers et al., 2002b). We previously reported that due to defective C&E movements, the PSM formed in *kny;tri* double mutants is extremely short anteroposteriorly and broad mediolaterally (Henry et al., 2000). Wild-type (WT) somites are composed of epithelial border cells and mesenchymal internal cells. In *kny;tri* double mutants, although the anteroposterior (AP) intrasegmental polarity and the somitic boundaries are established normally, the somites consist exclusively of border cells (Henry et al., 2000). It has not been addressed whether the somitic derivatives develop normally in *kny;tri* double mutants.

In zebrafish, somites give rise to sclerotome and myotome (Stickney et al., 2000), the latter being mainly composed of superficial slow muscles and medial fast muscles (Devoto et al., 1996). The precursors of slow and fast muscles are spatially segregated as early as during gastrulation (Hirsinger et al., 2004). Slow muscles originate from adaxial cells, which are specified as two patches of presomitic cells adjacent to the axial mesoderm during mid gastrulation (Devoto et al., 1996; Thisse et al., 1993). Adaxial cells can be recognized by their distinct cuboidal morphology and expression of the myogenic

basic helix-loop-helix transcription factors Myf5 and MyoD (Coutelle et al., 2001; Weinberg et al., 1996). During somitogenesis, majority of the adaxial cells migrate laterally through the somite to form a monolayer of slow muscle fibers at the surface of the myotome (Devoto et al., 1996). The migration of slow muscle cells initiates a wave of differentiation and morphogenesis of the fast muscle precursor cells, which are located more laterally in the somite (Henry and Amacher, 2004). Several studies have established that different levels of Hedgehog (Hh) signaling emanating from the axial mesoderm produce different cell types in the zebrafish somite: the specification and commitment to the adaxial cell fate require high Hh activity, whereas the lateral somitic cells receiving low levels of Hh are designated to become fast muscles (Blagden et al., 1997; Coutelle et al., 2001; Hirsinger et al., 2004; Wolff et al., 2003). Concurrent with the specification of adaxial cells during gastrulation, both axial and paraxial mesoderm undergoes marked C&E movements (Glickman et al., 2003; Henry et al., 2000; Myers et al., 2002b; Warga and Kimmel, 1990). Whether the morphogenesis of the axial and paraxial tissues has an influence on the adaxial cell fate remains to be investigated.

In this study, we demonstrate that *kny;tri* non-canonical Wnt mutants form fewer slow muscles and this reduction is a direct consequence of impaired C&E movements on the specification and maintenance of adaxial cell fate. During gastrulation, C&E affect the number of prospective adaxial cells specified by defining the AP dimension of the interface between the inducing axial and responding presomitic tissues. Convergence of prospective adaxial cells towards the notochord is essential for their fate maintenance during early segmentation, when the range of Hh signaling decreases. Our results

underscore the requirement for precise coordination between gastrulation movements and local inductive signals during cell fate specification.

Results

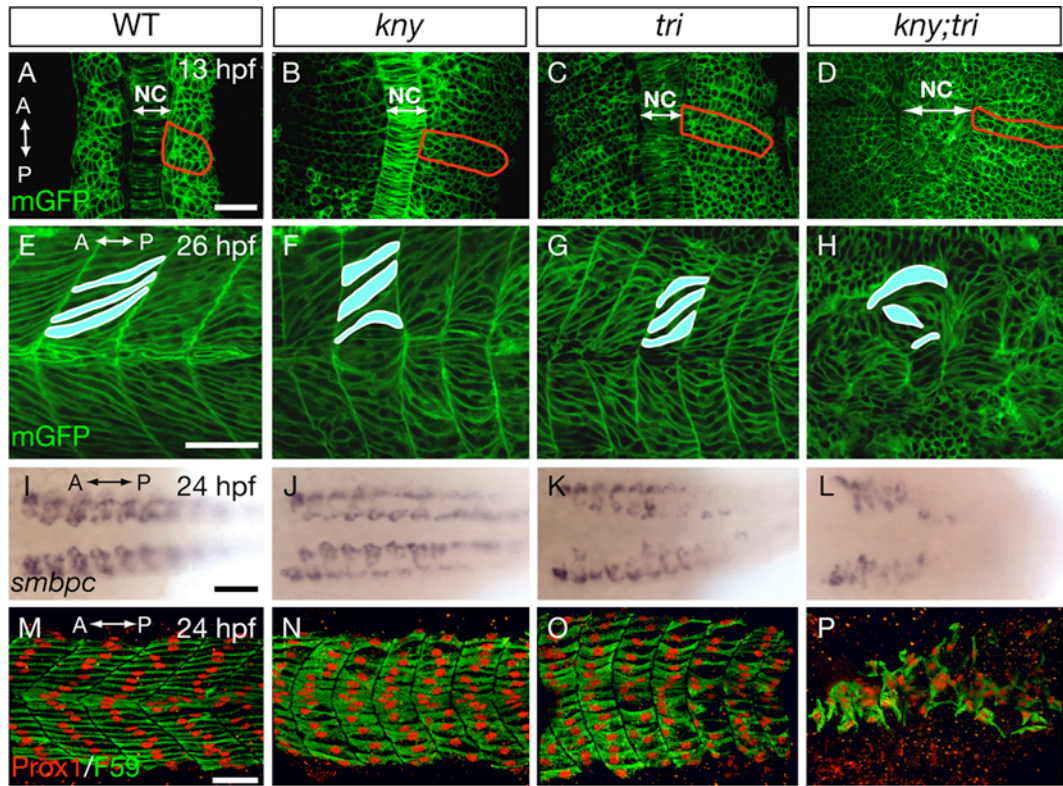
Simultaneous loss of Kny and Tri function impairs slow muscle development

Somites in *kny* and *tri* C&E mutants have shortened AP and broadened ML dimensions (Hammerschmidt et al., 1996; Henry et al., 2000; Solnica-Krezel et al., 1996), whereas *kny;tri* double mutants exhibit additive defects in C&E and somite morphology (Figure 2.1A-D) (Henry et al., 2000; Marlow et al., 1998). Given that *kny* and *tri* genes are continuously and broadly expressed in embryonic tissues, including the somites, throughout somitogenesis (Park and Moon, 2002; Topczewski et al., 2001), we decided to investigate whether Kny and Tri were also required for the later development of the somite. As revealed by membrane-localized GFP (mGFP) labeling (Wallingford et al., 2000) and confocal microscopy, at the end of segmentation, in WT the muscle fibers spanned the entire AP dimension of the chevron-shaped myotome and were oriented parallel to each other (Figure 2.1E) (Stickney et al., 2000). In *kny* and *tri* individual mutants, the myotomes were shortened anteroposteriorly and the parallel orientation of the muscle fibers was modestly impaired (Figure 2.1F, G). Strikingly, *kny;tri* double mutants formed very misshapen myotomes, composed of misaligned muscle fibers (Figure 2.1H).

The abnormal myotome morphology in *kny;tri* double mutants prompted us to investigate the development of slow and fast muscle fibers within the myotome by

examining the expression of cell-type specific genes. The expression of both slow and fast muscle markers was reduced and altered in the double mutants (Figure 2.1I-P and Figure 2.2). Because the lateral migration of slow muscle cells patterns the medial to lateral wave of fast muscle morphogenesis (Henry and Amacher, 2004), the fast muscle defects in the double mutants might be secondary to the impaired slow muscle development. Hence we focused on the analyses of slow muscles in this study. In WT embryo, *slow myosin binding protein C (smbpc)* gene is expressed in the slow muscle fibers that are located on either side of the notochord along the AP embryonic axis at 24 hours post fertilization (hpf) (Figure 2.1I) (Xu et al., 2000). The *smbpc* expression was discontinuous in the individual mutants (Figure 2.1J, K), and strongly downregulated and disorganized in the double mutants (Figure 2.1L). We examined two additional slow muscle makers in both WT and the mutants by immunohistochemistry: F59 antibody detects myosin heavy chain in amniotes and other species, and strongly labels the slow muscle fibers in zebrafish (Crow and Stockdale, 1986; Devoto et al., 1996); Prox1 antibody recognizes a homeobox protein and specifically labels the nuclei of slow muscle cells (Glasgow and Tomarev, 1998; Roy et al., 2001). Simultaneous labeling with both antibodies showed that the WT slow muscle fibers extended over the entire AP dimension of the myotome and were oriented parallel to the notochord (Figure 2.1M). In the individual mutants, the slow muscle fibers were shorter and less organized (Figure 2.1N, O). The slow muscle defects were significantly exacerbated in *kny;tri* double mutants, in which the slow muscle fibers were greatly reduced in number and highly disorganized (Figure 2.1P; Table 2.1). Therefore, combined loss of Kny and Tri function severely disrupts slow muscle development.

Figure 2.1. Loss of *Kny* and *Tri* function impairs zebrafish slow muscle development. (A-D) Confocal images of dorsal views of embryos expressing mGFP. Red lines delineate the outline of the 5th somite. (E-H) Trunk region of day1-embryos expressing mGFP, lateral views. (I-L) Dorsal views showing *smbpc* RNA expression in the slow muscles. (M-P) Lateral views of embryos stained with F59 antibody (green) that labels the cytoplasm of the slow muscle cells and Prox1 antibody (red) that labels their nuclei. A, anterior. P, posterior. NC, notochord. Scale bars, (A-H, M-P), 50 μ m. (I-L), 100 μ m.



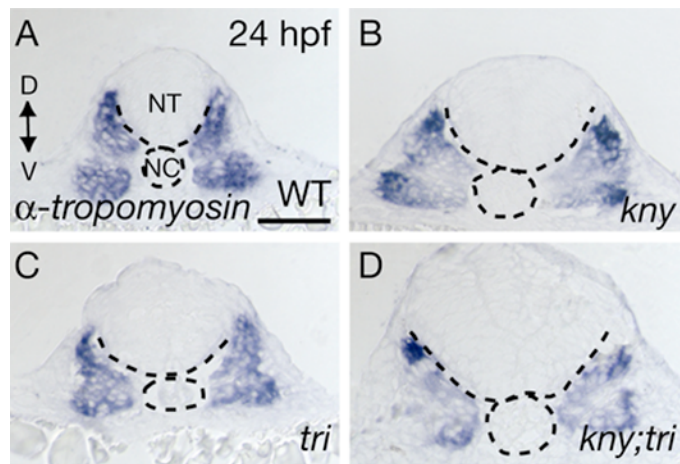
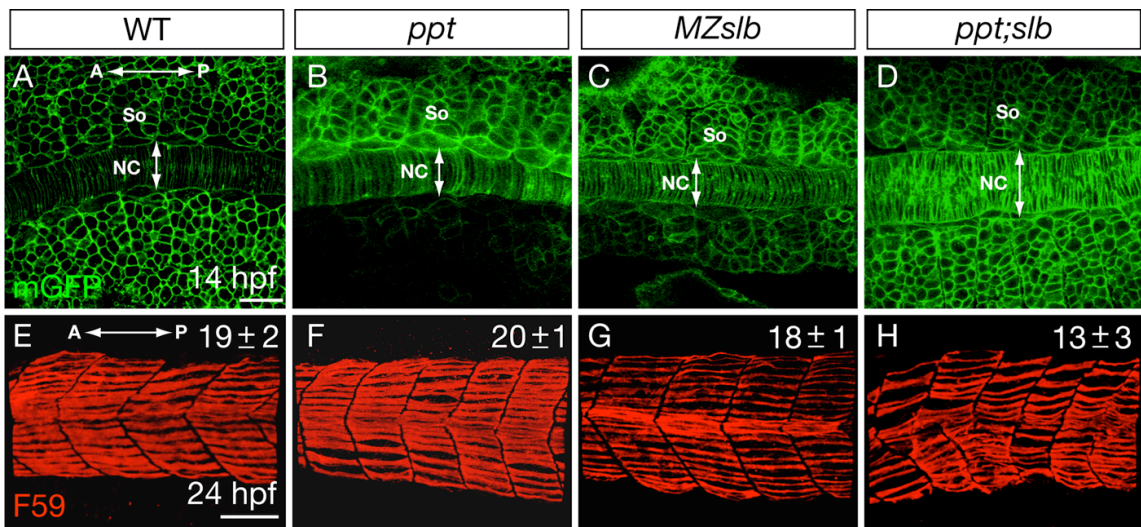


Figure 2.2. Fast muscle development in *kny;tri* double mutants. (A-D) α -tropomyosin is mainly expressed in the fast muscle component of the myotome in embryos at 24 hpf (Xu et al., 2000). Its expression was reduced and irregular in the double mutants (D). (A-D) Transverse sections. NT, neural tube. NC, notochord. D, dorsal. V, ventral. Scale bar, 100 μ m.

The slow muscle defects in *kny;tri* double mutants might be related to the impaired C&E gastrulation movements or might reflect a general requirement for the non-canonical Wnt/PCP pathway during zebrafish slow muscle development. Several genes that encode the PCP pathway components, such as *wnt5*, *kny*, and *tri*, are expressed in the paraxial mesoderm during gastrulation and segmentation (Jessen et al., 2002; Kilian et al., 2003; Park and Moon, 2002; Rauch et al., 1997; Topczewski et al., 2001). *wnt11*, which encodes another non-canonical Wnt ligand, is expressed in the axial mesoderm during gastrulation and early segmentation, and later in the slow muscle cells as they undergo lateral migration (Makita et al., 1998). To test the requirement for these PCP components in slow muscle development, we examined *pipetail/ppt* and *silberblick/slb* mutants that are defective in Wnt5 and Wnt11 function, respectively (Heisenberg et al., 2000; Rauch et al., 1997). As judged by the morphology of the notochord and somites during somitogenesis, *ppt* and *slb* individual mutants exhibited much milder C&E defects compared to *kny*, *tri*, and *kny;tri* mutant embryos (Figure 2.3B-C compared to Figure 2.1B-D), consistent with previous reports (Heisenberg et al., 2000; Rauch et al., 1997). At 24 hpf, *ppt* and *slb* individual mutants formed normal chevron-shaped myotomes, and the number and morphology of their slow muscle fibers were not significantly altered (Figure 2.3F-G). *ppt;slb* double mutants that lack the function of both Wnt ligands showed similar C&E phenotypes as seen in *kny* and *tri* individual mutants (Figure 2.3D) (Ciruna et al., 2006; Marlow et al., 2004; Westfall et al., 2003). The myotomes formed in these mutants were shortened and the slow muscle fibers were less organized and reduced in number (Figure 2.3H). These data indicate that PCP pathway itself is not absolutely essential for the establishment of slow muscle fate. However, there is a correlation

Figure 2.3. The somite morphology and slow muscle development in the non-canonical Wnt/PCP mutants. (A-D) Confocal images of the embryos expressing mGFP at the 10-somite stage, dorsal views. (E-H) Lateral views of day1-embryos stained with F59 antibody that labels the slow muscle fibers. The numbers of slow muscle fibers per somite are indicated in the up right corner. All the measurements were done in the 3rd and 4th myotomes. 10 embryos were analyzed for each genotype. NC, notochord. So, somite. A, anterior. P, posterior. Scale bar, 50 μ m.



between the degree of the C&E defect and the slow muscle defect: among all the PCP mutants examined, *ppt* and *slb* individual mutants exhibited the mildest C&E defects and formed slow muscle fibers with normal morphology and numbers. In *ppt;slb* double mutants, *kny* and *tri* individual mutants, characterized by intermediate C&E phenotypes, there were modest disorganization and deficiency of the slow muscle fibers. Finally, *kny;tri* double mutants exhibited the most severe defects in both C&E and slow muscle development.

Reduced numbers of prospective adaxial cells are specified in *kny;tri* double mutants

To distinguish whether the deficiency of slow muscle fibers in *kny;tri* double mutants was due to defects occurring during gastrulation or reflected a requirement for later roles of these genes, we asked at what stage slow muscle development was affected in the mutants. At the 10-somite stage (14 hpf), zebrafish somite contains two cell types. (1) The slow muscle precursors, known as adaxial cells, which form a monolayer next to the notochord (Cortes et al., 2003; Devoto et al., 1996). The adaxial cells are labeled strongly by a human Myf5 antibody, which has been recently implicated to detect primarily MyoD protein in zebrafish (Figure 2.7D) (Hammond et al., 2006; Tajbakhsh et al., 1998; Topczewska et al., 2001). (2) The lateral somitic cells, which give rise to fast muscles and express MyoD protein at much reduced levels (Coutelle et al., 2001; Devoto et al., 1996). WT embryos contained 106 ± 6 cells in each anterior somite, 16 of which were adaxial cells (Table 2.1) (Devoto et al., 1996). *kny;tri* double mutants had fewer cells in their anterior somites (84 ± 3 cells per somite) (Henry et al., 2000), only 7 of which were adaxial cells (Table 2.1). Notably, the ratio of adaxial cells to lateral somitic

Table 2.1. Numbers of slow muscle fibers and adaxial cells per somite

	24 hpf	14 hpf (the 10-somite stage)		
	No. of slow muscle fibers (embryos)	No. of adaxial cells (embryos)	Total numbers of somitic cells	Adaxial cell/lateral somitic cell
WT	19±2 (33)	16±1 (32)	106±6	0.15±0.03
<i>kny or tri</i>	14±2 (33)	11±2 (30)	103±7	0.10±0.02
<i>kny;tri</i>	9±1 (27)	7±1 (26)	84±3	0.07±0.01

All measurements were taken in the 3rd and 4th somites. The slow muscle fibers were recognized by co-labeling with the F59 and Prox1 antibodies, whereas the adaxial cells by their morphology, localization, and strong MyoD protein expression.

cells was significantly smaller in the double mutants compared to WT (0.15 for WT, 0.07 for the double mutants; $p < 3.3 \times 10^{-5}$). Therefore, *kny;tri* double mutants contain fewer adaxial cells during segmentation and such reduction is due to causes in addition to the smaller somite size.

We next asked whether defects in cell fate specification could account for the deficiency of adaxial cells in the double mutants. The prospective adaxial cells are specified at mid-gastrulation as two files of cells flanking the axial mesoderm, which is the source of the inductive signals (Hirsinger et al., 2004; Stickney et al., 2000). They can be recognized by their expression of the myogenic regulatory factor *myoD* gene (Figure 2.4A) (Coutelle et al., 2001; Rudnicki et al., 1993; Weinberg et al., 1996). At 95% epiboly (9 hpf), the ML width and dorsoventral depth of the *myoD*-expression domain in *kny;tri* double mutants were similar to that in WT (Figure 2.4A, C, Figure 2.5, and data not shown), indicating that the range of the inducing signals and their reception by the PSM are normal. However, the AP length of the *myoD*-expression domain was much shorter in the double mutants (78% of the WT length, $p < 0.0001$, 34 WT and 10 *kny;tri* embryos; Figure 2.4A, C), consistent with the overall reduction of their AP embryo length due to defective C&E movements (Henry et al., 2000; Marlow et al., 1998). Since the size and shape of the double mutant prospective adaxial cells were not significantly different from WT at this stage (Table 2.2), we propose that fewer prospective adaxial cells are specified along the AP dimension in the mutants. These data suggest that C&E movements influence the number of adaxial cells specified by defining the size of the interface between the inducing axial and responding presomitic tissues.

Figure 2.4. C&E movements define the number of prospective adaxial cells specified during gastrulation. (A-F) *myoD* RNA expression in the prospective adaxial cells. Purple lines delineate the interface between the axial and presomitic tissues. Arrowheads show the ML width of the *myoD*-expression domain. (G) Proliferation indices of the prospective adaxial cells (number of proliferating *myoD*-expressing cells/total number of *myoD*-expressing cells) at the tailbud stage (10 hpf). 10 embryos of each genotype were analyzed. Error bars represent the standard error. Asterisk: $p < 0.05$, *kny;tri* mutant versus WT. (H-J) *ptc1* RNA expression at the tailbud stage. (H'-J') *ptc1* RNA expression (red) detected by fast red staining. (A-F, H-J) Dorsal views. NC, notochord. Scale bars, (A-F, H-J) 100 μm ; (H'-J') 20 μm .

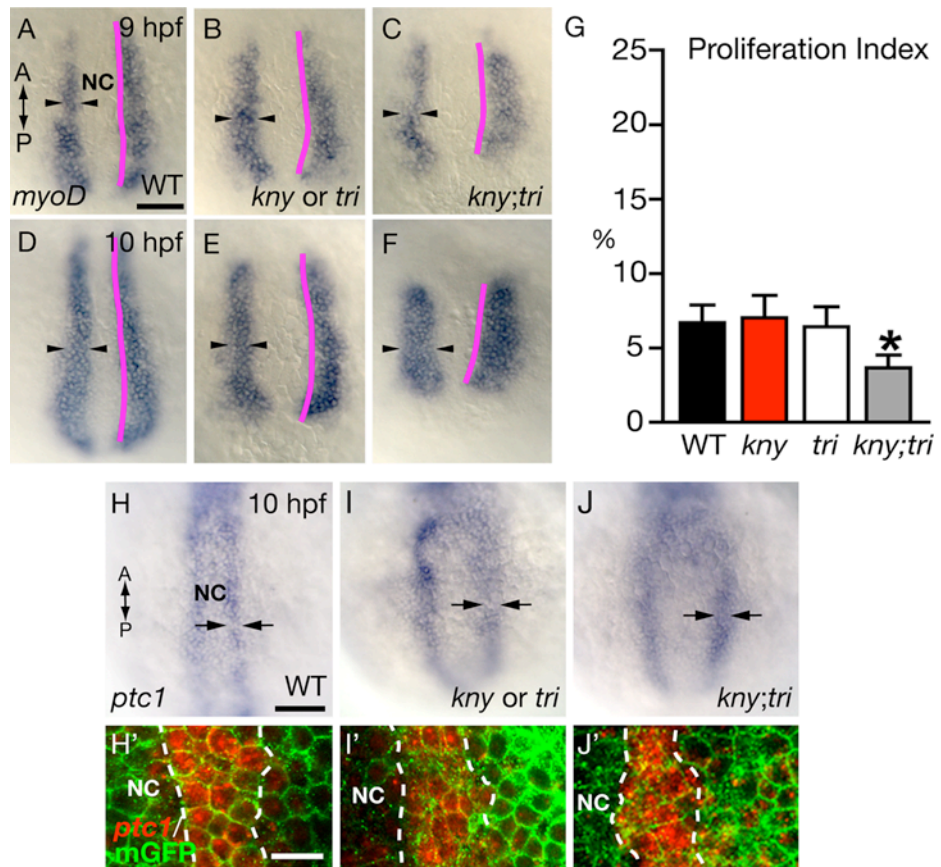


Figure 2.5. Numbers of *myoD*-expressing cells along the mediolateral dimension at 95% epiboly (9 hpf) and the tailbud stage (10 hpf). The positions where the numbers of *myoD*-positive cells were counted are indicated on the right. The mediolateral (ML) range of the *myoD* RNA expression in *kny;tri* double mutants is comparable to WT at 95% epiboly, but becomes significantly wider than WT at the tailbud stage. 34 WT, 24 *kny* or *tri* individual mutants, and 10 *kny;tri* double mutants were examined at 95% epiboly. 39 WT, 43 individual mutants, and 9 double mutants were examined at the tailbud stage. Error bars represent the standard deviation. Asterisks indicate values significantly different at $p < 0.05$.

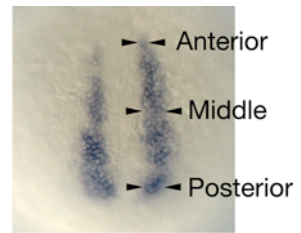
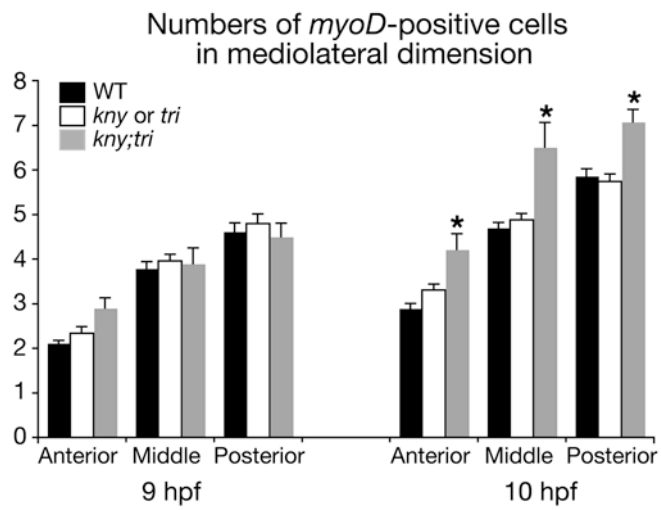


Table 2.2. Shape, size, and orientation of the prospective adaxial cells during late gastrulation

Genotype	Length/Width Ratio		Cell size (μm^2)		ML alignment (% \pm 30 ⁰) 1-somite	Cells/ Embryos
	95% epiboly, (9 hpf)	1-somite, (10.5 hpf)	95% epiboly, (9 hpf)	1-somite, (10.5 hpf)		
WT	1.38 \pm 0.25	1.51 \pm 0.32	132.2 \pm 27.3	118.9 \pm 25.2	67	208/10
<i>kny</i>	1.37 \pm 0.24	1.43 \pm 0.28 ^a	146.3 \pm 35.4	134.0 \pm 36.9	55 ^c	177/9
<i>tri</i>	1.38 \pm 0.27	1.50 \pm 0.33	148.0 \pm 30.0	132.5 \pm 32.8	60	233/10
<i>kny;tri</i>	1.35 \pm 0.23	1.40 \pm 0.26 ^b	134.9 \pm 31.0	121.6 \pm 31.5	52 ^d	246/10

^avs. WT, significantly different at $p < 0.05$.

^bvs. WT, significantly different at $p < 0.0003$.

^cvs. WT, significantly different at $p < 0.01$.

^dvs. WT, significantly different at $p < 0.001$.

The prospective adaxial cell population in *kny;tri* double mutants is defective in C&E movements at late gastrulation

As gastrulation continued and the tailbud formed, more *myoD*-expressing cells appeared in the posterior region when the nascent PSM encountered the midline tissues (Figure 2.4D) (Kanki and Ho, 1997). Meanwhile, C&E movements extended the *myoD*-expression domain and brought more laterally positioned cells towards the midline (Figure 2.4D). In *kny;tri* double mutants, AP extension of the *myoD*-expression domain was negligible (Figure 2.4F). Instead, the ML width of the *myoD* expression was broader in the double mutants than in WT (5-cell diameters wide for WT, 7-cell diameters for *kny;tri* double mutants, Figure 2.4D-F, and Figure 2.5). Three plausible mechanisms could account for the ML expansion of the *myoD* expression domain: First, this expansion could be due to increased cell proliferation along the ML dimension. Second, Hh signaling range might be expanded laterally in the double mutants, resulting in the formation of ectopic numbers of prospective adaxial cells (Blagden et al., 1997; Coutelle et al., 2001). Finally, in WT the *myoD*-expressing cells converge medially towards the notochord, whereas such medial convergence fails to occur in the double mutants, accounting for the abnormal accumulation of *myoD*-expressing cells in the PSM.

To distinguish between these possibilities, we first analyzed the proliferation rate of the *myoD*-expressing cells at different stages during late gastrulation (Materials and methods). At all the stages analyzed, the double mutant cells exhibited lower proliferation rates compared to WT and individual mutants (Figure 2.4G and data not shown), arguing against the notion that increased proliferation causes the ML expansion of the *myoD* expression.

Broader range of Hh signaling could induce prospective adaxial cells ectopically, accounting for the ML expansion of the *myoD* expression (Blagden et al., 1997). Moreover, a recent study in *X. laevis* indicated a requirement for PCP-related molecules in ciliogenesis that is essential for normal Hh signaling (Park et al., 2006). To test whether Hh signaling was affected in *kny;tri* PCP mutants, we examined the expression of *patched1/ptc1* gene that encodes the Hh receptor. *ptc1* expression is upregulated in response to Hh signaling and serves as a marker for the Hh responding cells (Concordet et al., 1996; Stone et al., 1996). At the end of gastrulation (10 hpf), *ptc1* was expressed at high levels within a range of 4-cell diameters from the axial-PSM boundary in WT (Figure 2.4H, H'). *kny;tri* double mutants exhibited equivalent ML dimension of the *ptc1* expression (Figure 2.4J, J'), indicating that the Hh signaling range in the PSM is not expanded in the double mutants.

The above results suggest that the ML expansion of the *myoD* expression in the double mutants is more likely caused by impaired medial convergence of this tissue. To study directly the C&E movements of the prospective adaxial cell population, we acquired Nomarski time-lapse recordings between 95% epiboly (9 hpf) and the 1-somite stage (10.5 hpf), and monitored the movements of a small population of cells at the intermediate depth of the PSM (Figure 2.6A-D). We used the first forming somitic boundary as a landmark to ensure that the analyzed cell populations were located at the equivalent AP position in each experimental embryo. The analyzed cells were located within 6-cell diameters from the axial-PSM boundary, thus representing a small portion of the prospective adaxial cells (referring to Figure 2.4A and Figure 2.5). During the recordings, the WT cell population underwent significant C&E as the tissue extended

anteroposteriorly and narrowed mediolaterally (10 embryos; Figure 2.6A, F; Movie S1). In the individual mutants, the tissue still converged and extended, but at reduced levels (9 *kny* mutants; 10 *tri* mutants; Figure 2.6B, C, F). Strikingly, the cell population in *kny;tri* double mutant exhibited little convergence and virtually no extension (10 embryos; Figure 2.6D, F; Movie S2).

Next, we tracked the positions of cells that were located 2-cell diameters away from the axial-PSM boundary at the beginning of the time-lapse. In WT, these prospective adaxial cells underwent active rearrangements, and 35% of them became adjacent to the midline by the end of the time-lapse (68 cells/10 embryos, Figure 2.6A). The percentage was 24% in *kny* (65 cells/9 embryos, Figure 2.6B), 27% in *tri* (68 cells/10 embryos, Figure 2.6C), but only 19% in *kny;tri* double mutants (68 cells/10 embryos, Figure 2.6D), providing direct evidence that the double mutant prospective adaxial cells are compromised in their medial convergence.

The lateral prospective adaxial cells in the double mutants fail to maintain their identity during segmentation

We next asked whether the ectopic columns of prospective adaxial cells in the double mutants maintained their fate during segmentation, when C&E movements continued to narrow and elongate the embryonic body (Myers et al., 2002b). By the 5-somite stage (11.7 hpf), the majority of the prospective adaxial cells in WT and individual mutants had converged medially and formed a monolayer of pseudo-epithelium flanking the notochord (Figure 2.7A, B) (Hirsinger et al., 2004). The adaxial cell marker, MyoD protein (Hammond et al., 2006; Tajbakhsh et al., 1998; Topczewska et al., 2001), was expressed in only one column of cells on either side of the notochord

Figure 2.6. C&E movements of the prospective adaxial cell population during late gastrulation. (A-D) Nomarski images of live embryos captured at the beginning and the end of the time-lapse recordings. Dorsal views, anterior to the top. Cells located two-cell diameters away from the notochord at the beginning of the time-lapse are labeled in red. Their positions at the end of the time-lapses are indicated in the right panels. Arrowheads point to the first somitic boundary. (E) Schematic of the tissue shape change in WT. (F) Quantifications of the tissue shape changes (Materials and methods). Error bars represent the standard error. Asterisk: $p < 0.05$, mutant versus WT. NC, notochord. M, medial. L, lateral. Scale bar, 50 μm .

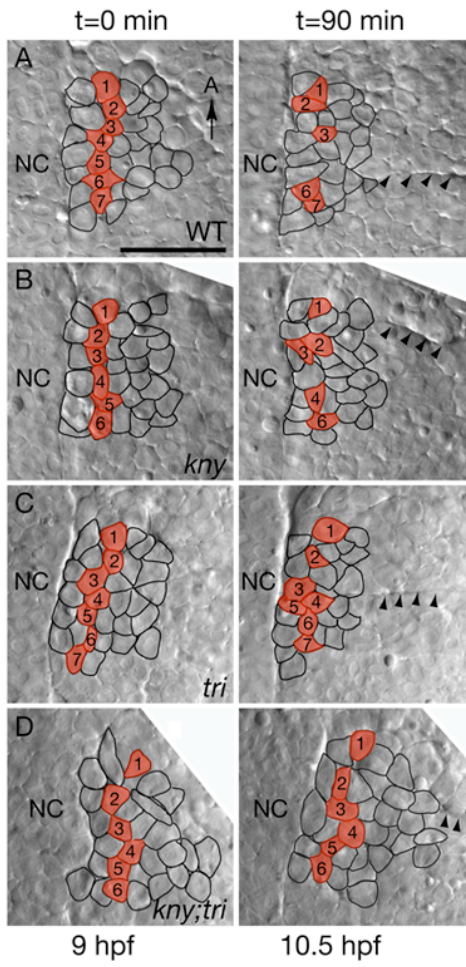
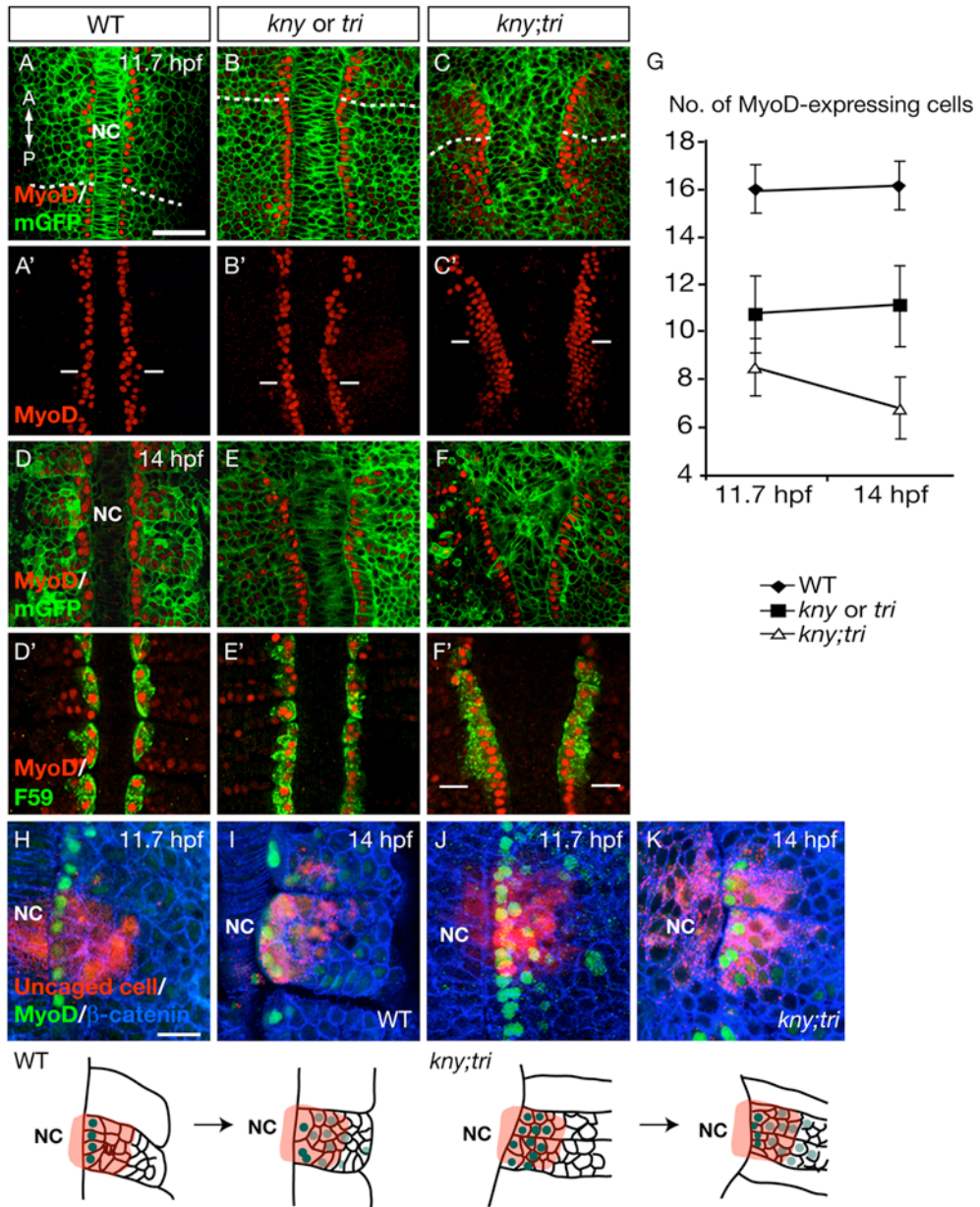


(Figure 2.7A, A', B, B'). Notably, although *kny* individual mutants exhibited severe convergence defect during late gastrulation (Figure 2.6F), such a defect was improved significantly during early segmentation so that most of the *kny* mutant prospective adaxial cells were located next to the notochord at the 5-somite stage (Figure 2.7B, B'). In the double mutants, by contrast, MyoD protein expression was expanded mediolaterally at the 5-somite stage (Figure 2.7C, C'), suggestive of persistent C&E defects in these embryos. Interestingly, among all the MyoD-expressing cells in the double mutants, only those immediately next to the notochord adopted an epithelial-like morphology (Figure 2.7C).

Strikingly, at the 10-somite stage (14 hpf), we no longer observed the expansion of MyoD protein expression in *kny;tri* double mutants. In both WT and the double mutants, MyoD protein was expressed throughout the somite, with the highest expression level detected in only one column of cells flanking the notochord (Figure 2.7D, F). The identity of these notochord-adjacent cells as adaxial cells that adopted a slow muscle fate was confirmed by the labeling with F59 antibody (Figure 2.7D', F') (Devoto et al., 1996). We quantified the numbers of MyoD-expressing cells at the 5-somite stage and the numbers of cells co-labeled by MyoD and F59 antibodies at the 10-somite stage. Within this time interval, whereas the number of cells expressing high levels of MyoD remained largely constant in WT and the individual mutants ($p > 0.08$), it was reduced drastically in the double mutants ($p < 0.0002$) (Figure 2.7G).

The above data suggest that in *kny;tri* double mutants some prospective adaxial cells expressing MyoD during early segmentation lost their adaxial identity by the 10-somite stage. To test this hypothesis, we carried out cell tracing experiments. At the 5-

Figure 2.7. The prospective adaxial cells in *kny;tri* double mutants fail to maintain their identity during early segmentation. (A-C) MyoD protein distribution detected by the human Myf5 antibody in the embryos also labeled with mGFP. Dashed lines highlight the somite-PSM boundary. (A'-C') show only the MyoD protein expression. (D-F) At the 10-somite stage, MyoD protein was strongly expressed in one column of adaxial cells flanking the notochord. Weak MyoD expression was detected in the lateral somitic cells at this stage. (D'-F') At the 10-somite stage, the notochord-adjacent adaxial cells were co-labeled by MyoD and F59 antibodies. Lines in (A'-C', F') indicate the somite-PSM boundary. (G) Quantification of the numbers of cells expressing MyoD protein at the 5-somite stage and cells co-labeled with MyoD and F59 antibodies at the 10-somite stage. Error bars represent standard deviation. (H-K) Cell tracing analyses of the prospective adaxial cell population. (H) Within the fluorescein-labeled cell population (red) in WT embryos (n=6), only one column of cells immediately next to the notochord expressed MyoD protein at the 5-somite stage. (I) The notochord-adjacent cells continued to strongly express MyoD protein at the 10-somite stage. (J) In the double mutants (n=6), at the 5-somite stage, majority of the fluorescein-labeled cells expressed MyoD. (K) At the 10-somite stage, only the column of cells flanking the notochord exhibit adaxial cell identity. (A-F, H-K) Dorsal views. NC, notochord. Scale bars, (A-F, A'-F'), 50 μm ; (H-K) 20 μm .



somite stage, we labeled uniformly sized small cell groups that were within 4-cell diameters from the notochord by photoactivation of caged fluorescein (Figure 2.7H, J) (Myers et al., 2002a), and assessed their positions at the 10-somite stage (Figure 2.7I, K). The prospective adaxial cells were identified based on the MyoD protein expression. At the 5-somite stage in the WT embryos, the prospective adaxial cells were restricted to one column of the fluorescein-labeled cells juxtaposing the notochord (Figure 2.7H), and only these cells exhibited strong MyoD expression at the 10-somite stage (Figure 2.7I). The remaining cells within the labeled group were the lateral somitic cells that did not express MyoD at the 5-somite stage and showed weak MyoD expression at the 10-somite stage (Figure 2.7H, I). In *kny;tri* double mutants, majority of the fluorescein-labeled cells were MyoD-expressing prospective adaxial cells at the 5-somite stage (Figure 2.7J). Between the 5- and 10-somite stages, the overall size, shape and cell number of the labeled cell group did not change significantly, indicating that these double mutant cells neither resumed C&E movements during segmentation, nor underwent cell death (Figure 2.7K and data not shown). At the 10-somite stage, strong MyoD expression was restricted to the notochord-adjacent cells (Figure 2.7K), whereas the labeled cells located more laterally exhibited much weaker MyoD expression, characteristic of the lateral somitic cell fate (Figure 2.7K). Taken together, our data suggest that the laterally-located prospective adaxial cells in the double mutants lose their adaxial cell identity during early segmentation and transdifferentiate into the lateral somitic cells that give rise to fast muscle.

Perturbed Hh signaling is not responsible for the defects in adaxial cell fate maintenance in *kny;tri* double mutants

We sought to understand the mechanisms underlying the defects in the maintenance of adaxial cell fate in *kny;tri* double mutants. Continuous Hh signaling is required for maintaining the adaxial cell identity (Coutelle et al., 2001; Hirsinger et al., 2004). Hence we examined *ptc1* expression to assess the Hh signaling during segmentation. Interestingly, between the tailbud and the 5-somite stages, the ML range of the *ptc1* expression decreased from 4-cell diameters to only 1-cell adjacent to the notochord, regardless of the embryo genotypes (Figure 2.4H'-J', Figure 2.8A-C, A'-C'). Thus the double mutant prospective adaxial cells that did not converge to the notochord stopped receiving Hh signal by the 5-somite stage.

To investigate whether the double mutant cells that failed to converge were still competent to respond to Hh signaling, we injected 100 pg of synthetic *sonic hedgehog/shh* RNA into the double mutants to achieve ectopic Shh expression in the PSM (Krauss et al., 1993). Injection of *shh* RNA did not suppress the C&E defects of *kny;tri* double mutants (data not shown), consistent with our previous report (Marlow et al., 1998). Rather, we detected excess MyoD-expressing cells in the injected double mutants at the 5-somite stage (Figure 2.8J). In contrast to the unmanipulated embryos, all of these MyoD-expressing cells maintained their adaxial cell identity and initiated slow muscle differentiation at the 10-somite stage as revealed by MyoD and F59 antibody labeling (Figure 2.8D-F, J). Thus, the loss of adaxial cell fate in *kny;tri* double mutants is not due to an incompetence of *kny;tri* cells to respond to Hh signaling. We also tested whether the *kny;tri* double mutant cells required higher levels of Hh signaling to maintain the adaxial cell identity compared to WT. We injected different doses of *shh* RNA, ranging from 100 pg up to 200 pg, into the embryo (data not shown). In both WT and

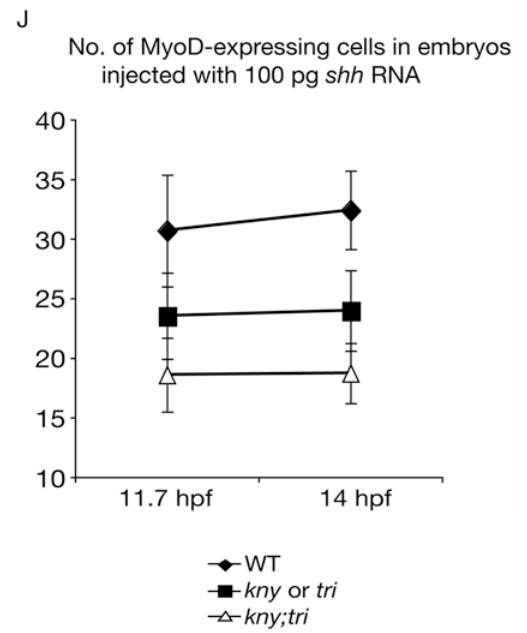
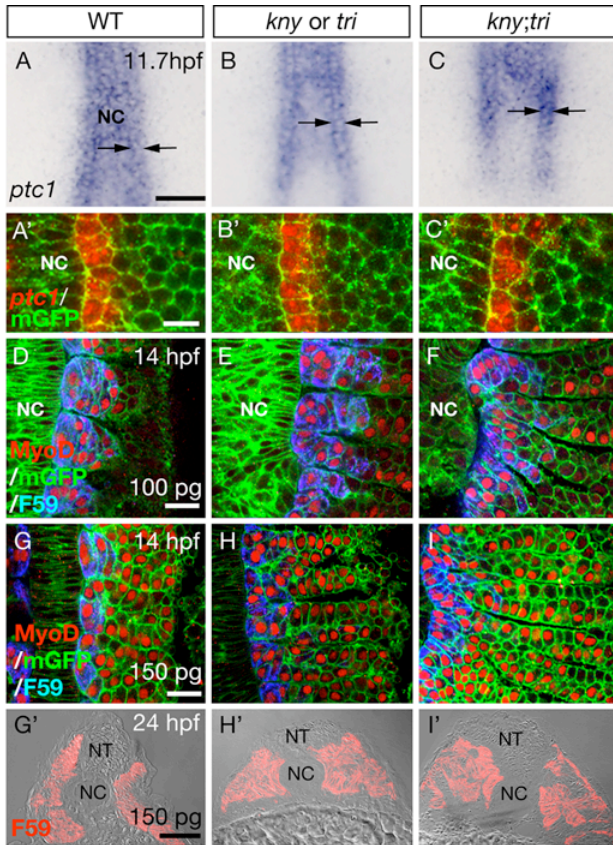
double mutants, at a minimum dose of 150 pg *shh* RNA, cells within the entire somite exhibited strong MyoD protein expression at the 10-somite stage and were strongly labeled by the F59 antibody at 24hpf (Figure 2.8G-I, G'-I'), suggesting that they were transformed into the slow muscle fate by the ectopic Hh signaling. This result indicates that the responsiveness of the double mutant prospective adaxial cells to Hh signaling is quantitatively similar to that of WT cells.

Our observations revealed a striking correlation between the decrease of Hh signaling range and the reduction of MyoD-expressing cells that occurred between the 5- and 10-somite stages in *kny;tri* double mutants. Hence we hypothesize that in the WT situation, the prospective adaxial cells specified during gastrulation all converge towards the notochord to receive continuous Hh signal, allowing them to maintain their adaxial cell fate during segmentation. By contrast, in *kny;tri* double mutants, the laterally specified prospective adaxial cells do not converge. Therefore they reside outside of the Hh signaling range during segmentation, and consequently fail to adopt the slow muscle fate.

Cell autonomy of Kny and Tri during adaxial cell specification and C&E movements

During gastrulation and early segmentation, both *kny* and *tri* genes are expressed broadly in the zebrafish embryo, including the prospective adaxial cells (Jessen et al., 2002; Park and Moon, 2002; Topczewski et al., 2001). Their ubiquitous expression patterns and our results described above are consistent with two models for the role of these genes in adaxial cell fate specification. One possibility is that Kny and Tri act cell-autonomously during the specification and maintenance of adaxial cell fate.

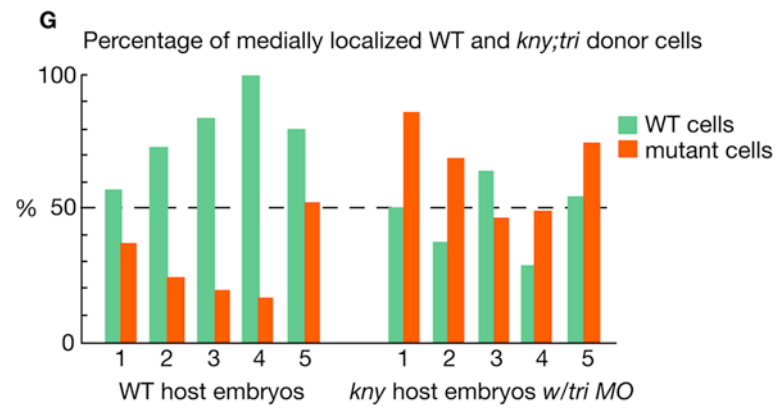
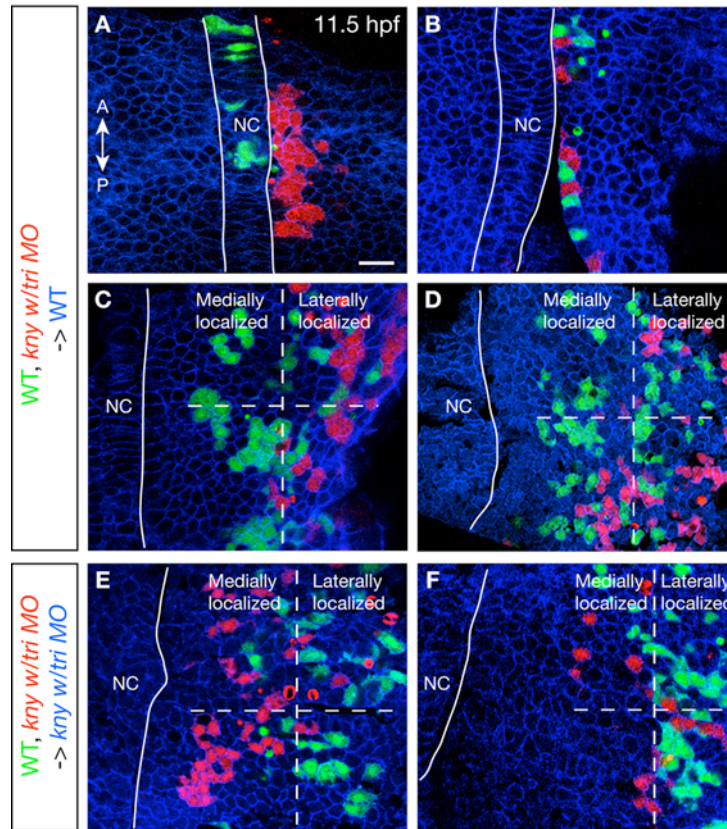
Figure 2.8. The range of Hh signaling in the PSM declines during early segmentation. (A-C, A'-C') *ptc1* RNA expression was restricted to one column of cells next to the notochord at the 5-somite stage in WT (A, A'), individual (B, B'), and *kny;tri* double mutants (C, C'). Arrows show the ML range of the *ptc1* expression. (D-F) Labeling of MyoD and F59 antibodies in embryos injected with 100 pg synthetic *shh* RNA to induce ectopic Shh activity. (G-I) In WT, individual mutants and double mutants, injection of 150 pg *shh* RNA caused strong MyoD protein expression throughout the somite at the 10-somite stage. (G'-I') Transverse sections of day1-embryos injected with 150 pg *shh* RNA and labeled with F59 antibody. (J) Numbers of MyoD-expressing cells at the 5-somite stage and numbers of cells co-labeled by MyoD and F59 antibodies at the 10-somite stage in embryos injected with 100 pg *shh* RNA. For each genotype, 10 embryos were examined at both stages and quantifications were all done within the 3rd somite. Error bars represent the standard deviation. (A-I) Dorsal views. NC, notochord. Scale bars, (A-C, G'-I') 100 μ m, (A'-C') 20 μ m, (D-I) 50 μ m.



Alternatively, Kny and Tri function is required for the movements of prospective adaxial cells to ensure their position within the range of the inducing Hh signal. To distinguish between these two possibilities, we performed transplantation experiments (Figure 2.9). Prospective somitic cells from the dorsolateral margin of the WT donor embryos and *kny* mutants injected with morpholino oligonucleotides (MO) targeting *tri* mRNA translation (Jessen et al., 2002), were co-transplanted deeply into the blastodermal margin of the WT host embryos at around 40% epiboly (4.5 hpf) (Materials and methods) (Yamashita et al., 2002). We examined the positions of the donor cells during early segmentation and found that the *kny;tri*-deficient donor cells were able to form adaxial cells in the WT hosts when located next to the notochord (Figure 2.9A, B, the adaxial cells were recognized by their characteristic epithelial-like morphology, 4 embryos). Such position-dependent behaviors of *kny;tri*-deficient cells indicate that Kny and Tri activities are not required cell-autonomously for the adaxial cell fate when located in the range of inducing signals.

Interestingly, the somitic cells from the WT and *kny;tri*-deficient donor embryos, which were co-transplanted into the same position in the WT host embryos right before the onset of gastrulation, became segregated from each other at early segmentation (Figure 2.9C, D, G). In all five WT host embryos examined, majority of the WT donor cells were localized in the medial half of the transplanted donor cell population, whereas most *kny;tri*-deficient donor cells were distributed in the lateral half (Figure 2.9C, D, G), indicating that the WT donor cells converged more medially than the *kny;tri*-deficient cells and the convergence defect of *kny;tri*-deficient cells is cell-autonomous. In contrast, when transplantation was performed using *kny;tri*-deficient hosts, cells from the WT and *kny;tri*-deficient donor embryos were intermingled with one another (Figure 2.9E, F, G).

Figure 2.9. Cell autonomy of Kny and Tri in adaxial cell specification and convergence movements of the PSM. Cells from WT (green) and *tri* MO-injected *kny* mutant embryos (red) were co-transplanted into the WT (A-D) or *kny;tri*-deficient (E-F) host embryos (Materials and methods). (A-F) Confocal images of the host embryos stained with β -catenin antibody at 11.5 hpf. (A-B) When located next to the notochord in the WT hosts, the *kny;tri*-deficient donor cells formed adaxial cells that exhibited the characteristic epithelial-like morphology. (C-D) In the WT hosts, the WT donor cells were located more medially than the *kny;tri*-deficient donor cells. (E-F) In the *kny;tri*-deficient hosts, the WT donor cells were intermingled with the mutant donor cells. In (C-F), the horizontal dashed lines show the ML range of the transplanted donor cell population. The vertical dashed lines separate the donor cell population into the medial and lateral halves. (A-F) Dorsal views. NC, notochord. Scale bar, 20 μ m. (G) Quantification of the proportions of WT and *kny;tri*-deficient donor cells that are located in the medial half of the transplanted donor cell population. Data from 5 WT and 5 *kny;tri* deficient host embryos are shown. Each host embryo contains on average of 43 WT donor cells and 38 mutant donor cells.



We interpret this result to mean that when positioned in a *kny;tri*-deficient environment, the WT cells exhibited similar convergence defects as the *kny;tri*-deficient cells. Consequently, these two types of donor cells failed to segregate from each other. Taken together, Kny and Tri regulate the convergence of somitic cells both cell-autonomously and non-autonomously, consistent with our previous observations that Kny and Tri function in both cell-autonomous and non-autonomous fashions to control the ML cell elongation underlying the C&E during gastrulation (Jessen et al., 2002) Topczewski and LSK, unpublished). Moreover, these data provide direct evidence to support the notion that in *kny;tri* double mutants, impaired convergence prevents the prospective adaxial cells from reaching the notochord-adjacent position, where they can receive the continuous midline Hh signal, necessary to maintain their identity.

Discussion

Cell fate specification during metazoan development frequently involves inductive interactions between tissues. How such inductive interactions are coordinated with the massive tissue rearrangements during gastrulation is only beginning to be understood. Here we address the relationship between defective C&E movements and the deficiency of slow muscle precursors in *kny;tri* non-canonical Wnt mutants. Our study reveals that C&E movements mediate two distinct steps of adaxial cell development. First, C&E movements regulate the number of prospective adaxial cells specified during gastrulation. Second, medial convergence is essential for the maintenance of adaxial cell fate, as it ensures the juxta-notochordal position of these cells during segmentation, when the Hh signaling range decreases. These results bring novel insights into the mechanisms

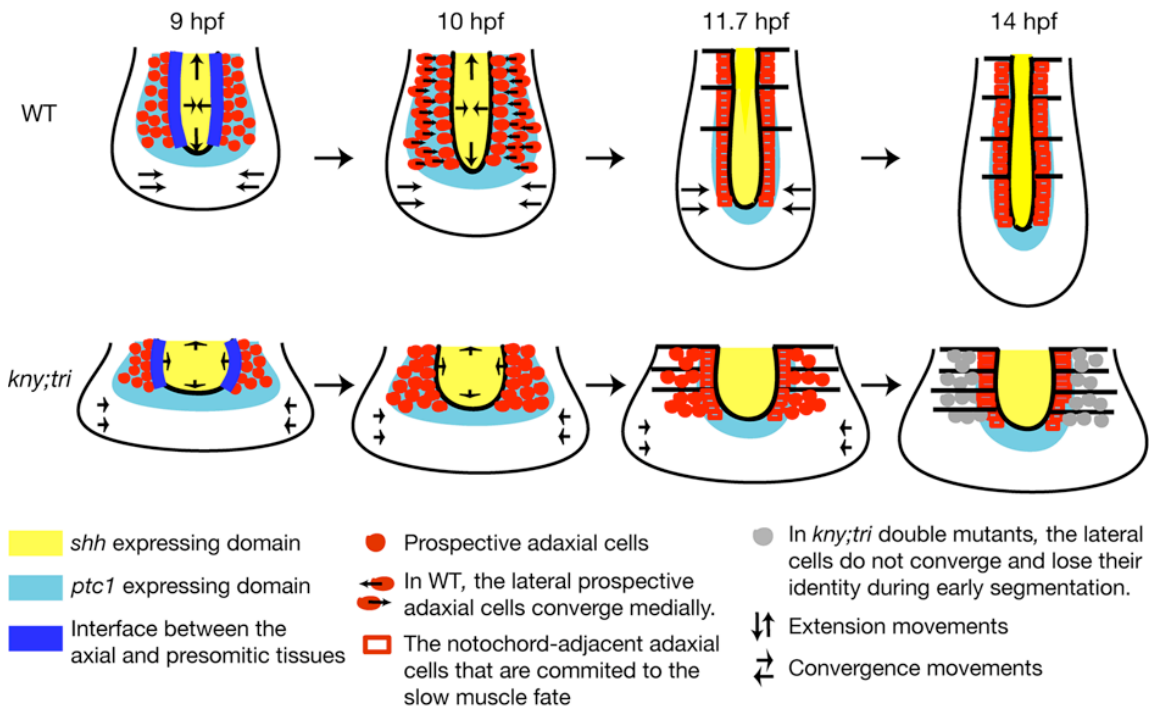
underlying zebrafish slow muscle development and establish critical roles for C&E gastrulation movements in the regulation of subsequent cell fate specification events.

C&E movements regulate the size of the contact area between the inducing and responding tissues during adaxial cell specification

We uncovered a significant deficit in slow muscle fibers and their precursors in *kny;tri* C&E mutants. Adaxial cells divide once between the onset of gastrulation and the 3-somite stage, and then become post-mitotic (Hirsinger et al., 2004). At the 10-somite stage, *kny;tri* double mutant somites contained only half the number of adaxial cells compared to WT (Table 2.1), while the difference in the proliferation rate of these cells was less than 3% between WT and the double mutants (Figure 2.4G). Therefore, we argue that although the double mutant cells undergo fewer cell divisions, such a defect is not sufficient to underlie the observed reduction of adaxial cell number.

Instead, our results indicate that fewer prospective adaxial cells are specified in *kny;tri* double mutants during gastrulation (Figure 2.10). Several studies demonstrated that the axial mesoderm is a source of signals that specify prospective adaxial cells in the adjacent PSM during gastrulation, and the inductive signals include, but are not limited to, Hh ligands (Blagden et al., 1997; Coutelle et al., 2001; Hirsinger et al., 2004). As a consequence of defective C&E movements, the axial mesoderm formed in *kny;tri* double mutants is much shorter anteroposteriorly compared to WT at mid-gastrulation (Figure 2.4) (Marlow et al., 1998), when the specification of prospective adaxial cells is thought to occur (Stickney et al., 2000). At this stage, a similar number of columns of prospective adaxial cells formed next to the axial mesoderm in both WT and *kny;tri* mutants (Figure 2.4). We interpret this to mean that the lateral range of the inducing signals and their

Figure 2.10. A model for C&E movements mediating the specification and maintenance of adaxial cell fate. During gastrulation, impaired C&E movements in *kny;tri* double mutants shorten the AP interface between the axial and presomitic tissues, thus reducing the number of prospective adaxial cells specified in the AP dimension. During early segmentation, when the range of Hh signal decreases in the PSM, all the WT prospective adaxial cells has converged medially to reside alongside the notochord. By contrast, the lateral prospective adaxial cells in the double mutants fail to converge, stop receiving Hh signal and consequently lose their adaxial cell identity.



reception by the PSM are normal in the mutants. We therefore attribute the specification of fewer prospective adaxial cells in the double mutants to the shortened AP interface between the axial and presomitic tissues (Figure 2.10). These data demonstrate that C&E gastrulation movements play an instructive role in adaxial cell fate specification by determining the geometric proportions and dimensions of the interacting tissues.

Medial convergence of prospective adaxial cells is crucial for their continuous reception of short-range Hh signal and fate maintenance

Between the end of gastrulation and early segmentation, several columns of prospective adaxial cells converge medially to form a monolayer alongside the notochord (Figure 2.10). Concurrently, Hh signaling range in the paraxial mesoderm decreases from 4 to 1-cell diameter (Figure 2.8 and 2.10). In both WT and double mutants, only the notochord-adjacent prospective adaxial cells maintained the expression of adaxial cell markers and adopted the slow muscle fate, supporting the notion that continuous Hh reception is required for the commitment of adaxial cell fate during early segmentation (Coutelle et al., 2001; Hirsinger et al., 2004).

The change of Hh range is unlikely due to the downregulation of Hh expression in the notochord, as previous studies show that both *shh* and *echidna hedgehog/ehh* RNAs are strongly expressed in the notochord until late segmentation (Currie and Ingham, 1996; Krauss et al., 1993). However, it is intriguing that coincident with the decrease of Hh signaling range in the PSM, the prospective adaxial cells immediately adjacent to the notochord form a monolayer of pseudo-epithelium (Figure 2.6A and Figure 2.7A) (Devoto et al., 1996). Such a process is independent of Hh signaling (Hirsinger et al., 2004), and occurs normally in *kny;tri* double mutants (Figure 2.7C). Formation of the

pseudo-epithelium might constrain the lateral diffusion of Hh ligands, either by setting up a physical barrier, or by inducing the subcellular redistribution of Hh signaling components within these juxta-notochordal adaxial cells. A recent study demonstrated that the Hh interacting protein Hhip functions synergistically with the Hh receptor Ptc to limit the transduction of Hh to the adaxial cells next to the notochord (Ochi et al., 2006). It would be interesting to examine the subcellular localization of these and other Hh components in the prospective adaxial cells before and after the pseudo-epithelium is formed.

Recently, several PCP-related molecules have been shown to affect Hh signaling by mediating ciliogenesis (Park et al., 2006). Our data do not support the notion that Hh signaling is perturbed in *kny;tri* PCP mutants. Instead, several lines of evidence suggest that the reduction of Hh signaling range in the PSM and the C&E movements of this tissue are two independent processes. First, the formation of the monolayered pseudo-epithelium next to the notochord and the change of Hh signaling range occur normally in *kny;tri* double mutants (Figure 2.7 and Figure 2.8). Second, no C&E defects have been reported in the embryos deficient in Hh signaling (van Eeden et al., 1996). Finally, overexpression of *shh* RNA did not suppress the C&E defects in *kny;tri* double mutants (Marlow et al., 1998). However, we demonstrate that the change of Hh signaling range and the C&E movements of the prospective adaxial cell population must be coordinated to ensure the fate maintenance of adaxial cells. In *kny;tri* double mutants, the lateral prospective adaxial cells fail to converge towards the notochord, stop receiving Hh signal during early segmentation, and consequently transdifferentiate into the fast muscle

precursors (Figure 2.7 and Figure 2.10). Our results reveal the significance of precisely coordinating morphogenetic and inductive events during adaxial cell fate specification.

Non-canonical Wnt/PCP pathway in adaxial cell specification and C&E movements of the paraxial mesoderm

In zebrafish, several components of non-canonical Wnt/PCP pathway are expressed in the paraxial mesoderm during gastrulation and segmentation, and a deficiency in any one of these molecules leads to C&E defects and consequently impairs somite morphology (Jessen et al., 2002; Kilian et al., 2003; Rauch et al., 1997; Topczewski et al., 2001). We provided several lines of evidence to show that PCP pathway is not absolutely essential for the specification of adaxial cell fate. First, the transplantation experiments showed that *kny;tri* double mutant cells, when positioned next to the notochord in the WT host embryos, were able to form adaxial cells. Second, mutants deficient in other PCP components still formed slow muscle cells. However, there is an interesting correlation between the degree of the C&E defects and the slow muscle defects: a gradation of slow muscle deficiency is observed from the mutants with the mildest C&E defect (*slb/wnt11* and *ppt/wnt5* individual mutants) to those with the most severe C&E phenotype (*kny;tri* double mutants). These results suggest that instead of being a determinant of the adaxial cell fate, PCP pathway governs the establishment of tissue architecture to ensure the formation of the correct number of adaxial cells.

In vertebrates, PCP pathway mediates intercellular communication that is essential for the establishment of tissue polarity and effective C&E movements (Klein and Mlodzik, 2005; Myers et al., 2002b; Tada et al., 2002). Previous studies demonstrated that during gastrulation, *Kny* and *Tri* act both cell-autonomously and non-

autonomously to regulate ML cell elongation, a behavior critical for cell migration and intercalation underlying C&E movements in the dorsal region of the zebrafish gastrulae (Concha and Adams, 1998; Jessen et al., 2002; Myers et al., 2002a) Topczewski and LSK, unpublished). By performing time-lapse analyses (Figure 2.6), we showed directly that the convergence of prospective adaxial cells was greatly compromised in *kny;tri* double mutants (Figure 2.6). Our transplantation experiments further revealed the cell-autonomous and non-autonomous roles of Kny and Tri in the convergence of PSM (Figure 2.9), thus confirming the direct link between impaired ML cell polarity and reduced convergence movements (Marlow et al., 2002; Topczewski et al., 2001; Wallingford et al., 2000). These results are consistent with the notion that impaired C&E movements prevent the prospective adaxial cells in *kny;tri* double mutants from reaching the juxta-notochordal position, where they can receive continuous Hh signal and maintain their identity.

Acknowledgements

We thank Drs. O. Pourquie, A.F. Schier, M.K. Cooper, M.S. Cooper, C. Henry, J. Topczewski, F. Marlow, D.S. Sepich, and A. Inbal for critical comments, and L.S.-K. lab members for discussions. We acknowledge excellent fish care by J. Clanton and A. Bradshaw. We also thank J.P. Wallingford, S. Krauss, F. Stockdale, Z. Gong, C. Kimmel, and E. Weinberg for generous gifts of antibodies and constructs. This work in the L.S.-K. laboratory is supported by NIH grants GM62283 and GM55101.

Experimental Procedures

Zebrafish maintenance, embryo generation, and staging

The *kny^{m119+/-}*, *tri^{m209+/-}*, and *kny^{m119+/-};tri^{m209+/-}* mutant zebrafish strains were maintained as described previously (Solnica-Krezel et al., 1994; Solnica-Krezel et al., 1996). Embryos were obtained from natural spawning and morphologically staged as described (Kimmel et al., 1995). The genotypes of the embryos were judged by described morphologic phenotypes (Henry et al., 2000; Marlow et al., 1998).

In situ hybridization, immunohistochemistry, and cell proliferation assay

Antisense RNA probe synthesis for *smbpc*, *myoD*, *ptc1*, and *α -tropomyosin* was as described previously (Sepich et al., 2000). Whole-mount in situ hybridization was performed according to Thisse et al. (Thisse et al., 1993). Embryos were photographed with a Zeiss Axiophot using an Axiocam digital camera.

Whole-mount immunohistochemistry was performed as described (Topczewska et al., 2001). Monoclonal F59 antibody (a gift from FE Stockdale, Stanford University) and polyclonal human Myf5 antibody (Santa Cruz Biotech.) were used at 1:100. Polyclonal Prox1 antibody (CHEMICON) was used at 1:1000. Monoclonal anti- β -catenin antibody (Sigma) was used at 1:250. Images were acquired using the Zeiss LSM 510 laser scanning inverted microscope and processed using Volocity (Improvision).

To assess the proliferation rates of prospective adaxial cells during late gastrulation, embryos were fixed at 80% epiboly (8.5 hpf), yolk plug closure (9.5 hpf), and the tailbud (10 hpf) stages. In situ hybridization was performed prior to immunohistochemistry by using digoxigenin-labeled *myoD* RNA probe detected with fast

red (Roche). M-phase cells were detected by polyclonal anti-phosphohistone antibody (Upstate Biotech.) at 1:1000 dilution (Chadee et al., 1995; Mahadevan et al., 1991).

Microinjections

Injections were performed at the one-cell stage as described (Marlow et al., 1998). Synthesis of the RNAs encoding membrane-GFP (the Ras membrane-localization (CAAX) sequence fused to the carboxy terminus of green fluorescein protein) and Shh, and the injection dosages were as described previously (Krauss et al., 1993; Marlow et al., 1998; Wallingford et al., 2000).

Time-lapse recording and analysis

Multi-plane DIC time-lapse recordings were collected at 1.5-minute intervals for 90 minutes from 90% epiboly (9 hpf) to the 1-somite stage (10.5 hpf) with Openlab software (Improvision) using a Zeiss Axiovert 200M. Manually dechorionated embryos were mounted in 1% low-melting-point agarose in 30% Danieau's Buffer as described (Sepich et al., 2005). After the recordings, embryos were allowed to develop until day 1 to determine their genotypes. Object-Image (Norbert Vischer, <http://simon.bio.uva.nl/object-image.html>) was used to label and track cells. Data were exported to Excel (Microsoft) for calculation of the cell shape and size. The orientation and angular deviation were analyzed using VectorRose (P.A. Zippi, <http://pazsoftware.com/>). Statistical analyses were performed using Student's two-tailed *t*-test.

The tissue shape changes were calculated as followed:

$$\text{Extension rate} = \frac{(\text{Total cell No./column No.})_{t=90} - (\text{Total cell No./column No.})_{t=0}}{(\text{Total cell No./column No.})_{t=0}}$$

$$\text{Convergence rate} = - \frac{(\text{Total cell No./row No.})_{t=90} - (\text{Total cell No./row No.})_{t=0}}{(\text{Total cell No./row No.})_{t=0}}$$

Cell lineage tracing/uncaging analysis

Embryos were injected with fluorescein-caged dye (Molecular Probes) at the one-cell stage as described (Sepich et al., 2000). At the 5-somite stage, cells at the 3rd somite level and located within 4-cell diameters from the notochord were labeled by photoactivation performed according to Myers et al. (Myers et al., 2002a). Half of the embryos were fixed immediately after uncaging, the remaining were allowed to develop and fixed at the 10-somite stage. All embryos were processed for immunohistochemistry and the uncaged cells were detected using anti-fluorescein antibody (Roche).

Transplantation experiments

Genetic mosaic analyses were performed essentially as described (Yamashita et al., 2002). WT donor embryos were injected with 0.5% fluorescein-dextran (Molecular Probes) at the one-cell stage. *kny* mutant donor embryos were injected at the same stage with 0.5% rhodamine-dextran (Molecular Probes) and 4 ng of *tri* morpholino oligonucleotides (Jessen et al., 2002). Between 4 and 5 hpf, before the embryonic shield became morphologically distinct, 10-30 deep cells at the blastoderm margin were aspirated from one WT and one *kny;tri*-deficient donor embryo using the same transplantation needle. The mixture of donor cells was immediately transplanted into the margin of a host embryo to ensure that the initial positions of the WT and *kny;tri*-

deficient donor cells were identical. The host embryos were fixed at the 3-somite stage and stained with anti- β -catenin antibody that labels the cell membrane. The donor and host embryos were genotyped by their morphological phenotypes and PCR amplification followed by restriction digest as previously described (Henry et al., 2000; Marlow et al., 2004; Marlow et al., 1998).

CHAPTER III

COOPERATION OF POLARIZED CELL INTERCALATIONS DRIVES CONVERGENCE AND EXTENSION OF PRESOMITIC MESODERM DURING ZEBRAFISH GASTRULATION

This paper has been submitted under the same title to *Nature Cell Biology*.

Chunyue Yin¹, Maria Kiskowski², Philippe-Alexandre Pouille³, Emmanuel Farge³, and Lilianna Solnica-Krezel¹

¹Department of Biological Sciences, Vanderbilt University, Nashville, Tennessee, US.

²Biomathematics Study Group, Department of Mathematics, Vanderbilt University, Nashville, Tennessee, US.

³Mechanics and Genetics of Embryonic and Tumoral Development Group, UMR 168 Physico-Chimie Curie, Institut Curie, Centre de Recherche, 11 rue Pierre et Marie Curie, 75005 Paris, France.

Summary

During vertebrate gastrulation, massive cell movements transform an initially unstructured group of cells into a triploblastic gastrula with a defined body plan (Keller et al., 2003; Solnica-Krezel, 2005; Warga and Kimmel, 1990). Key components of gastrulation are convergence and extension (C&E) movements, which narrow and lengthen the embryonic tissues, respectively. In zebrafish gastrula, regional differences in rates of C&E have been observed (Myers et al., 2002), however the underlying cell behaviors are less understood. Here, we combined both *in vivo* and *in silico* approaches to demonstrate that C&E movements of the medial presomitic mesoderm (PSM) during

gastrulation are achieved by the cooperation of planar and radial intercalations. Unexpectedly, the radial intercalations preferentially separate anteroposterior neighbors. In *knypek; trilobite* non-canonical Wnt mutants, C&E movements are compromised: the frequency of cell intercalations is altered and the anteroposterior bias in radial intercalation is lost. Polarized radial intercalation represents a novel cellular behavior that promotes tissue extension and is the first evidence of non-canonical Wnt signaling polarizing cell movements between different cell layers. We further reveal that during C&E of the dorsal mesoderm, the non-canonical Wnt component Prickle is localized at the anterior cell edge, whereas Dishevelled is enriched near the posterior cell membrane. The asymmetric localization of Dishevelled and Prickle strongly suggests the presence of anteroposterior polarity cues that define differential properties of anterior and posterior cell edges to underlie the biased orientation of cell intercalations.

Results and Discussion

Vertebrate gastrulation employs evolutionarily conserved morphogenetic movements to shape the germ layers (Keller et al., 2003; Solnica-Krezel, 2005). Internalized mesodermal cells undergo C&E movements in a region-specific manner (Myers et al., 2002). In zebrafish gastrula, the lateral mesodermal cells converge medially by directed migration at increasing speeds as they move closer to the nascent axial mesoderm (Myers et al., 2002). In the dorsal region where strong extension movements are accompanied by limited convergence (Glickman et al., 2003; Myers et al., 2002), the axial mesodermal cells engage in mediolateral (ML) intercalation to achieve the similar

rates of convergence, but three-fold higher extension than the adjacent PSM (Glickman et al., 2003; Wood and Thorogood, 1994).

To obtain insight into the cell behaviors underlying the distinct C&E movements of the axial and presomitic mesoderm, we made Nomarski time-lapse recordings between 95% epiboly (9 hpf) and the 1-somite stage (10.5 hpf). The field of view covered the middle portion of both tissues (Figure 3.1A), and was focused on the intermediate depth of the mesoderm. To gain a quantitative description of the cell movements in the entire field, we applied Particle Image Velocimetry (PIV) analysis (Raffel, 1998; Supatto et al., 2005). The PIV algorithm generates a displacement field based on local correlation calculations between two consecutive images, allowing visualization of the velocity field of the movements. In the wild-type (WT) gastrula, cells at different positions exhibited distinct speeds and directions of movements (Figure 3.1B,C; Figure 3.2). In the axial mesoderm, ML cell movements were towards the field center and anteroposterior (AP) movements were away from the center, consistent with a previous report (Glickman et al., 2003). Moreover, cells located away from the field center moved faster than those closer to the center (Figure 3.1C). In the PSM, all the cells in the analyzed field migrated towards the midline, with the more lateral cells migrated faster than the medial ones (Figure 3.1C). Compared to the axial mesodermal cells, the presomitic cells exhibited less anterior or posterior bias in their movement directions, providing a possible mechanism for the lower extension rate of the PSM compared to the axial mesoderm.

In vertebrates, non-canonical Wnt signaling, a vertebrate equivalent of the *D. melanogaster* planar cell polarity (PCP) pathway that polarizes cells within the plane of epithelium (Klein and Mlodzik, 2005), is the key regulator of C&E gastrulation

Figure 3.1. Patterns of C&E movements in the dorsal mesoderm. (A, D) Lateral views of live embryos at the 1-somite stage (10.5 hpf). The regions where the time-lapse recordings were taken are shown by brackets. (B, E) Snapshots of the PIV analyses of the C&E movements at the 1-somite stage. The arrows indicate the direction of cell movements, while their length represents the movement speed. The red squares in (E) show the regions where the movement directions of neighboring cells were disrupted but highly correlated. (C, F) are the same images as (B, E) except that different movement velocities were presented in a color-coded manner. Purple lines delineate the axial mesoderm. (B-C, E-F) Dorsal views, anterior to the top. (G-J) Snapshots of the analyzed medial PSM cell population at the beginning and the end of the time-lapse recordings. Dorsal views, anterior to the top. The red arrows illustrate the length and width of the analyzed cell population when the time-lapses started. (K) Quantification of the tissue shape changes (Experimental procedures). 10 embryos of each genotype were analyzed. Error bars represent the standard error. *, $p < 0.05$; **, $p < 0.005$, mutant vs. WT. A, anterior. P, posterior. Scale bars, (A, D) 100 μm ; (B-C, E-F, G-J) 20 μm .

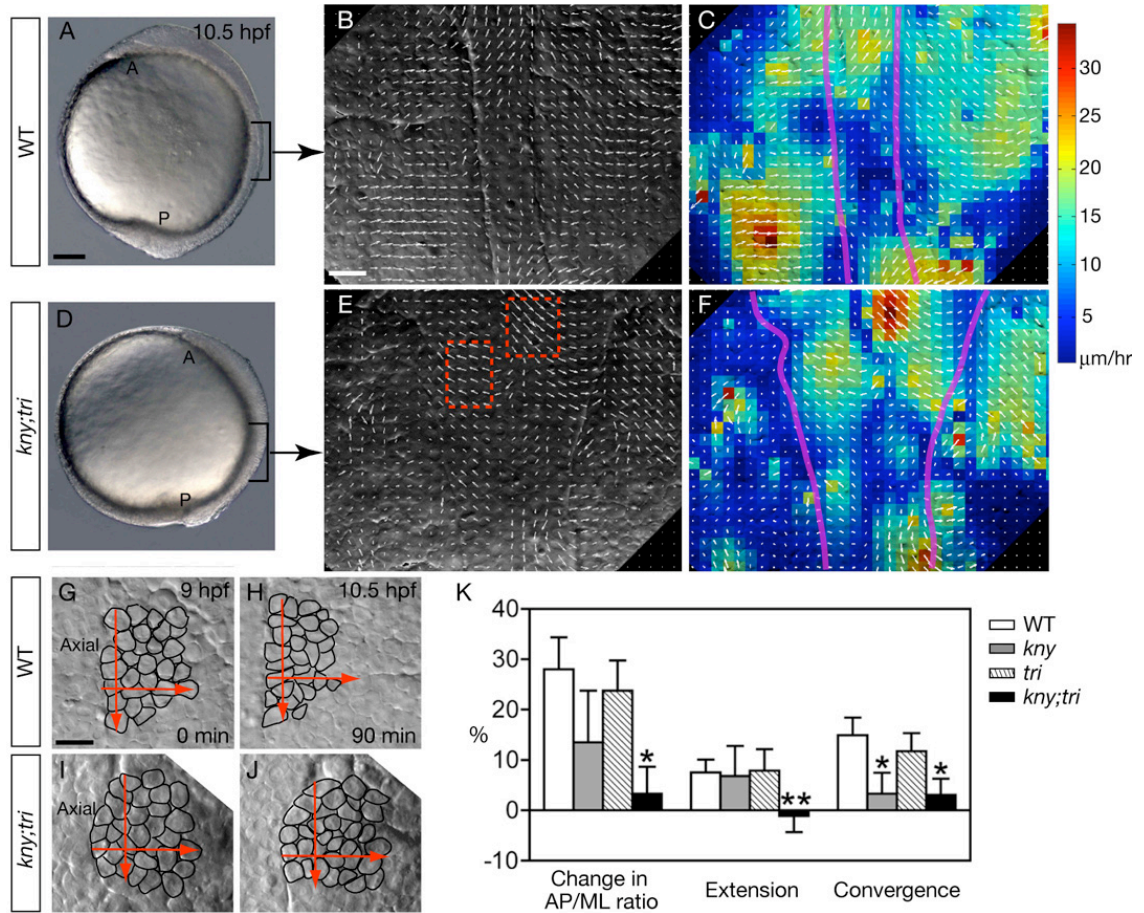
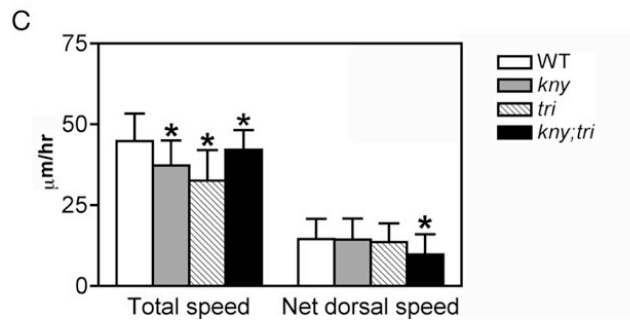
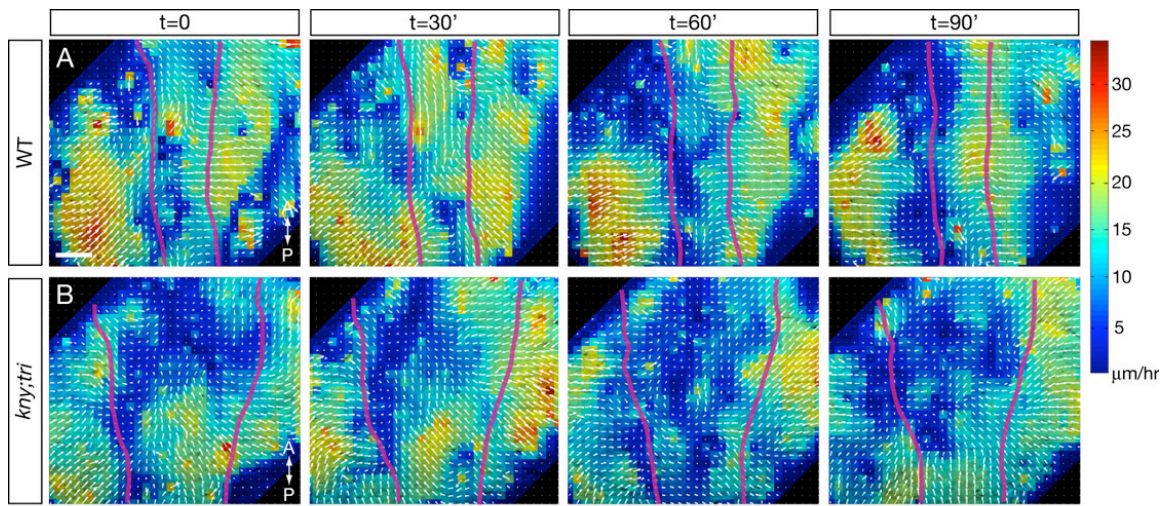


Figure 3.2. C&E movements of the axial mesoderm and medial PSM. (A, B) Time series of the C&E movement patterns in WT (A) and *kny;tri* double mutants (B) generated by PIV analyses. The movement directions are indicated by the arrows and the speeds are illustrated in a color-coded fashion. Purple lines delineate the axial mesoderm. Dorsal views. Scale bar, 20 μm . A, anterior; P, posterior. (C) Measurements of the movement speeds of the medial presomitic cells. The speeds of individual cells within the analyzed cell population were calculated. Total speed accounts for movement in all directions, whereas net dorsal speed shows only the medial movement. Error bars represent the standard error. Asterisk: $p < 0.05$, WT vs. mutant.



movements (Myers et al., 2002). Two non-canonical Wnt signaling components, the heparan sulfate proteoglycan Knypek/Glypican4 (Kny) (Topczewski et al., 2001), and the transmembrane protein Trilobite/Strabismus/Van Gogh like 2 (Tri) (Jessen and Solnica-Krezel, 2004; Jessen et al., 2002), regulate the ML cell elongation and orientation critical for the planar cell behaviors driving C&E, including directed migration and ML intercalation (Jessen et al., 2002; Lin et al., 2005; Topczewski et al., 2001). Mutations inactivating either molecules result in anteroposteriorly shortened and mediolaterally broadened embryonic axes, and the C&E defects are dramatically exacerbated in *kny;tri* double mutants (Henry et al., 2000; Marlow et al., 1998; Yin and Solnica-Krezel, 2006) (Figure 3.1D). To investigate the cellular and molecular mechanisms underlying the C&E of the axial and presomitic mesoderm, we acquired time-lapse recordings and performed PIV analyses of the equivalent dorsal mesodermal cell populations in *kny;tri* double mutants as in WT (Figure 3.1D-F). The double mutant cells migrated at significantly reduced speeds and in a random fashion (Figure 3.1F; Figure 3.2). The stereotyped cell movement patterns seen in WT were largely absent in the double mutants. Interestingly, the cell movements in the double mutants were not completely randomized. Instead, there were regions where the aberrant movement directions of neighboring cells showed a high correlation, resulting in distinctive swirling patterns of cell movements (Figure 3.1E,F; Figure 3.2), indicating a loss of large length scale coordination with short length scale coordination reminiscence. Swirling patterns were also observed in bristle and hair orientation in the fly PCP mutants (Gubb and Garcia-Bellido, 1982; Wong and Adler, 1993), and in the skin hair in *frizzled6*-deficient mice (Guo et al., 2004). This lack of complete randomness suggests that other PCP-independent mechanisms of cell

communication also contribute to the local orchestration of the cell movements of zebrafish dorsal mesoderm.

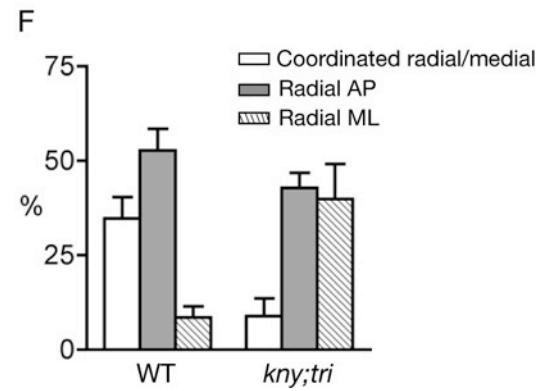
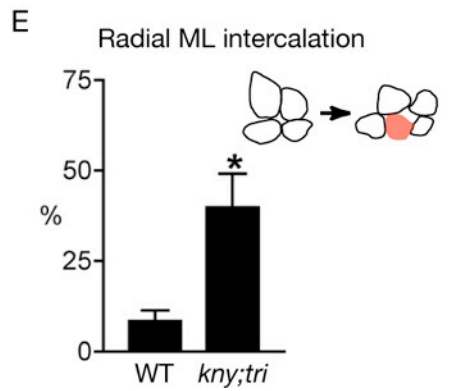
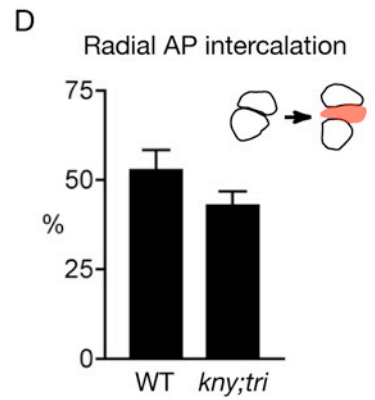
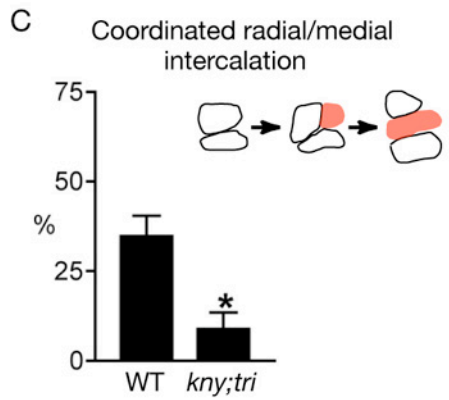
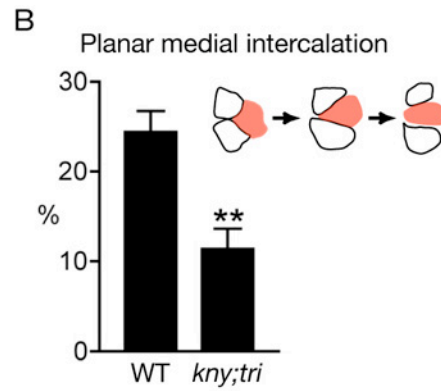
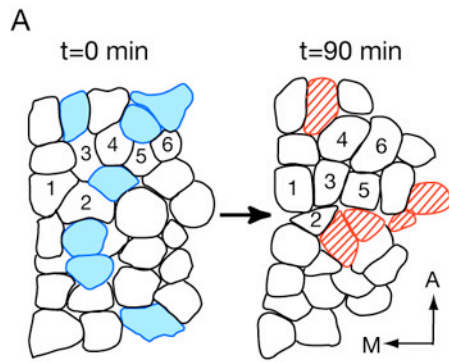
The different C&E patterns between the axial and presomitic mesoderm likely reflect distinct underlying cell behaviors. The axial mesoderm C&E is driven by ML cell intercalation, whereby cellular rearrangements along the ML axis narrow the tissue mediolaterally and lengthens it along the AP axis (Glickman et al., 2003). In this study, we wished to elucidate the cell behaviors driving the PSM C&E and to identify defective cell behaviors that account for the C&E defects in *kny;tri* double mutants. We monitored the movements of a small presomitic cell population within 6-cell diameters from the axial mesoderm throughout the time-lapse recordings. Our previous study showed that cells in this region form slow-twitch muscles during somitogenesis (Yin and Solnica-Krezel, 2006). In WT, the analyzed cell population narrowed mediolaterally and extended anteroposteriorly during the recordings (Yin and Solnica-Krezel, 2006) (Figure 3.1G,H, and K). C&E movements of the equivalent cell population were reduced in *kny*, *tri* individual mutants and largely inhibited in *kny;tri* double mutants (Yin and Solnica-Krezel, 2006) (Figure 3.1I-K).

To investigate the cellular behaviors during the medial PSM C&E, we tracked the positions of individual cells within the analyzed cell layer throughout the recordings. In WT, the analyzed cells frequently exchanged neighbors while moving medially (Figure 3.3A). The amount of cell rearrangements was greatly reduced in *kny;tri* double mutants. Whereas 60% of analyzed cells in the double mutants (320 cells/10 embryos) moved medially without any neighbor exchanges, such behavior was observed only for 34% of the equivalent WT cells (299 cells/10 embryos). Towards identifying the cellular

behaviors underlying the neighbor exchanges, we observed two types of planar cell intercalation behaviors that occur in the analyzed cell layer. In the predominant planar intercalation behavior, medial intercalation, a cell intercalates medially to separate two AP neighboring cells (Figure 3.3B; Movie S1). Medial intercalation simultaneously increases the cell number along the AP axis and decreases it in the ML dimension, thus contributing to both convergence and extension (Keller et al., 2000). At very low frequencies (4%), we observed lateral intercalation, in which a cell intercalates laterally, thus counteracting convergence (Movie S1). In *kny;tri* double mutants, lateral intercalation was also very infrequent (<4%). However, the frequency of medial intercalation was dramatically reduced in the double mutants compared to WT (Figure 3.3B), supporting a non-canonical Wnt-dependent contribution of medial intercalation to C&E (Keller et al., 2000; Solnica-Krezel, 2006).

Once a cell intercalates medially, it leaves behind an empty space. We followed the events after medial intercalations. In WT, the lateral neighboring cell filled the empty space in 96% of the observed medial intercalation events (n=73). We interpret this result to mean that medial is the favored movement direction for the presomitic cells, and we name this bias a “medial preference”. In *kny;tri* double mutants, although fewer medial intercalations occurred, the presomitic cells still exhibited an obvious medial preference: in 88% of the observed events (n=41), the lateral neighbor filled the hole generated by medial intercalation. Therefore, the double mutant cells were able to distinguish between the medial and lateral directions and preferentially moved medially. This is consistent with the notion that signals other than non-canonical Wnts provide the midline instructive

Figure 3.3. C&E movements of the medial PSM entail multiple cell intercalations. (A) Schematic of the WT cell population being analyzed. Cells leaving the analyzed layer during the recording are shown in blue; cells entering the layer are shown in red. 6 cells are assigned numbers to show the dynamic neighbor exchanges. (B-E) Frequencies of cells undergoing planar medial intercalation, coordinated radial/medial intercalation, radial AP intercalation, and radial ML intercalation, respectively. Schematics of the intercalation behaviors are also shown. Medial is to the left. (F) Frequencies of the three types of radial intercalations listed in (C-E). (B-F) Error bars represent the standard error. *, $p < 0.05$; **, $p < 0.005$, mutant vs. WT. A, anterior. M, medial.



cues to guide the direction of C&E movements (Sepich et al., 2005; Solnica-Krezel, 2006).

To date, all described cellular behaviors contributing to C&E occur within a plane of a single cell layer (planar) (Keller et al., 2000; Myers et al., 2002). Surprisingly, we noted cells entering or leaving the analyzed cell layer during the medial PSM C&E (Figure 3.3A). The frequencies of cell entry and exit events were both reduced in the double mutants (entry, 14%; exit, 13%) compared to WT (entry, 21%; exit, 21%; $p < 0.05$). To enter or leave a cell layer, cells move between the cells in a deeper or more superficial layer, so-called radial intercalation behavior (Keller et al., 2003). Radial intercalation is best known for its role in epiboly movements that spread and thin the blastoderm during gastrulation (Keller et al., 2003; Warga and Kimmel, 1990). We did not observe evident changes in the total cell number or thickness of the analyzed tissue during the time-lapse recordings of WT or the double mutant embryos, probably because the cell entry and exit events occurred at comparable frequencies, thus balancing each other.

In epiboly movements, radial intercalation occurs in a random fashion with respect to the AP and ML embryo axes, resulting in isotropic tissue expansion (Keller et al., 2003; Warga and Kimmel, 1990). It has been hypothesized that radial intercalation should be polarized to produce an anisotropic expansion, whereby tissue expands more along one dimension than another (Wilson and Keller, 1991; Wilson et al., 1989). Our examination of radial intercalations into the analyzed cell layer revealed three types of behaviors (Movie S3). First, coordinated radial/medial intercalation: a cell enters the layer and immediately intercalates medially (Figure 3.3C). This behavior introduces new

cells in the AP dimension, thus contributing to AP extension. We observed coordinated radial/lateral intercalation in the opposite direction, but at low frequency (<4%). Second, radial AP intercalation: a new cell intercalates, taking a position between two anterior and posterior neighbors (Figure 3.3D). This behavior also promotes AP extension. Third, radial ML intercalation: a new cell intercalates, separating two medial and lateral neighbors (Figure 3.3E). This behavior leads to ML expansion, thus counteracting the C&E movements. Interestingly, WT cells exhibited a strong bias towards the behaviors that promote AP extension: among the cells entering the analyzed layer, 35% underwent coordinated radial/medial intercalation, 53% carried out radial AP intercalation, but only 9% entered by means of radial ML intercalation (Figure 3.3C-F). In *kny;tri* double mutants, the frequency of coordinated radial/lateral intercalation was similar to WT (<4%, $p>0.5$, data not shown), while there was a significant increase in the frequency of radial ML intercalations in the double mutants (Figure 3.3E). Conversely, the frequencies of both coordinated radial/medial intercalation and radial AP intercalation were reduced in the double mutants compared to WT (Figure 3.3C,D). Therefore, the bias of radial intercalations towards the types that promote AP extension was largely lost in the double mutants (Figure 3.3F).

We next examined whether the events of cells leaving the analyzed layer occurred in a polarized manner. Arguing against this notion, cells exited the analyzed layer from between either their AP or ML neighbors at similar frequencies, and the double mutant cells did not behave differently from the WT (Movie S3; data not shown).

Our observation of multiple cell intercalations during the medial PSM C&E is unexpected and contrasts previous studies showing that C&E within distinct regions of

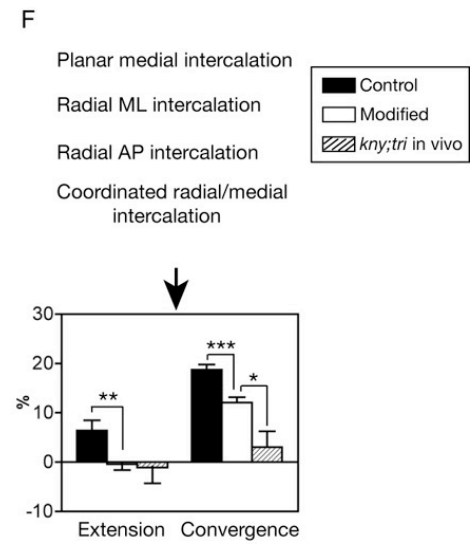
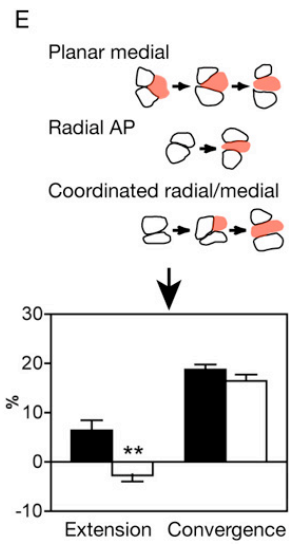
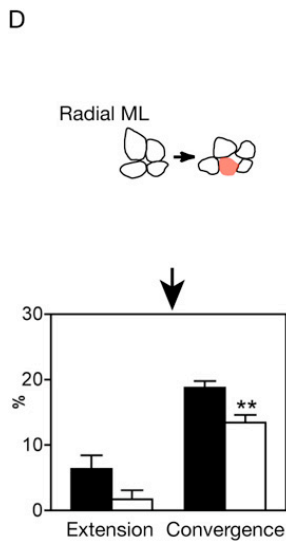
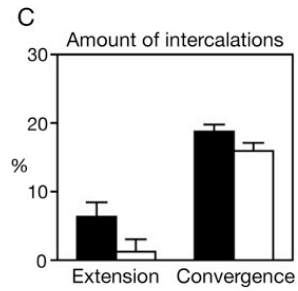
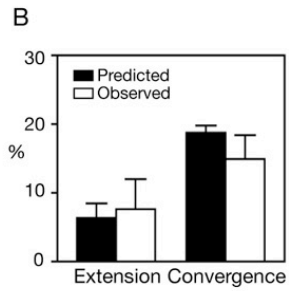
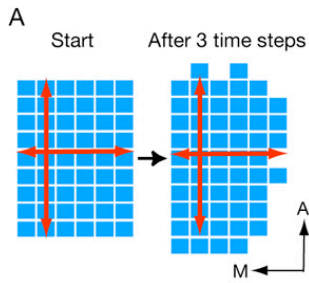
the zebrafish gastrula is driven by one predominant cell movement behavior (Myers et al., 2002). Hence, it is important to understand the relative contributions of each intercalation behavior to the C&E of the medial PSM. Direct *in vivo* analyses cannot address this question since cells are engaged in various movements and rearrangements simultaneously, and are changing shape, size and protrusive activities over time. Computational models have been employed in biology to evaluate how individual components of a complex biological system interact with each other to produce a specific result (Endy and Brent, 2001). Therefore we developed a computational model to query the contributions of individual intercalation behaviors to C&E and to investigate whether the defects in cell intercalations could account for the impaired C&E in *kny;tri* double mutants. To study the effects of cell rearrangements independent of other variables, we assumed that cells do not change shape or size in the simulation. We did not include cell division in the simulation since we observed only one or two proliferation events in the time-lapse recordings of both WT and double mutant populations (data not shown). The simulation initiated with 48 cells arranged in a two-dimensional 6X8 lattice, representing the analyzed cell population *in vivo* (Figure 3.4A). Each simulation contains three time steps. In each step, every cell was selected exactly once in a random order to undergo planar medial intercalation, one type of radial intercalations, or remain in its initial position. The probabilities of specific behaviors that each cell would perform in the simulation were based on the frequencies obtained from the time-lapse analyses. Neighbors of the intercalating cells would move with directions based on the *in vivo* observations to accommodate intercalation events. The detailed rules implemented in the simulation are described in the Supplementary information.

To determine whether the observed cell intercalations are capable of producing C&E, we applied the frequencies of intercalation behaviors in WT to the simulation. The resulting C&E rates were consistent with the *in vivo* data ($p>0.3$; Figure 3.4A,B), indicating that the specific cell behaviors and rules implemented in the simulation are sufficient to generate the C&E of the medial PSM.

Our time-lapse analyses of *kny;tri* double mutants correlated the impaired C&E movements with significant reduction of cell rearrangements and changes in the frequencies of individual intercalation behaviors. First, to examine whether reduced intercalations were responsible for the C&E defects in the double mutants, we increased the probability of cells “not intercalating” to the double mutant level (from 34% to 60%), while preserved the WT ratios for the relative probabilities of different intercalations. This modification modestly reduced the C&E rates (Figure 3.4C, $p>0.07$), suggesting that reduced cell intercalations alone cannot account for the C&E defects in *kny;tri* double mutants.

Next, to investigate the contribution of individual intercalation behaviors, we modified the probability of one behavior at a time by applying the double mutant data, and assessed how each modification affected the simulation result. We identified three types of radial intercalations by which cells entered a cell layer: radial AP intercalation, coordinated radial/medial intercalation, and radial ML intercalation (Figure 3.3). WT cells exhibited a strong bias for the first two behaviors that promote AP extension, and such bias was lost in the double mutants (Figure 3.3F). When we increased the probability of radial ML intercalation to the double mutant level in the simulation, the resulting convergence rate was significantly reduced compared to the control simulation,

Figure 3.4. Computational modeling predicts the contributions of individual cell intercalations to C&E. (A) Tissue shape change predicted by the simulation. Each blue block represents a single cell. (B) Quantitative comparison of the tissue shape changes based on the time-lapse observation and the simulation. Error bars represent the standard error. $p > 0.3$. (C-F) Comparison of the results from the WT control simulation and the simulations in which the cell behaviors were modified in one of the four ways: reducing the total amount of intercalations (C), increasing radial ML intercalation (D), reducing planar medial, radial AP, and coordinated radial/medial intercalations (E), and reducing planar medial, radial AP, and coordinated radial/medial intercalations, while increasing radial ML intercalation (F). 20 independent simulations were performed for each condition. Error bars represent the standard error. *, $p < 0.05$; **, $p < 0.005$; ***, $p < 0.0005$. A, anterior; M, medial.



whereas extension was mildly affected ($p>0.2$) (Figure 3.4D). Therefore limiting radial ML intercalation is crucial for convergence, but not extension.

Planar medial intercalation, radial AP intercalation, and coordinated radial/medial intercalations promote AP extension, and their frequencies were reduced in *kny;tri* double mutants (Figure 3.3). Whereas reducing the probabilities of these behaviors independently in the simulations only caused a mild reduction of extension ($p>0.1$; data not shown), modification of all three behaviors in a single simulation specifically blocked extension (Figure 3.4E). We therefore concluded that planar medial intercalation, radial AP intercalation, and coordinated radial/medial intercalations contribute additively to tissue extension.

Finally, when the probabilities of planar medial intercalation and polarized radial intercalation were modified in one simulation, convergence was greatly reduced and extension was completely inhibited in the simulated tissue (Figure 3.4F). This indicates that polarized medial and radial intercalations cooperate to underlie the C&E movements of the medial PSM. Notably, modification of intercalation behaviors alone in the simulation caused less severe C&E defects than observed in *kny;tri* double mutants (Figure 3.4F), suggesting that additional cellular defects may also impair the medial PSM C&E in the double mutants.

Our modeling analyses demonstrate that the medial PSM C&E is achieved by the cooperation of planar medial intercalation and polarized radial intercalation. It is noteworthy that both intercalation behaviors preferentially separate anterior and posterior neighbors in one layer (Figure 3.3). This suggests that within in a cell layer, the contacts between AP neighboring cells may be weaker or otherwise different from the ML

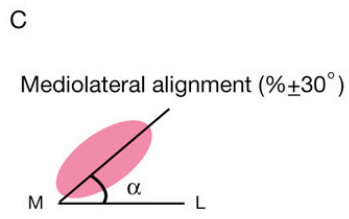
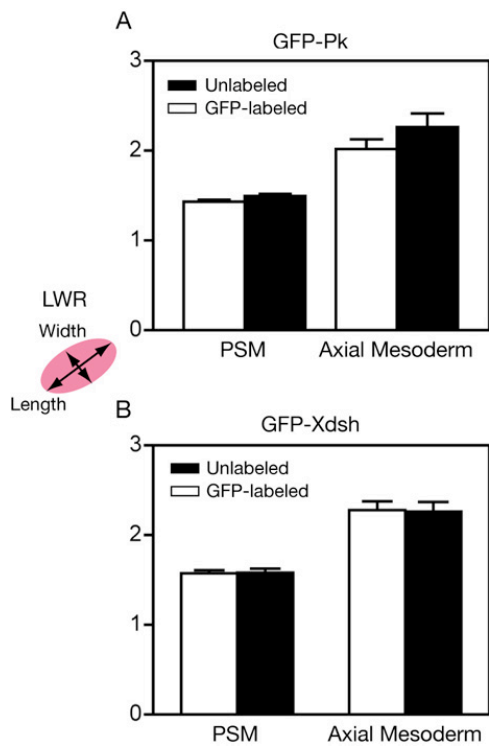
neighbor contacts, providing a mechanism for preferential separation of anterior and posterior neighbors in the medial and polarized radial intercalations. The *kny;tri* double mutant cells underwent fewer medial intercalations and did not exhibit an AP bias in radial intercalation. We therefore propose that non-canonical Wnt signaling is required not only for the ML orientation and elongation of cell body and the elaboration of ML protrusions (Myers et al., 2002; Wallingford et al., 2000), but also for defining unique properties of the anterior and posterior cell membranes that underlie the biased orientation of planar and radial intercalations.

In *D. melanogaster*, PCP pathway components are expressed asymmetrically at the cell membrane (Adler, 2002; Klein and Mlodzik, 2005; Strutt, 2002). However, asymmetric localization of non-canonical Wnt signaling components has not been investigated in the intercalating cells during vertebrate gastrulation. A recent study using zebrafish showed that enhanced green fluorescent protein (EGFP)-tagged Prickle (Pk) (Jenny et al., 2003; Jiang et al., 2005), which encodes a cytoplasmic protein that is recruited to the cell membrane by Tri/Strabismus (Stbm) (Jenny et al., 2003), is localized at the anterior edge of the notochord and neural tube cells during somitogenesis (Ciruna et al., 2006). To examine the subcellular localization of GFP-Pk during gastrulation, we mosaically expressed GFP-Pk and collected confocal images of the dorsal mesoderm in live embryos at the tailbud stage (10 hpf), when both the axial and presomitic cells undergo active cell intercalations underlying C&E (Glickman et al., 2003; Myers et al., 2002). The amount of GFP-Pk expressed did not detectably alter the ML cell polarity (Figure 3.5). In the dorsal mesoderm of the WT embryo, GFP-Pk was expressed in dynamic punta next to the anterior cell membranes (Figure 3.6A, G; Movie S4), similar

to its expression in the notochord and neural tube cells at later stages (Ciruna et al., 2006). The anterior localization of GFP-Pk was correlated with the ML elongation of the dorsal mesodermal cells, as the GFP-Pk puncta were distributed randomly within these cells at 75% epiboly (8 hpf), prior to their ML elongation (Myers et al., 2002) (Figure 3.6E, F). In *kny* and *tri* individual mutants, the GFP-Pk puncta were not restricted to the anterior cell membranes (Figure 3.6B, C, G), while in *kny;tri* double mutants, GFP-Pk was mainly expressed in the cytoplasm (Figure 3.6D, G). We interpret these results to mean that the asymmetric localization of GFP-Pk requires both Kny and Tri function. In the individual mutants, the presence of maternal Kny and Tri proteins enables some recruitment of GFP-Pk to the cell membrane, but is not sufficient for its anterior-restricted localization. In contrast, in *kny;tri* double mutants in which the function of both molecules are lacking, GFP-Pk fails to be recruited to the cell surface.

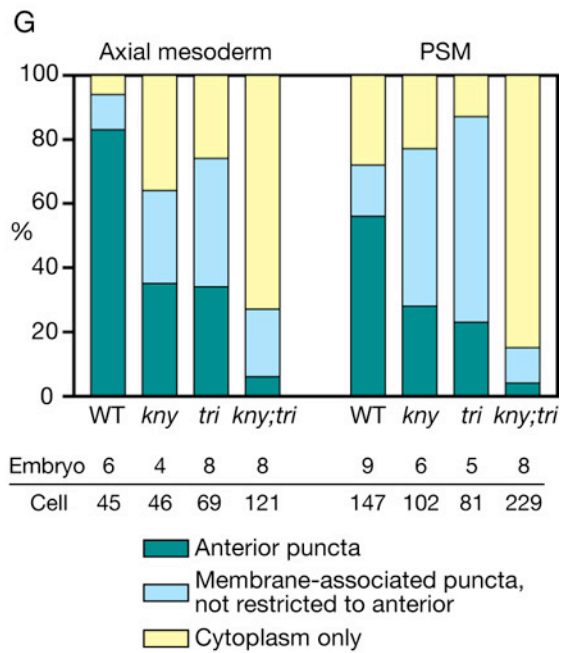
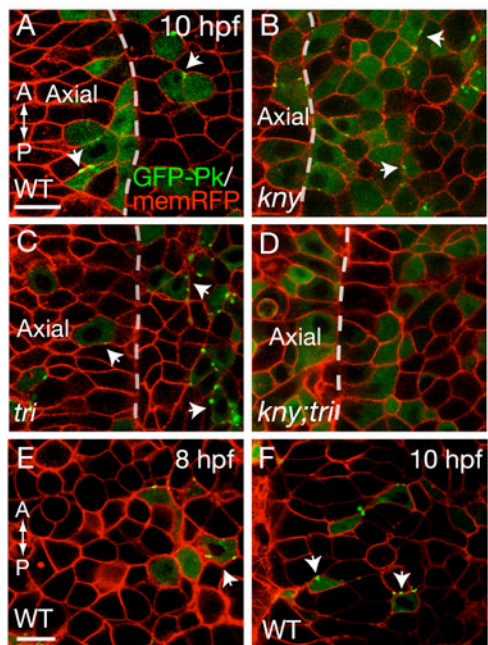
In the developing fly wing epithelium, Stbm and Pk are distributed at the proximal cell membrane, forming a complex that antagonizes the Frizzled/Dishevelled (Dsh) complex localized at the distal side of the cell (Klein and Mlodzik, 2005). In *X. laevis*, GFP-tagged Xdsh expression was shown to be enriched at the ML tips of the intercalating cells in the dorsal marginal zone explants (Kinoshita et al., 2003). To visualize the localization of GFP-Xdsh in zebrafish during C&E, we injected into the embryos a moderate amount of GFP-Xdsh synthetic RNA (Rothbacher et al., 2000; Wallingford et al., 2000), which had no obvious effect on the ML polarity of the labeled cells (Figure 3.5). Consistent with the observations in the fly and frog that activation of PCP pathway promotes Dsh recruitment to the cell membrane (Adler, 2002; Klein and Mlodzik, 2005; Wallingford et al., 2000), we detected GFP-Xdsh expression along the

Figure 3.5. The amount of GFP-Pk and GFP-Xdsh expressed has no detectable effect on the mediolateral polarity of the labeled cells. (A-B) Comparison of the cell shape between the unlabeled cells and GFP-labeled cells within the same embryo based on their length-to-width ratio (LWR). Error bars represent standard error. $p > 0.08$, unlabeled vs. labeled. Numbers of cells and embryos analyzed are shown in (C). (C) The mediolateral orientation of cells with and without GFP-labeling. $p > 0.1$, unlabeled vs. labeled.



	PSM	Cell/ Embryo	Axial mesoderm	Cell/ Embryo
Unlabeled	61%	107/10	96%	21/5
GFP-Pk labeled	54%	103/10	96%	21/5
Unlabeled	54%	116/11	94%	48/7
GFP-Xdsh labeled	55%	121/11	94%	47/7

Figure 3.6. Subcellular localization of GFP-Pk during C&E. (A-D) Confocal images of GFP-Pk localization in the dorsal mesoderm in live embryos at the tailbud stage (10 hpf). (E-F) GFP-Pk localization in the dorsal mesoderm of the same WT embryo (4 embryos) at 8hpf (E) and 10 hpf (F). (G) Quantification of GFP-Pk localization observed at the end of gastrulation (Experimental procedures). (A-F) Dorsal views. Scale bar, 20 μ m. A, anterior. P, posterior.



membrane in the dorsal mesodermal cells at the tailbud stage (Figure 3.7G; Figure 3.8), when non-canonical Wnt signaling regulates the C&E movements of this tissue (Myers et al., 2002). The membrane-localization of GFP-Xdsh was also correlated with the ML elongation of the dorsal mesodermal cells (Figure 3.7E-F, E'-F'). Surprisingly, in the axial mesoderm, 64% of the labeled cells showed strong GFP-Xdsh expression specifically along the posterior membrane, opposite to where GFP-Pk was localized (Figure 3.7A, A', G). In *kny* individual mutants, although GFP-Xdsh was localized to the membrane in 60% of the labeled axial mesodermal cells, fewer cells exhibited posterior restricted localization of GFP-Xdsh compared to WT (Figure 3.7C, C', G, $p < 0.02$). Membrane-localization of GFP-Xdsh was greatly reduced in *tri* individual mutants (Figure 3.7D, D', G, $p < 0.03$) and abolished in *kny;tri* double mutants (Figure 3.7B, B', G, $p < 2 \times 10^{-7}$), consistent with the previous reports that Tri/Stbm is required for recruitment of Dsh to the cell membrane (Bastock et al., 2003; Park and Moon, 2002).

In the medial PSM, GFP-Xdsh localization differed from cell to cell. In WT, GFP-Xdsh was expressed along the cell membrane in 65% of the labeled cells, but only 30% cells showed asymmetric GFP-Xdsh localization at the posterior edge (Figure 3.8). Given that multiple dynamic cell behaviors occurred during the medial PSM C&E (Figure 3.3), we hypothesized that the asymmetric localization of GFP-Xdsh might be a transient event and correlated with specific cell behaviors. Consistent with this notion, the posterior localization of GFP-Xdsh was more prominent in the axial mesoderm where every cell was engaged in ML intercalation (Glickman et al., 2003). Similar to what was observed in the axial mesoderm (Figure 3.7), the membrane localization of GFP-Xsh was less seen in the PSM of the individual mutants and eliminated in the double mutants

Figure 3.7. Subcellular localization of GFP-Xdsh in the axial mesoderm during C&E. (A-D) Confocal images of the axial mesoderm in live embryos expressing GFP-Xdsh. (A'-D') The same embryos as shown in (A-D) but co-labeled with membrane-RFP (memRFP). The histograms of the fluorescein intensity of the selected cells (*) are shown in the right panels. Green lines represent the fluorescein intensity of GFP-Xdsh and the red lines represent the intensity of memRFP. (E-F, E'-F') In the axial mesoderm of the same WT embryo (n=4), GFP-Xdsh was detected mainly in the cytoplasm at 75% epiboly (8 hpf) (E, E'), but became restricted to the posterior membrane at the tailbud stage (10 hpf) (F, F'). (G) Quantification of GFP-Xdsh localization in the axial mesoderm during late gastrulation (Experimental procedures). (A-F, A'-F') Dorsal views. Scale bar, 20 μ m. A, anterior. P, posterior.

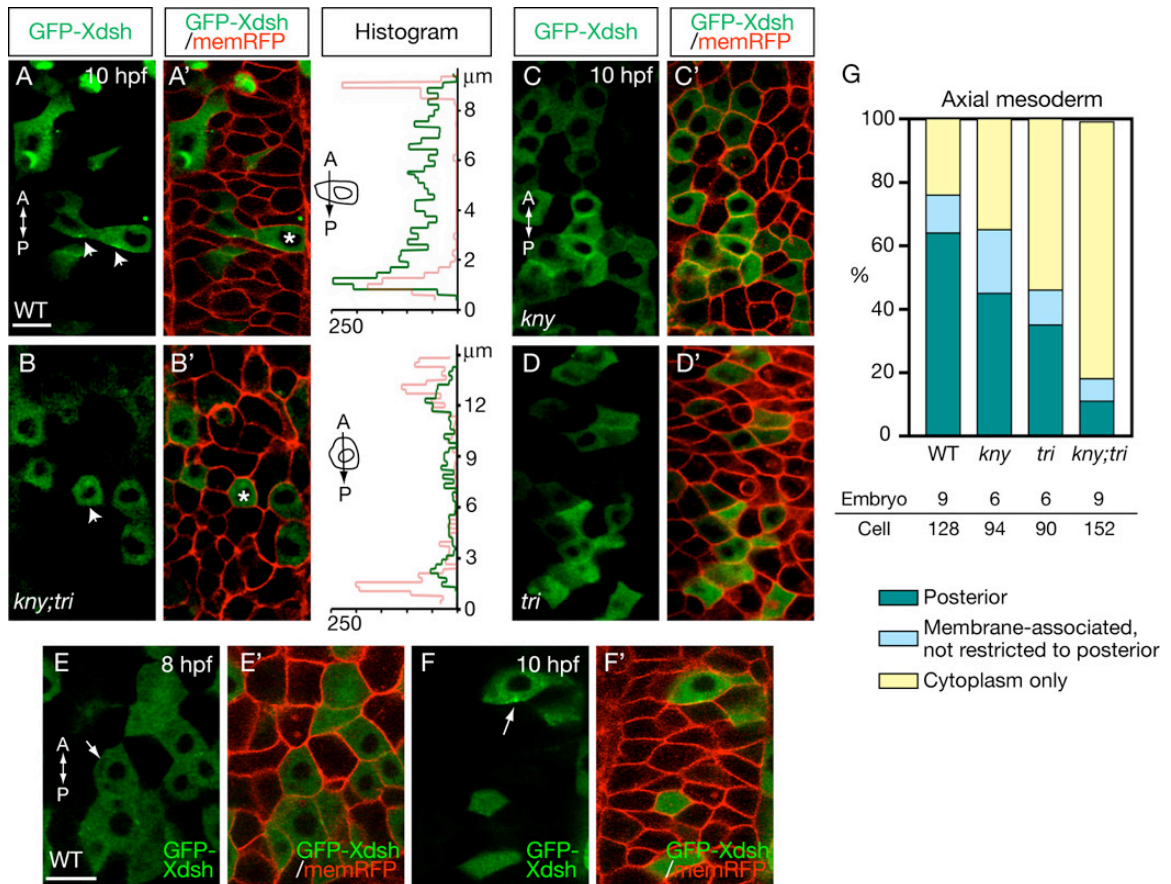
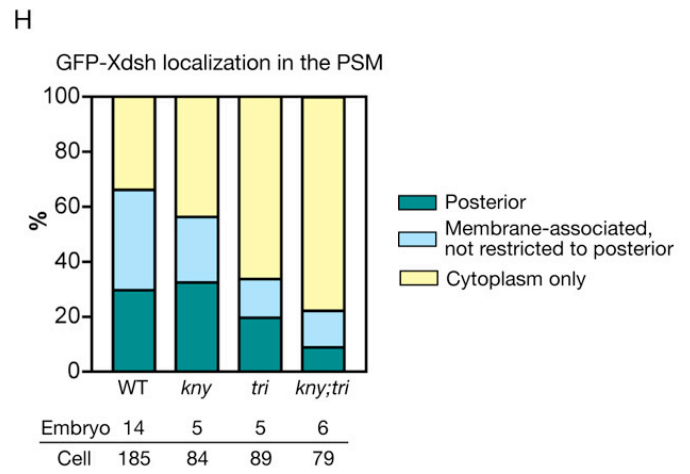
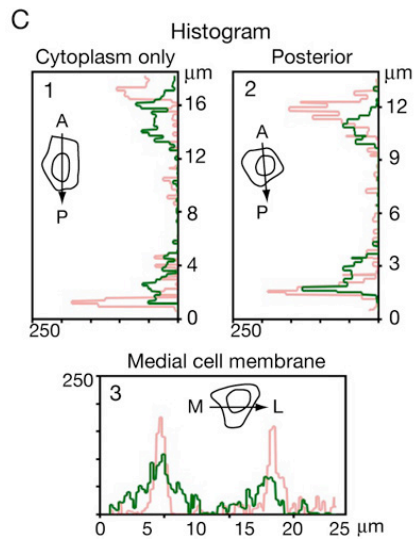
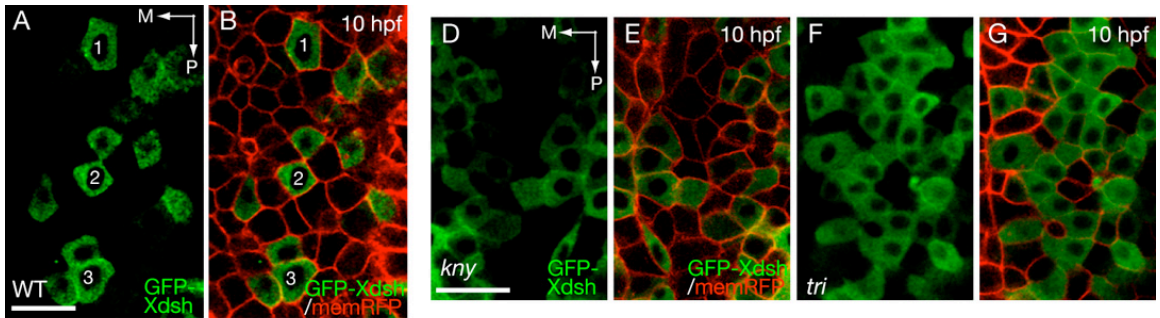


Figure 3.8. Subcellular localization of GFP-Xdsh in the medial PSM at the tailbud stage (10 hpf). (A) Confocal image showing GFP-Xdsh localization in the medial PSM in live WT embryo. (B) Same embryo as shown in (A) but co-labeled with membrane-RFP. Three cells with different GFP-Xdsh localization are selected and the histograms of their fluorescein intensity are shown in (C). (C) Green lines represent the fluorescein intensity of GFP-Xdsh, whereas red lines represent the intensity of memRFP. (D-G) GFP-Xdsh localization in the medial PSM in *kny* and *tri* individual mutants. (H) Quantification of GFP-Xdsh localization in the medial PSM at the tailbud stage. (A-B, D-G) Dorsal views. Scale bar, 20 μm . A, anterior; P, posterior; M, medial; L, lateral.



(Figure 3.8). Taken together, our study revealed novel asymmetric localizations of non-canonical Wnt components within the intercalating cells during vertebrate gastrulation. The anterior localization of GFP-Pk and posterior localization of GFP-Xdsh in the dorsal mesoderm of zebrafish gastrula are reminiscent of the proximal distribution of Pk and distal distribution of Dsh in the fly wing (Adler, 2002; Klein and Mlodzik, 2005), suggesting that the interactions between these molecules during tissue polarization are evolutionarily conserved.

Combining *in vivo* and *in silico* approaches, we performed a comprehensive analysis of the cellular behaviors underlying the C&E movements of the medial PSM during zebrafish gastrulation. Unlike the adjacent axial mesoderm, where C&E is driven mainly by ML intercalation, the medial PSM C&E is achieved by the cooperation of multiple cell intercalation behaviors: planar medial, radial AP, and coordinated radial/medial intercalations contribute additively to extension, whereas limiting radial ML intercalation is essential for convergence. We discovered anteroposteriorly polarized radial intercalation as a novel cellular behavior that generates anisotropic tissue extension. In *D. melanogaster*, PCP pathway establishes cell polarization within the epithelial sheets (Adler, 2002; Klein and Mlodzik, 2005). Likewise, in vertebrates, non-canonical Wnt signaling regulates C&E cell movement behaviors in a plane of a single cell layer (Gong et al., 2004; Myers et al., 2002). Our observation that *kny;tri* double mutants are defective in polarized radial intercalations, provides the first evidence that non-canonical Wnt signaling polarizes cell behaviors between different cell layers.

The molecular mechanisms defining the anteroposteriorly-biased orientation of planar and radial intercalations are not clear. In *D. melanogaster*, genes controlling AP

pattern are essential for ML intercalation during germ band extension (Zallen and Wieschaus, 2004). Similarly, in the *Xenopus* chordamesoderm, graded activin-like signaling that establishes AP polarity was proposed to act in parallel or upstream of non-canonical Wnt pathway to regulate the orientation of ML intercalation (Ninomiya et al., 2004). Our discovery of asymmetric GFP-Pk localization to the anterior cell edge together with enrichment of GFP-Xdsh at the posterior cell edge suggests the presence of an intrinsic AP polarity in the zebrafish dorsal mesoderm during C&E. In *kny* and *tri* individual mutants, although some GFP-Pk and Xdsh were recruited to the membrane, their asymmetric localization was compromised, indicating that non-canonical Wnt signaling is necessary for the dorsal mesodermal cells to incorporate the AP polarity signal. Studies in *X. laevis* suggest that non-canonical Wnt signaling constrains the lamellipodial protrusions to the ML tips of the cells, which is essential for ML intercalation (Keller et al., 2000; Wallingford et al., 2000). Other reports have connected non-canonical Wnt signaling with cell adhesion (Ulrich et al., 2005; Ungar et al., 1995; Witzel et al., 2006). We therefore propose that in the dorsal mesoderm of the zebrafish gastrula, AP polarity cues activate non-canonical Wnt signaling along the AP axis, which in turn regulates the mediolaterally-biased protrusive activities and differential cell adhesions to direct where cells should intercalate. Whereas previous studies emphasized the role of non-canonical Wnt signaling in controlling cell shape and orientation, and the formation of polarized cellular protrusions, our work underscores the significance of this pathway in defining distinct anterior and posterior edges of the mediolaterally-elongated cells during biased cell intercalations that drive C&E during gastrulation.

Experimental Procedures

Zebrafish maintenance, embryo generation, and staging

The *kny*^{m119+/-}, *tri*^{m209+/-}, and *kny*^{m119+/-};*tri*^{m209+/-} mutant zebrafish strains were maintained as described previously (Solnica-Krezel et al., 1994; Solnica-Krezel et al., 1996). Embryos were obtained from natural matings and morphologically staged as described (Kimmel et al., 1995). The genotypes of the embryos were determined by described morphologic phenotypes (Henry et al., 2000; Marlow et al., 1998).

RNA microinjections

To obtain mosaic expression of GFP-Pk or GFP-Xdsh in the embryo, 200 pg of RNA encoding membrane-RFP (the ras membrane-localization (CAAX) sequence fused to the carboxy terminus of RFP) was injected at the one-cell stage as described (Marlow et al., 1998). At the 16-cell stage (1.5 hpf), either 15 pg of RNA encoding GFP-Pk or 30 pg of RNA encoding GFP-Xdsh was injected into one of the blastomeres (Ciruna et al., 2006; Rothbacher et al., 2000; Wallingford et al., 2000). Synthesis of the RNAs encoding memRFP, GFP-Pk, and GFP-Xdsh were described previously (Marlow et al., 1998; Wallingford et al., 2000).

Time-lapse recording and analysis

Multi-plane Nomarski images were collected at 1.5-minute intervals for 90 minutes from 90% epiboly (9 hpf) to the 1-somite stage (10.5 hpf) with Openlab software (Improvision) using a Zeiss Axiovert 200M. Embryos were dechorinated and mounted as

described (Sepich et al., 2005). After the recordings, embryos were allowed to grow until 24 hpf to determine their genotypes. Object-Image (Norbert Vischer, <http://simon.bio.uva.nl/object-image.html>) was used to label and track cells. Data was exported to Excel (Microsoft) for calculation of the movement speeds and frequencies of different intercalation behaviors. Statistical analyses were performed using Student's two-tailed *t*-test.

The C&E rates were calculated as follows:

$$\text{Extension rate} = \frac{(\text{Total cell No./column No.})_{t=90} - (\text{Total cell No./column No.})_{t=0}}{(\text{Total cell No./column No.})_{t=0}}$$

$$\text{Convergence rate} = - \frac{(\text{Total cell No./row No.})_{t=90} - (\text{Total cell No./row No.})_{t=0}}{(\text{Total cell No./row No.})_{t=0}}$$

$$\text{AP/ML change} = \frac{\left(\frac{\text{AP cell No.}_{\text{max}}}{\text{ML cell No.}_{\text{max}}}\right)_{t=90} - \left(\frac{\text{AP cell No.}_{\text{max}}}{\text{ML cell No.}_{\text{max}}}\right)_{t=0}}{\left(\frac{\text{AP cell No.}_{\text{max}}}{\text{ML cell No.}_{\text{max}}}\right)_{t=0}}$$

Confocal imaging

To visualize the localization of GFP-Pk and GFP-Xdsh, live embryos expressing either fusion protein were mounted in 0.8% low-melting agarose. Confocal z-stacks were collected at the end of gastrulation using the Zeiss LSM 510 laser scanning inverted microscope. Three-dimensional projections were made from the z-stacks so that the localization of GFP signal within the entire cell body could be visualized three-dimensionally. Images were processed using Volocity (Improvision). The cell length-width ratio was measured by using Object-Image. The orientation and angular deviation were analyzed using VectorRose (P.A. Zippi, <http://pazsoftware.com/>). The histogram of

fluorescein intensity was measured using LSM Examiner (Zeiss). To investigate the correlation between ML cell elongation and the asymmetric localization of GFP-Pk and GFP-Xdsh, confocal images of the dorsal mesoderm in four WT embryos mosaically expressing either GFP-Pk or GFP-Xdsh were collected at 8 hpf and 10 hpf.

PIV analyses

Velocimetric estimation of morphogenetic movements was performed on the Nomarski time-lapses by using PIV analysis as described (Raffel, 1998). Time-lapse images were analyzed by using the MATPIV software package (J. K. Sveen, University of Oslo, Oslo). Practically, the algorithm first divides each time-lapse image into several so-called interrogation small windows of a few tenths of pixels. Then, for each window, it estimates by statistical correlation between two successive frames the best displacement of the window pattern, which gives, knowing the time interval, an estimation of the velocity vector.

Computational modeling of the cell intercalation behaviors

The computational model was developed using a Matlab software package (Mathworks Inc.). Detailed rules are given in the Supplementary Information.

Acknowledgements

We would like to thank Drs. O. Pourquie, A.F. Schier, B. Ciruna, M.K. Cooper, F. Marlow, A. Inbal, D. Carlin, and D.S. Sepich for critical comments, and L. S.-K. lab members for technical advices and discussions. We acknowledge excellent fish care by J.

Clanton, J. Ruddick, H. Beck and A. Bradshaw. We also thank J.P. Wallingford and B. Ciruna for generous gifts of constructs. Work in L. S.-K. laboratory is supported by NIH grants GM2283 and GM55101. Work in E. Farge laboratory is supported in part by Microsoft Research through the European PhD Scholarship Programme, as well as by the Inserm and Cnrs (ITS2005), and the HSFP.

Supplementary information

Computational modeling of the cell intercalation behaviors during C&E

To analyze the contributions of individual intercalation behaviors to the C&E movements of the medial PSM, we generated a computational model using a Matlab software package. We model cells in a single cell layer as occupied nodes of a two-dimensional 6x8 lattice. Each cell occupies a unique node (x,y) , where x refers to a specific row and y refers to a specific column. The left side of the lattice is defined as the axial-PSM boundary and we refer to this side as medial. The value of each node represents the number of cells occupying the node: “1” for one cell, “2” for two cells, and “0” for an empty space. The maximum number of cells occupying a node is two. In the simulations, we model intercalations and rearrangements of neighboring cells in response to these intercalations according to the time-lapse observations. Referring to the frequencies of different intercalation behaviors occurred during the time-lapse recordings, 30 minutes is the approximate time scale over which at least one cell intercalation event occurs. Thus we define three time steps in the simulation, each representing 30 minutes.

Our time-lapse analyses showed that the entire analyzed cell population moved toward the axial mesoderm. No other cell rearrangement was observed at the cell positions where cells moved medially without the intercalations described in the text. Since all cells were moving together, there was no net relative motion between cells. In the simulation, we assume that every cell moves medially at the same speed unless it is chosen to undergo a certain intercalation behavior. Thus we define an additional event, default planar medial migration, in which cells do not intercalate and remain in their original node. While this net medial migration does not affect the relative position of cells since all cells are moving at a uniform velocity, it may bias the motion of neighboring cell rearrangements after intercalations occur.

In time-lapse analyses we observed seven intercalation behaviors: planar medial intercalation and planar lateral intercalation in which cells move within a single cell layer, cells leaving the analyzed cell layer, and radial AP intercalation, radial ML intercalation, coordinated radial/medial intercalation and coordinated radial/lateral intercalation in which cells enter the cell layer. We do not include planar lateral intercalation or coordinated radial/lateral intercalation in the simulations because they occurred at very low frequencies (<4%) irrespective of the embryo genotype. We subdivide the remaining five types of intercalation behaviors into three lattice events: cells moving within the analyzed cell layer (planar medial intercalation), cells moving out of the analyzed cell layer, and cells entering the cell layer (radial AP intercalation, radial ML intercalation, and coordinated radial/medial intercalation). In each simulation time step, each *cell* has a probability of moving within the cell layer or leaving the cell layer, while each *node* has a probability that a new cell appears.

Probabilities of lattice events were deduced from the time-lapse analyses (Fig. 2). For example, the time-lapses of WT embryos showed that within the 90-minute time scale, the frequencies of planar medial intercalation or a cell leaving the analyzed layer were 24%, and 21% per cell, respectively, corresponding to probabilities of 8% and 7% per time step per cell in the simulation, respectively. The probability of a new cell appearing within the layer is 21%, corresponding to a probability of 0.15% (7%/48) per time step per node. Lattice events are implemented according to the following rules:

Planar medial intercalation: If a cell is assigned a planar medial intercalation event, it will be removed from the chosen node to the immediate medial node if the medial node has fewer than two cells. If the medial node already has two cells, which is the maximum number of cells a node can hold, the cell will remain in its original position and the intercalation behavior will not occur. Because we define the left edge of the lattice as the axial-PSM boundary, according to the experimental observation, the probability for cells in the left-most column (i.e. $y=1$) to undergo medial intercalation is defined as 0.

Cell leaving the analyzed layer: If a cell is assigned the behavior to leave the analyzed cell layer, it will be deleted from the chosen node.

Cell entering the analyzed layer: If a node is assigned the behavior of a cell entering the analyzed plane, one cell is added to the current node if the node has fewer than two cells. If the node already has two cells, which is the maximum number of cells a node can hold, no new cell will be added.

At the simulation onset, every node of the lattice is occupied by exactly one cell. However, in the course of simulation, cell rearrangements result in local inhomogeneities. For instance, planar medial intercalations and cells entering the analyzed layer produce

nodes with more than one cell, whereas planar medial intercalations and cells leaving the analyzed layer generate holes within the lattice. In the embryo, by contrast, we observed a confluent cell layer with no holes and rare double occupancies. To produce a more realistic representation of the *in vivo* situation, we model random cell motions in response to intercalations, which simulates the way neighboring cells accommodate the intercalating cells. In each time step, after intercalation events have occurred, each node is chosen randomly. If the value of a node is greater than 1, one of the cells in that node will move one node medial, lateral, anterior or posterior. If the value of a node is less than 1, a cell from an adjacent node anterior, posterior, medial or lateral will move to fill that node. In the case of no bias, the probability of a cell at a high-density node choosing an AP or an ML movement direction is equal (0.5) and the probability of a low-density node being occupied by a neighboring cell of anterior, posterior, medial or lateral direction is equal (0.25).

We distinguished three types of radial intercalations when a cell entered the analyzed layer, based on how they separate the neighboring cells: radial AP or ML intercalation, or coordinated radial/medial intercalation, respectively. The different types of radial intercalations are modeled by imposing an AP bias in the way cells move away from high-density nodes, which are created by cells entering the analyzed cell layer. To model the anteroposteriorly biased radial intercalation, the probability of a cell at a high-density node to move along the AP dimension is assigned the probability B_{AP} . In the WT situation, 35% cell entry occurred by coordinated radial/medial intercalation, 50% by radial AP intercalation, and 9% by radial ML intercalation. Accordingly, in the control

simulation, the probability of a cell at a high-density node to move in the AP direction is assigned the probability $B_{AP}=0.90$ ($B_{AP} = (0.35+0.50) / (0.35+0.50+0.09)$).

During planar medial intercalation, the intercalating cell leaves a hole in the lattice. Our time-lapse analyses showed that lateral neighboring cells often filled the holes generated by medial intercalation events. Thus we introduce a medial preference to fill in lattice holes. In WT, there is a 96% chance a hole will be filled by the lateral neighbor. Correspondingly, the value of medial preference is 0.96 in WT. In *kny;tri* double mutants, the value of medial preference is 0.88. When a cell leaves the analyzed cell layer, it also generates a hole in the lattice. According to the *in vivo* observations, cells exited the analyzed layer from between either their AP or ML neighbors at similar frequencies. Therefore, in the simulation, we assume that after a cell exits, the hole will be filled by the anterior, posterior, medial or lateral neighbor at equal probabilities (0.25).

To investigate the contributions of different cell intercalation behaviors to C&E, we increased or decreased the probability of one behavior at a time while keeping the probabilities of other intercalation behaviors unchanged. Meanwhile, we modified the probability of “no intercalating” events so that the sum of the probabilities of all cell behaviors would always remain as 1.

We quantified the tissue shape change by measuring the rates of C&E (Experimental procedures). For each condition (WT control simulation or simulations with the modifications of individual behaviors), 20 simulations were performed. The number of simulations required to evaluate the difference between the control and the modified situations was determined by the condition of a vanishing variation of the calculated average with respect to the number of computer runs. The raw data were

exported to Excel (Microsoft) for calculation of the average values and standard errors.

Statistical analyses were done using Student's two-tailed *t*-tests.

CHAPTER IV

CONVERGENCE AND EXTENSION MOVEMENTS AFFECT DYNAMIC NOTOCHORD-SOMITE INTERACTIONS ESSENTIAL FOR ZEBRAFISH SLOW MUSCLE MORPHOGENESIS

Chunyue Yin and Lilianna Solnica-Krezel

Department of Biological Sciences, Vanderbilt University, Nashville, Tennessee

Summary

The basic body plan of vertebrate embryos is established during gastrulation by evolutionarily conserved morphogenetic movements. However, the manner in which gastrulation movements affect later embryogenesis is not completely understood. In vertebrates, segmented somites form the vertebral column, skeletal fast and slow muscles, and dermis. During gastrulation, convergence and extension (C&E) movements elongate the presomitic mesoderm anteroposteriorly and bring it close to the axial mesoderm, which produces signals patterning the somites. In zebrafish, simultaneous inactivation of two non-canonical Wnt signaling components, *Knypek* and *Trilobite*, severely impairs C&E movements, resulting in misshapen somites and reduction of slow muscle precursors, the adaxial cells. Here, we demonstrated that C&E movements play essential roles in slow muscle morphogenesis. During segmentation, the adaxial cells dramatically change shapes and migrate laterally to form the slow muscle fibers at the myotome surface. The shape changes and lateral migration of slow muscle cells were perturbed in *knypek;trilobite* double mutants due to cell non-autonomous defects. Using confocal

imaging techniques, we showed that the adaxial cell changed shapes via a sequence of cellular behaviors, including dorsoventral elongation, anterior-ward rotation, and anteroposterior elongation. In *knypek; trilobite* double mutants, the adaxial cells maintained prolonged contact with the notochord and consequently failed to accomplish the anterior-ward rotation. The prolonged notochord-adaxial cell contact was correlated with the persistent expression of Fibronectin on the notochord surface. The adaxial cell rotation defect could be suppressed either by physical removal of the double mutant notochord or by introducing the wild-type notochord cells into the double mutants. We propose that in *knypek; trilobite* double mutants, defective C&E disrupts normal notochord development, which in turn impedes the adaxial cell shape changes and likely interferes with their lateral migration. Moreover, C&E gastrulation movements ensure proper differentiation of organ rudiments, which is necessary for tissue interactions during later development.

Introduction

During vertebrate gastrulation, evolutionarily conserved morphogenetic movements transform an initially unstructured blastula into a multilayered embryo with defined body axes (Keller et al., 2003; Solnica-Krezel, 2005). Internalization movements bring the presumptive mesoderm and endoderm from the outer layer of the early gastrula to the deeper layers underneath the future ectoderm. Epiboly movements spread and thin the germ layers. Concurrent convergence and extension (C&E) movements narrow the embryonic tissues mediolaterally and elongate them from head to tail. Impaired internalization and epiboly movements are often accompanied by severe patterning

defects and early developmental arrest, respectively (Carmany-Rampey and Schier, 2001; Feldman et al., 2000; Kane et al., 2005; Shimizu et al., 2005). By contrast, mutants defective in C&E movements form a short body axis, but precede embryonic development normally and do not exhibit significant patterning defects during gastrulation (Hammerschmidt et al., 1996; Myers et al., 2002; Solnica-Krezel et al., 1996). The relative influence of C&E gastrulation movements on cell fate specification and tissue morphogenesis during later development is only beginning to be unraveled. We recently reported that C&E movements regulate the specification and fate maintenance of zebrafish slow muscle precursors, thus demonstrating the significance of precise coordination between C&E movements and local inductive events during somite formation (Yin and Solnica-Krezel, in press). In this study, we have further queried the roles of C&E movements during somite differentiation.

Segmented somites are transient mesodermal structures that serve as a scaffold for the vertebrate body plan and give rise to the vertebrae and muscle of the trunk and tail (Pourquie, 2001). In zebrafish, the presomitic mesoderm resides at the dorso-lateral blastoderm margin at the onset of gastrulation, and is shaped and positioned alongside the axial mesoderm by gastrulation movements (Stickney et al., 2000). Simultaneous inactivation of two non-canonical Wnt signaling components Knypek/Glypican4 (Kny) and Trilobite/Van gogh-like2/Strabismus (Tri) impairs C&E movements (Jessen et al., 2002; Topczewski et al., 2001). Consequently, the somites formed in *kny;tri* double mutants are broad mediolaterally and short anteroposteriorly (Henry et al., 2000; Marlow et al., 1998). Zebrafish somites contain two types of muscle precursors: the adaxial cells, which are located next to the axial mesoderm and give rise to the slow muscle fibers, and

the lateral somitic cells, which form the fast muscles (Devoto et al., 1996). The specification and differentiation of adaxial cells are dependent on Hedgehog signaling emanating from the axial mesoderm (Blagden et al., 1997; Coutelle et al., 2001; Hirsinger et al., 2004; Wolff et al., 2003). In addition, we have demonstrated that *kny;tri* double mutants form fewer slow muscle cells and adaxial cells. This reduction is a direct consequence of impaired C&E movements on the specification and maintenance of adaxial cell fate (Yin and Solnica-Krezel, in press).

Both *kny* and *tri* genes are continuously expressed in the somites throughout somitogenesis (Park and Moon, 2002; Topczewski et al., 2001). The slow muscle fibers formed in *kny;tri* C&E mutants are not only reduced in number, but also highly disorganized, suggestive of defects in late slow muscle development in the double mutants (Yin and Solnica-Krezel, in press). During somitogenesis, the adaxial cells elongate along the anteroposterior embryonic axis and then migrate laterally to form a monolayer of slow muscle fibers at the surface of the myotome (Devoto et al., 1996; Stickney et al., 2000). Some adaxial cells do not migrate, but remain juxtaposed to the notochord, where they differentiate as the muscle pioneers and express the Engrailed proteins (Hatta et al., 1991). The lateral migration of slow muscle cells is crucial for zebrafish somite development as it initiates the medial to lateral wave of fast muscle differentiation and morphogenesis (Henry and Amacher, 2004). Although Hedgehog signaling is required for the specification and differentiation of slow muscle cells, mutant analyses argue against a role of Hedgehog in the shape changes or lateral migration of these cells (Barresi et al., 2000; Baxendale et al., 2004; Nakano et al., 2004; Roy et al., 2001). Rather, the migration of slow muscle cells was shown to follow a dynamic wave

of *m-* and *n-cadherin* co-expression moving mediolaterally through the developing somite (Cortes et al., 2003). The large extracellular polysaccharide Hyaluronan and its synthesizing enzymes also regulate the slow muscle migration, though the underlying mechanism is still unclear (Bakkers et al., 2004). Aside from these pioneer studies, our understanding of the cellular and molecular basis of slow muscle morphogenesis remains elusive.

In this study, we investigated slow muscle development in *kny;tri* non-canonical Wnt mutants and provided evidence that C&E gastrulation movements affect the dynamic interactions between the notochord and adaxial cells essential for slow muscle morphogenesis. The adaxial cells undergo three-step shape changes prior to their lateral migration: (1) dorsoventral elongation, (2) anterior-ward rotation, and (3) anteroposterior elongation. In *kny;tri* double mutants, although the adaxial cells differentiate into slow muscles normally, they fail to undergo proper cell shape changes and subsequent lateral migration. By performing genetic mosaic analyses, we demonstrated that Kny and Tri function is not required cell-autonomously for the slow muscle morphogenesis. Instead, the defective C&E movements in *kny;tri* double mutants impairs notochord development, which in turn impedes the adaxial cell shape changes and likely their subsequent lateral migration.

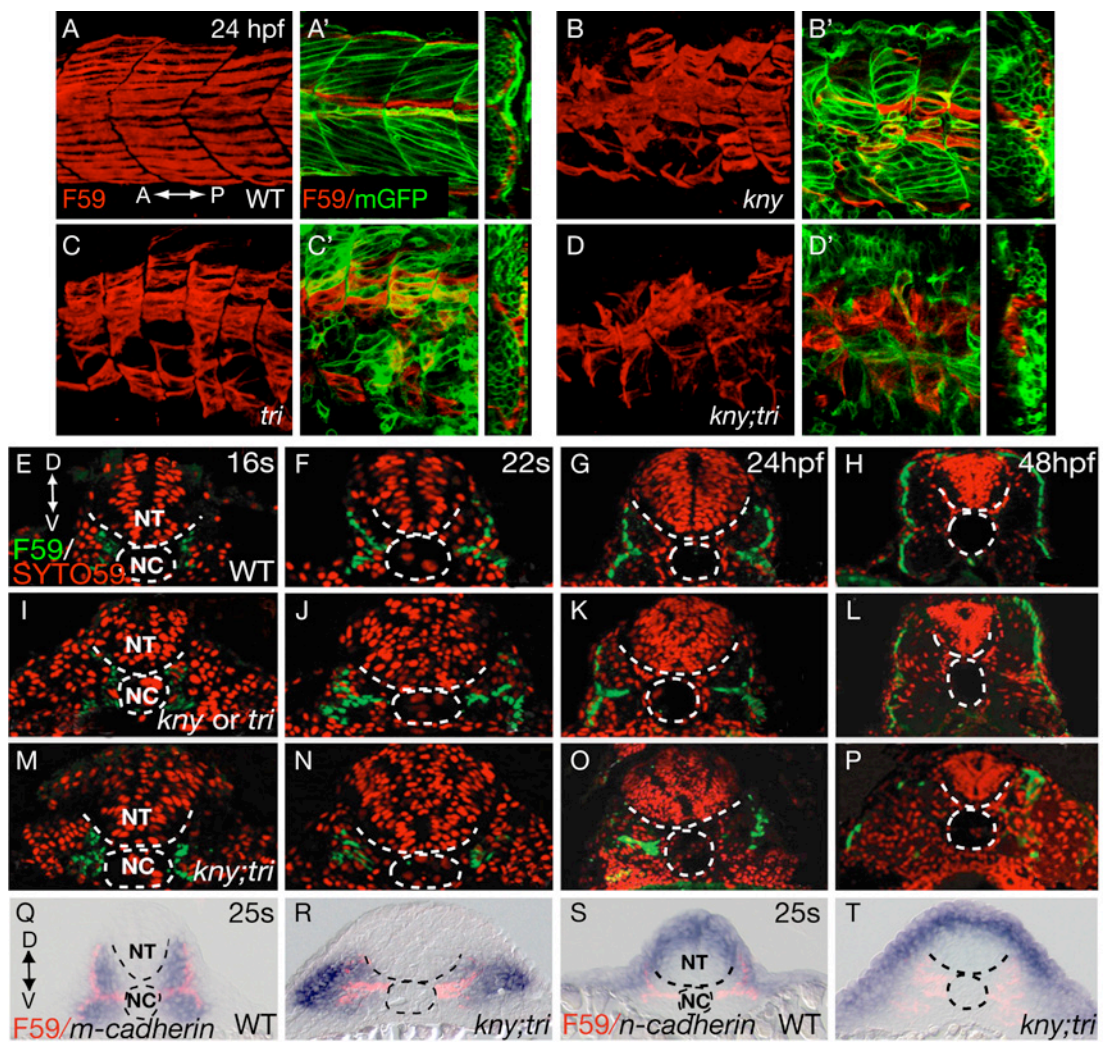
Results

Lateral migration of the slow muscle cells is compromised in *kny;tri* double mutants

Our recent study showed that the slow muscle cells formed in *kny;tri* C&E mutants are reduced in number and highly disorganized (Yin and Solnica-Krezel, in press). To address the cellular basis of the disorganization of slow muscle fibers in the double mutants, we collected confocal z-stacks of the embryos stained with the slow muscle marker F59 at 24 hours post fertilization (hpf) (Crow and Stockdale, 1986; Devoto et al., 1996). Given that F59 antibody labels the cytosolic portion of the slow muscle cells (Devoto et al., 1996), both impaired slow muscle localization and altered intracellular distribution of the myofibril bundles within the slow muscle cells could result in disorganized F59 labeling. To visualize the morphology and localization of the slow muscle cells, we co-labeled the embryos with global membrane-localized GFP (mGFP) (Figure 4.1A'-D') (Wallingford et al., 2000). In wild-type (WT) embryos, the slow muscle fibers were oriented parallel to the anteroposterior embryonic axis and spanned the entire width of the myotome (Figure 4.1A,A'). The slow muscle fibers in *kny* and *tri* individual mutants were shorter and less organized (Figure 4.1B-C,B'-C'), and these defects were greatly exacerbated in *kny;tri* double mutants (Figure 4.1D,D'). As revealed by three-dimensional (3D) reconstruction, the slow muscle fibers in WT and the individual mutant embryos were mainly located at the myotome surface by 24 hpf, with the exception of the muscle pioneers juxtaposed to the notochord (Figure 4.1A-C). By contrast, most slow muscle fibers in *kny;tri* double mutants did not assume the lateral position, but resided in the middle of the myotome (Figure 4.1D).

Based on the above observations, we hypothesized that the lateral migration of slow muscle cells was impaired in *kny;tri* double mutants. To monitor the migration process, we examined the positions of migrating slow muscle cells at consecutive time

Figure 4.1. *kny;tri* double mutants are defective in slow muscle migration. (A-D) Lateral views of the trunk region of embryos stained with the slow muscle marker F59 antibody. Confocal z-series were collected and merged into one focal plane. (A'-D') Left panels show the lateral views of the same embryos in (A-D), but only one single focal plane of the z-series is presented. The embryos are labeled with mGFP to highlight the morphology of the myotome and individual muscle fibers. Left panels show the confocal 3D reconstructed transverse sections. (E-P) Localization of the slow muscle cells between the 16-somite stage and 48 hpf as revealed by F59 antibody staining. SYTO59, which labels nuclei, highlights the embryonic structures. (Q-T) *m-* and *n-cadherin* expression (blue) and the localizations of the slow muscle cells shown by F59 labeling (pink) at the 25-somite stage. (E-T) Transverse sections of the second or third somite. A, anterior. P, posterior. D, dorsal. V, ventral. NT, neural tube. NC, notochord.



points during somitogenesis by employing F59 antibody immunohistochemistry. Because the lateral migration of slow muscle cells occurs sequentially along the anteroposterior embryonic axis (Devoto et al., 1996; Stickney et al., 2000), we analyzed the transverse sections of the second and third somites in the embryos of different genotypes to ensure that the investigated cells were at the equivalent developmental stages. Between the 16-somite stage (17 hpf) and 24 hpf, in WT and individual mutants, most slow muscle cells migrated from medial to lateral positions and eventually reached the myotome surface (Devoto et al., 1996) (Figure 4.1E-L). By contrast, the lateral migration of slow muscle cells was largely blocked in *kny;tri* double mutants (Figure 4.1M-P). Even at 48 hpf, long after normal migration should conclude (Devoto et al., 1996), some slow muscle cells in the double mutants were still apparent in the middle of the myotome (Figure 4.1P).

Given that the lateral migration of slow muscle cells is guided by the reciprocal waves of *n-* and *m-cadherin* expression in the somite (Cortes et al., 2003), we asked whether the defective slow muscle migration observed in *kny;tri* double mutants coincided with alterations in *m-* and *n-cadherin* expression. In WT, *m-cadherin* expression expands in medial to lateral direction through the developing myotome during somitogenesis, with its lateral boundary advancing in front of the migrating slow muscle cells (Figure 4.1Q) (Cortes et al., 2003). By contrast, *n-cadherin* transcripts are initially detected throughout the somite, but become downregulated mediolaterally with the most medial aspect of *n-cadherin* expression domain corresponding to the position of migrating slow muscle cells (Cortes et al., 2003) (Figure 4.1S). We examined the expression of *m-* and *n-cadherin* at various time points during somitogenesis, and did not observe any significant differences between WT and the double mutants (data not

shown). At the 25-somite stage (21.5 hpf), a strong co-expression domain of *m-* and *n-cadherin* was seen at the lateral edge of the myotome in *kny;tri* double mutants, indicating that the wave of *m-* and *n-cadherin* expression still occurred in these embryos (Figure 4.1R,T). However, the *kny;tri* slow muscle cells did not follow the wave, but rather remained close to the notochord (Figure 4.1R,T). These data indicate that the slow muscle cells in *kny;tri* double mutants fail to migrate properly, despite the normal dynamic expression of *m-* and *n-cadherin* in the myotome.

The *kny;tri* adaxial cells fail to undergo cell shape changes prior to lateral migration

We next asked whether the failure of slow muscle migration in *kny;tri* double mutants was due to earlier defects in adaxial cell development. Prior to their lateral migration, the adaxial cells elongate down the anteroposterior axis until they span the length of the somite (Devoto et al., 1996; Stickney et al., 2000). To investigate the process of adaxial cell shape changes, we expressed mGFP in the embryos and fixed them every 20 minutes between the 5-somite (11.7 hpf) and 8-somite (13 hpf) stages. We then collected z-series of confocal images along the dorsoventral embryo axis and performed 3D reconstruction (Figure 4.2). Using this approach, we identified a sequence of cellular behaviors occurring during the adaxial cell shape changes. In each WT somite, three to five rows of cuboidal adaxial cells formed a monolayer flanking the notochord at the 5-somite stage (Figure 4.3A). At the 6-somite stage (12 hpf), the adaxial cells elongated dorsoventrally to become aligned perpendicular to the notochord. At around the 7-somite stage (12.5 hpf), the dorsal aspect of the adaxial cells rotated toward the anterior somitic boundary. Upon finishing the rotation at the 8-somite stage, the adaxial

Figure 4.2. Quantification of the shape changes of adaxial cells prior to lateral migration. (A-H) Time course analyses monitoring the shape changes of the adaxial cells in WT (A-D) and *kny;tri* double mutants (E-H). Embryos expressing mGFP were fixed at 20-minute intervals between the 5- and 8-somite stages and confocal z-stacks of the adaxial cells were acquired. Upper panels show the dorsal views, focusing on the third somite. Dashed lines mark the somitic boundaries and boundaries between the adaxial cells and lateral somitic cells. Red boxes show the confocal 3D-reconstructed sagittal sections. Dashed lines delineate the third somite. (I) Measurements of the shape changes of the adaxial cells within the second and third somites in the anteroposterior and dorsoventral dimensions. For individual genotype, 4 embryos were analyzed at each time point. Error bars show the standard deviations. A, anterior. P, posterior. D, dorsal. V, ventral. NC, notochord.

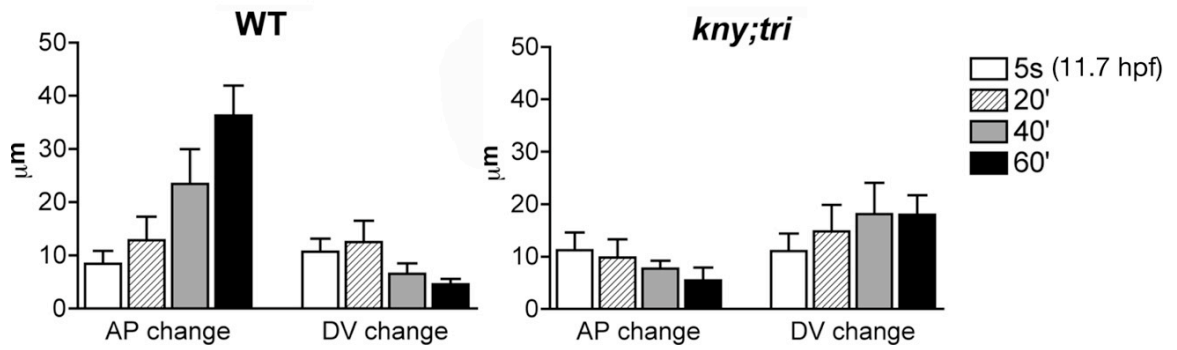
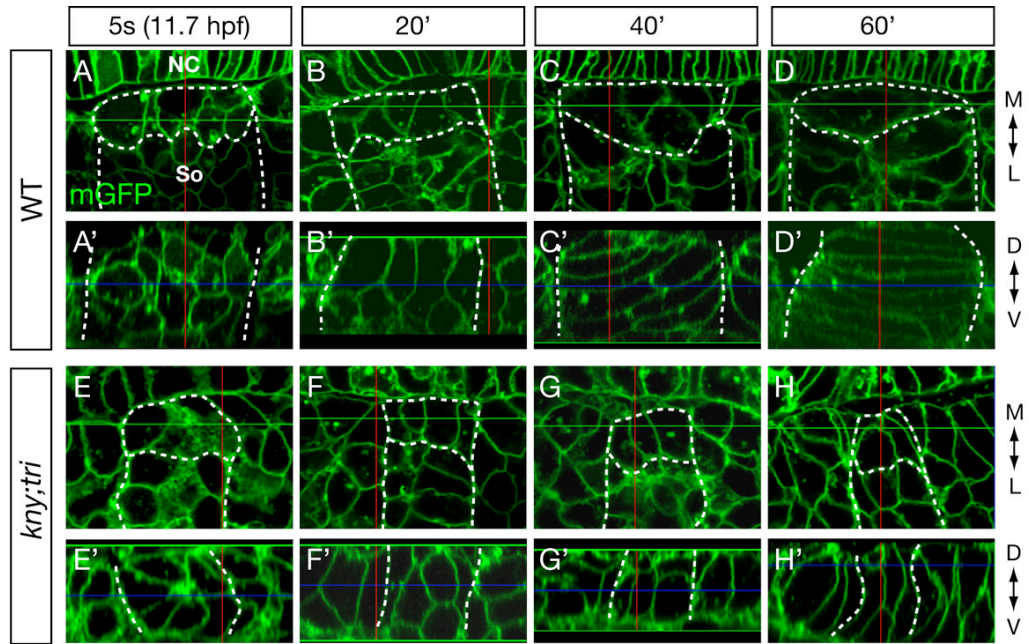
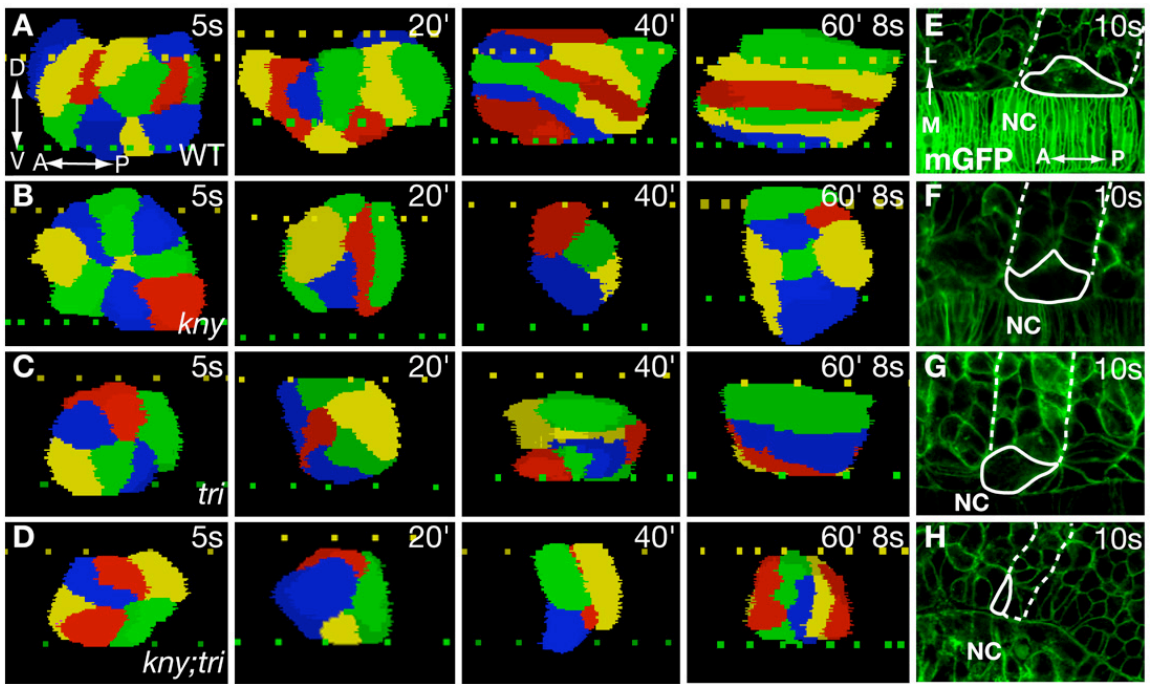


Figure 4.3. The *kny;tri* adaxial cells fail to undergo proper shape changes before lateral migration. (A-D) 3D reconstruction of the adaxial cells within the third somite (Material and methods). Lateral views. Individual cells are colored for clarity. Dashed lines denote the dorsal (yellow) and ventral (green) edges of the notochord. (E-H) Dorsal views of embryos expressing mGFP, one adaxial cell and the corresponding somitic boundaries are highlighted. A, anterior. P, posterior. D, dorsal. V, ventral. M, medial. L, lateral. NT, neural tube. NC, notochord. So, somite.



cells elongated further anteroposteriorly, and oriented themselves parallel to the notochord (8 embryos, 97 cells. Figure 4.2; Figure 4.3A,E). The consecutive shape changes of the adaxial cells occurred simultaneously within the five most anterior somites. In the more posterior somites, however, we did not observe the dorsoventral elongation or anterior-ward rotation behavior. Rather, the adaxial cells in the posterior somites elongated directly along the anteroposterior dimension (data not shown).

In the anterior somites of *kny* and *tri* individual mutants, half of the adaxial cells exhibited rotation and elongation behaviors similar to the WT (Figure 4.3B-C). At the 8-somite stage, 56% of *kny* cells (8 embryos, 72 cells) and 53% of *tri* cells (8 embryos, 60 cells) spanned the entire AP dimension of the somite. In *kny;tri* double mutants, the adaxial cells were of a similar size and shape as WT before they started to change shape (Figure 4.2; Figure 4.3D,I). However, after the dorsoventral elongation, none of the *kny;tri* cells rotated towards the anterior somitic boundary (6 embryos, 58 cells). Instead, they remained aligned perpendicular to the notochord at the 8-somite and later stages (Figure 4.3D; data not shown). Therefore, the adaxial cells in *kny;tri* double mutants fail to undergo proper shape changes that normally precede their lateral migration (Figure 4.3I).

The morphogenetic defects of the *kny;tri* adaxial cells are cell non-autonomous

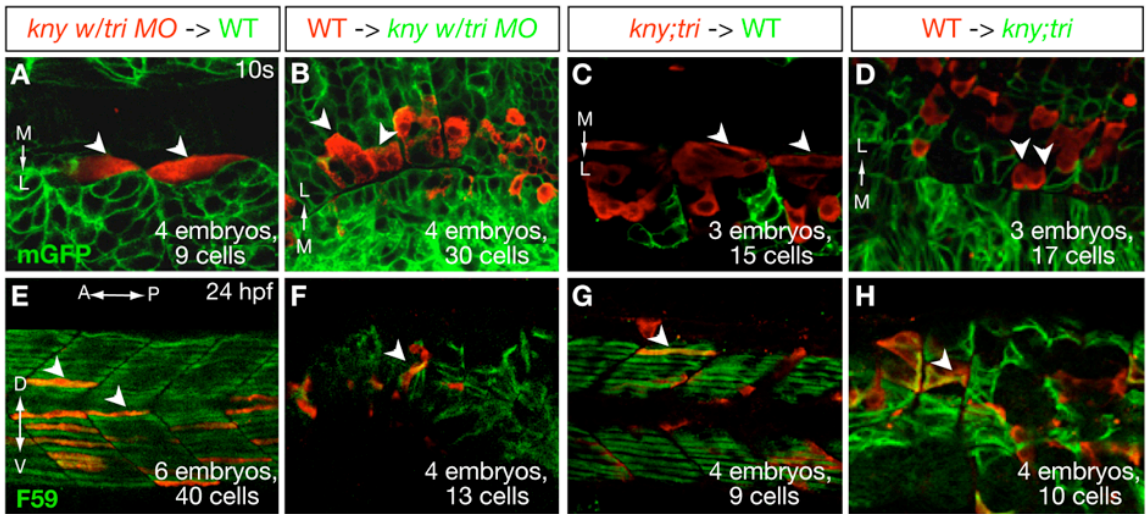
Kny and Tri are crucial regulators of the C&E movements during gastrulation (Jessen et al., 2002; Topczewski et al., 2001). They function in both cell-autonomous and non-autonomous fashions to mediate the mediolateral cell elongation underlying C&E (Jessen et al., 2002), and to regulate the dorsal convergence of the presomitic mesoderm

(Yin and Solnica-Krezel, in press). This suggests that both *Kny* and *Tri* are required for intercellular communication critical for cell polarization. To test whether *Kny* and *Tri* have similar cell-autonomous and non-autonomous roles during slow muscle morphogenesis, we performed genetic mosaic analyses. When the adaxial cells from *kny* blastulae injected with *tri* morpholino oligonucleotides (MO) were transplanted into WT hosts (Jessen et al., 2002), they underwent normal shape changes and lateral migration (Figure 4.4A,E). In contrast, WT cells failed to behave properly in an environment deficient for both *Kny* and *Tri* function (Figure 4.4B,F). The same results were observed when *kny;tri* double mutants were used as donors or hosts in the transplantation experiments (Figure 4.4C,D,G,H). Therefore, unlike the situation during gastrulation, *Kny* and *Tri* function is required only cell non-autonomously for the slow muscle morphogenesis during segmentation.

Close apposition of the somitic boundaries is not responsible for the adaxial cell morphogenesis defects in *kny;tri* double mutants

Our transplantation results indicate that the impaired morphogenesis of the slow muscle cells in *kny;tri* double mutants is due to defects in the environment rather than disrupted cell-autonomous properties. As the consequence of impaired C&E movements, the somites formed in *kny;tri* double mutants contain only two rows of cells and the somitic boundaries are positioned extremely close to one another (Henry et al., 2000). Therefore, it is plausible that close apposition of the somitic boundaries in the double mutants restrains the rotation of the dorsoventrally elongated adaxial cells. To test the roles of somitic boundaries in slow muscle morphogenesis, we employed *fused somite* (*fss/tbx24*) mutants that lack the somitic boundaries (Nikaido et al., 2002). It has been

Figure 4.4. Kny and Tri act in cell non-autonomous fashion during slow muscle morphogenesis. Confocal images of host embryos expressing mGFP (A-D) or immunostained with F59 antibody (E-H). Transplanted donor cells are labeled with Rhodamine dextran (red). (A, B, E, F) Transplantation experiments using *kny* embryos injected with *tri* MO as donors (A, E) or hosts (B, F). (C, D, G, H) Transplantation analyses using *kny;tri* double mutants as donors (C, G) or hosts (D, H). (A-D) Dorsal views of embryos at the 10-somite stage. (E-H) Lateral views of the embryos at 24 hpf, arrowheads point to the selected donor cells. A, anterior. P, posterior. D, dorsal. V, ventral. M, medial. L, lateral.

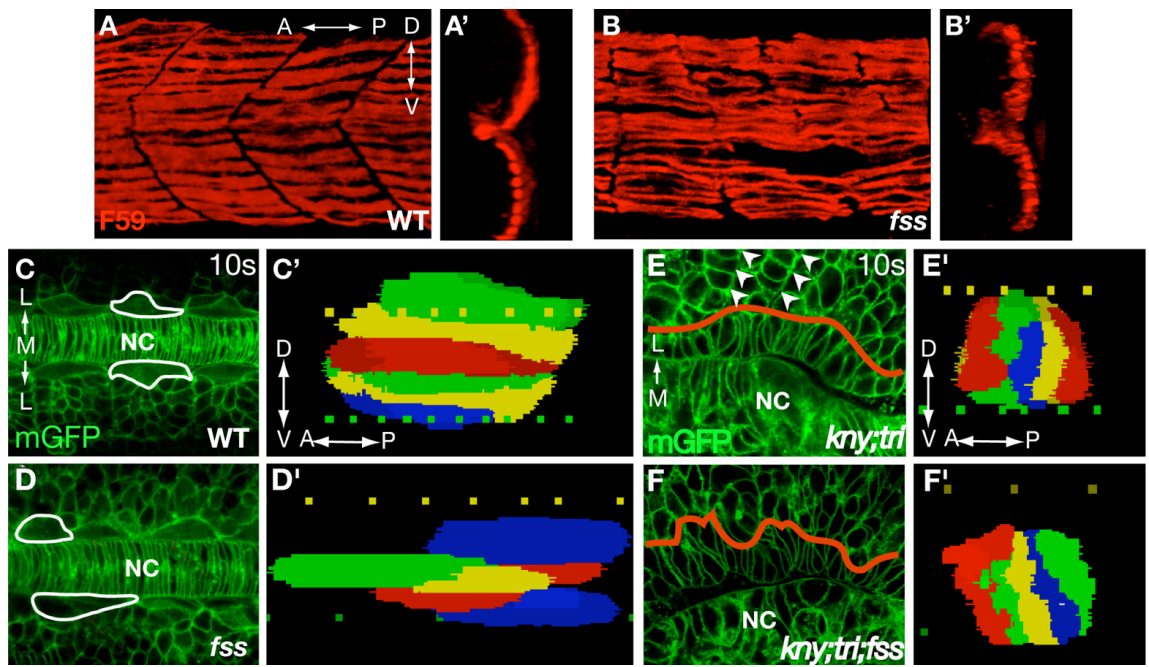


shown that interactions between muscle fibers and somitic boundaries limit to what extent muscle cells can elongate (Henry et al., 2005). Consistently, we found that the slow muscle fibers in *fss* mutants did not exhibit clear segmental arrangement at 24 hpf (Figure 4.5B) (Barrios et al., 2003; van Eeden et al., 1996). However, majority of the *fss* mutant slow muscle fibers were located at the lateral surface of the myotome with the exception of muscle pioneers, indicating that somitic boundaries are dispensable for the slow muscle migration (Figure 4.5B').

We next asked whether the presence of somitic boundaries is required for the shape changes of adaxial cells prior to their lateral migration. Between the 5-somite and 8-somite stages, the *fss* mutant adaxial cells underwent dorsoventral elongation and anterior-ward rotation (data not shown). However, they elongated to variable degrees and their characteristic somitic organization was lost (Figure 4.5D,D'). These results lead us to the conclusion that somitic boundaries function to limit the adaxial cell elongation and ensure their segmental organization. However, the presence of somitic boundaries is not essential for the shape changes of the adaxial cells.

If the close apposition of somitic boundaries in *kny;tri* double mutants blocks the adaxial cell rotation, such a defect should be suppressed in *kny;tri;fss* triple mutants, where the somitic boundaries would not form. We generated *kny;tri;fss* triple mutants, and as expected, the somitic boundaries were missing in these mutants (Figure 4.5F). However, in the triple mutants, the adaxial cells still failed to accomplish their normal shape changes (Figure 4.5F,F'). Thus compression of somitic boundaries alone cannot account for the impaired adaxial cell rotation in *kny;tri* double mutants.

Figure 4.5. Somitic boundaries are not required for the shape changes or lateral migration of the adaxial cells. (A-B) Lateral views of embryos stained with F59 antibody. (A'-B') show the reconstructed transverse sections. (C-D) Dorsal views of embryos expressing mGFP. White lines outline the selected adaxial cells. (E, F) Dorsal views of *kny;tri* (E) and *kny;tri;fss* (F) embryos expressing mGFP. Red lines highlight the boundary between the adaxial cell and the lateral somitic cells. Arrowheads in (E) mark the somitic boundaries, which are missing in the *kny;tri;fss* embryos (F). (C'-F') 3D reconstruction of the adaxial cells labeled with mGFP at the 10-somite stage, lateral views. A, anterior. P, posterior. M, medial. L, lateral. D, dorsal. V, ventral. NT, neural tube. NC, notochord.



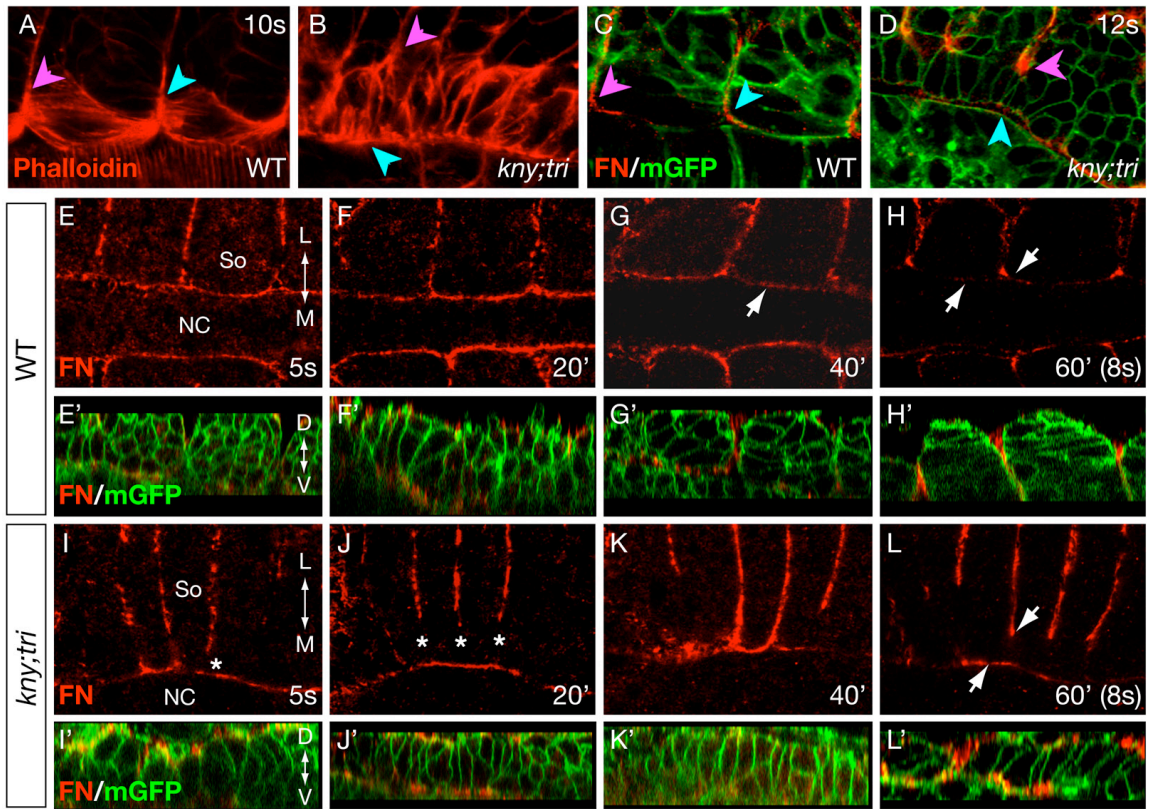
The *kny;tri* double mutant adaxial cells exhibit prolonged contacts with the notochord

The cell non-autonomous requirements for Kny and Tri function during the adaxial cell shape changes suggested that these cells make important interactions with their extracellular environment. Actin cytoskeleton is engaged in the establishment of cell adhesion and plays critical roles in cell shape changes (Carthew, 2005). Hence we investigated the contacts between the adaxial cells and the neighboring environment during their shape changes by visualizing F-actin distribution with phalloidin staining. Before the adaxial cells initiated the shape changes, F-actin was localized ubiquitously near the plasma membrane of the adaxial cells, regardless of their genotypes (data not shown). At the 10-somite stage (14 hpf) when the adaxial cell rotation was completed in WT and individual mutants, we observed long bundles of actin filaments forming in the anteroposteriorly elongated adaxial cells and these bundles were oriented parallel to the notochord (Felsenfeld et al., 1991) (Figure 4.6A; data not shown). Interestingly, F-actin was enriched at the positions where the adaxial cells attached to the somitic boundaries (Figure 4.6A). Moreover, the level of F-actin at the notochord-adaxial cell boundary was greatly reduced, suggesting that the adaxial cells have little contact with the notochord after they become anteroposteriorly aligned. By contrast, in *kny;tri* double mutant embryos, the F-actin bundles, like the cell body of the adaxial cells, were misaligned and perpendicular to the notochord at the 10-somite stage (Figure 4.6B). F-actin was enriched at two ends of the double mutant adaxial cells, with one end touching the anterior somitic boundary (pink arrowhead), whereas the other still in contact with the notochord (blue arrowhead). The persistent F-actin enrichment at the notochord-adaxial cell boundary in

the double mutants suggests prolonged contact between the adaxial cells and the notochord in *kny;tri* double mutants.

In zebrafish, the notochord is constrained by a sheath of extracellular matrix (ECM) (Parsons et al., 2002; Scott and Stemple, 2005). We thus hypothesized that the *kny;tri* double mutant adaxial cells might maintain prolonged contact with the notochord via cell-matrix adhesion. Fibronectin (Fn) is a large ECM glycoprotein that mediates a wide variety of cellular interactions with the ECM (Miyamoto et al., 1998). During zebrafish segmentation, *fn* RNA is expressed in the notochord, whereas its main receptor *integrin α 5* is expressed in the adaxial cells, suggesting a possible role of Fn-Integrin interactions during the adaxial cell shape changes (Julich et al., 2005; Koshida et al., 2005). We investigated the distribution of Fn protein in the somites and found a correlation between the changes in Fn protein expression and the three-step shape changes of the adaxial cells in WT. Prior to the adaxial cell shape changes, as well as during their dorsoventral elongation, Fn protein was expressed at the somitic boundaries and the notochord-adaxial cell boundary (Crawford et al., 2003) (Figure 4.6E,F). At the 7-somite stage when the adaxial cells started to rotate towards the anterior somitic boundary, the level of Fn expression was unchanged at the somitic boundaries, but became reduced at the notochord-adaxial cell boundary (Figure 4.6G). Finally, after the adaxial cells completed their rotation, Fn expression was significantly downregulated at the notochord surface (Figure 4.6C,H). Meanwhile, Fn became enriched at the anterior and posterior ends of the anteroposteriorly elongated adaxial cells (Figure 4.6C,H). In *X. laevis*, perturbing the expression of non-canonical Wnt components, such as Tri/Vangl2, disrupts the Fn fibril assembly on mesodermal tissue surfaces (Goto et al., 2005). We did

Figure 4.6. The adaxial cells in *kny;tri* double mutants keep prolonged contact with the notochord. (A, B) F-actin distribution at the 10-somite stage as revealed by phalloidin staining. (C, D) Expression of Fn protein at the 12-somite stage. In *kny;tri* double mutants, Fn is persistently enriched at the notochord-somitic boundary (arrowheads). In (A-D), the pink arrowheads point to the places where the adaxial cells touch the anterior somitic boundary, whereas the blue arrowheads point to the other end of the adaxial cells. (E-L) Time course of the Fn expression between the 5- and 8-somite stages. (E'-L') Confocal reconstructed images showing the sagittal sections of the adaxial cells expressing mGFP and Fn between the 5- and 8-somite stages. (A-L) Dorsal views, anterior to the left. A, anterior. P, posterior. M, medial. L, lateral. D, dorsal. V, ventral. NC, notochord. So, somite.



not observe any significant alteration of Fn expression in *kny* and *tri* individual mutants during the adaxial cell shape changes (data not shown). Likewise, in *kny;tri* double mutants, Fn was highly expressed at the notochord surface and the somitic boundaries before and during the dorsoventral elongation of the adaxial cells (Figure 4.6I,J). However, Fn expression was often absent at the positions where the adaxial cells contacted the somitic boundaries (Figure 4.6I,J, asterisks). At the 8-somite stage, when Fn expression at the notochord-adaxial cell boundary was largely diminished in WT, we observed persistent high level of Fn deposition at the notochord surface in *kny;tri* double mutants (Figure 4.6D,L). The persistent Fn expression is correlated with the prolonged contacts between the adaxial cell and the notochord in *kny;tri* double mutants, and might be correlated with the adaxial cell morphogenesis defects in these mutants.

An intact notochord is not required for normal slow muscle morphogenesis

The discovery that the notochord in *kny;tri* double mutants maintained persistent contact with the adaxial cells during their shape changes prompted us to investigate the role of notochord in slow muscle morphogenesis. We took advantage of the *floating head/flh* mutants that fail to form a notochord (Talbot et al., 1995). The *flh* mutation inactivates a homeobox gene homologous to *Xnot* and causes transdifferentiation of chordamesoderm into muscle (Halpern et al., 1993; Talbot et al., 1995). As revealed by F59 antibody labeling, the *flh* mutant adaxial cells were located at the dorsal midline rather than assuming the “adaxial” position as in WT (Figure 4.7A,B) (Blagden et al., 1997). Despite their abnormal location, 92% of the *flh* adaxial cells became anteroposteriorly elongated and occupied the entire anteroposterior dimension of the

somite by the 10-somite stage (Figure 4.7B; 10 embryos, 84 cells, the adaxial cells within the 3rd somite were analyzed). Moreover, majority of the *flh* mutant slow muscle cells migrated to the lateral surface of the myotome by 24 hpf (Figure 4.7C-F).

We also investigated the slow muscle development in *bozozok* and *no tail* mutants that affect notochord specification and differentiation, respectively (Fekany et al., 1999; Schulte-Merker et al., 1994; Solnica-Krezel and Driever, 2001). In both mutants, the early deficiency of notochord tissue significantly reduces the number of specified slow muscle cells (Blagden et al., 1997) (data not shown). However, the adaxial cells in both mutants underwent normal shape changes and subsequent lateral migration, similar to the observations in *flh* mutants (data not shown). Taken together, these data support a permissive rather than an instructive role of the notochord in slow muscle morphogenesis.

Abnormal notochord properties impede the adaxial cell rotation in *kny;tri* double mutants

To test directly whether the persistent notochord-adaxial cell contacts blocked the adaxial cell rotation in *kny;tri* double mutants, we physically removed the notochord by excising the embryonic shield, the dorsal organizer in zebrafish, at the onset of gastrulation (Saude et al., 2000; Shih and Fraser, 1996). Because notochord is the source of Hedgehog signal that specifies the adaxial cell fate (Blagden et al., 1997), we injected synthetic *sonic hedgehog/shh* RNA into the embryos prepared for shield extirpation to ensure that they still formed adaxial cells in the absence of the notochord (Krauss et al., 1993). Consistent with previous reports, the shield-depleted embryos formed brain, spinal cord and segmented somites, whereas the notochord was largely missing (Figure 4.8E,F;

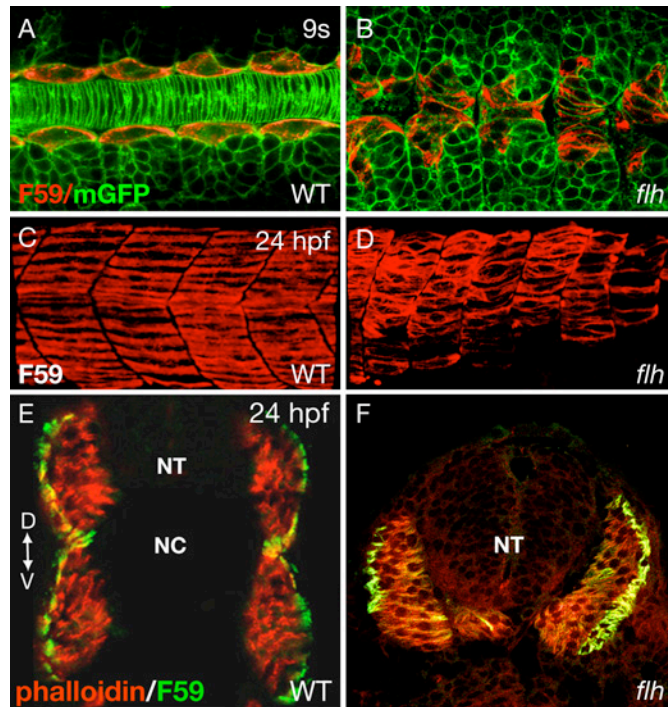


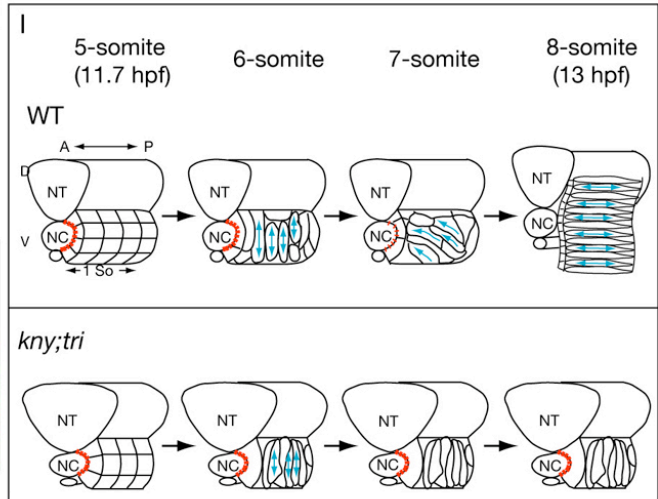
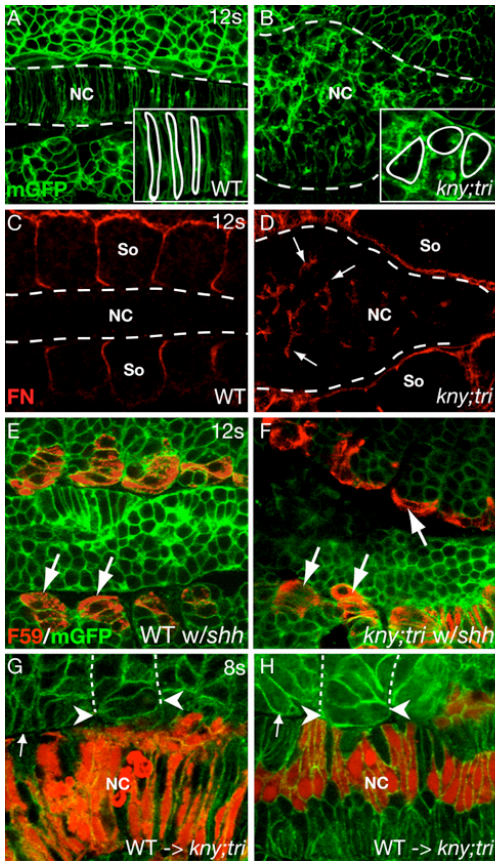
Figure 4.7. The presence of an intact notochord is not essential for slow muscle morphogenesis. (A, B) Dorsal views of the 9-somite embryos labeled with mGFP and the slow muscle marker F59 antibody. (C, D) Lateral views of the trunk region of embryos stained with F59 antibody. (E, F) Transverse sections of the anterior myotomes stained with the slow muscle marker F59 antibody, and phalloidin that recognizes both the fast and slow muscle fibers (Henry and Amacher, 2004). A, anterior. P, posterior. D, dorsal. V, ventral. NT, neural tube. NC, notochord.

data not shown) (Shih and Fraser, 1996). Shield ablation did not disrupt the adaxial cell shape changes in the operated WT embryos (n=4) (Figure 4.8E), in agreement with the permissive role of notochord in this process. Remarkably, when the notochord was removed from *kny;tri* double mutants, the mutant adaxial cells were able to accomplish the proper shape changes and became anteroposteriorly elongated by the 12-somite stage (n=10) (Figure 4.8F).

The fact that removal of the notochord suppressed the adaxial cell rotation defects in *kny;tri* double mutants provides strong support for the notion that abnormal notochord properties prevent the double mutant adaxial cells from rotating normally. Due to the C&E movement defects during gastrulation, the notochord formed in *kny;tri* double mutants was extremely broad and misshaped (Figure 4.8A,B) (Henry et al., 2000; Marlow et al., 1998; Yin and Solnica-Krezel, in press). At the 12-somite stage, the WT notochord cells were highly elongated in the mediolateral dimension and aligned parallel to each other (Figure 4.8A). By contrast, the double mutant notochord cells exhibited very irregular shapes and were oriented in random directions (Figure 4.8B). Moreover, whereas Fn protein was excluded from the notochord in WT at the 12-somite stage, it accumulated ectopically in the middle of the double mutant notochord (Figure 4.8D). The abnormal cell morphology and the aberrant Fn deposition suggest that the notochord morphogenesis and differentiation are impaired in *kny;tri* double mutants.

To investigate whether defective notochord properties in *kny;tri* double mutants accounted for the prolonged contact between the notochord and the adaxial cells, we performed shield transplantation experiments (Saude et al., 2000; Shih and Fraser, 1996). In all experiments in which a portion of the embryonic shield from a WT donor embryo

Figure 4.8. Abnormal notochord properties impede the shape changes of adaxial cells. (A-B) The WT and double mutant embryos expressing mGFP at the 12-somite stage. Lower windows show the notochord cells under higher magnification. (C-D) Expression of Fn protein at the 12-somite stage. Dashed lines delineate the notochord-somitic boundaries. Arrows in (D) point to the ectopic Fn expression inside of the notochord in *kny;tri* double mutants. (E-F) Dorsal views of the shield-depleted embryos at the 12-somite stage. The adaxial cells (arrows) are stained by F59 antibody. (G-H) Introducing WT notochord cells suppresses the rotation defects of the double mutant adaxial cells lying next to them (white arrowheads). Transplanted cells are labeled with Rhodamine dextran (red). β -catenin antibody (green), which labels the cell membrane, delineates the embryonic structures. (A-H) Dorsal views, anterior to the left. NC, notochord. So, somite. (I) A model for the shape changes of the adaxial cells in WT and *kny;tri* double mutant embryos. Between the 5- and 8-somite stages, the WT adaxial cells undergo three-step cell shape changes: (1) Dorsoventral elongation, (2) anterior-ward rotation, and (3) anteroposterior elongation. Prior to the step of anterior-ward rotation, the adaxial cells are in direct contact with the notochord, likely via cell-matrix adhesion (Red). The contacts become reduced at around the 7-somite stage so that the adaxial cells are released from the notochord and rotate towards the anterior somitic boundary. In *kny;tri* double mutants, the contacts between the notochord and the adaxial cells persist so that the adaxial cells fail to rotate and remain perpendicular to the notochord.



was transplanted into a double mutant host, the resulting notochord was two to three cells wide in the mediolateral dimension, composed of a mixture of WT and double mutant cells (Figure 4.8G,H; 5 embryos). Interestingly, although introducing WT notochord cells had no obvious effect on the body length or somite morphology of the *kny;tri* host embryos, the WT cells significantly corrected the shape and orientation of their neighboring double mutant notochord cells (Figure 4.8G,H). In the double mutant host embryos, each somite was in direct contact with 4 to 7 notochord cells. When more than 25% of these notochord cells were of the WT genotype, the adaxial cells within the adjacent somite, but not those positioned in the more anterior or posterior neighboring somites, were able to rotate and elongate normally (Figure 4.8G,H, arrows; Table 4.1). The shield transplantation results provide direct evidence to show that abnormal notochord properties in *kny;tri* double mutants are responsible for the failure of adaxial cell shape changes.

Discussion

Morphogenesis of organ rudiments requires precise interactions between neighboring tissues. Ensuring that such interactions occur at the proper time and between the proper tissues relies on the correct basic body plan established by the morphogenetic movements during gastrulation. Here, we studied slow muscle morphogenesis in *kny;tri* double mutants that are defective in C&E gastrulation movements (Marlow et al., 1998; Henry et al., 2000; Yin and Solnica-Krezel, in press). During segmentation, the adaxial cells change shapes and migrate laterally through the somite to form the slow muscle fibers at the surface of the myotome (Devoto et al., 1996; Stickney et al., 2000). We

Table 4.1. Introducing WT notochord cells suppressed the rotation defect of the *kny;tri* double mutant adaxial cells

	The first three pairs of somites in <i>kny;tri</i> hosts* (H)	Proportion of transplanted WT NC cells adjacent to the somite (No. of WT cells/total No. of NC cells)		Minimum percentage of WT NC cells correlated with suppressing the adaxial cell rotation defect
H1		s1a: 5/5	s1b: 3/5	40%
H2		s1a: 4/6	s1b: 1/8	33%
H3		s1a: 3/5	s1b: 1/4	25%
H4		s1a: 2/7	s1b: 2/5	29%
H5		s1a: 2/4	s1b: 0/4	40%

**kny;tri* host somites in which the adaxial cell rotation defect was suppressed are shown in red, those in which rotation defect was not suppressed are shown in black. NC, notochord. S, somite. A, anterior.

revealed a sequence of cellular behaviors during the adaxial cell shape changes, which is dependent on the dynamic interactions between the notochord and adaxial cells. In *kny;tri* double mutants, the adaxial cells failed to change shapes properly. Such a defect is not due to the close apposition of somitic boundaries caused by the early C&E defects in these mutants. Rather, impaired C&E gastrulation movements perturb the normal differentiation and morphogenesis of the notochord in *kny;tri* double mutants, resulting in the prolonged contact between the notochord and the adaxial cells. This in turn impedes the adaxial cell shape changes and likely interferes with their lateral migration.

The adaxial cells undergo dramatic cell shape changes preceding lateral migration

During zebrafish segmentation, the adaxial cells first undergo shape changes and then migrate laterally to form a monolayer of slow muscle fibers at the myotome surface (Devoto et al., 1996). By using confocal imaging and 3D reconstructions, we revealed that the shape changes of adaxial cells within the anterior somites entail three consecutive steps: (1) dorsoventral elongation, (2) anterior-ward rotation, and (3) anteroposterior elongation (Figure 4.8I). The adaxial cells in *kny;tri* double mutants failed to rotate towards the anterior somitic boundary and consequently remained perpendicular to the notochord.

In *X. laevis*, the paraxial mesoderm forms blocks of cells that rotate 90° to become oriented parallel to the notochord (Afonin et al., 2006; Hamilton, 1969; Youn and Malacinski, 1981). The three-step sequence of the zebrafish adaxial cell shape changes shares remarkable similarities with the somite rotation in *X. laevis*, suggesting that these behaviors are evolutionarily conserved (Keller, 2000; Youn and Malacinski, 1981).

Moreover, the *X. laevis* somites contain two distinct types of muscle cells analogous to the superficial slow and medial fast muscle fibers of zebrafish (Grimaldi et al., 2004). The precursors of the superficial slow muscles are specified next to the notochord upon Hedgehog signal and migrate to the lateral somite surface to form slow muscles (Grimaldi et al., 2004), similar to what was reported for the zebrafish slow muscle development (Blagden et al., 1997; Coutelle et al., 2001; Devoto et al., 1996). However, there are also differences between the somitic cell rotation in frog and the adaxial cell shape changes in zebrafish. In *X. laevis*, somitic cells rotate individually and somite rotation occurs in a dorsal-to-ventral gradient (Youn and Malacinski, 1981), whereas in zebrafish, we did not observe an obvious gradation of the adaxial cell shape changes along the dorsoventral axis. In *X. laevis*, every cell in the somite elongates and rotates 90° to align parallel to the notochord, a process that begins simultaneously with the segmentation of the presomitic mesoderm (Keller, 2000). Perturbation of somitic cell rotation is often associated with impaired somitic boundary formation (Youn and Malacinski, 1981). In zebrafish, the adaxial cell shape changes occur normally in *fss* mutants in which the somitic boundaries are missing (Figure 4.5). Conversely, in mutants that are defective in Hedgehog signaling or notochord formation, the adaxial cells are largely absent whereas the somitic boundaries form on schedule (Blagden et al., 1997; van Eeden et al., 1996). These results suggest that the adaxial cell shape changes and segmentation of the presomitic mesoderm are independent of each other in zebrafish.

Abnormal notochord properties impede the adaxial cell shape changes in *kny;tri* double mutants

Our transplantation experiments indicated that the defects in the adaxial cell shape changes in *kny;tri* double mutants are cell non-autonomous. We further revealed novel interactions between the adaxial cells and the environment during their shape changes. By investigating slow muscle development in *fss* individual mutants lacking somitic boundaries, we showed that although not being essential for the shape changes of adaxial cells to take place, somitic boundaries provide cues to limit their elongation. Our results are consistent with the recent report that the somitic boundaries ensure the segmented organization of slow muscle fibers (Henry et al., 2005). However, given that the adaxial cells in *kny;tri;fss* triple mutant exhibited the same rotation defect as observed in *kny;tri* double mutants, we concluded that compression of somitic boundaries alone is not responsible for the defects of adaxial cell rotation in *kny;tri* double mutants.

Notochord was implicated in mediating somitic cell rotation in *X. laevis*, though its actual role remains controversial. Whereas *in vitro* analyses suggest that notochord induces somitic cell rotation (McCaig, 1986), laser ablation of notochord in *X. laevis* explants did not block the rotation (Keller, 2000). We showed that in zebrafish, the adaxial cells in *flh* and other notochord-deficient mutants rotated and elongated normally, arguing against an instructive role of notochord in the adaxial cell shape changes. Studies using *X. laevis* notochordal explants demonstrated that physically hindering C&E movements interrupts normal notochord differentiation (Domingo and Keller, 1995). Consistently, we showed that in zebrafish *kny;tri* double mutants, C&E defects severely impair the shape and alignment of the notochord cells (Figure 4.8A,B). Although the double mutant notochord cells adopt the correct cell fate as revealed by the normal expression of many notochord markers (data not shown), we detected persistent F-actin

localization and Fn protein expression at the notochord surface. We therefore hypothesize that defective C&E movements disrupt normal notochord development in *kny;tri* double mutants. This causes the prolonged contact between the notochord and the adaxial cells and consequently impedes the adaxial cell shape changes. In support of this notion, we showed that the adaxial cell rotation defects were suppressed by physical removal of the double mutant notochord or by introducing the WT notochord cells into the double mutants (Figure 4.8). Interestingly, in the shield transplantation experiments, the presence of a relatively small number of WT notochord cells was sufficient for the adjacent double mutant adaxial cells to change shapes (Table 4.1). Furthermore, the morphology and orientation of the double mutant notochord cells were improved significantly when they were next to the WT cells. These results suggest that Kny and Tri are not required cell-autonomously for the normal contact between the notochord and the adaxial cells. The prolonged notochord-adaxial cell contact in the double mutants is likely the consequence of defective polarization of the double mutant notochord cells, which can be suppressed by the WT cells in a cell non-autonomous manner. Notably, the suppression of defective notochord cell polarization by WT donor cells during segmentation contrasts our previous observations that Kny and Tri act in both cell-autonomous and non-autonomous fashion to control ML cell elongation during gastrulation (Jessen et al., 2002; Topczewski and Solnica-Krezel, unpublished). This suggests that the mechanisms by which Kny and Tri regulate cell polarity might be different between gastrulation and segmentation.

It is noteworthy that in *X. laevis*, disruption of the cell adhesion molecules, such as paraxial protocadherin (Kim et al., 1998), Type I cadherins (Giacomello et al., 2002), and the Ena/VASP family of actin regulatory proteins (Kragtorp and Miller, 2006),

impairs somitic cell rotation. Learning whether cell adhesion molecules have a role in the adaxial cell shape changes in zebrafish requires further investigation.

Fn and the adaxial cell shape changes

Concurrent with the adaxial cell shape changes between the 5- and 8-somite stages, Fn protein is expressed dynamically at the notochord-somite boundary (Figure 4.6). Fn expression is initially strong, then becomes downregulated as the adaxial cells rotate towards the anterior somitic boundary, and diminishes from the notochord surface when the adaxial cells are anteroposteriorly elongated and aligned. In *X. laevis*, perturbing non-canonical Wnt signaling disrupts polarized Fn fibril assembly on mesodermal tissue surfaces (Goto et al., 2005). Consistently, we observed aberrant Fn protein expression inside the notochord and at the notochord-somite boundary in *kny;tri* double mutants (Figure 4.6 and 4.8). The molecular regulation of the Fn expression along the notochord is not clear. It has been shown that during ECM remodeling, the turnover of matrix proteins, such as Fn, is regulated by the matrix metalloproteases (MMPs) (McCawley and Matrisian, 2001). In zebrafish, both *mmp-9* and *mmp-14a* genes are expressed in the notochord during segmentation (Thisse et al., 2004; Yoong et al., 2007), and the enzymes they encode may regulate the expression levels of Fn at the notochord surface. To test this, it will be necessary to examine the expression of these *mmps* in *kny;tri* double mutants, in which Fn expression fails to diminish at the notochord surface.

The dynamic expression of Fn protein is highly correlated with the three-step shape changes of the adaxial cells (Figure 4.6). Furthermore, *integrin α 5* gene, which encodes a subunit of Fn receptor, is expressed in the adaxial cells during segmentation

(Julich et al., 2005; Koshida et al., 2005), supporting the notion that the Fn/Integrin mediated cell-matrix adhesion may have a role in the adaxial cell shape changes. It has been reported that mutations in zebrafish *integrin α 5* disrupt anterior somite formation, whereas the slow muscle development is rather normal in these mutants (Julich et al., 2005). Our preliminary results also showed that in zebrafish *natter/fn* mutants (Trinh and Stainier, 2004) and WT embryos injected with the MO blocking *fn* translation, the adaxial cells rotated and elongated normally (Yin and Solnica-Krezel, unpublished). These data suggest that Fn-Integrin interaction is not required for the adaxial cells to change shapes. Instead, the dynamic Fn expression is likely to mediate the timing of the adaxial cell shape changes. It is still unclear whether the prolonged Fn expression at the notochord-adaxial cell boundary is directly responsible for the failed adaxial cell shape changes in *kny;tri* double mutants, or other defects of the double mutant notochord also contribute to their adaxial cell defects. Our initial study supports the latter possibility as knocking down Fn function by MO injection failed to suppress the adaxial cell morphogenesis defects in *kny;tri* double mutants (Yin and Solnica-Krezel, unpublished).

Slow muscle migration in *kny;tri* double mutants

Shortly after their shape changes, the adaxial cells migrate through the entire myotome towards its lateral surface, where they differentiate into slow muscle fibers (Devoto et al., 1996). The lateral migration of slow muscle cells is also impaired in *kny;tri* double mutants. Several genes encoding the non-canonical Wnt signaling components, including *wnt5*, *kny*, and *tri*, are expressed in the paraxial mesoderm during segmentation (Jessen et al., 2002; Kilian et al., 2003; Park and Moon, 2002; Rauch et al., 1997; Topczewski et al., 2001). *wnt11*, which encodes non-canonical Wnt ligand, is

expressed in the slow muscle cells as they migrate laterally (Makita et al., 1998). However, in *kny*, *tri* individual mutants, as well as in other non-canonical Wnt mutants, such as *silberblick/wnt11*, *pipetail/wnt5* individual mutants and *silberblick;pipetail* double mutants, the slow muscle migration is largely normal (Yin and Solnica-Krezel, in press). This suggests that non-canonical Wnt signaling is not absolutely essential for the slow muscle migration.

Our transplantation experiments indicate that the failure of slow muscle migration in *kny;tri* double mutants is due to defects in the environment rather than abnormal slow muscle cell properties. Monitoring the migration of the double mutant slow muscle cells revealed that most cells continued to maintain contacts with the notochord during the time period when normal lateral migration should be underway (Figure 4.1). The reciprocal wave of *n-* and *m-cadherin* expression was shown to generate differential adhesive environments to guide the slow cell migration (Cortes et al., 2003), and our data indicated that such a wave still occurs in *kny;tri* double mutants (Figure 4.1). It is tempting to hypothesize that the prolonged contacts with the notochord may prevent the double mutant slow muscle cells from catching the *cadherin* expression wave on time. Therefore, when these cells become separated from the notochord during later segmentation, they cannot migrate laterally as the migration cues are no longer available. In this view, normal notochord development that is dependent on C&E gastrulation movements, may also be important for the slow muscle cells to receive and respond to the proper migration signal at the proper time. In addition, due to the early C&E movement defects, the somites in *kny;tri* double mutants are severely malformed. Our previous analyses showed that the fast muscle fibers in *kny;tri* double mutants are short and

misoriented, and their expression of fast muscle marker gene is reduced (Yin and Solnica-Krezel, in press). Therefore, the environment in which the lateral migration of slow muscle cells takes place is abnormal in *kny;tri* double mutants. To determine whether defective notochord and fast muscle development affects slow muscle migration in *kny;tri* double mutants, it would be interesting to investigate whether transplantation of WT notochord alone can suppress the migration defects of the slow muscle cells in the double mutants.

Experimental Procedures

Zebrafish maintenance, embryo generation, and staging

The *kny^{m119+/-}*, *tri^{m209+/-}*, *fs^{s-/-}*, *flh^{n1-/-}*, *kny^{m119+/-};tri^{m209+/-}*, and *kny^{m119+/-};tri^{m209+/-};fs^{s+/-}* mutant zebrafish strains were maintained as described previously (Solnica-Krezel et al., 1994). Embryos were obtained from natural spawnings and morphologically staged as described (Kimmel et al., 1995). The genotypes of the embryos were judged by the described morphologic phenotypes (Henry et al., 2000; Marlow et al., 1998; Solnica-Krezel et al., 1996; Talbot et al., 1995; van Eeden et al., 1996).

In situ hybridization and immunohistochemistry

Antisense RNA probe synthesis for *m-* and *n-cadherin* was as described (Sepich et al., 2000). Whole-mount in situ hybridization was performed according to (Thisse et al., 1993). Embryos for sectioning were embedded in 1.5% agar/5% sucrose and frozen in 2-methyl-butane chilled by liquid nitrogen. 10 μ m sections were obtained using a cryostat

microtome. Sections were photographed with a Zeiss Axiophot using Axiocam digital camera.

Whole-mount immunohistochemistry was performed essentially as described (Topczewska et al., 2001). Monoclonal F59 antibody (anti-slow MyHC, a generous gift from FE Stockdale, Stanford University) (Crow and Stockdale, 1986), and anti- β -catenin antibody (Sigma) were used at 1:100 and 1:250 dilution, respectively. Polyclonal anti-Fibronectin antibody (Sigma) was used at 1:200 dilution. SYTO59 (Molecular Probes) staining was performed after antibody staining. Embryos were incubated for 30 minutes at room temperature by using a dilution of 1:10000 in PBT-2%DMSO. Phalloidin (Molecular Probes) staining was performed as described (Barrios et al., 2003). Images were acquired using the Zeiss LSM 510 laser scanning inverted microscope.

For 3D reconstruction of the adaxial cells, confocal z-series of somitic cells expressing mGFP were acquired and processed using Object-Image (Vischer, <http://rsb.info.nih.gov/nih-image>) and reconstructed using Rotater 3.5 (Kloeden, craig@raru.adelaide.edu.au). Briefly, confocal z-stacks were opened in Object-Image and the adaxial cells were outlined using the Region of Interest (ROI) function, which allows to draw a freehand polygon, encode the cell shape using the X, Y, Z coordinates of the corners and specify the color of the line as a fourth variable. These xyz data were exported as a Rotater file and the stacked outlines of cells were examined in Rotater that reads a set of 3D points and lines and plots them into a 3D image. All measurements were performed using ImageJ 1.29x (Wayne Rasband, <http://rsb.info.nih.gov/ij/Java1.3.1>) and analyzed using Microsoft Excel and GraphPad Prism. Statistical analyses were performed using Student' *t*-test.

Microinjections

Injections were performed at the one-cell stage as described (Marlow et al., 1998). The *tri/vangl2* morpholino oligonucleotide, and synthetic RNAs encoding Sonic Hedgehog and mGFP (the ras membrane-localization (CAAX) sequence fused to the carboxy terminus of GFP) were described previously (Jessen et al., 2002; Krauss et al., 1993; Marlow et al., 1998; Sokol, 1996; Wallingford et al., 2000).

Transplantation and shield ablation experiments

Genetic mosaic analyses were performed as described (Westerfield, 2000). To determine the cell autonomy of Kny and Tri function during adaxial cell shape changes, host embryos were injected with RNA encoding mGFP and fixed at the 10-somite stage. To determine the cell autonomy during the migration of slow muscle cells, host embryos were allowed to develop until 24 hpf, when they were fixed and stained with F59 antibody.

Shield ablation and transplantation were performed essentially as described (Saude et al., 2000). For shield ablation experiments, the embryos were injected with 100 pg of synthetic *shh* RNA at the 1-cell stage to ensure that the shield-ablated embryos still formed adaxial cells (Krauss et al., 1993; Marlow et al., 1998). For shield transplantation experiments, host embryos were fixed at the 10-somite stage and stained with anti- β -catenin antibody. *kny;tri* double mutant hosts were identified based on the morphological characteristics, such as anteroposteriorly shortened and mediolaterally broadened somite morphology and the lack of internal cells (Henry et al., 2000).

CHAPTER V

ATP7A DETERMINES A HIERARCHY OF COPPER METABOLISM DURING EMBRYOGENESIS ESSENTIAL FOR NOTOCHORD DEVELOPMENT

Running Title: Zebrafish copper metabolism

This paper has been published under the same title in *Cell Metabolism*, 2006.

Bryce A. Mendelsohn*[§], Chunyue Yin^{‡§}, Stephen L. Johnson[†], Thomas Wilm[‡], Lilianna Solnica-Krezel[‡] and Jonathan D. Gitlin*[†]

Departments of Pediatrics* and Genetics[†], Washington University School of Medicine, St. Louis, Missouri and [‡]Department of Biological Sciences, Vanderbilt University, Nashville, Tennessee

[§]These authors contributed equally to this work.

The sequence of the zebrafish *atp7a* has been deposited in GenBank under the accession number AAZ07896.

Summary

The critical developmental and genetic requirements of copper metabolism during embryogenesis are unknown. Utilizing a chemical genetic screen in zebrafish, we identified small molecules that perturb copper homeostasis. Our findings reveal a role for copper in notochord formation and demonstrate a hierarchy of copper metabolism within the embryo. To elucidate these observations, we interrogated a genetic screen for embryos phenocopied by copper deficiency, identifying *calamity*, a mutant defective in the zebrafish ortholog of the Menkes disease gene (*atp7a*). Copper metabolism in

calamity is restored by human ATP7A and transplantation experiments reveal that *atp7a* functions cell-autonomously, findings with important therapeutic implications. The gene dosage of *atp7a* determines the sensitivity to copper deprivation, revealing that the observed developmental hierarchy of copper metabolism is informed by specific genetic factors. Our data provide insight into the developmental pathophysiology of copper metabolism and suggest that suboptimal copper metabolism may contribute to birth defects.

Introduction

Copper is an essential transition metal that plays a critical role in the biochemistry of aerobic organisms. Enzymes utilize the reactivity of this metal to undertake a series of facile electron transfer reactions in a select number of metabolic pathways essential for cellular respiration, iron oxidation, pigment formation, connective tissue biogenesis, peptide amidation, neurotransmitter biosynthesis and antioxidant defense (Pena et al., 1999). The signs and symptoms of copper deficiency are the result of impaired function of these cuproenzymes. This reactivity of copper also accounts for the toxicity of this metal when metabolism is perturbed and for this reason specific pathways have evolved for the intracellular trafficking and compartmentalization of copper (O'Halloran and Culotta, 2000; Rosenzweig, 2002). The inherited disorders of copper metabolism, Menkes disease and Wilson disease, underscore both the essential need for copper and the toxicity of this metal and elucidation of the molecular genetic basis of these diseases has enhanced our understanding of the biochemical mechanisms of copper metabolism (Culotta and Gitlin, 2001; Shim and Harris, 2003).

Considerable clinical and experimental data indicates that copper is an essential nutrient for normal development. In children with Menkes disease, an inability to acquire copper *in utero* due to inherited loss-of-function mutations in the gene encoding a copper-transport ATPase (*ATP7A*), results in metaphyseal dysplasia, cerebellar degeneration and severe failure to thrive (Hamza et al., 2001; Voskoboinik and Camakaris, 2002). Similarly, in a variety of mammals copper deficiency during pregnancy either due to nutrient deprivation or genetic manipulation results in embryo resorption or offspring with severe neurologic impairment and presumed organogenesis defects in multiple tissues including the heart and skeleton (Hamza et al., 2001; Keen et al., 1998). While these data indicate a role for specific transporters and chaperones in supplying copper to the developing fetus (Mercer and Llanos, 2003), the mechanisms and timing of developmental events dependent on copper metabolism remain unknown due to the lack of models affording facile genetic and biochemical analysis during embryogenesis.

We hypothesized that the zebrafish might provide advantages for the analysis of copper metabolism during vertebrate development. The optical clarity and rapid external development of embryos permits detailed characterization of deficient phenotypes from the moment of fertilization. Furthermore, zebrafish embryos have been used in small molecule screens, permitting the identification of specific developmental phenotypes and the associated genetic pathways (Peterson et al., 2000a; Stern et al., 2005; Zon and Peterson, 2005). In this current study, we have utilized chemical genetics combined with a genetic screen (Solnica-Krezel et al., 1994) to elucidate the critical developmental and genetic requirements of copper metabolism during embryogenesis. Our findings provide

insight into the developmental pathophysiology of copper metabolism and suggest an experimental approach towards elucidating the biology of gene-nutrient interaction essential for early human development.

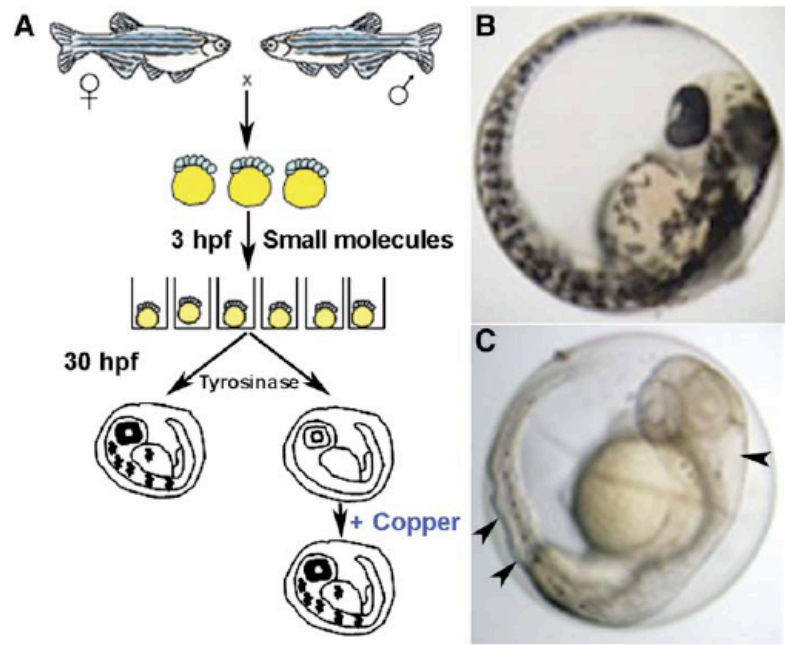
Results

Small molecules allow the specific manipulation of copper during development

To obtain precise, temporal control of copper metabolism during development, we determined the minimum copper concentration in the zebrafish embryo to be 0.5-1.0 μM based upon data from oocytes (Riggio et al., 2003). This internal copper pool largely present within the yolk sac is entirely sufficient for embryonic development as treatment of developing embryos with nonpermeable copper chelators was without effect (data not shown). To identify tools with which to alter this internal copper pool, we employed a chemical genetic screen, reasoning that small molecules interfering with copper metabolism would prevent melanin pigmentation by blocking the activity of tyrosinase, a copper-containing oxidase required for melanin-based pigment in the zebrafish embryo (Rawls et al., 2001). The specificity of this effect was determined by examining these Embryos for recovering of tyrosinase activity following the addition of exogenous copper (Figure 5.1).

Of the small molecules screened (Table 5.1), 7 of diverse chemical structure prevented melanin pigmentation in a manner entirely reversible by the addition of exogenous copper (Table 5.2). These small molecules each yielded an identical and striking pleiotropic phenotype, as illustrated in Figure 5.1 following exposure to

Figure 5.1. Schematic of the small-molecule screen for drugs perturbing copper metabolism. (A) Embryos from wild-type zebrafish were arrayed in a 96-well format and treated with drugs at 5 mM beginning at 3 hr post fertilization (hpf). At 30 hpf, the embryos were assayed for the development of melanin pigment. In a second screen, embryos were again exposed at 3 hpf to drugs that abrogated melanin formation but this time were supplemented with 25 mM CuCl₂. In this screen, all drugs that prevented pigmentation in a manner reversible by the addition of exogenous copper were considered as perturbing copper homeostasis. (B and C) As compared to wild-type embryos (B), copper-deficient embryos treated with neocuproine (C) lacked pigment and displayed a strikingly wavy notochord and enlarged hindbrain ventricle (arrowheads).



neocuproine. Each drug gave the same phenotype at the same time of treatment. Although there were differences in effectiveness of the compounds as reflected by the doses used, in every case the identical hierarchy of phenotypes was observed (see below). These small molecules did not affect melanocyte differentiation or migration as determined by *in situ* hybridization with a melanocyte marker and did not directly inhibit tyrosinase as determined by an in-gel assay (data not shown). Consistent with these experimental findings, review of the literature revealed that each molecule has been associated with copper chelating activity. Furthermore none of these compounds has reported teratogenic activity, supporting the concept that the phenotypes observed arise directly from copper deficiency. The identification in this screen of two drugs used in clinical medicine raises the intriguing possibility that unidentified alterations in nutrient metabolism may underlie the therapeutic or toxic mechanisms of additional prescription drugs.

Examination of the copper-deficient phenotype in greater detail was undertaken following treatment of developing embryos with the minimum dose (10 μ M) of neocuproine that gave the most robust phenotype. In the zebrafish embryo, the notochord consists of a collection of vacuolated cells surrounded by a sheath, adjacent to the dorsal aorta and the developing floor plate (Figure 5.2A, left). Copper deficiency profoundly altered notochord development resulting in an undulating structure that contains vacuolated cells but was interrupted by additional tissue structures and surrounded by a thickened floor plate and deformed aorta (Figure 5.2A, right). Further phenotypic analysis of copper-deficient embryos also revealed impaired cartilage and vascular development (Figure 5.2B,C), an absence of hematopoiesis (Figure 5.2D) and impaired

Table 5.1 Small molecules utilized for copper homeostasis screen

AMD 3100	Clonazepam	Imidazole	Paclitaxel
Acemetacin	Clonidine	Isoniazid	Piroxicam
Acetylcholine	Ciglitazone	Itraconazole	Procainamide
N-2-(4-aminophenyl)ethyladenosine	Captopril	Indomethacin	Phenylarsine oxide
Amantadine	Carbamazepine	Kojic Acid	Reserpine
Amiloride	Cystamine	Ketamine	Ranitidine
Amiodarone	4-Chromanol	LiCl	Ritodrine
3-aminopropionitrile	Cyclophosphamide	Lithium carbonate	Reserpine
Amrinone	Cyclosporin A	Lansoprazole	Riluzole
Acetazolamide	Cyclothiazide	Loratidine	Risperidone
Allopurinol	Cyclopamine	Loperamide	Retinoic acid
Alloxan	Diethyldithiocarbamate	Mifepristone	13-cis-retinoic acid
Amitriptyline	Daidzein	Metoclopramide	Roscovitine
Astemizole	Daphnetin	Minoxidil	Ritanserlin
Aminopterin	Daunorubicin	Metformin	Scopolamine
Arecoline hydrobromide	Desipramine	Methotrexate	Salbutamol
Atenolol	Doxycycline	Mevastatin	Sulfasalazine
Actinomycin D	Dyclonine	Minocycline	Sulfanilamide
AZT (3-azido-3-deoxy thymidine)	Diethyldithiocarbamate	4-aminophenyl mercuric acetate	Sulfisoxazole
Amphotericin B	Diphenylhydantoin	Melatonin	Sulfipyrazone
Atropine	Dexamthasone	Melanin	Shikonin
Acetaminophen	Deferoxamine mesylate	Menandione	Streptozocin
Acetylsalicylic acid	Dexamethasone	Metoclopramide	Tetrakis
Artemisin	Diethylenertiaminepentaacetate	Methimazole	2,3,2-tetraamine
Bathophenanthroline disulfonate	Diltiazem	Mimosine	Tolbuamide
Benoxinate	Methyl Dopa	Methoxyestradiol	Tolmetin
Baclofen	Droperidol	Nocodazole	Thiourea
Buspirone	Dantrolene	Neocuprione	Tamoxifen
Bupropin	Domperidone	Nitro-L-arginine	Tetraethylenpolyamine
Bathocuproine disulfonate	Domperidone	NBQX	Tetraethylenepentamidine
Barium chloride	Diazepam	Nalidixic acid	Tetracycline
2-Hydroxy-5-sulfobenzoate	Dobutamine	Oxypurinol	Thalidomide
Clomipramine	Disulfiram	Omperazole	Triethylenetetramine
Clotrimazole	Eserine	N-phenylthiourea (PTC - phenylthiocarbamide)	
Chloroquine	Etoposide	1-phenyl-3-2-thiazolyl-2-thiourea	
Cadaverine	Etodolac	Pentamidine	
Cysteine	Erythromycin ethylsuccinate	Phenoxybenzamine	
Cisplatin	Furosemide	Propranolol	
Colchicine	Fluphenazine	Picrotoxin	
Caffeine	Fenofibrate	Phenelzine	
Copper chloride	Glutathione	Pentoxifylline	
Camptothecin	Gemfibrozil	Phenylephrine	
Chlorambucil	Glybenclamide	Pirenzepine	
Chlorothiazide	Genistin	Phloridzin	
Cimetidine	Genistein	Phloretin	
	Hypoxanthine	Prazosin	
	Hydralazine	Primidone	
	Haloperidol	Promethazine	
	Hydroxyzine	Pyrrolidine dithiocarbamate (ammonium)	
	Hydroxyurea		
	2-amino-7-phosphoheptanoic acid		

Table 5.2 Small molecules perturbing copper homeostasis

Disulfuram (Antabuse)

N-phenyl thiourea

Neocuproine

Clonazepam (Klonopin)

Diethyldithiocarbamate

Pyrrolidine dithiocarbamate

1-phenyl-3-(2-thiazolyl)-2-thiourea

neurogenesis affecting both the midbrain-hindbrain region of the developing brain (Figure 5.2E) as well as the primary motor neurons (Figure 5.2F). Interestingly, the hematopoietic defect involved multiple cell lineages (data not shown) analogous to what is observed in mammalian copper deficiency, although the mechanisms of this effect are not well understood. These identical phenotypes were observed with each of the other small molecules identified in this screen and in all cases were prevented by treatment with 25 μ M copper chloride dissolved in the egg water at 5 hours post fertilization (hpf) but not other transition metals including zinc, iron, cobalt, cadmium and molybdenum (data not shown). These findings also reveal that copper readily enters the embryo from the surrounding water, presumably entering cells through plasma membrane transport, although the route and mechanism of this process is unknown.

These phenotypes of copper deficiency were readily demonstrable following relatively short and early incubation times with the small molecules suggesting a mechanism of action that permanently renders copper inaccessible to the embryo (Figure 5.3). Surprisingly, careful observation of embryos treated for brief time periods (Figure 5.3A-D) or with submaximal doses of drugs (Figure 5.3E-F) revealed that the threshold of drug for each aspect of the phenotype differed. Thus, while untreated embryos had normal notochords and melanin pigmentation (Figure 5.3A), treatment for 10 min in 10 μ M neocuproine resulted in absence of melanin pigment but a normal notochord (Figure 5.3B). When such treatment was extended to 20 min the notochord was clearly abnormal (Figure 5.3C), and by 60 min the entire phenotype including the enlarged hindbrain ventricle was observed and did not worsen with longer treatment (Figure 5.3D). Similarly, embryos incubated continuously starting at 3 hpf in 100 nM neocuproine

Figure 5.2. Copper-deficient embryos display a pleiotropic phenotype. DIC image of notochord from a control embryo at 28 hpf (A, left) reveals normal development of the central canal (c), floor plate (f), notochord (n), and aorta (a), while a copper-deficient embryo of the same age treated with neocuproine (NeoC) (A, right) shows malformations including distorted floor plate (arrow), undulating notochord, additional tissue structures (arrowhead), and displaced aorta. Alcian blue staining of 96 hpf control (B, left) and copper-deficient (B, right) embryos reveals reduced cartilage formation with compression (arrowhead) and impaired jaw elongation. At 48 hpf, *fli1*:GFP copper-deficient embryos (C) exhibit disorganization of the intersegmental vasculature with microaneurysms (arrowheads). O-dianisidine staining at 72 hpf (D) reveals a marked decrease in hematopoiesis (arrowheads) in a copper-deficient embryo (top) compared to control (bottom). DIC image at 32 hpf reveals an abnormal midbrain hindbrain boundary (arrowheads) in copper-deficient (E, right) versus control (E, left) embryos. Antibody staining (*Znp-1*) reveals loss of primary motor neurons (arrow) and associated axons (arrowhead) in copper-deficient (F, right) versus control (F, left) embryo at 28 hpf.

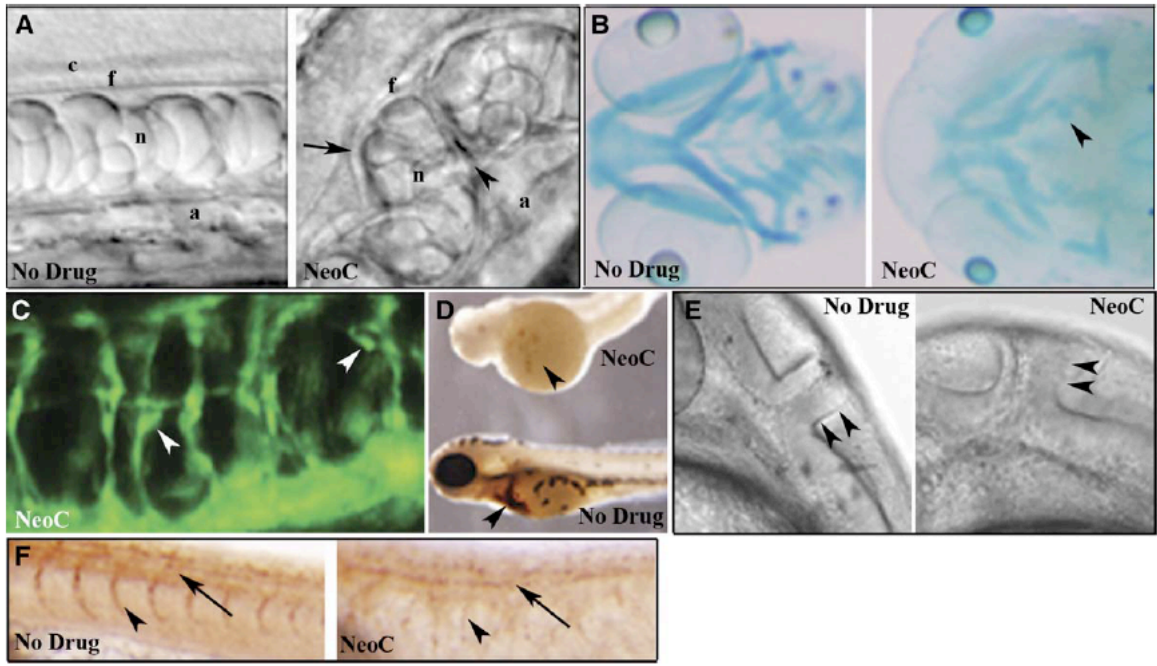
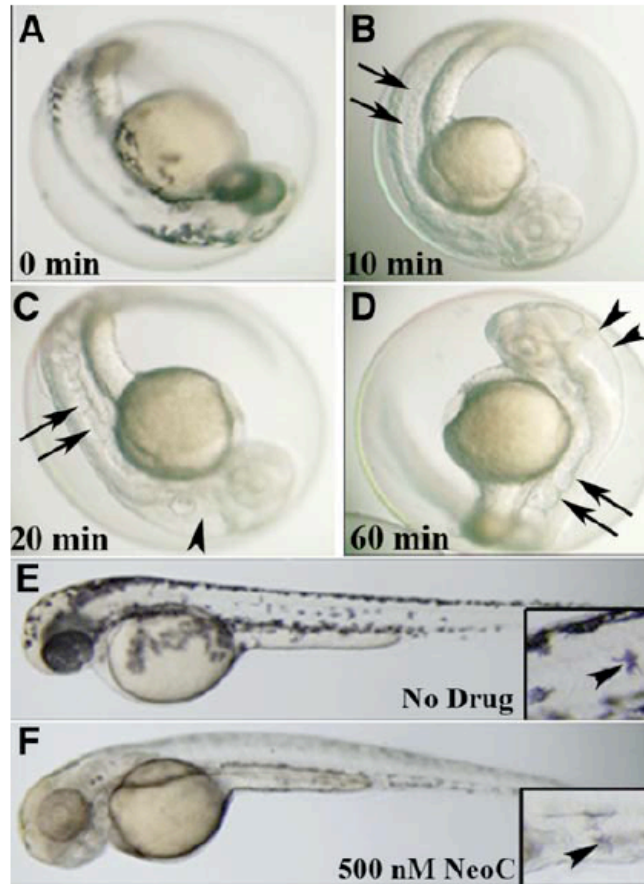


Figure 5.3. Small-molecule effects are rapid, saturable, and dose and time dependent. Examination of embryo at 48 hpf following no treatment reveals normal melanin pigmentation and notochord (A), while treatment with 10 mM neocuproine for 10 min at 3 hpf abrogates melanin pigmentation but does not affect the notochord (arrows) (B). Treatment with 10 mM neocuproine for 20 min starting at 3 hpf reveals both abrogated pigmentation, enlarged hindbrain ventricle (arrowhead), and a wavy notochord (arrows) (C). Treatment with 10 mM neocuproine for 60 min at 3 hpf does not increase the severity of the pigment, notochord (arrows), or ventricle (arrowheads) phenotype (D), indicating that the effect is saturable. Untreated 48 hpf embryo (E) shows the normal distribution of melanocytes with melanin pigmentation (inset, arrowhead) and normal notochord, while treatment at 3 hpf with 500 nM neocuproine (one-twentieth of the dose of neocuproine resulting in the complete phenotype) (F) impairs only melanin pigmentation (inset, arrowhead).



appeared normal, while treatment with 1 μ M drug prevented pigmentation but did not affect the notochord. These findings reveal a hierarchy of copper distribution within the developing embryo that may reflect specific metabolic adaptations based upon the availability of this metal and the essential requirements of each diverse biochemical pathway.

Copper deficiency phenocopies *calamity*^{vu69}

To further understand the molecular genetic basis of such metabolic adaptations in copper homeostasis during embryogenesis, we next interrogated a genetic screen for mutant embryos phenocopied by copper deficiency. Utilizing an ENU-mutagenesis genetic screen, we identified *calamity* (*cal*^{vu69}) (Figure 5.4A,B), a recessive lethal mutant with a striking resemblance to the chemically-induced copper-deficient phenotype, particularly the lack of melanin pigment and wavy notochord. Initial mapping experiments localized *cal* to a region of chromosome 14, 3.5cM from the *knypek/glypican 4* locus (Topczewski et al., 2001), in proximity to a gene suggested by a BLAST search to encode a copper-transport ATPase. Phylogenetic analysis (Figure 5.4C) and sequence comparison (Figure 5.5) indicate that this ATPase identified on chromosome 14 is the ortholog of the human Menkes disease gene, *ATP7A*. A second zebrafish ATPase identified in the BLAST search is the ortholog of the human Wilson disease gene, *ATP7B* (Figure 5.4C). As Menkes disease is in part characterized by reduced melanin pigmentation, we considered *atp7a* to be a candidate gene for the locus mutated in *cal*. Sequence analysis of the zebrafish *atp7a* gene from *cal* mutant embryos identified a mutation creating a cryptic splice acceptor in the intron before exon 9 (Figure 5.4D),

Figure 5.4. The zebrafish mutant *calamity*^{vu69} is defective in the zebrafish ortholog of the Menkes disease gene and is phenocopied by copper deficiency. (A and B) Copper-deficient embryo (A) and a *cal* homozygote (B) at 48 hpf. (C and D) Phylogeny of copper-transport P type ATPases (C) displayed as maximum-likelihood tree with bootstrap values as shown. Aligned nucleotide sequence chromatograms (D) from genomic DNA from a portion of the *atp7a* gene from wildtype, *cal* heterozygote, and mutant embryos reveals a T/A transversion (box) in the intron 50 to exon 9. (E) Analysis of cDNA reverse transcribed from mRNA reveals that this mutation acts as a cryptic splice acceptor causing the insertion of seven nucleotides (TTCTCAG) into the mRNA. (F) Restriction digests of a region amplified from *atp7a* cDNA reveal a novel DdeI site corresponding to the 7 bp insertion at the *cal* locus (arrowheads).

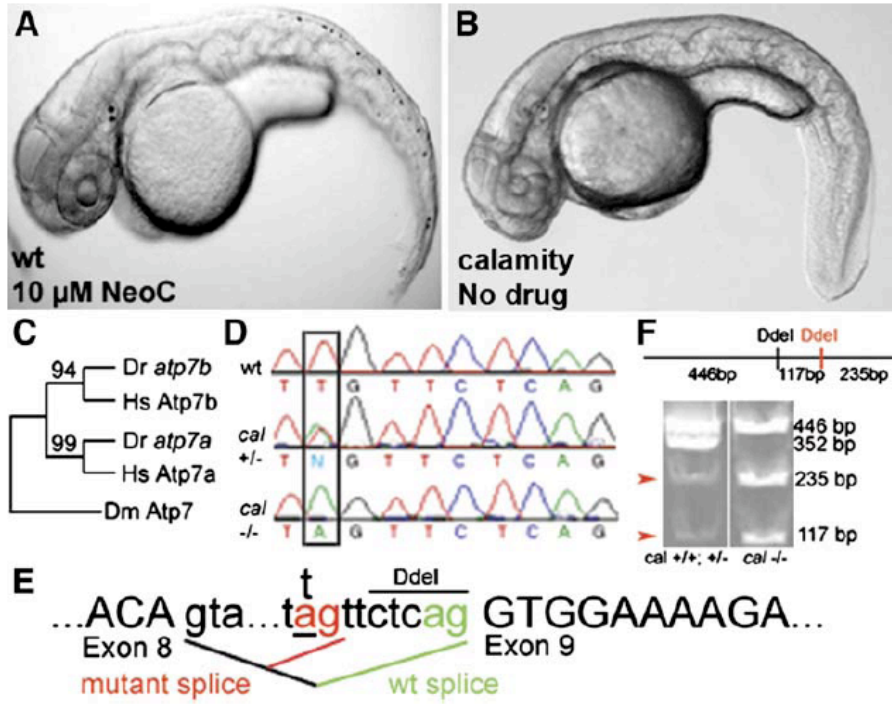


Figure 5.5. Alignment of amino acid sequence of human and zebrafish *atp7a*. Sequence alignment reveals 64.5% identity with marked conservation of CPC copper transport domain (underlined in black), all 6 MXCXXC copper-binding motifs (underlined in red), the invariant aspartate (underlined in blue) and the conserved SEHPL sequence required for trafficking (underlined in green).

DrATP7a HALSTNLCRVTLGVEGHTCGSCVQSTIEGRIGGPGVVIHQVSLQNNATVYIHTQHTTQSADAIEDMGFESSLTHATSTPVQTEKVF 90
 HsATP7a MDPSHGQNSVTISVEGHTCNSCVWTIEQQIGRWNGVHHIKVSLLEKRNATHIYDPKIQTKTQEAIDDMGFDAVHHMDDPLPVLTDTLFL 90

DrATP7a SKAGCSADSVQQAALSTLAQIKGVIEIQESADNOGLAVTIVFSPVSEDOQGEVVKCLAFDTACRPFLLSFKEGSTSRSTSGVEATKMRTEGM 180
 HsATP7a TVTASLTLPLWDHIQSTLLKTKGVTDIKIYYPKQRTAVTIIHPSVFNANQRELVPESLDTGTLEKRSACACEDHSMQAAGIVVKKMKVEGH 180

DrATP7a VCLSCSTTIEGKIGKLGVEIKIKVSLSESQEAAMVYVPIITVDFIVKQIEVAGFKATVFSKPRQLKLSAIFVERLLSAPKOTSEKLS-- 268
 HsATP7a TCHSCTSTIEGKIGKLGQVQRIKVSLEDNQEAITVYQPHLISVEMKQIEAMGFPAFVHKQPHYLKLGATLVERLKNTPVKSSEGSQQRS 270

DrATP7a PPAADSTVITLFOVITGMHCNSCVVNIQDNISKLPVAVTSVVVSLNROASIQHNPKQVSVVELOKAIEALPPGNFKAITPASPPEPG----- 352
 HsATP7a PSYTNDSATFIIIDGMHCNSCVVNIESTLSALQYVSSIVVSLNRSATIKYVNASSTPESLRKAIEAVSPGLYRVSTSEVESTSNPSS 360

DrATP7a -----FLQPLVSVAEIHIEGHTCGSCVQSTIEGTLISCKKGVRSQAQVSLANHQGTFEYDPLLTSPHELRAAIEDMGFADLPETNSL 432
 HsATP7a SSLQKIFLNVSQPLTQETVINIDGHTCNSCVQSTIEGTLISKRFVGRSIRVSLANSNGTVEYDPLLTSPETLRGAIEDMGFADLSDTN-- 448

DrATP7a VPSVVKSPSPSVSSLSPVRSVAVKENEAESDAEPTNIIKSKFIQIGGHTCASCVANIERNLKNEVGIHSLVALHASKAEVRYSPSVI 522
 HsATP7a -EPHVVIAQPSSEMPLLTSTNEFYTKGMTPVQDKEEGKSSKCYIQVGTGHTCASCVANIERNLREEGTIVSHLVALHAGKAEVRYVPAVI 537

DrATP7a DPLRIAELEIRELGFHATVMDNYDGS DGSLELVVRGHTCASCVHKIESNLKQHGILYASVALSTNKAKIKYDPEVIGPRDIIILLENMGI 612
 HsATP7a QPHIAEPIRELGFATVMDNADGDGVLELVVRGHTCASCVHKIESLTKHGHILYCSVALSTNKAKIKYDPEVIGPRDIIITISLGF 627

DrATP7a TASLVKDRPGSHLDHREIRQVRSFQISLFFCVPVGMNIYVIVVDHMDIKYHGHATAEDRAKYHSTMFLEKOLLPGLSTMNLSF 702
 HsATP7a EASLVKDRSASHLDHREIRQVRSFVLSLFFCIPVGMNIYVIVVDHMFATLHNNQMSREMINLHSMFLERQILPGLSMNLSF 717

DrATP7a LFCVVPQFVGGRYFYVQAYKAKKHTANMDVLIVLATTIAFYVSVVLLVAMVERAKVNPITFFDTPPHLFFVIALGRWLEIAKSKTSE 792
 HsATP7a LFCVVPQFVGGRYFYVQAYKAKKHTANMDVLIVLATTIAFYVSLIILLVAMVERAKVNPITFFDTPPHLFFVIALGRWLEIAKSKTSE 807

DrATP7a ALSKLSLQATEATVTLNEDHSLVSEEQVDVELVQRGDVKVVPVGGKFPVDGRVIEGSHADESLITGEAMPVTKKPGSTVIAGSINQN 882
 HsATP7a ALAKLSLQATEATVTLNEDHSLVSEEQVDVELVQRGDIKVVVGGKFPVDGRVIEGSHADESLITGEAMPVAKKPGSTVIAGSINQN 897

DrATP7a GSLLIKATHVGDITTLTSLQIVKLVEEAQTSKAPIQQFADKISSYFVFPFIVVSNLTLTLLAVIIGFVNFSLVQTYFPGDKSISEAEAVIRF 972
 HsATP7a GSLLIKATHVGDITTLTSLQIVKLVEEAQTSKAPIQQFADKISSYFVFPFIVVSNLTLTLLAVIIGFVNFSLVQTYFPGDKNRISRTETIRF 987

DrATP7a AFQASITVLCIACPCSLGLATPTAVNVGTGVGAQNGILIKGGEFLEMAHKIKQSVVFDKTGTITTYGAPHVVQVKKLAEGRNLPKSLLAIV 1062
 HsATP7a AFQASITVLCIACPCSLGLATPTAVNVGTGVGAQNGILIKGGEFLEMAHKVQVVFDKTGTITHTGTPVNVQVKKLAEGRNLPKSLLAIV 1077

DrATP7a GTAENSSEHPLGTAITKYCKQELGTESLCTCFDFCAVPGCGIISCLVSNTEENLKRKEDSDISEENQHNVAVLQISDAR--AHSTHPLTMDP 1150
 HsATP7a GTAENSSEHPLGTAITKYCKQELDTELTGTCDFQVVPGCCGISCKVTEHGLLHKNNWNIEENNIKNASVQIDASNEQSSSTSSSHIDA 1167

DrATP7a QPLTVVQTASYIVLIGNREWHRNALQVRADVDEAMTEHERRGCTAVLVAVDMELCAMVAIADTVKPEAEALAVHVLSSMGLLEVVLHTGDN 1240
 HsATP7a QISNALNAQQYKVLIGNREWHRNGLVINNDVNDFNTEHERRGCTAVLVAVDMELCGLVAIADTVKPEAEALAHILSSMGLLEVVLHTGDN 1257

DrATP7a SKTARIAAQVGIKRVFAEVLPSHKVAKVEQLQQAQKRVAMVGDGNDSPALAMAVGIAIGTGDVAIEAADVLLIRNDLLDVVGSIDL 1330
 HsATP7a SKTARIAAQVGIKRVFAEVLPSHKVAKVEQLQQAQKRVAMVGDGNDSPALAMAVGIAIGTGDVAIEAADVLLIRNDLLDVVASIDL 1347

DrATP7a SKKTVKRIRINVFVALLHYNLVGPIAAGVFMVGLVLPQPMGSAAHALSSVSUVLSSLILKCVTRPTVEKLRRLGDVVRTHGSLSDVSVH 1420
 HsATP7a SKKTVKRIRINVFVALLHYNLVGPIAAGVFMVGLVLPQPMGSAAHALSSVSUVLSSLILKCVTRPTVEKLRRLGDVVRTHGSLSDVSVH 1437

DrATP7a IGHGELRRPSPKLSLLDRFVNYSRASINSLSDKHSNNSHALSEPDKHSLLVGDDHCDNIV- 1482
 HsATP7a VCHDITSRNSPKLGLLDRFVNYSRASINSLSDKRSNNSVVTSEPDKHSLLVGDFHEDDITL 1500

inserting 7 additional bases into the mRNA and causing a frameshift and premature stop codon at amino acid 674 of 1482 (Figure 5.4E). The resulting open reading frame, if translated, would lack all transmembrane and catalytic domains, and would therefore be nonfunctional. Restriction digestion of a fragment PCR-amplified from zebrafish *atp7a* cDNA revealed the absence of wild-type message in *cal* homozygous mutant embryos and a mixture of wild-type and mutant mRNA in their siblings (Figure 5.4F).

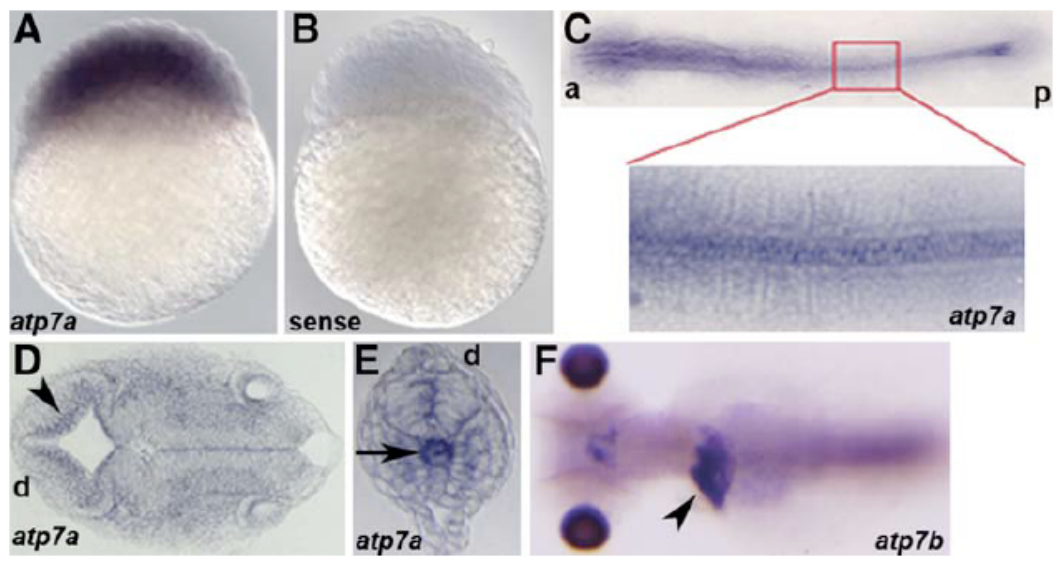
The expression pattern of zebrafish *atp7a* correlates with observed phenotypes

In situ hybridization with a probe to zebrafish *atp7a* revealed ubiquitous and early expression (Figure 5.6A). A sense-control probe yielded no staining (Figure 5.6B). Later, significant expression was observed in the developing notochord with ubiquitous weaker expression in other tissues of the embryo (Figure 5.6C). Sections revealed *atp7a* expression along the ventricles (Figure 5.6D) and in the distal notochord (Figure 5.6E) at 24 hpf. These patterns of expression correlate with the observed *cal* phenotype. A probe to the zebrafish ortholog of the Wilson disease protein at 5 dpf revealed expression in the liver (Figure 5.6F), consistent with the known expression pattern of *ATP7B* in mammals and demonstrating the conservation of liver-specific expression across metazoans over millions of years of evolution.

Rescue of *calamity* with human ATP7A and assessment of cell autonomy

To confirm the role of *atp7a* deficiency in the *cal* phenotype, synthetic RNA encoding human ATP7A was injected into the zygotes from a *cal* heterozygous cross, significantly suppressing pigmentation and notochord defects in genotypically-mutant

Figure 5.6. Expression pattern of *atp7a* via in situ hybridization. Anterior (a), posterior (p), and dorsal (d) are as indicated. (A) *atp7a* message is present in all cells at 3 hpf. (B) Staining is specific, as a sense-control probe does not show staining. (C) At 8 somites, *atp7a* is expressed most abundantly in the notochord and is expressed ubiquitously at lower levels. (D and E) Sectioning at 24 hpf reveals staining along the ventricle (D) (arrowhead) and in the distal notochord (E) (arrow). (F) In situ analysis of *atp7b* reveals expression in the liver (arrowhead) in a 5 dpf embryo as shown in this dorsal view.

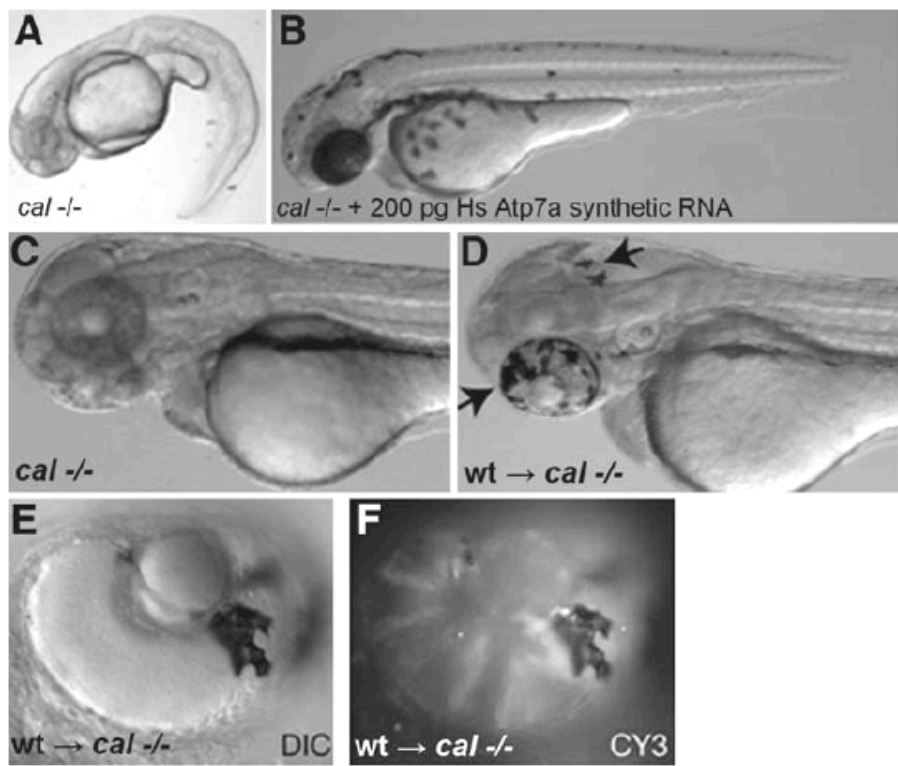


embryos (Figure 5.7A). In three separate experiments, 72% of *cal* embryos were entirely rescued by this approach (Figure 5.7B) while the remainder displayed some normalization of pigmentation and notochord structure. Mechanisms of iron homeostasis have been conserved between humans and zebrafish over millions of years of evolution (Donovan et al., 2000). The restoration of complex developmental phenotypes following expression in the zebrafish of the orthologous human copper transporter similarly demonstrates the functional evolutionary conservation of the genetic and biochemical mechanisms of copper metabolism and provides for a unique experimental system to assess the function of genetic variants of the human Menkes copper transporter. The availability of a vertebrate model of Menkes disease in an organism where embryonic cell transplantation is possible allowed for a direct analysis of the requirement for *atp7a* in inter- and intra-cellular copper transport during development. Therefore, we transplanted cells from wild-type donors into *cal* embryos to assess the cell autonomy of the genetic defect. *cal* ^{-/-} embryos lack melanin pigmentation (Figure 5.7C) while in contrast 35 out of 48 *cal* embryos from three separate transplantation experiments exhibited pigmented donor melanophores or retinal pigment epithelium (Figure 5.7D-F). Most interestingly, these transplantation experiments reveal that zebrafish Atp7a acts cell autonomously in melanocytes, suggesting that it is required for proper copper utilization in individual cells and may not be essential for copper transport from the yolk sac or within the embryo.

Gene dosage of zebrafish *atp7a* determines the sensitivity to copper deprivation

The developmental hierarchy of copper metabolism observed in embryos treated

Figure 5.7. Rescue of *cal* with human ATP7A and transplantation experiments. The *calamity* mutant phenotype (A) is rescued by injection with synthetic RNA encoding the human Menkes ATPase (B). Although *cal* embryos display a complete lack of melanin pigment at 48 hpf (C), transplantation of rhodamine-dextran-injected wild-type cells into *cal* embryos (D) yields embryos mosaic for pigmented melanophores (arrows). In all cases, the pigmented cells shown here in the retinal epithelium (E) correspond to the rhodamine-labeled donor cells as detected by fluorescence for CY3 in this same epithelium (F).



with variable time or dose exposure to small molecules as well as the cell autonomy observed in the transplantation experiments suggests a complex developmental program of copper metabolism dependent upon both the availability of copper and the function of *atp7a*. To elucidate this complexity of gene-nutrient interaction we took advantage of our small molecule screen to precisely modulate copper availability in a specific genetic context. While 100 nM neocuproine did not affect melanin pigmentation in wild-type embryos (Figure 5.8A), this dose prevented melanin pigment in *cal* heterozygotes (Figure 5.8B), and worsened the notochord phenotype in *cal* homozygotes (compare Figure 5.4B and Figure 5.8C). To more precisely examine this effect, we next utilized an antisense morpholino oligonucleotide (MO) directed against a splice junction in the *atp7a* transcript at a dose that resulted in no apparent phenotype and preserved some wild-type message (Figure 5.9). Comparison of control MO-injected embryos (Figure 5.8D-G) with *atp7a* MO-injected embryos (Figure 5.8H-K) at increasing doses of neocuproine revealed that knockdown of *atp7a* strikingly increased the sensitivity of zebrafish embryos to developmental copper deficiency. Most notably, a dose of neocuproine that affected neither pigmentation nor the notochord (Figure 5.8E) together with a dose of *atp7a* MO that yielded no phenotype (Figure 5.8I) caused a severe phenotype when combined (Figure 5.8J). Taken together, these findings support the hypothesis that the gene dosage of *atp7a* informs the sensitivity of each phenotype to copper deficiency.

Figure 5.8. Interaction of *atp7a* dosage and developmental copper deficiency. (A and B) Wild-type embryos appear normal in 100 nM neocuproine (A); *cal* heterozygotes display loss of all melanin pigment at this same dose (B). (C) The pleiotropic phenotype of copper deficiency is observed in all *cal* homozygotes in 100 nM neocuproine. (D–K) Embryos injected with control MO (D–G) display a phenotypic dose-response curve in neocuproine of the notochord (arrowheads) and melanin pigment (arrows) that is altered in embryos injected with *atp7a*-targeted MO (H–K). All embryos were treated continuously from 3 hpf with the indicated dose of drug.

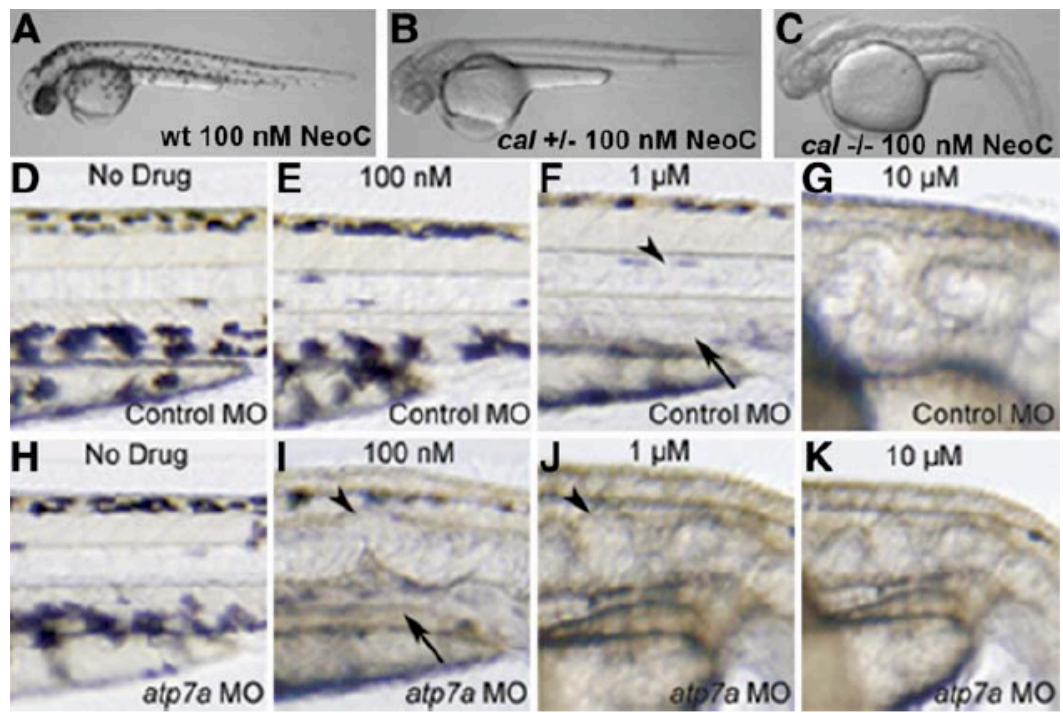
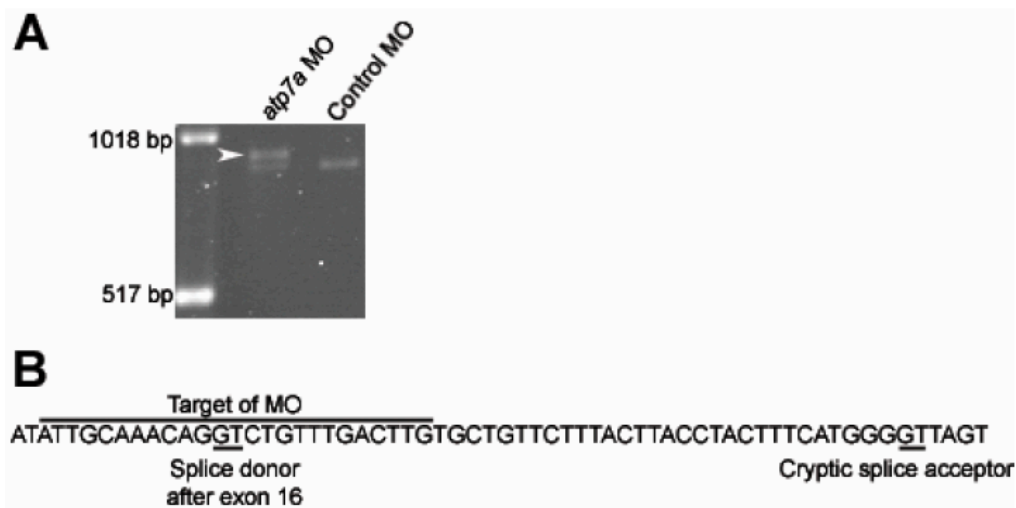


Figure 5.9. *atp7a* morpholino causes abnormal splicing of the zebrafish *atp7a* transcript. (A) PCR amplification from cDNA of the region surrounding the target of this MO reveals a single band of expected size from embryos injected with control MO, and an additional larger band (arrowhead) in embryos injected with MO to *atp7a*. (B) Sequence analysis of this band reveals a transcript resulting from a cryptic splice donor 44 nucleotides into the intron, causing a frame shift. The predicted resulting ORF, when translated, would contain 46 incorrect amino acids and terminate prematurely, removing the final 354 amino acids, including two transmembrane domains.



Discussion

In this current study, we have utilized chemical genetics combined with a genetic screen to elucidate the critical developmental and genetic requirements of copper metabolism during embryogenesis. Our findings reveal an adaptive hierarchy of copper metabolism as evidenced, for example, by the notochord abnormality, a lethal defect for the developing embryo, that is preferentially preserved when copper availability is limited (Figure 5.3). Presumably all such developmental events ultimately depend upon the incorporation of copper into specific cuproenzymes and thus the mechanisms of this adaptive metabolic hierarchy must arise from differences in either the localization of copper to embryonic structures or the relative affinity of intracellular copper transporters, chaperones or specific cuproenzymes for this metal (Bertinato and L'Abbe, 2004). This differing threshold of drug for each aspect of the phenotype is not due to differences in tissue penetration as treatment is initiated prior to any significant differentiation (Figure 5.3). Our genetic studies suggest that the sensitivity of each phenotype to copper deficiency is determined by gene dosage of *atp7a* (Figure 5.8), while the transplantation experiments reveal that this sensitivity is cell-autonomous such that any cell with sufficient Atp7a for the given availability of copper will produce active cuproenzymes (Figure 5.7). These observations suggest that in the developing embryo, as copper becomes limiting, tissues expressing higher levels of Atp7a would be advantaged, and in support of this concept *in situ* analysis reveals that *atp7a* mRNA is most abundantly expressed in the notochord and ventricles (Figure 5.6) paralleling the observed hierarchy of sensitivity to copper deficiency.

The notochord is the defining structure of chordates and has essential roles in vertebrate development as a skeletal element and in the patterning of the surrounding tissues (Stemple, 2005). Our data demonstrate that copper is essential for notochord formation (Figure 5.2) and raise the interesting possibility that some of the vascular and neurologic abnormalities observed in the offspring of copper-deficient animals and patients with Menkes disease may result from patterning defects secondary to notochord abnormalities. While we have not elucidated the mechanisms of impaired notochord formation in copper deficiency, recent studies in *Xenopus laevis* demonstrate abundant expression of lysyl oxidases within the developing notochord (Geach and Dale, 2005), suggesting that we may have uncovered a role for these cuproenzymes in connective tissue biosynthesis critical for notochord development (Csiszar, 2001). In mammalian cells, lysyl oxidases are synthesized within the secretory pathway of mesenchymal cells where copper incorporation is dependent upon ATP7A (Voskoboinik and Camakaris, 2002), a finding that would support the hypothesis that the abnormal notochord formation in *cal* (Figure 5.4) arises from impaired lysyl oxidase activity. In humans, the notochord eventually becomes ossified in regions forming vertebrae and contributes to the nucleus pulposus of the intervertebral discs (Linsenmayer et al., 1986). Our observations that copper is essential for notochord structure raise the intriguing possibility that suboptimal copper availability either due to dietary factors or genetic variation in *ATP7A* or lysyl oxidases during the period of notochord formation or subsequent ossification may contribute to structural birth defects such as congenital scoliosis where axial skeletal structure is impaired (Blank et al., 1999).

calamity is a newly-described zebrafish mutant and a useful model of Menkes disease. Our data demonstrate that *cal* is phenocopied by copper-deficiency (Figure 5.4), a finding to be anticipated in any legitimate model of this disorder. Importantly, while a well-established mammalian model of this disease exists in the *mottled* mouse, the rapid external development of the optically clear zebrafish embryo permits a precise characterization of the genesis of developmental abnormalities and allows for cellular and genetic manipulations such as transplantation (Figure 5.7) not possible with *in utero* development. Indeed, our observation of the cell-autonomy of this disorder suggests that therapeutic strategies focused upon tissue-specific gene replacement may be a legitimate approach in affected patients. Furthermore, consistent with the observation of cell-autonomy, exogenous CuCl_2 did not improve the *cal* phenotype. The discovery of a zebrafish model of Menkes disease now permits high-throughput chemical suppression screens (Peterson et al., 2004; Stern et al., 2005) for compounds that restore cuproenzyme function in the setting of a deficiency of the Menkes Atpase, an approach also not possible with the existing murine models. Such drugs would be of immediate clinical relevance.

The relevance of nutrition during development is revealed by recent data highlighting the importance of folate intake before and during pregnancy for preventing neural tube defects (Copp et al., 2003). Despite these observations, the metabolic factors that place specific pregnancies at higher risk remain unknown. Having described the gene-nutrient interactions of copper metabolism and *atp7a* during development, our findings demonstrate the potential of chemical and genetic screens to elucidate the

metabolic and genetic interplay of other nutrients that may provide insight into the roles of suboptimal nutrition and genetic variation in human birth defects.

Acknowledgements

J.D.G. was supported by HD39952, L. S-K. was supported by GM55101, S.L.J. was supported by GM56988.

Experimental Procedures

Zebrafish maintenance and analysis

SJD and C32 strains were utilized to obtain large numbers of synchronously *in vitro* fertilized zebrafish eggs. Embryos were maintained and staged as described previously (Kimmel et al., 1995). The *fli1:EGFP* transgenic fish are described elsewhere and were generously provided by Brant Weinstein (Motoike et al., 2000). *calamity*^{vu69} arose from an ENU-mutagenesis screen for mutants defective in gastrulation and is in the AB/TL background (Solnica-Krezel et al., 1994). Eggs from individual females were collected, and fertilized *in vitro* with sperm and allowed to develop at 28.5°C. Synchronized wild-type developing embryos were arrayed as three embryos per well in 96-well plates containing 180 µl of embryo buffer supplemented with methylene blue and ampicillin. Differential interference contrast images (DIC) were obtained using an Olympus IX71 microscope fitted with a Nomarski objective and images were acquired with a TH4-100 camera and Olympus microsuite software. Fluorescently labeled embryos were visualized utilizing a laser scanning confocal microscope (BX61WI

FV500; Olympus), equipped with argon 488 13 and krypton 568 lasers utilizing the 10X objective. Representative fish were imaged using identical confocal settings and serial Z stacks were acquired using a pinhole aperture of 150 μM . Images were collected with Fluoview software (Olympus).

Pharmacologic compounds

Approximately 250 small molecules representing all of the major classes of compounds used in clinical medicine as well as a series of known metal chelators were purchased from Sigma, prepared as 5mg/ml stocks in dimethyl sulfoxide and then transferred as 20 μl aliquots into individual wells, followed by dilutions to ranges from 1 mM to 1 nM for each drug. In addition, an array of pharmacologically active small molecules (Sigma Chemical Company, St. Louis, LOPAC¹²⁸⁰) was utilized at 1000-fold dilution for a final concentration of 10 μM . All small molecules were added to the arrayed zebrafish embryos at the 256-cell stage unless otherwise stated and embryos were examined with an Olympus SZX12 stereomicroscope at 1, 2, and 3 days post fertilization (dpf). Phenotypes were recorded when exhibited by each embryo in the well (Peterson et al., 2000b). For those drugs identified as potentially interfering with copper homeostasis on the basis of lack of melanin pigment at 2 dpf, this analysis was repeated in the presence of 25 μM CuCl_2 dissolved in the media.

Immunohistochemistry and in situ hybridization

Embryos raised in phenylthiourea were dechorionated and fixed in 4% paraformaldehyde/PBS for 4 hr at RT or overnight at 4° C. Embryos were washed in

PBS, then water, and permeabilized for 7 min in -20° acetone, followed by washes in water. The embryos were then blocked for 30 min in PBS/1% DMSO/0.05% Tween-20/10% FBS, and incubated overnight in Znp-1 (1:500) antisera (Developmental Studies Hybridoma Bank) in the blocking solution. The antibody was removed and the embryos washed extensively for 2 hr (Schulte-Merker et al., 1992). Staining was carried out using the Vectastain anti-mouse IgG peroxidase assay (Vector Laboratories) according to manufacturer's instructions. To generate an in-situ probe, a 1.6 kb region corresponding to nt 807 - 2467 of the zebrafish *atp7a* cDNA was PCR amplified and used as template to prepare a probe using the DIG-labeling kit (Roche). Various stage embryos were collected and fixed in fresh 4% paraformaldehyde overnight at 4°C, dechorionated, dehydrated with an ascending methanol series (30%, 50%, and 100%) and stored in methanol at -20°C overnight. In-situ hybridization was performed as previously described (Thisse et al., 1993).

Alcian Blue Staining

Embryos at 4 dpf raised in phenyl-thiourea (PTU) were fixed overnight in 3.7% formaldehyde/PBS, rinsed in PBT (PBS, 0.1% Tween-20), and stained overnight in 0.1% Alcian Blue (Sigma) dissolved in 80% ethanol and 20% glacial acetic acid. Embryos were then rehydrated in ethanol:PBT to 100% PBT, and cleared in 0.05% trypsin in PBS for 1.5h at RT, followed by several washes in PBS. Embryos were gradually transferred to 70% glycerol and visualized (Detrich et al., 2004).

Dianisidine Staining

Dechorionated 3 dpf embryos were stained at RT for 15 minutes in 2.0 ml o-dianisidine (100mg/70 ml ethanol), 0.5 ml 0.1M acetate buffer (pH 4.7), 2.0 ml deionized water, 0.1 mL hydrogen peroxide (30%), followed by rinsing in water (Iuchi and Yamamoto, 1983).

Tyrosinase Assay

96 hpf embryos were de-yolked and lysed in protein extraction buffer (10 mM Tris, pH 7.4, 2% Triton-X 100) plus protease inhibitor cocktail (Calbiochem) for 30 min on ice. 100 µg of lysate without beta-mercaptoethanol or boiling was run on a 10% SDS gel and assayed for tyrosinase activity as described (Orlow et al., 1993).

Calamity Sequence Analysis

RNA was isolated from 48 hpf *cal* mutant and wild-type siblings using the Trizol method (Invitrogen). First-strand cDNA was generated using the SuperScript III kit (Invitrogen). Gene-specific PCR primers were created using available genomic cDNA sequence, and were used to amplify two fragments encompassing the zebrafish *atp7a* open reading frame, which were then cloned into the TA cloning vector pCRII (Invitrogen). The insert was sequenced using internal primers and primers to the flanking vector sequence. A 798 kb PCR product surrounding the 7 bp insertion was amplified from *cal* mutant cDNA and from wild-type sibling cDNA, digested with DdeI (NEB) for 3 hours, and run on a 5% polyacrylamide gel. Phylogenetic analysis of zebrafish copper transport P-type Atpases was determined using neighbor-joining and maximum likelihood methods to construct trees (Felsenstein). Accession numbers as follows: *Homo*

sapiens ATP7A, gi:1351993; *Homo sapiens* ATP7B, gi:55957861; *D rerio* *atp7a*, gi:70724999; *D rerio* *atp7b*, FGENESH00000051998; *D melanogaster* *Atp7*, gi:45446920.

Cloning of zebrafish *atp7a*

Putative exons encoding the zebrafish *atp7a* gene were found by TBLASTN from the Ensembl zebrafish genome website (http://www.ensembl.org/Danio_rerio/) available as of January 2005. 5' RACE was used to identify the first exon. The primers used were: forward primer 5'-CGAAGAATGGCGCTGAGCAC-3' and reverse primer 5'-GCTCCAGAGACCCTCAGACT-3'. These primers were used to amplify from 32 hpf cDNA, and the resulting product was completely sequenced. The coding sequence has been deposited into GenBank with the accession number DQ100352. Alignment of the zebrafish *atp7a* amino acid sequence to human sequences were performed using ClustalW (Thompson et al., 1994).

Morpholino and mRNA Injection

A morpholino oligonucleotide (Nasevicius and Ekker, 2000) (MO) 5'-CAAGTCAAGCAGACCTGTTTGCAAT-3' targeting the splice donor site following exon 16 (Gene Tools) was synthesized, dissolved in Danieau's buffer/Phenol Red and injected into 1-4 cell embryos as 12 ng MO per embryo. A second MO (5'-TTAGTGCTCAGCGCCATTCTTCGTC-3') targeting the start codon of *atp7a* yielded a similarly increased sensitivity to neocuproine. A standard control MO (Gene Tools) was injected in parallel at the same dose. Synthetic RNA encoding the human Menkes Atpase

was generated from pJFM19 using the T7 mMessage mMachine kit (Ambion), and polyadenylated with the Poly(A)-Tailing Kit (Ambion). 200 pg/embryo was injected.

Transplantation

Rhodamine dextran was injected as a lineage tracer into 1-cell wild-type embryos. At the sphere stage, approximately 30 donor cells below the animal pole were transplanted into zygotes of the same age from *cal* heterozygous parents (Lin et al., 2005).

CHAPTER VI

OVERVIEW AND FUTRUE DIRECTIONS

In this thesis I described work towards elucidating the cellular and molecular basis of convergence and extension (C&E) gastrulation movements and in what manner C&E affects somite development in the zebrafish embryo. I employed time-lapse analyses and computational simulations to demonstrate that the C&E movements of the medial presomitic mesoderm (PSM) are achieved by the cooperation of polarized planar and radial cell intercalations. The radial intercalations preferentially separate anterior and posterior neighbors, presenting as a novel cellular behavior that contributes to anisotropic tissue extension. In *knypek;trilobite* (*kny;tri*) mutants in which two components of non-canonical Wnt signaling are inactivated, C&E movements are compromised: the frequencies of cell intercalations are dramatically reduced and the anteroposterior (AP) bias of radial intercalation is lost. This provides the first evidence that non-canonical Wnt signaling not only regulates cell polarity within a plane of a single cell layer, but also controls polarized cell behaviors between different cell layers. Towards identifying molecular mechanisms underlying the biased orientation of both planar and radial intercalations, I discovered that during the dorsal mesoderm C&E in zebrafish, the non-canonical Wnt signaling component Prickle (Pk) is localized at the anterior cell edge, whereas Dishevelled (Dsh) is enriched near the posterior cell membrane. The anterior localization of Pk and posterior localization of Dsh in the dorsal mesoderm of zebrafish gastrula are reminiscent of the proximal distribution of Pk and distal distribution of Dsh

in the fly wing, thus providing evidence to support the notion that the molecular mechanisms by which non-canonical Wnt/PCP pathway regulates cell polarity are conserved between vertebrates and invertebrates. Pk and Dsh expression is distributed randomly along the cell membrane in *kny* and *tri* individual mutants, and remains in the cytoplasm in *kny;tri* double mutants. The abnormal distribution of these two proteins is correlated with the defects in polarized cell intercalations in these mutant embryos. Based on the above observations, I propose that non-canonical Wnt signaling defines different properties of the AP and mediolateral (ML) cell edges to bias the orientation of cell intercalations.

By conducting cell tracing analyses and genetic manipulations, I demonstrated that C&E gastrulation movements play critical roles in multiple aspects of zebrafish slow muscle development. During gastrulation, C&E movements regulate the number of the specified prospective adaxial cells by defining the size of the interface between the inductive axial and target presomitic tissues. Shortly after the first somites form, the ML range of Hedgehog (Hh) signaling in the paraxial mesoderm declines. Convergence of the prospective adaxial cells at the time when the Hh signaling range declines ensures their continuous Hh signaling reception and fate maintenance. Later during somite differentiation, the adaxial cells undergo dramatic shape changes and subsequent lateral migration. The defective notochord properties in *kny;tri* double mutants, caused by early C&E movement defects, impede the adaxial cell shape changes and likely interfere with their lateral migration. These studies delineate discrete cellular mechanisms through which C&E gastrulation movements mediate cell fate specification and morphogenetic events during later development.

In addition, through a genetic screen for modifiers of the *kny*^{m818} phenotype, I isolated several novel mutations that affect C&E movements and early embryogenesis in zebrafish. Further molecular analyses of these mutations will contribute to our understanding of vertebrate gastrulation and embryogenesis. In a parallel standard screen, I identified the mutation *calamity*^{vu69}, which is genetically linked to the *kny* locus and impairs pigmentation and notochord development. *calamity*^{vu69} inactivates a zebrafish homolog of the human Menkes *atp7a* gene, which is critical for copper homeostasis in humans. Using genetic mosaic analyses, I showed that *atp7a* gene acts cell-autonomously in melanocytes to ensure the normal function of cuproenzymes producing melanin. This work underscores unexpected roles of copper during embryogenesis and demonstrates the potential of chemical and genetic screens to elucidate the biology of gene-nutrient interactions essential for early human development. Because *calamity*^{vu69} mutation enhances aspects of the *kny* mutant phenotype, it also affords a new tool to study interactions between copper and glypicans.

Diverse cellular behaviors underlie regional C&E movements

Previous work in our laboratory has revealed the presence of three distinct C&E movement domains in the zebrafish gastrula (Figure 6.1) (Jessen et al., 2002; Myers et al., 2002b; Sepich et al., 2005). Mesodermal cells within the ventral “no convergence no extension zone” migrate directly towards the vegetal pole, thus engaging in epiboly rather than convergence or extension movements (Figure 6.1A). In the lateral domain, mesodermal cells initially travel on meandering but dorsally oriented paths, which for

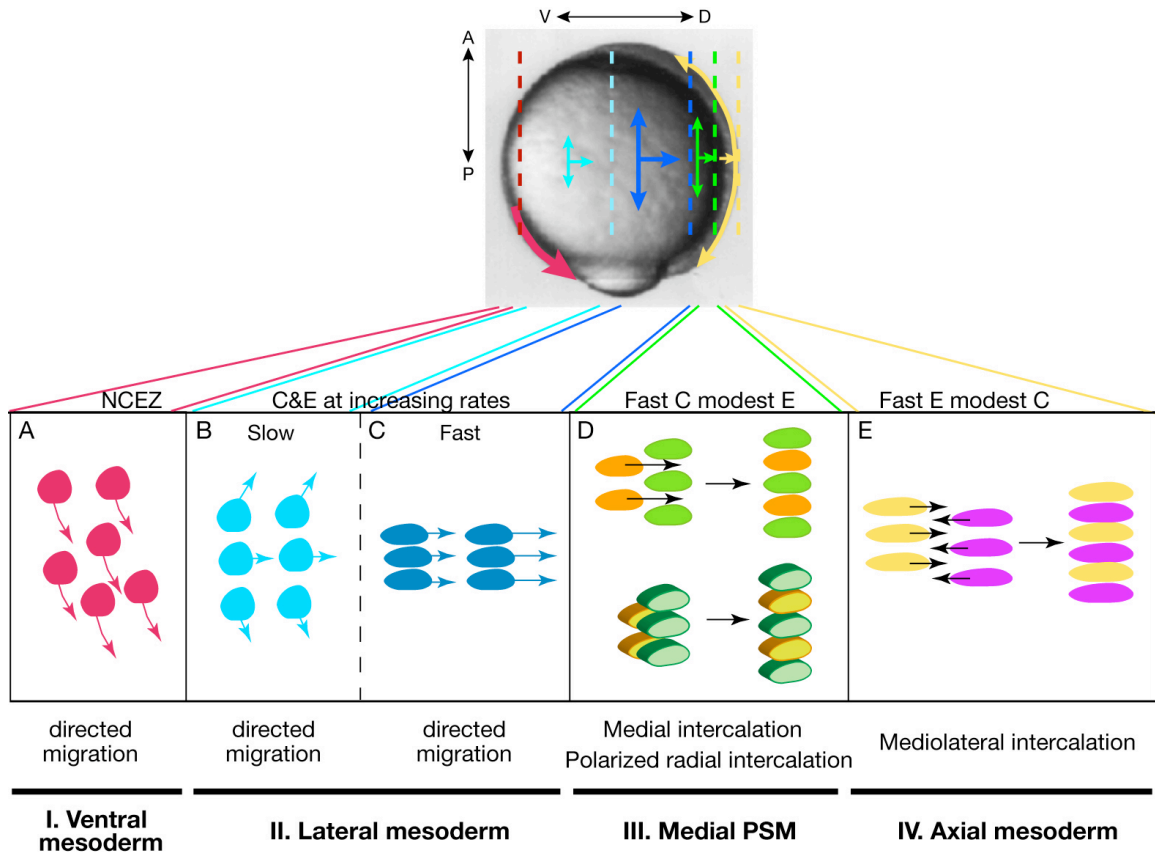


Figure 6.1. Four distinct domains of C&E movements in the zebrafish gastrula and the underlying cell movement behaviors. NCEZ, no convergence no extension zone. A, anterior. P, posterior. D, dorsal. V, ventral.

cells in more animal locations are biased animally and cells closer to the vegetal pole are biased vegetally (Figure 6.1B). This “fanning” of cell trajectories culminates in slow C&E movements (Sepich et al., 2005). As the lateral mesodermal cells move closer to the midline, they become closely packed, acquiring mediolaterally elongated morphology and orientation, and converge as a cohort at faster speeds along straight paths (Figure 6.1C) (Jessen et al., 2002; Myers et al., 2002b). Dorsally, the axial mesodermal cells undergo ML intercalation to achieve strong convergence and limited extension (Figure 6.1E) (Glickman et al., 2003; Myers et al., 2002b). Adjacent to the axial mesoderm, the medial PSM exhibits the same convergence rate as the adjacent axial mesoderm, but much lower extension rate compared to the axial mesoderm (Figure 6.1D) (Glickman et al., 2003). Therefore, it is tempting to hypothesize that the medial PSM constitutes a fourth C&E domain and its morphogenesis may involve cellular behaviors different from those observed in the other three C&E domains (Glickman et al., 2003; Keller et al., 2003). In support of this notion, I demonstrated that the C&E of the medial PSM is achieved by the cooperation of multiple polarized planar and radial cell intercalations (Figure 6.1D). The identification of multiple cell intercalation behaviors during the medial PSM C&E is unexpected and contrasts previous studies showing that C&E within distinct regions of the zebrafish gastrula is driven by one predominant cell movement behavior (Figure 6.1) (Myers et al., 2002b).

It is intriguing that during vertebrate gastrulation embryos use a limited repertoire of cell behaviors to drive the distinct morphogenetic movements, but these behaviors are employed in different geometric territories of the gastrula, and with different timing. My discovery that the medial PSM utilizes a unique set of cell intercalations to drive C&E

further demonstrates that different combinations of cell movement behaviors define the spatial pattern of C&E movements during gastrulation.

To date, the described cellular behaviors contributing to the C&E of the mesoderm, such as directed migration (Heisenberg et al., 2000; Jessen et al., 2002; Myers et al., 2002b; Ulrich et al., 2003), ML intercalation (Glickman et al., 2003; Keller and Tibbetts, 1989), and oriented cell division (Gong et al., 2004), all occur within the plane of a single cell layer (Figure 6.1 and 6.2). However, I observed three types of radial intercalations by which the medial presomitic cells from one cell layer enter another cell layer. The wild-type (WT) cells exhibit a strong bias towards the radial AP intercalation and coordinated radial/medial intercalation that promote AP extension, while the radial ML intercalation events are uncommon. In frog and fish, radial intercalation thins and spreads the blastoderm in all directions, and is recognized as the main cellular behavior underlying epibolic movements (Keller et al., 2003; Keller, 1980; Warga and Kimmel, 1990). In contrast, I showed that during zebrafish late gastrulation, the radial intercalations in the medial PSM do not produce an isotropic expansion, but rather extend and narrow the tissue. Studies in *X. laevis* reported that in the first half of gastrulation, deep mesenchymal cells in the dorsal mesoderm and the prospective posterior neural tissues undergo radial intercalations to produce fewer layers of greater length (Keller et al., 2003; Wilson and Keller, 1991). Keller and colleagues hypothesized that to generate an anisotropic expansion, radial intercalation has to occur in a polarized fashion, whereby cells intercalate primarily along one axis (Keller and Tibbetts, 1989; Wilson and Keller, 1991). In agreement with this notion, I showed that radial intercalations preferentially separate AP neighbors within the zebrafish medial PSM (Figure 6.2). My work provided

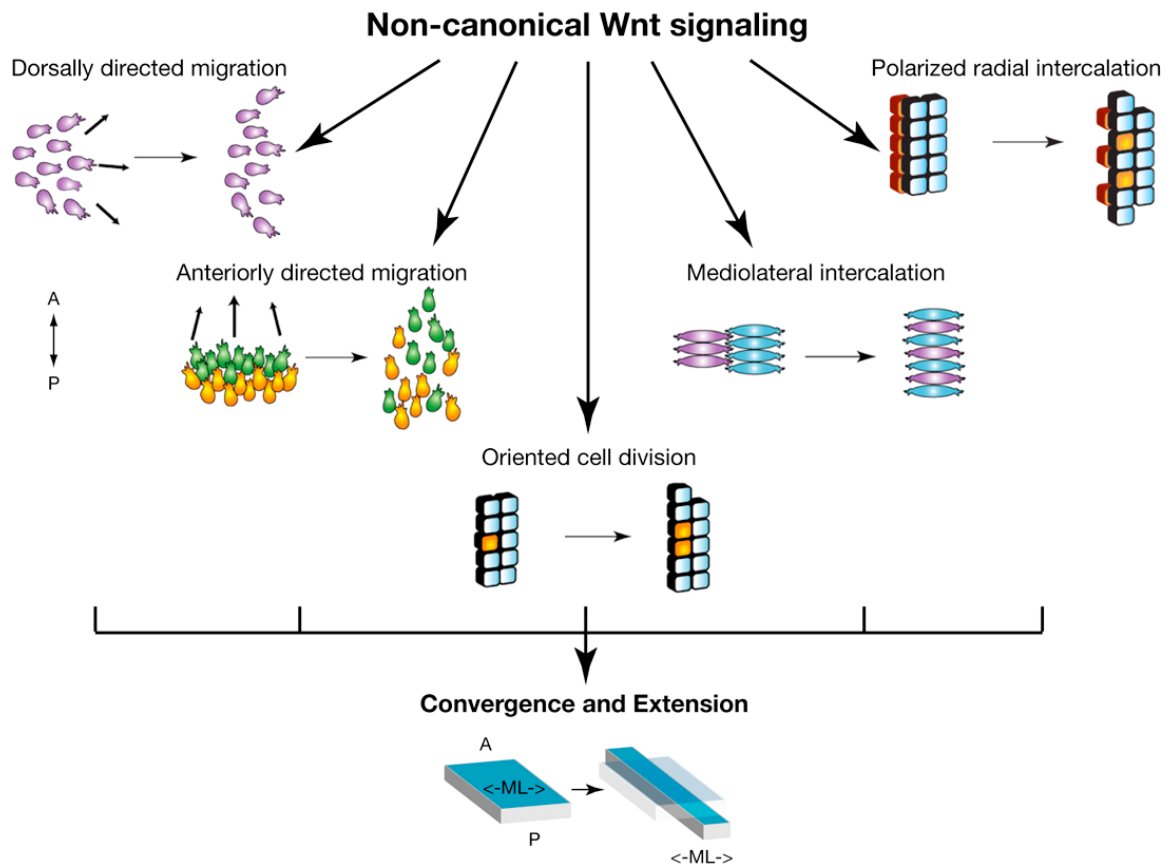


Figure 6.2. Non-canonical Wnt signaling regulates diverse cellular behaviors that underlie C&E movements. A, anterior; P, posterior. M, medial. L, lateral.

the first quantitative evidence for polarized radial intercalation during anisotropic tissue morphogenesis.

Molecular regulation of region-specific C&E movements

Recent studies have begun to elucidate the molecular determinants of region-specific C&E movements. Different pathways and molecules function to either control the directionality of cell movements or regulate the distinct cell movement behaviors within different C&E domains. In the lateral domain, mesodermal cells converge dorsally via directed migration at increasing speeds, reminiscent of active cell migration along a chemoattractant gradient (Figure 6.1B,C) (Jessen et al., 2002; Myers et al., 2002b). Computational modeling predicted that a minimum of two chemoattractant cues, one at the prechordal mesoderm and a second one located more vegetally in the dorsal midline, is sufficient to orient the cell movement paths towards dorsal (Sepich et al., 2005). The molecular nature of the dorsal guidance cues is not clear. While embryos deficient in non-canonical Wnt signaling are defective in C&E movements (Heisenberg et al., 2000; Jessen et al., 2002; Rauch et al., 1997; Topczewski et al., 2001), the existing data do not support an instructive role for non-canonical Wnt signaling in C&E. For example, ubiquitous expression of WT *wnt11* RNA rescues the *silberblick/wnt11* mutant phenotype (Heisenberg et al., 2000). In *kny* and *tri* non-canonical Wnt mutants, dorsal convergence of the lateral mesoderm initiates normally (Sepich et al., 2005). My study of *kny;tri* double mutants also indicates that the double mutant cells are able to distinguish between dorsal and ventral directions and preferentially migrate towards dorsal. These results

support the notion that non-canonical Wnt signaling does not have a role in defining the directionality of dorsal convergence of the lateral mesoderm.

A promising lead in identifying the dorsal guidance cue is the JAK/Stat3 signaling pathway. Stat3 signaling is activated by maternal β -catenin at the dorsal side of the blastula and was shown to be required in the prechordal and anterior chordamesoderm to provide attracting cues for convergence of the lateral mesoderm (Miyagi et al., 2004; Yamashita et al., 2002). In Stat3-depleted embryos, dorsal convergence of the lateral mesoderm is delayed and reduced (Sepich et al., 2005; Yamashita et al., 2002). Such defects are due to cell non-autonomous requirement of Stat3 and can be suppressed by restoring Stat3 expression in the axial mesoderm alone (Miyagi et al., 2004; Yamashita et al., 2002). Further analyses showed that Stat3 activates the small GTPase Rho in the lateral cells to regulate the ML cell elongation and alignment (Miyagi et al., 2004). Stimulating non-canonical Wnt signaling in Stat3-depleted embryos can rescue the defect in cell elongation, but not the orientation of the lateral mesodermal cells (Miyagi et al., 2004). These results are consistent with the model that a Stat3-dependent signal activated at the dorsal midline provides cues to define the directionality of convergence movements, whereas non-canonical Wnt signaling is required for the lateral mesodermal cells to refine the midline cues and establish the ML cell polarity essential for effective C&E movements.

Whereas Stat3 signaling likely provides the guidance cues for convergence movements, what is the molecular regulation of region-specific cell behaviors underlying C&E? In zebrafish, C&E of the lateral and axial mesoderm is achieved by distinct cell movement behaviors (Figure 6.1B-E). Several lines of evidence indicate that the dorsal

directed migration of lateral cells and the ML intercalation of axial cells are controlled by different molecules and pathways. In zebrafish, mutation in the T-box transcription factor *no tail/brachyury* blocks the ML intercalation of axial cells, whereas the dorsal convergence of lateral cells is unaffected in the mutants (Glickman et al., 2003). Hyaluronic acid synthesizing enzyme 2 (Has2) acts through the small GTPase Rac1 to regulate the formation of lamellipodia. It is required cell-autonomously for dorsal convergence, but not extension. Moreover, ectopic *has2* expression in the axial cells appears to transform them from intercalating to migratory cells (Bakkers et al., 2004).

Despite the differences between the movement behaviors of lateral and axial cells, they also share some common molecular components. For example, the fast directed migration of lateral cells during late gastrulation and the ML intercalation of axial cells are both dependent on non-canonical Wnt signaling (Heisenberg et al., 2000; Jessen et al., 2002; Marlow et al., 2002; Topczewski et al., 2001). Also, the persistence of directed migration in convergence of lateral cells is controlled by G α 12/13 as is the ML intercalation in the axial mesoderm (Lin et al., 2005). Because non-canonical Wnt signaling is required for both directed migration and ML intercalation, it is tempting to speculate that there are functional interactions between non-canonical Wnt signaling and other signaling pathways to drive the two different cell behaviors (Solnica-Krezel, 2006). It is noteworthy that embryos deficient in other signaling pathways or molecules form short and broad embryo axes reminiscent of non-canonical Wnt mutants. Initial analyses have established their roles in certain types of cell behaviors driving C&E. For instance, activation of Stat3 in the dorsal mesoderm is essential for the directed migration of lateral cells (Yamashita et al., 2002). COX-1-Ptges-EP4 signaling, on the other hand, controls

the speed of lateral cells during directed migration (Cha et al., 2006). It has not been addressed whether Stat3 or EP4 signaling have roles in ML intercalation of the axial cells. Nonetheless, further investigation of the distinct cellular behaviors in different C&E domains is required to determine whether these pathways are common regulators of diverse cell behaviors or are required for one or few specific cell behaviors.

Last, my study uncovered polarized radial intercalation as a novel cell behavior contributing to C&E (Figure 6.2). The AP bias in radial intercalation is lost in *kny;tri* double mutants, providing the first evidence that non-canonical Wnt signaling polarizes cell movement behaviors between different cell layers (Figure 6.2). The involvement of other pathways in regulating polarized radial intercalation is not known. Moreover, as the C&E of the medial PSM is achieved by multiple cell intercalations, it will be also important to explore the molecular regulations that underlie the cooperation of these different cellular behaviors.

Non-canonical Wnt signaling defines polarized cell intercalations during C&E

I described in this thesis that non-canonical Wnt signaling regulates polarized planar and radial intercalations to drive the C&E movements of the medial PSM (Figure 6.1). Both intercalation behaviors preferentially separate anterior and posterior neighbors in one layer (Figure 6.2). However, how non-canonical Wnt signaling defines this biased orientation of cell intercalation is not clear. Studies in frog showed that non-canonical Wnt signaling establishes polarized protrusive activities essential for ML intercalation during C&E (Wallingford et al., 2000). In frog, the dorsal mesodermal cells engaged in ML intercalation display large lamellipodial protrusions at their medial and lateral ends

Figure 6.3. Polarized protrusive activities in cells undergoing C&E. (A) An image adapted from Keller, 2002. Intercalating frog mesodermal cells are visualized at two levels: the surface of the explant (red) and 5 μm deep in the tissue (green). The explant mosaically expresses the GAP-43 GFP that labels the cell membrane. The labeled cells are elongated mediolaterally and are polarized by lamellipodia at their medial and lateral ends (arrows) and adhere by short filiform contacts on their anterior and posterior surfaces (arrow heads). (B) An image from Keller et al., 2000. Scanning electron image at high magnification show the mediolaterally polarized protrusive activities in the intercalating cells in *X. laevis*. (C-F) Dorsal views of live zebrafish embryos at the end of gastrulation (10 hpf). These embryos were injected first with memRFP RNA at the 1-cell stage to achieve memRFP expression in every cell, at the 4-cell stage, one of the four blastomeres was injected with mGFP to achieve mosaic labeling. Cells in the axial mesoderm and the medial PSM both exhibit mediolaterally polarized protrusions during C&E (arrow), similar to what was observed in frog. Notably, in the axial mesoderm (D), cells form special blebbing-like protrusions at the position where it touches the boundary of the axial mesoderm (arrow head). A, anterior; P, posterior.

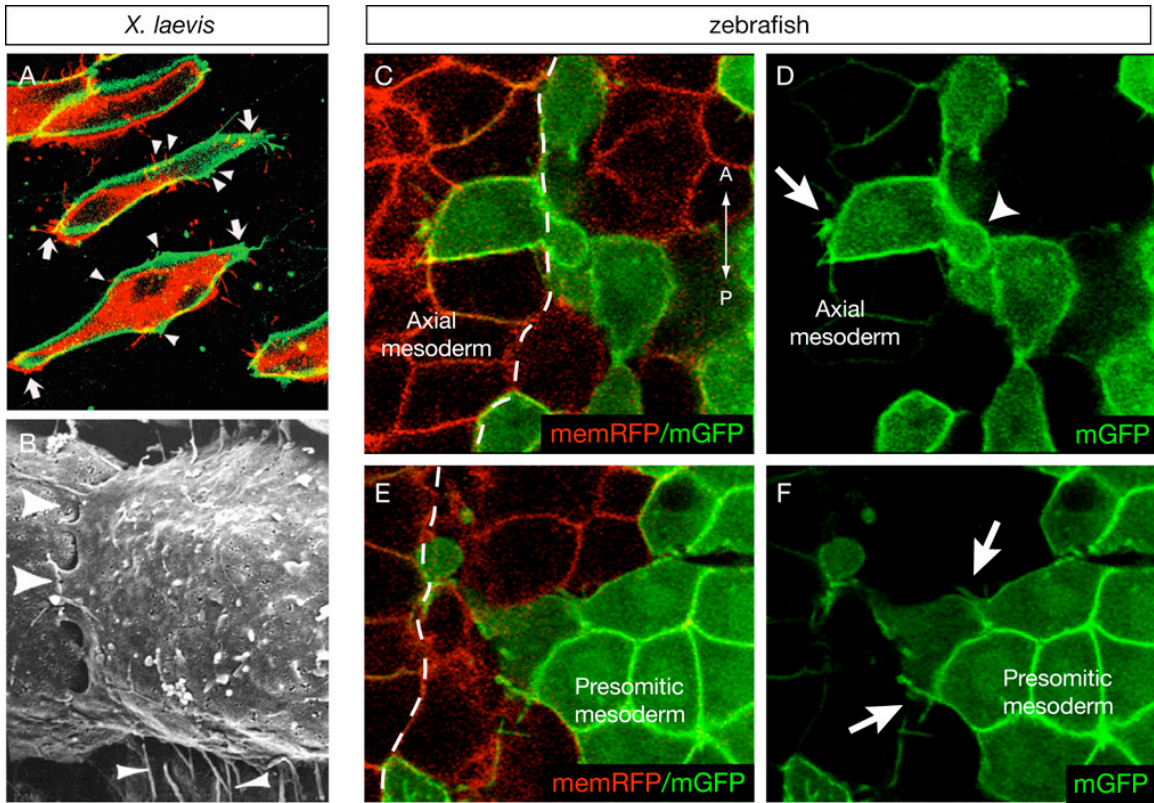


(Figure 6.3A,B) (Keller et al., 2000). These lamellipodia exert traction on neighboring cell bodies, thereby pulling cells between one another mediolaterally. Meanwhile, cells adhere by many small filiform protrusions and contact points on their elongated anterior and posterior surfaces (Figure 6.3A, B) (Keller et al., 2000). These contacts are being made and broken rapidly, which provides local, transient openings that allow the cells to intercalate (Keller et al., 2000). When non-canonical Wnt signaling is perturbed, cells exhibit a round morphology, fail to orient their body mediolaterally (Jessen et al., 2002; Topczewski et al., 2001), and form random or unstable protrusions (Wallingford et al., 2000). Accordingly, ML intercalation is impaired in these embryos. I observed similar polarized cellular protrusions in the medial presomitic cells in WT embryos in zebrafish (Figure 6.3E,F) (Yin and L. S-K, unpublished), suggesting that mediolaterally biased protrusive activities may also contribute to the polarized planar and radial intercalations.

Non-canonical Wnt signaling regulates actin cytoskeleton rearrangements by activating members of the Rho family of small GTPases, including Rho, Cdc42, and Rac (Nobes and Hall, 1999). Studies in cell culture established that each small GTPase has a distinct role in regulating cytoskeleton, cell polarity and protrusive activities. Cdc42 mediates cell polarity and formation of filopodia. Rac is essential for lamellipodia formation, whereas Rho promotes formation of stress fibers and focal adhesions (Hall and Nobes, 2000). Meanwhile, non-canonical Wnt signaling activates these small GTPases through independent and parallel pathways (Veeman et al., 2003a; Wallingford and Habas, 2005). Downstream of Dsh, the Formin homology protein Daam1 binds to the PDZ domain of Dsh and activates RhoA. RhoA in turn leads to the activation of the Rho-associated kinase Rock (Habas et al., 2001; Katoh et al., 2001; Marlow et al., 2002;

Winter et al., 2001). Rac is activated through interaction with the DEP domain of Dsh (Habas et al., 2003). Wnt11/Fz was shown to activate Cdc42 through G protein and protein kinase C (Penzo-Mendez et al., 2003), whereas other studies placed Cdc42 downstream of Wnt/Ca²⁺ pathway that affects C&E movements and tissue separation during gastrulation (Choi and Han, 2002). Therefore, one interesting possibility is that non-canonical Wnt signaling controls differential activation of the small GTPases at the AP and ML cell surface. Rac would constrain the lamellipodial protrusions to the ML ends of the intercalating cells, whereas Cdc42 would establish small filopodia at the AP cell surface. This, in turn, would define the anteroposteriorly biased orientation of planar and radial intercalations (Figure 6.4B,C).

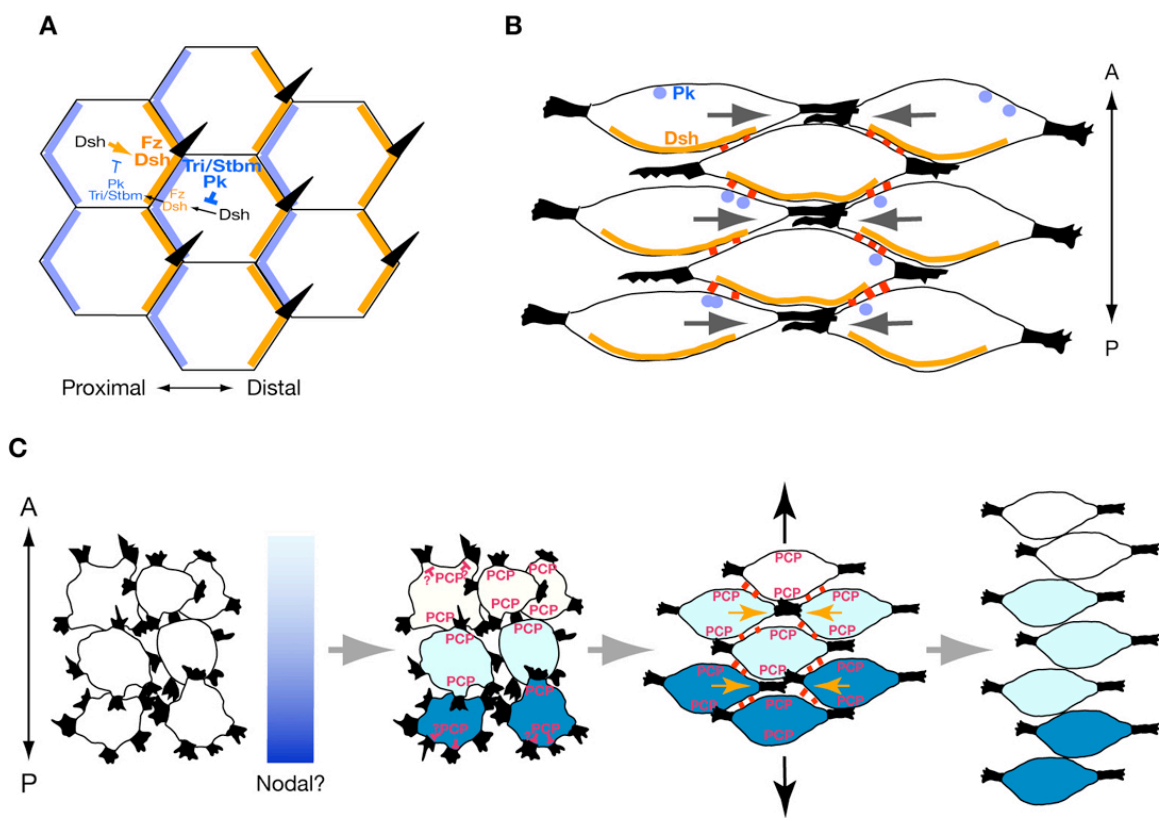
The AP bias in the polarized planar and radial intercalations during the medial PSM C&E also suggests that within a cell layer, the contacts between AP neighboring cells may be weaker or otherwise different from the ML neighbor contacts, providing another possible mechanism for preferential separation of anterior and posterior neighbors in the polarized planar and radial intercalations. In support of this, several lines of evidence have connected non-canonical Wnt signaling with cell adhesion (Torres et al., 1996; Ulrich et al., 2005; Ungar et al., 1995; Witzel et al., 2006). In zebrafish, Wnt11 locally promotes cell contact by accumulating Fz and Dsh to the cell surface (Witzel et al., 2006). This may involve the activation of Rho and Rac downstream of Dsh as both molecules can modulate cadherin-dependent cell-cell contact (Braga, 2002). Another study showed that Wnt11 mediates E-cadherin endocytosis and recycling to control cohesion of prechordal plate progenitors required for directed and coherent cell migration (Ulrich et al., 2005). These studies lead to the hypothesis that non-canonical Wnt

signaling regulates differential cell adhesions within the medial PSM to define where cells should intercalate.

Establishment of ML cell polarity by non-canonical Wnt signaling during C&E

The mechanism by which non-canonical Wnt signaling regulates ML cell polarity during C&E remains elusive. In fly, planar cell polarity (PCP) pathway establishes the cell polarity within a plane of epithelium (Adler, 2002; Klein and Mlodzik, 2005). PCP pathway in the fly contains the same set of “core proteins” as non-canonical Wnt signaling in vertebrates, including Strabismus/Van Gogh-like2 (Stbm), Frizzled (Fz), Dsh, Pk, Flamingo (Fmi), and Diego (Dg) (Adler, 2002; Klein and Mlodzik, 2005). In the fly, PCP components are asymmetrically localized at the cell membranes (Figure 6.4A) (Adler, 2002; Klein and Mlodzik, 2005). In the fly wing epithelium, for example, each cell orients itself with respect to the proximo-distal axis, developing near the distal cell edge a distally pointing actin-based hair (Figure 6.4A) (Adler, 2002; Mlodzik, 2002). In fly, PCP pathway is activated through Fz receptor apparently without the binding of a Wnt ligand (Adler, 2002; Klein and Mlodzik, 2005). Recent studies suggest that the interactions between the transmembrane/secreted protein Four-jointed and two protocadherin, Dachshous and Fat, might regulate Fz activity in the fly eye and wing (Matakatsu and Blair, 2004; Simon, 2004; Yang et al., 2002a). Upon activation of the pathway, PCP components, which are initially distributed evenly in the cell, become first localized uniformly on the apical cell edge, and then become asymmetrically localized at either distal or proximal side of the cell (Strutt, 2002). Fz recruits and forms a complex with Dsh at the distal edge of the

Figure 6.4. Non-canonical Wnt signaling regulates the polarized orientation of cell intercalations during C&E. (A) Cellular interactions between the components of PCP pathway that establish the cell polarity in the fly wing epithelium. (B) In zebrafish, the dorsal mesodermal cells exhibit asymmetric localization of non-canonical Wnt components during C&E, with Pk localized to anterior edge and Dsh localized to the posterior edge. The subcellular localization of PK and Dsh in zebrafish is reminiscent of the Pk and Dsh localization in the fly wing disc (A). (C) A model of anteroposterior (AP) polarity cues activating non-canonical Wnt signaling to bias the orientation of cell intercalations. In zebrafish gastrula, the dorsal mesodermal cells initially exhibit round morphology and send out protrusions in random directions. Gradients of gene expression in the AP dimension specify anteroposteriorly graded cell properties. Upon the AP polarity cues, non-canonical Wnt signaling is activated at the anterior and posterior sides of the cell. It may function to constrain the lamellipodia protrusions to the medial and lateral ends of the cell or may establish the differential cell adhesions within the dorsal mesoderm. Polarized cellular protrusions and differential cell adhesions subsequently define the biased orientation of cell intercalations. A, anterior; P, posterior.



wing cell. Stbm, on the other hand, brings Pk to the membrane and the Stbm/Pk complex becomes enriched at the proximal cell membrane (Figure 6.4A) (Adler, 2002; Klein and Mlodzik, 2005). The Stbm/Pk complex inhibits the Fz/Dsh complex from forming on the proximal cell edge, thereby functioning in a feedback loop that amplifies differences between Fz/Dsh levels on the adjacent cell surface (Figure 6.4A) (Tree et al., 2002).

Whether non-canonical Wnt signaling utilizes similar mechanisms to establish ML cell polarity during vertebrate gastrulation is unknown. Consistent with the observations in the fly, vertebrate Dsh is recruited to the cell membrane upon activation of non-canonical Wnt signaling (Rothbacher et al., 2000; Wallingford et al., 2000). Stbm/Vangl2 forms a complex with Pk at the cell membrane (Jenny et al., 2003). Pk in turn inhibits Fz-mediated Dsh localization to the membrane, likely by removing Dsh from the membrane to the cytoplasm, or by directly binding to and degrading Dsh (Carreira-Barbosa et al., 2003). In *X. laevis*, Dsh was reported to be highly expressed at the medial and lateral ends of the intercalating cells in dorsal marginal zone explants (Kinoshita et al., 2003). Pk, on the other hand, was shown to be localized at the anterior edge of the cells in the notochord and neural tube during zebrafish somitogenesis (Ciruna et al., 2006). However, asymmetric localization of non-canonical Wnt components has not been investigated in the intercalating cells during vertebrate gastrulation.

Towards elucidating the molecular mechanisms defining the polarized planar and radial intercalations, I revealed that in the dorsal mesoderm of the zebrafish gastrula, Pk is localized to the anterior side of the cell, whereas Dsh is transiently enriched near the posterior cell membrane (Figure 6.4B). The anterior localization of Pk and posterior localization of Dsh in the zebrafish dorsal mesoderm are reminiscent of the asymmetric

distribution of the fly homologs of these proteins in the wing epithelium, where Pk exhibits proximal distribution and Dsh is localized distally (Strutt, 2002). This suggests that the interactions between these molecules during tissue polarization are evolutionarily conserved. The asymmetric localization of Pk and Dsh is dependent on non-canonical Wnt signaling and is correlated with the ML cell elongation at late gastrulation. Based on the above observations and other studies (Keller et al., 1992; Shih and Keller, 1992a; Shih and Keller, 1992b; Wallingford et al., 2000), I propose a model of how non-canonical Wnt signaling regulates polarized cell intercalations in the dorsal mesoderm of the zebrafish gastrula (Figure 6.4C): upon internalization, the dorsal mesodermal cells initially display a round morphology, produce lamellipodia in all directions, and move away from the blastopore by directed migration without significant cell intercalations. At late gastrulation, non-canonical Wnt signaling becomes activated at the anterior and posterior cell edges. This would lead to the activation of Cdc42 and small filopodia formation at the AP cell surface, while constraining the Rac activity and lamellipodia protrusions at the medial and lateral cell ends. Meanwhile, the activation of non-canonical Wnt signaling along the AP axis may also establish differential cell adhesions within the dorsal mesoderm. The mediolaterally biased protrusive activities and differential cell adhesions consequently underlie the polarized orientation of planar and radial intercalations. Notably, the lateral mesodermal cells engaged in fast directed migration also acquire ML polarity under the control of non-canonical Wnt signaling (Figure 6.1C) (Jessen et al., 2002). Whether the lateral cells exhibit the same asymmetric Dsh and Pk localization as the dorsal cells still remains open.

What activates non-canonical Wnt signaling in the dorsal mesoderm of the zebrafish gastrula? At late gastrulation, *wnt5* RNA is expressed in the posterior PSM (Rauch et al., 1997), whereas *wnt11* is expressed in the anterior PSM and the lateral neuroectoderm (Heisenberg et al., 2000). Therefore, the expression pattern of *wnt5* and *wnt11* cannot explain the activation of non-canonical Wnt signaling along the AP axis in the dorsal mesoderm. In *D. melanogaster*, genes controlling AP patterning are essential for ML intercalation during germ band extension (Zallen and Wieschaus, 2004). Similarly, in the *X. laevis* chordamesoderm, graded activin-like signaling that establishes AP polarity was proposed to act in parallel or upstream of non-canonical Wnt pathway to regulate the orientation of ML intercalation (Ninomiya et al., 2004). My discovery of anterior localization of Pk and posterior localization of Dsh, as well as the loss of asymmetric Pk and Dsh expression in *kny* and *tri* individual mutants, strongly suggests that an AP polarity signal is present in the dorsal mesoderm during zebrafish C&E and acts upstream of non-canonical Wnt signaling (Figure 6.4C). During zebrafish gastrulation, a Nodal activity gradient originated from the blastoderm margin patterns different cell fate along the animal-vegetal axis (Schier and Talbot, 2005). Zebrafish double mutants for the nodal-related genes *squint(sqt)* and *cyclops(cyc)*, as well as maternal-zygotic *one-eyed pinhead (MZOep)* mutants in which a EGF-CFC gene essential for Nodal signaling transduction is mutated, exhibit severe defects in internalization gastrulation movements and lack mesodermal and endodermal derivatives (Feldman et al., 1998; Gritsman et al., 1999). Interestingly, in these mutants, convergence movements of the non-internalized neural tissues occur relatively normally, whereas extension seems to be reduced (Erter et al., 2001; Gritsman et al., 1999). This movement defect is

correlated with their shortened body axis and the formation of an abnormal thickening at the dorsal side during gastrulation. Furthermore, simultaneous interference with the function of both Nodal antagonists *Lefty1* and *Lefty2* in zebrafish with antisense morpholino oligonucleotides also leads to severe gastrulation abnormalities (Agathon et al., 2001; Feldman et al., 2002). These observations make Nodal signaling a good candidate for establishing the AP polarity cues upstream of non-canonical Wnt signaling. One informative experiment to test this would be to interfere with the endogenous Nodal activity gradient by providing ectopic Nodal in the anterior dorsal gastrula and analyze the cell movements and subcellular localization of Pk and Dsh in the region between the margin and the ectopic Nodal source.

Roles of C&E movements in zebrafish slow muscle development

The main role of gastrulation movements is to shape the tissue primordia and position them precisely along the dorsoventral (DV) and AP embryo axes. However, in what manner gastrulation movements influence subsequent cell fate specification and tissue morphogenesis is an important but not fully elucidated area of research. To address this question, I studied somite development in zebrafish *kny;tri* C&E mutants. During gastrulation, C&E movements shape and position the PSM alongside the axial mesoderm (Henry et al., 2000; Schoenwolf and Smith, 2000; Stickney et al., 2000). Our group previously showed that as a consequence of impaired C&E movements, the somites formed in *kny;tri* double mutants are extremely broad mediolaterally and narrow anteroposteriorly (Henry et al., 2000). WT somites are composed of epithelial border cells and mesenchymal internal cells. In *kny;tri* double mutants, although the AP

intrasegmental polarity and the somitic boundaries are established normally, the somites consist exclusively of border cells (Henry et al., 2000). Whereas these previous studies had mainly focused on the morphological defects of the somites in *kny;tri* double mutants, my work delineated how defective C&E movements affect the specification and morphogenesis of slow muscle lineages in the somite in the double mutants.

In *kny;tri* double mutants, the slow muscle fibers are reduced in number and highly disorganized. These defects are not due to a cell-autonomous requirement for non-canonical Wnt signaling in slow muscle development. Rather, I uncovered a significant correlation between the degree of C&E defects and slow muscle defects in different C&E mutants: a gradation of slow muscle deficiency and disorganization is observed from the mutants with the mildest C&E defect (*silberblick/wnt11* and *pipetail/wnt5* individual mutants) to those with the most severe C&E phenotype (*kny;tri* double mutants). This indicates that C&E gastrulation movements and slow muscle development are closely related.

Using cell tracing analyses and genetic manipulations, I demonstrated that the reduction of slow muscle fibers in *kny;tri* double mutants is a direct consequence of impaired C&E movements on specification and fate maintenance of slow muscle precursors, the adaxial cells. The prospective adaxial cells are specified in the PSM in response to midline inducing signals during mid-gastrulation (Coutelle et al., 2001; Devoto et al., 1996; Thisse et al., 1993; Weinberg et al., 1996). Defective C&E movements in *kny;tri* double mutants shorten the AP interface between the inducing axial and target presomitic tissues, resulting in the specification of fewer prospective adaxial cells.

C&E movements continue to narrow and elongate the paraxial mesoderm during early segmentation (Myers et al., 2002b). In WT, all prospective adaxial cells converge medially to form a single column flanking the notochord. Simultaneously, the ML range of Hedgehog (Hh) signaling in the paraxial mesoderm decreases to one-cell diameter from the notochord. Little is known about the molecular mechanisms underlying the change of Hh signaling range during early segmentation. Consistent with previous reports, I observed that coincident with the decrease of Hh signaling range, the prospective adaxial cells immediately adjacent to the notochord form a monolayer of pseudo-epithelium (Hirsinger et al., 2004). This pseudo-epithelium might constrain the lateral diffusion of Hh ligands, either by setting up a physical barrier, or by inducing the subcellular redistribution of the downstream components of Hh signaling within these juxta-notochordal adaxial cells. To test this, it would be interesting to examine the localization of Hh signaling components in the notochord-adjacent prospective adaxial cells before and after the formation of pseudo-epithelium.

A recent study in *X. laevis* showed that the PCP effectors Inturned and Fuzzy affect Hh signaling by mediating ciliogenesis (Park et al., 2006). The interrelationship between PCP pathway and Hh signaling demands further analyses as no Hh-related phenotypes have been reported in embryos deficient in the PCP core proteins in zebrafish. My data indicate that Hh signaling is not compromised in *kny;tri* double mutants. In these embryos, the notochord-adjacent prospective adaxial cells still form a monolayered pseudo-epithelium, and the decrease of Hh signaling range in the paraxial mesoderm occurs normally. Moreover, the prospective adaxial cells in the double mutants exhibit quantitatively similar responsiveness to Hh signaling as WT. However, I

demonstrated that the change of Hh signaling range and the C&E movements of the prospective adaxial cell population must be coordinated to ensure the fate maintenance of the adaxial cells. In *kny;tri* double mutants, the prospective adaxial cells fail to converge, stop receiving Hh signal during early segmentation. Consequently, they lose the adaxial cell identity and transdifferentiate into the fast muscle precursors.

Later during segmentation, the adaxial cells adopt an anteroposteriorly elongated morphology and subsequently migrate towards the lateral somite surface (Stickney et al., 2000). The shape changes and lateral migration of the adaxial cells are compromised in *kny;tri* double mutants and transplantation experiments showed that both defects are cell non-autonomous. Little is known about the cellular behaviors and molecular mechanisms underlying the slow muscle morphogenesis in zebrafish. Through confocal imaging analyses, I revealed that the shape changes of adaxial cells within the anterior somites entail three consecutive steps: (1) DV elongation, (2) anterior-ward rotation, and (3) AP elongation. In *kny;tri* double mutants, the adaxial cells fail to rotate towards the anterior somitic boundary and consequently remain aligned perpendicular to the notochord. I provided evidence to show that the defect in adaxial cell shape changes in *kny;tri* double mutants is due to the prolonged contacts between the adaxial cells and notochord in these embryos. Such a defect could be suppressed either by physical removal of the double mutant notochord or by introducing the WT notochord cells into the double mutants. Studies using *X. laevis* notochordal explants demonstrated that physically hindering C&E movements interrupts notochord differentiation (Domingo and Keller, 1995). Consistently, I found that the notochord formed in *kny;tri* C&E mutants is extremely misshaped. I therefore propose that defective C&E gastrulation movements disrupt

notochord development in *kny;tri* double mutants, which in turn impedes the adaxial cell shape changes. However, it is also possible that non-canonical Wnt signaling has a more direct role in notochord development, which is required for adaxial cell morphogenesis.

What are the molecular and cellular mechanisms underlying the prolonged contacts between the notochord and adaxial cells in *kny;tri* double mutants? The zebrafish notochord is constrained by a sheath of extracellular matrix (ECM) (Parsons et al., 2002; Scott and Stemple, 2005). During segmentation, the transcripts of *fibronectin* (*fn*) gene, which encodes a large ECM protein, is expressed in the notochord, whereas its main receptor *integrin α 5* is expressed in the adaxial cells, suggesting a possible role of Fn-Integrin association in adaxial cell morphogenesis (Julich et al., 2005; Koshida et al., 2005). In *X. laevis*, perturbation of non-canonical Wnt signaling disrupts Fn fibril assembly on mesodermal tissue surfaces (Goto et al., 2005). Consistently, I found that in *kny;tri* double mutants, Fn protein is distributed ectopically inside the notochord and fails to disappear from the notochord-somite boundary during the adaxial cell shape changes. Whether the persistent Fn expression directly accounts for the adaxial cell defects in *kny;tri* double mutants requires further investigation.

The early adaxial cell shape change defects and the later slow muscle migration defects in *kny;tri* double mutants might be connected. Monitoring the migration of the double mutant slow muscle cells revealed that most cells continue to maintain contacts with the notochord during the time period when normal lateral migration should be underway. Meanwhile, the reciprocal waves of *n-* and *m-cadherin* expression that guide the lateral migration of slow muscle cells occur normally in *kny;tri* double mutants (Cortes et al., 2003). Therefore, I hypothesize that the prolonged contacts between the

notochord and adaxial cells may prevent the adaxial cells from responding to the lateral migration cues on time. When these cells are separated from the notochord during later segmentation, they cannot migrate laterally as the migration cues are no longer available.

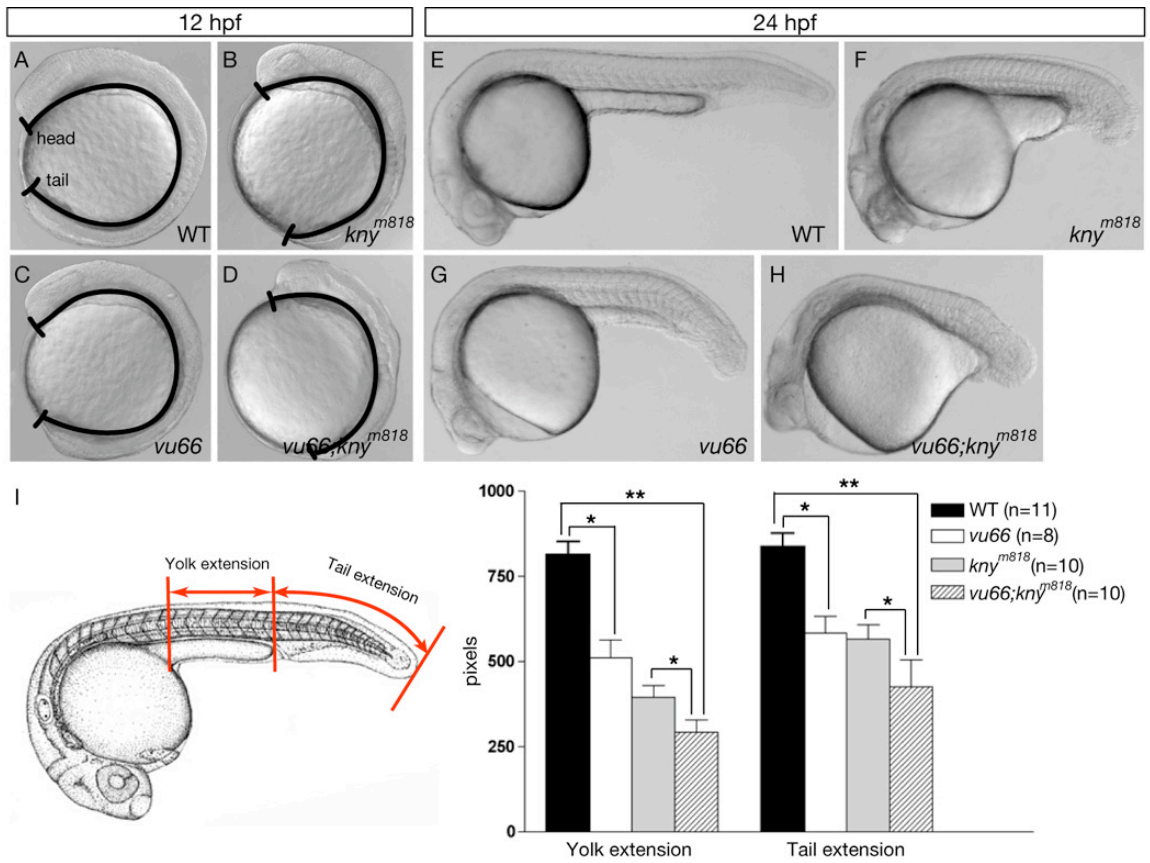
Taken together, my study of somite development in *kny;tri* double mutants uncovers novel cellular behaviors and tissue interactions that underlie the slow muscle development in zebrafish. Moreover, it provides an important example of how C&E gastrulation movements establish proper tissue geometry essential for inductive and morphogenetic events during later development.

Modifier screen to identify genes essential for early embryogenesis

To identify additional genes essential for C&E movements and early embryogenesis, I conducted a genetic screen for mutations that exacerbate the phenotype of the hypomorphic *kny^{m818}* allele. Previous screens have identified many alleles of the *tri/vangl2* locus (Hammerschmidt et al., 1996a; Solnica-Krezel et al., 1996), indicating that it is a highly mutable gene. As expected, I found a new *tri^{vu64}* mutant allele (Y219Stop) in the screen. In addition, I isolated four mutations that cause further shortening of the *kny^{m818}* mutant body axis (*vu63*, *vu66*, and *vu84*), thus likely interacting with *kny* during C&E movements. Two other mutations interact with *kny^{m818}* allele in developmental processes other than gastrulation, such as tail morphogenesis (*vu65*) and fin formation (*vu61*).

One of the mutants, *vu66*, exhibits a shortened body, malformed brain, edema, and reduced blood circulation (Figure 6.5). Acridine orange labeling revealed excess cell death in the head and trunk region of the *vu66* homozygotes (Yin and L.S-K,

Figure 6.5. *vu66* mutation impairs C&E and enhances *kny^{m818}* mutant phenotype. (A-H) Lateral views of WT, *vu66*, *kny^{m818}* individual and *vu66;kny^{m818}* double mutant embryos at (A-D) early somitogenesis, and (E-H) 24 hpf stages. (I) Morphometric measurements of length of the trunk and tail regions: *vu66* individual mutants form shorter body axis compared to WT. *vu66;kny^{m818}* double mutants are significantly shorter than the *kny^{m818}* individual mutants. Note opaque head region of double mutants suggestive of neural degeneration. *, p<0.05. **, p<0.01.



unpublished). The phenotype of *vu66* individual mutants is reminiscent of that reported for zebrafish embryos injected with *liv1* morpholino oligonucleotides (Yamashita et al., 2004). *liv1* encodes a breast-cancer-associated zinc transporter protein, which acts downstream of Stat3 to promote the nuclear localization of zinc-finger protein Snail, a master regulator of epithelial-mesenchymal transition (Yamashita et al., 2004). *liv1* acts cell-autonomously to regulate the anterior migration of the axial mesendoderm. *vu66;kny^{m818}* double mutants exhibit additive shortening of the body, increased apoptosis in the brain, and cardia bifida that is not seen in *vu66* or *kny^{m818}* individual mutants (Figure 6.5) (Yin and L.S-K, unpublished), suggesting that *vu66* acts as a recessive enhancer of the *kny^{m818}* mutant allele. Given that the C&E defects seen in *vu66* individual mutants are relatively mild compared to *kny* or other non-canonical Wnt signaling mutants (Hammerschmidt et al., 1996a; Solnica-Krezel et al., 1996) (Figure 6.5), it is possible that *vu66* mutation only modestly affects some aspects of the cellular behaviors required for C&E. Further phenotypic and molecular characterization of *vu66* mutation may reveal novel interactions between non-canonical Wnt signaling and other pathways during C&E, as well as the roles of *kny* in cardiogenesis and neural development.

Two important issues about the *kny* modifier screen should be addressed. First, to identify real enhancers of the *kny^{m818}* allele, one needs to understand the range of the variations in the *kny^{m818}* phenotype, in particular during gastrulation. In the screen, we found that some *kny^{m818}* mutants had shorter body axis or abnormal tail morphology compared to the others. Several rounds of re-screening would be necessary to determine whether these defects are caused by newly-induced mutations in addition to *kny^{m818}*, or just the variations in the *kny^{m818}* phenotype due to existing genetic polymorphisms. It

would also be critical to calculate the ratio of embryos showing different phenotypes to see whether it fits the ratio predicted by the principle of genetics. Second, in this screen, we isolated mutants based on the morphological defects. Because of the variations in the *kny*^{m818} phenotype, we might miss the mutations that subtly modify the *kny*^{m818} defects. To improve the screen strategy, one may include in situ or immunohistochemistry into the next round of screen or conduct the screen in a transgenic line that expresses GFP reporter in the tissues of interest.

Nevertheless, the fact that several recessive enhancers of the *kny*^{m818} allele have been isolated from this pilot screen strongly suggests that it is an efficient strategy towards identifying additional regulators of gastrulation. Similar screen strategy has been applied in our laboratory to look for modifiers of the patterning defects in *chordino* mutants (Inbal and L.S-K, unpublished). Through molecular characterization of the loci that functionally interact with *kny*, we may identify novel molecules that regulate C&E and new components of non-canonical Wnt signaling, or reveal connections between non-canonical Wnt signaling and other known genes. It is noteworthy that *kny* gene is continuously and broadly expressed after gastrulation, including in the forming somites, pronephric ducts, neural retina, midbrain-hindbrain boundary, nascent pectoral fins, branchial arches, and the ventral spinal cord (Topczewski et al., 2001). Therefore, identification and characterization of the mutations that interact with *kny* during later development may also reveal novel function of *kny* separate from non-canonical Wnt signaling.

Potential interactions between copper and glypicans during embryogenesis

In this thesis, I described the characterization of *calamity*^{vu69} (*cal*^{vu69}) mutation, which impairs pigmentation and notochord development in zebrafish. Through mapping experiments, we determined that *cal*^{vu69} inactivates the zebrafish homolog of the human Menkes disease gene *atp7a*, which is essential for copper homeostasis in humans. *cal*^{vu69} was originally identified from the double mutants that result from two independent but simultaneously-induced mutations, one *vu69* inactivating the *cal* gene, and a second one *vu68* affecting the *kny* locus (a missense mutation L227P). *cal*^{vu69} is genetically linked to the *kny* locus, and the two loci reside 3.5 cM apart on chromosome 14. Interestingly, my initial analyses suggest that the *cal* and *kny* loci also interact functionally (Figure 6.6). First, compared to *cal*^{vu69} and *kny*^{vu68} individual mutants, *cal*^{vu69};*kny*^{vu68} double mutants exhibit shorter body axis and more strongly folded notochord at day 1. Second, there is a larger accumulation of the red blood cells in the blood island of the double mutants than in the individual mutants. Third, red blood cells are frequently seen distributed broadly in the trunk region of the double, but not the individual mutants, suggesting that *kny* and *cal* interact during normal blood vessel formation (Figure 6.6D).

How do *kny* and *cal* interact during embryogenesis? Studies from *in vitro* system and the mammalian model of Menkes disease have provided detailed description of the roles of ATP7a Menkes protein in copper homeostasis (Lutsenko and Petris, 2003; Voskoboinik and Camakaris, 2002). At normal intracellular copper levels, the Menkes protein is predominantly localized to the trans-Golgi network (TGN) and delivers cytoplasmic copper to the secreted cuproenzymes via protein-protein interactions. Meanwhile it cycles between the TGN and the plasma membrane to efflux copper. When

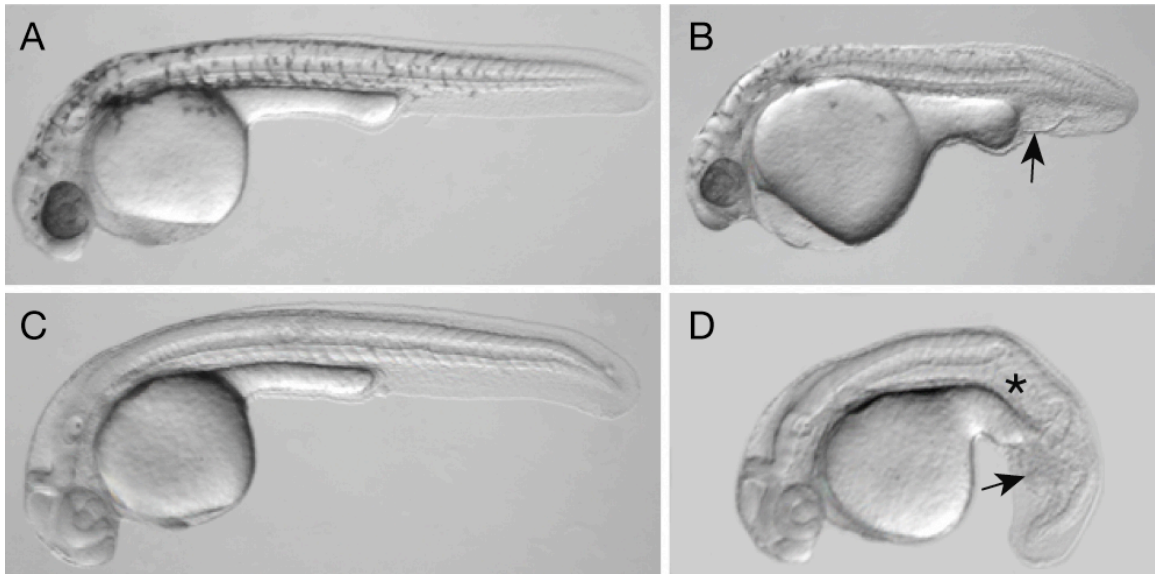


Figure 6.6. *calamity* (cal^{vu69}) mutation functionally interacts with kny^{vu68} mutation. (A-D) Lateral views of live embryos at day 1, anterior to the left. In cal^{vu69} individual mutants and $cal^{vu69}; kny^{vu68}$ compound mutants, the lack of pigmentation and notochord defects are associated with the cal^{vu69} mutation. In addition, $cal^{vu69}; kny^{vu68}$ compound mutants show shorter body, more severe notochord defects and ectopic blood accumulation in the tail region (arrow), as well as hemorrhages in the trunk (asterisk).

cells are exposed to excessive copper, the Menkes protein is rapidly relocalized to the plasma membrane where it functions mainly in copper efflux. Therefore, the Menkes protein is critical for the regulation of copper levels within the cell. In agreement with this notion, the defects seen in *cal^{vu69}* mutants, such as folded notochord and lack of pigmentation, can be phenocopied by treatments of WT zebrafish embryos with neocuproine, a copper chelator that blocks copper uptake (Figure 6.7I). Neocuproine treatments exacerbated the *cal^{vu69};kny^{vu68}* double mutant phenotypes (Figure 6.7F, J), and enhanced the defects of *kny^{m119}* and *kny^{m818}* individual mutants (Figure 6.7C-L). Based on these observations, I hypothesize that the interactions between *cal/atp7a* and *kny* might be indirect and the synergistic phenotypes seen in *cal^{vu69};kny^{vu68}* double mutants might reflect the requirement of normal copper homeostasis for Kny function.

Recent studies of Glypican1 recycling provide direct evidence to show that glypicans can be modified in a copper-dependent manner (Figure 6.8) (Fransson, 2003; Fransson et al., 2004). In cell culture, Glypican1 binds the cargo molecules via the heparan sulfate (HS) side chains at the cell surface and carry them into the cell when it is internalized by a caveolae-associated mechanism. During recycling, the HS is cleaved both by heparanase and by nitric oxide (NO)-dependent deaminative cleavage. The cargo is released and transported across the endosomal membrane. After resynthesis of the HS on the core protein, Glypican1 returns to the cell surface. It has been shown that copper is required for the self-cleavage of the recycling Glypican1 (Fransson, 2003; Fransson et al., 2004). The NO required for deaminative cleavage of the HS is derived from intrinsic S-nitroso groups in the Glypican1 core protein. Loading and unloading of NO is dependent on a $\text{Cu}^{2+}/\text{Cu}^{+}$ redox cycle. A recent report revealed that a cuproprotein PrP^c co-

Figure 6.7. Treatments of WT embryos with neocuproine phenocopy the *cal^{vu69}* defects and enhance the *cal^{vu69}* and *kny* mutant phenotypes. *cal^{vu69}* individual mutants are hypersensitive to neocuproine treatments as their notochord becomes more folded at low drug concentration (F, arrow) compared to the untreated control (B). Upon neocuproine treatments, both *kny^{m119}* (G, K) and *kny^{m818}* (H, L) mutant embryos exhibit shortened body axis and increased blood accumulation in the tail (asterisks) compared to the untreated controls (C, D).

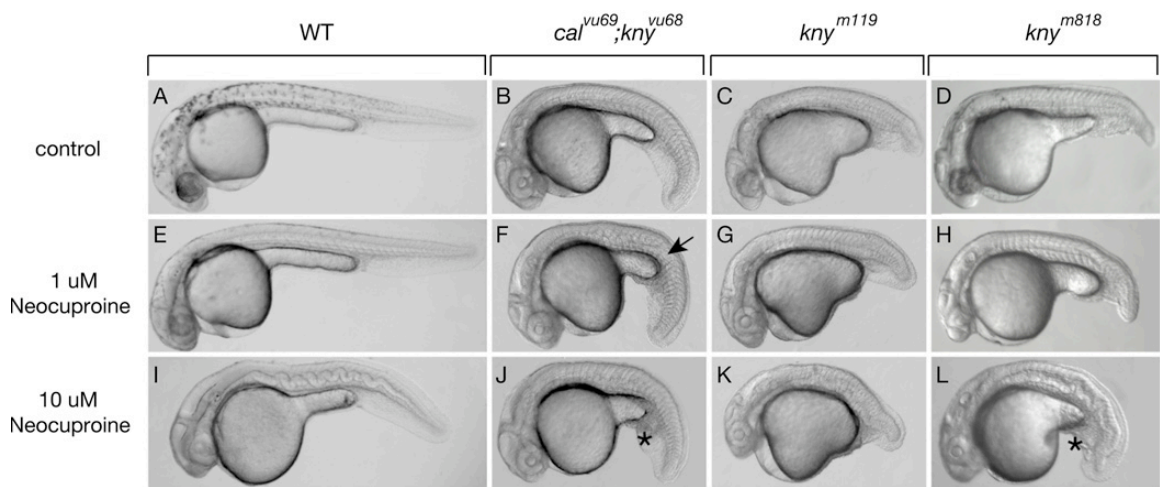
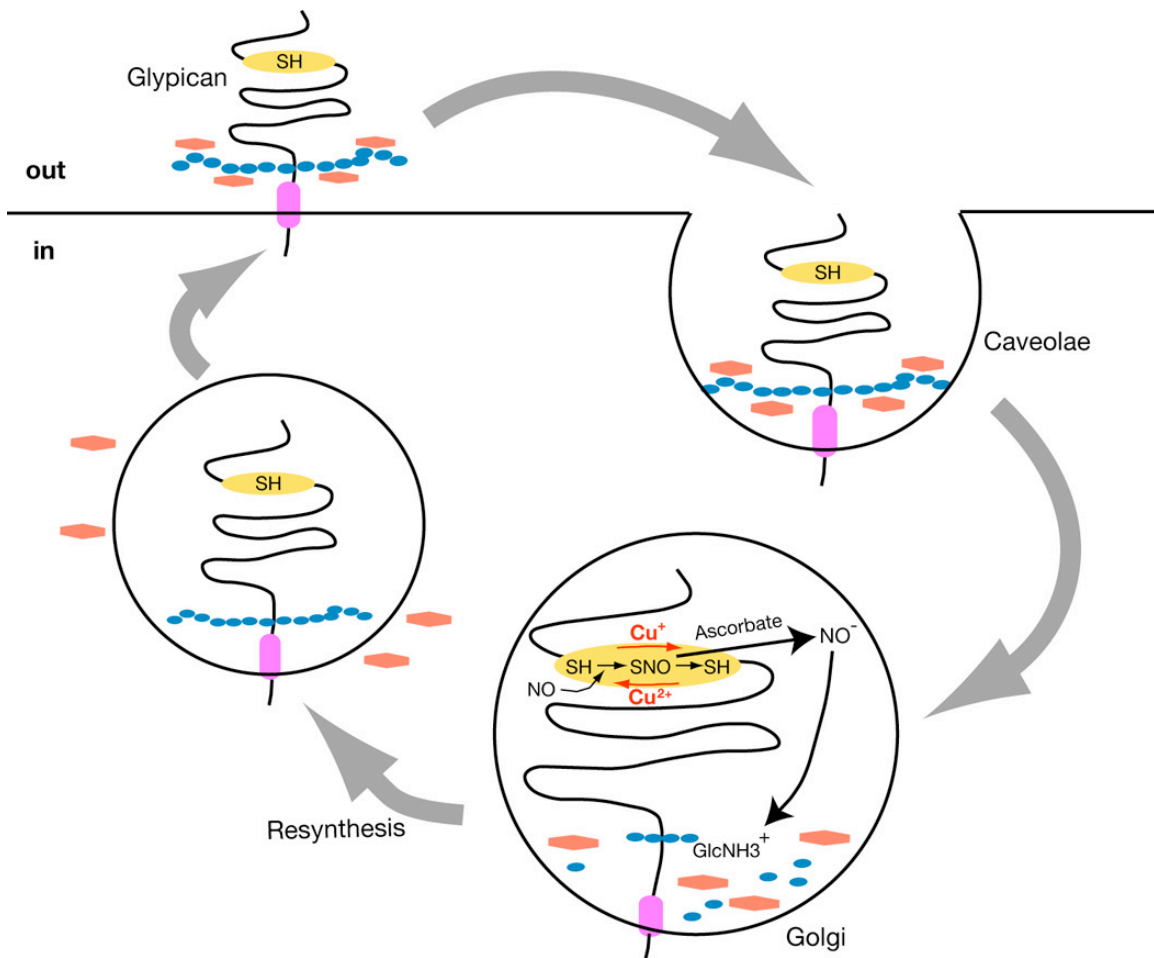


Figure 6.8. Glypican1 recycling in cell culture and the involvement of copper. The GPI-linked Glypican1 binds cargo molecules to its heparan sulfate (HS) side chains and carries them into the cell when Glypican1 is internalized, possibly via caveolae. During recycling, the HS is cleaved by heparanase and by nitric oxide (NO)-dependent deaminative cleavage at GlcNH_3^+ . The NO required for deaminative cleavage of HS is derived from intrinsic S-nitroso (SNO) groups in the Glypican1 core protein. Loading and unloading of NO is dependent on a $\text{Cu}^{2+}/\text{Cu}^+$ redox cycle. Cargo molecules are released upon the HS disassembly and transported across the endosomal membrane. Subsequently, Glypican1 resynthesizes its HS chains and goes back to the plasma membrane.



internalizes with Glypican1 and functions to deliver Cu^{2+} to Glypican1 (Cheng et al., 2006). In fibroblasts lacking the function of PrP^c, the HS chains of Glypican-1 are poorly degraded. The addition of either Cu^{2+} ions, NO donors, or ectopic expression of PrP^c protein could restore the HS degradation. These findings uncover the intriguing connections between glypicans and copper homeostasis.

Whether Kny/Glypican4 undergoes similar recycling is not known. We previously showed that a Flag-tagged Kny protein (Kny C-Flag), upon overexpression in the zebrafish embryo, is mainly localized at the cell surface (Topczewski et al., 2001). However, some punctate expression of Kny C-Flag is also detected in the cytoplasm, suggesting that Kny might cycle between the cell surface and cytoplasm. In the future, we would like to investigate whether Kny undergoes S-nitrosylation and HS pruning in a copper-dependent manner. Furthermore, it has been proposed that Kny serve as a co-receptor of Fz in non-canonical Wnt signaling (Topczewski et al., 2001). In *X.laevis*, Glypican4 was shown to bind directly to XWnt5 and XWnt11 (Ohkawara et al., 2003). Therefore, copper homeostasis may also play a role in the transduction of non-canonical Wnt signaling. To test this, it would be interesting to analyze the effects of copper depletion on *ppt/wnt5* and *slb/wnt11* mutants by either treating these mutant embryos with neocuproine or constructing the double mutants with *cal^{nu69}*.

REFERENCES

- Adams, R. J., and Kimmel, C.B.** (2004). Morphogenetic Cellular Flows during Zebrafish Gastrulation. In *Gastrulation. From Cells to embryo*, (ed. C. D. Stern), pp. 305-316. New York: Cold Spring Harbor Laboratory Press.
- Adler, P. N.** (2002). Planar signaling and morphogenesis in *Drosophila*. *Dev Cell* **2**, 525-35.
- Afonin, B., Ho, M., Gustin, J. K., Meloty-Kapella, C. and Domingo, C. R.** (2006). Cell behaviors associated with somite segmentation and rotation in *Xenopus laevis*. *Dev Dyn* **235**, 3268-79.
- Agathon, A., Thisse, B. and Thisse, C.** (2001). Morpholino knock-down of *antivin1* and *antivin2* upregulates nodal signaling. *Genesis* **30**, 178-82.
- Agathon, A., Thisse, C. and Thisse, B.** (2003). The molecular nature of the zebrafish tail organizer. *Nature* **424**, 448-52.
- Amsterdam, A., Yoon, C., Allende, M., Becker, T., Kawakami, K., Burgess, S., Gaiano, N. and Hopkins, N.** (1997). Retrovirus-mediated insertional mutagenesis in zebrafish and identification of a molecular marker for embryonic germ cells. *Cold Spring Harb Symp Quant Biol* **62**, 437-50.
- Bakkers, J., Kramer, C., Pothof, J., Quaedvlieg, N. E., Spaink, H. P. and Hammerschmidt, M.** (2004). *Has2* is required upstream of *Rac1* to govern dorsal migration of lateral cells during zebrafish gastrulation. *Development* **131**, 525-37.
- Barresi, M. J., Stickney, H. L. and Devoto, S. H.** (2000). The zebrafish slow-muscle-omitted gene product is required for Hedgehog signal transduction and the development of slow muscle identity. *Development* **127**, 2189-99.
- Barrios, A., Poole, R. J., Durbin, L., Brennan, C., Holder, N. and Wilson, S. W.** (2003). Eph/Ephrin signaling regulates the mesenchymal-to-epithelial transition of the paraxial mesoderm during somite morphogenesis. *Curr Biol* **13**, 1571-82.

- Bastock, R., Strutt, H. and Strutt, D.** (2003). Strabismus is asymmetrically localised and binds to Prickle and Dishevelled during *Drosophila planar* polarity patterning. *Development* **130**, 3007-14.
- Baxendale, S., Davison, C., Muxworthy, C., Wolff, C., Ingham, P. W. and Roy, S.** (2004). The B-cell maturation factor Blimp-1 specifies vertebrate slow-twitch muscle fiber identity in response to Hedgehog signaling. *Nat Genet* **36**, 88-93.
- Bertinato, J. and L'Abbe, M. R.** (2004). Maintaining copper homeostasis: regulation of copper-trafficking proteins in response to copper deficiency or overload. *J Nutr Biochem* **15**, 316-22.
- Blagden, C. S., Currie, P. D., Ingham, P. W. and Hughes, S. M.** (1997). Notochord induction of zebrafish slow muscle mediated by Sonic hedgehog. *Genes Dev* **11**, 2163-75.
- Blank, R. D., Raggio, C. L., Giampietro, P. F. and Camacho, N. P.** (1999). A genomic approach to scoliosis pathogenesis. *Lupus* **8**, 356-60.
- Braga, V. M.** (2002). Cell-cell adhesion and signalling. *Curr Opin Cell Biol* **14**, 546-56.
- Brennan, C., Amacher, S. L. and Currie, P. D.** (2002). Somitogenesis. *Results Probl Cell Differ* **40**, 271-97.
- Carmany-Rampey, A. and Schier, A. F.** (2001). Single-cell internalization during zebrafish gastrulation. *Curr Biol* **11**, 1261-5.
- Carreira-Barbosa, F., Concha, M. L., Takeuchi, M., Ueno, N., Wilson, S. W. and Tada, M.** (2003). Prickle 1 regulates cell movements during gastrulation and neuronal migration in zebrafish. *Development* **130**, 4037-46.
- Carthew, R. W.** (2005). Adhesion proteins and the control of cell shape. *Curr Opin Genet Dev* **15**, 358-63.
- Cha, Y. I., Kim, S. H., Sepich, D., Buchanan, F. G., Solnica-Krezel, L. and DuBois, R. N.** (2006). Cyclooxygenase-1-derived PGE2 promotes cell motility via the G-protein-coupled EP4 receptor during vertebrate gastrulation. *Genes Dev* **20**, 77-86.

- Chadee, D. N., Taylor, W. R., Hurta, R. A., Allis, C. D., Wright, J. A. and Davie, J. R.** (1995). Increased phosphorylation of histone H1 in mouse fibroblasts transformed with oncogenes or constitutively active mitogen-activated protein kinase kinase. *J Biol Chem* **270**, 20098-105.
- Chen, Y. and Schier, A. F.** (2001). The zebrafish Nodal signal Squint functions as a morphogen. *Nature* **411**, 607-10.
- Cheng, F., Lindqvist, J., Haigh, C. L., Brown, D. R. and Mani, K.** (2006). Copper-dependent co-internalization of the prion protein and glypican-1. *J Neurochem* **98**, 1445-57.
- Choi, S. C. and Han, J. K.** (2002). Xenopus Cdc42 regulates convergent extension movements during gastrulation through Wnt/Ca²⁺ signaling pathway. *Dev Biol* **244**, 342-57.
- Ciruna, B., Jenny, A., Lee, D., Mlodzik, M. and Schier, A. F.** (2006). Planar cell polarity signalling couples cell division and morphogenesis during neurulation. *Nature* **439**, 220-4.
- Concha, M. L. and Adams, R. J.** (1998). Oriented cell divisions and cellular morphogenesis in the zebrafish gastrula and neurula: a time-lapse analysis. *Development* **125**, 983-94.
- Concordet, J. P., Lewis, K. E., Moore, J. W., Goodrich, L. V., Johnson, R. L., Scott, M. P. and Ingham, P. W.** (1996). Spatial regulation of a zebrafish patched homologue reflects the roles of sonic hedgehog and protein kinase A in neural tube and somite patterning. *Development* **122**, 2835-46.
- Conlon, F. L., Barth, K. S. and Robertson, E. J.** (1991). A novel retrovirally induced embryonic lethal mutation in the mouse: assessment of the developmental fate of embryonic stem cells homozygous for the 413.d proviral integration. *Development* **111**, 969-81.
- Conlon, F. L., Lyons, K. M., Takaesu, N., Barth, K. S., Kispert, A., Herrmann, B. and Robertson, E. J.** (1994). A primary requirement for nodal in the formation and maintenance of the primitive streak in the mouse. *Development* **120**, 1919-28.
- Copp, A. J., Greene, N. D. and Murdoch, J. N.** (2003). The genetic basis of mammalian neurulation. *Nat Rev Genet* **4**, 784-93.

Cortes, F., Daggett, D., Bryson-Richardson, R. J., Neyt, C., Maule, J., Gautier, P., Hollway, G. E., Keenan, D. and Currie, P. D. (2003). Cadherin-mediated differential cell adhesion controls slow muscle cell migration in the developing zebrafish myotome. *Dev Cell* **5**, 865-76.

Coutelle, O., Blagden, C. S., Hampson, R., Halai, C., Rigby, P. W. and Hughes, S. M. (2001). Hedgehog signalling is required for maintenance of myf5 and myoD expression and timely terminal differentiation in zebrafish adaxial myogenesis. *Dev Biol* **236**, 136-50.

Crawford, B. D., Henry, C. A., Clason, T. A., Becker, A. L. and Hille, M. B. (2003). Activity and distribution of paxillin, focal adhesion kinase, and cadherin indicate cooperative roles during zebrafish morphogenesis. *Mol Biol Cell* **14**, 3065-81.

Crow, M. T. and Stockdale, F. E. (1986). Myosin expression and specialization among the earliest muscle fibers of the developing avian limb. *Dev Biol* **113**, 238-54.

Csiszar, K. (2001). Lysyl oxidases: a novel multifunctional amine oxidase family. *Prog Nucleic Acid Res Mol Biol* **70**, 1-32.

Culotta, V. and Gitlin, J. (2001). Disorders of Copper Transport. In *The Molecular and Metabolic Basis of Inherited Disease*, vol. 3 (ed. C. Scriver A. Beaudet W. Sly and D. Valle), pp. 3105-3136. New York: McGraw-Hill.

Currie, P. D. and Ingham, P. W. (1996). Induction of a specific muscle cell type by a hedgehog-like protein in zebrafish. *Nature* **382**, 452-5.

D'Amico, L. A. and Cooper, M. S. (2001). Morphogenetic domains in the yolk syncytial layer of axiating zebrafish embryos. *Dev Dyn* **222**, 611-24.

Davidson, A. E., Balciunas, D., Mohn, D., Shaffer, J., Hermanson, S., Sivasubbu, S., Cliff, M. P., Hackett, P. B. and Ekker, S. C. (2003). Efficient gene delivery and gene expression in zebrafish using the Sleeping Beauty transposon. *Dev Biol* **263**, 191-202.

Detrich, H. W., Westerfield, M. and Zon, L. I. (2004). The zebrafish: cellular and developmental biology. In *Methods in cell biology*, v. 76, (ed., pp. xx, 632, [36]. Amsterdam; Boston: Elsevier Academic Press.

Devoto, S. H., Melancon, E., Eisen, J. S. and Westerfield, M. (1996). Identification of separate slow and fast muscle precursor cells in vivo, prior to somite formation. *Development* **122**, 3371-80.

Devoto, S. H., Stoiber, W., Hammond, C. L., Steinbacher, P., Haslett, J. R., Barresi, M. J., Patterson, S. E., Adiarte, E. G. and Hughes, S. M. (2006). Generality of vertebrate developmental patterns: evidence for a dermomyotome in fish. *Evol Dev* **8**, 101-10.

Domingo, C. and Keller, R. (1995). Induction of notochord cell intercalation behavior and differentiation by progressive signals in the gastrula of *Xenopus laevis*. *Development* **121**, 3311-21.

Dougan, S. T., Warga, R. M., Kane, D. A., Schier, A. F. and Talbot, W. S. (2003). The role of the zebrafish nodal-related genes *squint* and *cyclops* in patterning of mesendoderm. *Development* **130**, 1837-51.

Driever, W., Solnica-Krezel, L., Schier, A. F., Neuhauss, S. C., Malicki, J., Stemple, D. L., Stainier, D. Y., Zwartkruis, F., Abdelilah, S., Rangini, Z. et al. (1996). A genetic screen for mutations affecting embryogenesis in zebrafish. *Development* **123**, 37-46.

Driever, W., Stemple, D., Schier, A. and Solnica-Krezel, L. (1994). Zebrafish: genetic tools for studying vertebrate development. *Trends Genet* **10**, 152-9.

Endy, D. and Brent, R. (2001). Modelling cellular behaviour. *Nature* **409**, 391-5.

Erter, C. E., Wilm, T. P., Basler, N., Wright, C. V. and Solnica-Krezel, L. (2001). *Wnt8* is required in lateral mesendodermal precursors for neural posteriorization in vivo. *Development* **128**, 3571-83.

Fekany, K., Yamanaka, Y., Leung, T., Sirotkin, H. I., Topczewski, J., Gates, M. A., Hibi, M., Renucci, A., Stemple, D., Radbill, A. et al. (1999). The zebrafish *bozozok* locus encodes Dharma, a homeodomain protein essential for induction of gastrula organizer and dorsoanterior embryonic structures. *Development* **126**, 1427-38.

Fekany-Lee, K., Gonzalez, E., Miller-Bertoglio, V. and Solnica-Krezel, L. (2000). The homeobox gene *bozozok* promotes anterior neuroectoderm formation in zebrafish through negative regulation of BMP2/4 and Wnt pathways. *Development* **127**, 2333-45.

Feldman, B., Concha, M. L., Saude, L., Parsons, M. J., Adams, R. J., Wilson, S. W. and Stemple, D. L. (2002). Lefty antagonism of Squint is essential for normal gastrulation. *Curr Biol* **12**, 2129-35.

Feldman, B., Dougan, S. T., Schier, A. F. and Talbot, W. S. (2000). Nodal-related signals establish mesendodermal fate and trunk neural identity in zebrafish. *Curr Biol* **10**, 531-4.

Feldman, B., Gates, M. A., Egan, E. S., Dougan, S. T., Rennebeck, G., Sirotkin, H. I., Schier, A. F. and Talbot, W. S. (1998). Zebrafish organizer development and germ-layer formation require nodal-related signals. *Nature* **395**, 181-5.

Felsenfeld, A. L., Curry, M. and Kimmel, C. B. (1991). The fub-1 mutation blocks initial myofibril formation in zebrafish muscle pioneer cells. *Dev Biol* **148**, 23-30.

Felsenstein, J., (ed).

Formstone, C. J. and Mason, I. (2005). Combinatorial activity of Flamingo proteins directs convergence and extension within the early zebrafish embryo via the planar cell polarity pathway. *Dev Biol* **282**, 320-35.

Fransson, L. A. (2003). Glypicans. *Int J Biochem Cell Biol* **35**, 125-9.

Fransson, L. A., Belting, M., Cheng, F., Jonsson, M., Mani, K. and Sandgren, S. (2004). Novel aspects of glypican glycobiology. *Cell Mol Life Sci* **61**, 1016-24.

Furthauer, M., Van Celst, J., Thisse, C. and Thisse, B. (2004). Fgf signalling controls the dorsoventral patterning of the zebrafish embryo. *Development* **131**, 2853-64.

Geach, T. J. and Dale, L. (2005). Members of the lysyl oxidase family are expressed during the development of the frog *Xenopus laevis*. *Differentiation* **73**, 414-24.

Giacomello, E., Vallin, J., Morali, O., Coulter, I. S., Boulekbache, H., Thiery, J. P. and Broders, F. (2002). Type I cadherins are required for differentiation and coordinated rotation in *Xenopus laevis* somitogenesis. *Int J Dev Biol* **46**, 785-92.

Glasgow, E. and Tomarev, S. I. (1998). Restricted expression of the homeobox gene *prox 1* in developing zebrafish. *Mech Dev* **76**, 175-8.

Glickman, N. S., Kimmel, C. B., Jones, M. A. and Adams, R. J. (2003). Shaping the zebrafish notochord. *Development* **130**, 873-87.

Gong, Y., Mo, C. and Fraser, S. E. (2004). Planar cell polarity signalling controls cell division orientation during zebrafish gastrulation. *Nature* **430**, 689-93.

Gore, A. V., Maegawa, S., Cheong, A., Gilligan, P. C., Weinberg, E. S. and Sampath, K. (2005). The zebrafish dorsal axis is apparent at the four-cell stage. *Nature* **438**, 1030-5.

Goto, T., Davidson, L., Asashima, M. and Keller, R. (2005). Planar cell polarity genes regulate polarized extracellular matrix deposition during frog gastrulation. *Curr Biol* **15**, 787-93.

Griffin, K. J., Amacher, S. L., Kimmel, C. B. and Kimelman, D. (1998). Molecular identification of spadetail: regulation of zebrafish trunk and tail mesoderm formation by T-box genes. *Development* **125**, 3379-88.

Grimaldi, A., Tettamanti, G., Martin, B. L., Gaffield, W., Pownall, M. E. and Hughes, S. M. (2004). Hedgehog regulation of superficial slow muscle fibres in *Xenopus* and the evolution of tetrapod trunk myogenesis. *Development* **131**, 3249-62.

Gritsman, K., Zhang, J., Cheng, S., Heckscher, E., Talbot, W. S. and Schier, A. F. (1999). The EGF-CFC protein one-eyed pinhead is essential for nodal signaling. *Cell* **97**, 121-32.

Grunwald, D. J. and Streisinger, G. (1992). Induction of mutations in the zebrafish with ultraviolet light. *Genet Res* **59**, 93-101.

Gubb, D. and Garcia-Bellido, A. (1982). A genetic analysis of the determination of cuticular polarity during development in *Drosophila melanogaster*. *J Embryol Exp Morphol* **68**, 37-57.

Guo, N., Hawkins, C. and Nathans, J. (2004). Frizzled6 controls hair patterning in mice. *Proc Natl Acad Sci U S A* **101**, 9277-81.

Habas, R., Dawid, I. B. and He, X. (2003). Coactivation of Rac and Rho by Wnt/Frizzled signaling is required for vertebrate gastrulation. *Genes Dev* **17**, 295-309.

Habas, R., Kato, Y. and He, X. (2001). Wnt/Frizzled activation of Rho regulates vertebrate gastrulation and requires a novel Formin homology protein Daam1. *Cell* **107**, 843-54.

Haffter, P., Granato, M., Brand, M., Mullins, M. C., Hammerschmidt, M., Kane, D. A., Odenthal, J., van Eeden, F. J., Jiang, Y. J., Heisenberg, C. P. et al. (1996). The identification of genes with unique and essential functions in the development of the zebrafish, *Danio rerio*. *Development* **123**, 1-36.

Hall, A. and Nobes, C. D. (2000). Rho GTPases: molecular switches that control the organization and dynamics of the actin cytoskeleton. *Philos Trans R Soc Lond B Biol Sci* **355**, 965-70.

Halpern, M. E., Ho, R. K., Walker, C. and Kimmel, C. B. (1993). Induction of muscle pioneers and floor plate is distinguished by the zebrafish no tail mutation. *Cell* **75**, 99-111.

Hamilton, L. (1969). The formation of somites in *Xenopus*. *J Embryol Exp Morphol* **22**, 253-64.

Hammerschmidt, M. and Mullins, M. C. (2002). Dorsoventral patterning in the zebrafish: bone morphogenetic proteins and beyond. *Results Probl Cell Differ* **40**, 72-95.

Hammerschmidt, M., Pelegri, F., Mullins, M. C., Kane, D. A., Brand, M., van Eeden, F. J., Furutani-Seiki, M., Granato, M., Haffter, P., Heisenberg, C. P. et al. (1996a). Mutations affecting morphogenesis during gastrulation and tail formation in the zebrafish, *Danio rerio*. *Development* **123**, 143-51.

Hammerschmidt, M., Serbedzija, G. N. and McMahon, A. P. (1996b). Genetic analysis of dorsoventral pattern formation in the zebrafish: requirement of a BMP-like ventralizing activity and its dorsal repressor. *Genes Dev* **10**, 2452-61.

Hammond, C. L., Hinits, Y., Osborn, D. P., Minchin, J. E., Tettamanti, G. and Hughes, S. M. (2006). Signals and myogenic regulatory factors restrict pax3 and pax7 expression to dermomyotome-like tissue in zebrafish. *Dev Biol*.

Hamza, I., Faisst, A., Prohaska, J., Chen, J., Gruss, P. and Gitlin, J. D. (2001). The metallochaperone Atox1 plays a critical role in perinatal copper homeostasis 10.1073/pnas.111058498. *PNAS* **98**, 6848-6852.

Harland, R. M. (2004). Dorsoventral patterning of the mesoderm. In *Gastrulation: From cells to Embryos.*, (ed. C. D. Stern), pp. 373-388. New York: Cold Spring Harbor Laboratory Press.

Hashimoto, H., Itoh, M., Yamanaka, Y., Yamashita, S., Shimizu, T., Solnica-Krezel, L., Hibi, M. and Hirano, T. (2000). Zebrafish Dkk1 functions in forebrain specification and axial mesendoderm formation. *Dev Biol* **217**, 138-52.

Hatta, K., Bremiller, R., Westerfield, M. and Kimmel, C. B. (1991). Diversity of expression of engrailed-like antigens in zebrafish. *Development* **112**, 821-32.

Heisenberg, C. P., Tada, M., Rauch, G. J., Saude, L., Concha, M. L., Geisler, R., Stemple, D. L., Smith, J. C. and Wilson, S. W. (2000). Silberblick/Wnt11 mediates convergent extension movements during zebrafish gastrulation. *Nature* **405**, 76-81.

Henry, C. A. and Amacher, S. L. (2004). Zebrafish slow muscle cell migration induces a wave of fast muscle morphogenesis. *Dev Cell* **7**, 917-23.

Henry, C. A., Hall, L. A., Burr Hille, M., Solnica-Krezel, L. and Cooper, M. S. (2000). Somites in zebrafish doubly mutant for knypek and trilobite form without internal mesenchymal cells or compaction. *Curr Biol* **10**, 1063-6.

Henry, C. A., McNulty, I. M., Durst, W. A., Munchel, S. E. and Amacher, S. L. (2005). Interactions between muscle fibers and segment boundaries in zebrafish. *Dev Biol* **287**, 346-60.

Hirsinger, E., Stellabotte, F., Devoto, S. H. and Westerfield, M. (2004). Hedgehog signaling is required for commitment but not initial induction of slow muscle precursors. *Dev Biol* **275**, 143-57.

Ho, R. K. and Kane, D. A. (1990). Cell-autonomous action of zebrafish spt-1 mutation in specific mesodermal precursors. *Nature* **348**, 728-30.

Holtfreter, J. (1933). Die totale Exogastrulation, eine Selbstablosung des Ektoderms vom Entomesoderm. *Roux' Arch. F. Entw. mech.* **129**, 669-793.

Iuchi, I. and Yamamoto, M. (1983). Erythropoiesis in the developing rainbow trout, *Salmo gairdneri irideus*: histochemical and immunochemical detection of erythropoietic organs. *J Exp Zool* **226**, 409-17.

- Jenny, A., Darken, R. S., Wilson, P. A. and Mlodzik, M.** (2003). Prickle and Strabismus form a functional complex to generate a correct axis during planar cell polarity signaling. *Embo J* **22**, 4409-20.
- Jessen, J. R. and Solnica-Krezel, L.** (2004). Identification and developmental expression pattern of van gogh-like 1, a second zebrafish strabismus homologue. *Gene Expr Patterns* **4**, 339-44.
- Jessen, J. R., Topczewski, J., Bingham, S., Sepich, D. S., Marlow, F., Chandrasekhar, A. and Solnica-Krezel, L.** (2002). Zebrafish trilobite identifies new roles for Strabismus in gastrulation and neuronal movements. *Nat Cell Biol* **4**, 610-5.
- Jiang, D., Munro, E. M. and Smith, W. C.** (2005). Ascidian prickle regulates both mediolateral and anterior-posterior cell polarity of notochord cells. *Curr Biol* **15**, 79-85.
- Julich, D., Geisler, R. and Holley, S. A.** (2005). Integrin α 5 and delta/notch signaling have complementary spatiotemporal requirements during zebrafish somitogenesis. *Dev Cell* **8**, 575-86.
- Kane, D. A. and Kimmel, C. B.** (1993). The zebrafish midblastula transition. *Development* **119**, 447-56.
- Kane, D. A., McFarland, K. N. and Warga, R. M.** (2005). Mutations in half baked/E-cadherin block cell behaviors that are necessary for teleost epiboly. *Development* **132**, 1105-16.
- Kanki, J. P. and Ho, R. K.** (1997). The development of the posterior body in zebrafish. *Development* **124**, 881-93.
- Katoh, K., Kano, Y., Amano, M., Onishi, H., Kaibuchi, K. and Fujiwara, K.** (2001). Rho-kinase--mediated contraction of isolated stress fibers. *J Cell Biol* **153**, 569-84.
- Kazakova, N., Li, H., Mora, A., Jessen, K. R., Mirsky, R., Richardson, W. D. and Smith, H. K.** (2006). A screen for mutations in zebrafish that affect myelin gene expression in Schwann cells and oligodendrocytes. *Dev Biol* **297**, 1-13.
- Keen, C., Uriu-Hare, J., Hawk, S., Jankowski, M., Daston, G., Kwik-Urbe, C. and Rucker, R.** (1998). Effect of copper deficiency on prenatal development and pregnancy outcome

. *Am J Clin Nutr* **67**, 1003S-1011.

Keller, R. (2000). The origin and morphogenesis of amphibian somites. *Curr Top Dev Biol* **47**, 183-246.

Keller, R. (2005). Cell migration during gastrulation. *Curr Opin Cell Biol* **17**, 533-41.

Keller, R., Davidson, L., Edlund, A., Elul, T., Ezin, M., Shook, D. and Skoglund, P. (2000). Mechanisms of convergence and extension by cell intercalation. *Philos Trans R Soc Lond B Biol Sci* **355**, 897-922.

Keller, R., Davidson, L. A. and Shook, D. R. (2003). How we are shaped: the biomechanics of gastrulation. *Differentiation* **71**, 171-205.

Keller, R., Shih, J. and Domingo, C. (1992). The patterning and functioning of protrusive activity during convergence and extension of the *Xenopus* organiser. *Dev Suppl*, 81-91.

Keller, R. and Tibbetts, P. (1989). Mediolateral cell intercalation in the dorsal, axial mesoderm of *Xenopus laevis*. *Dev Biol* **131**, 539-49.

Keller, R. E. (1980). The cellular basis of epiboly: an SEM study of deep-cell rearrangement during gastrulation in *Xenopus laevis*. *J Embryol Exp Morphol* **60**, 201-34.

Kilian, B., Mansukoski, H., Barbosa, F. C., Ulrich, F., Tada, M. and Heisenberg, C. P. (2003). The role of Ppt/Wnt5 in regulating cell shape and movement during zebrafish gastrulation. *Mech Dev* **120**, 467-76.

Kim, S. H., Yamamoto, A., Bouwmeester, T., Agius, E. and Robertis, E. M. (1998). The role of paraxial protocadherin in selective adhesion and cell movements of the mesoderm during *Xenopus* gastrulation. *Development* **125**, 4681-90.

Kimmel, C. B., Ballard, W. W., Kimmel, S. R., Ullmann, B. and Schilling, T. F. (1995). Stages of embryonic development of the zebrafish. *Dev Dyn* **203**, 253-310.

- Kimmel, C. B., Kane, D. A., Walker, C., Warga, R. M. and Rothman, M. B.** (1989). A mutation that changes cell movement and cell fate in the zebrafish embryo. *Nature* **337**, 358-62.
- Kimmel, C. B., Warga, R. M. and Schilling, T. F.** (1990). Origin and organization of the zebrafish fate map. *Development* **108**, 581-94.
- Kinoshita, N., Iioka, H., Miyakoshi, A. and Ueno, N.** (2003). PKC delta is essential for Dishevelled function in a noncanonical Wnt pathway that regulates *Xenopus* convergent extension movements. *Genes Dev* **17**, 1663-76.
- Kishimoto, Y., Lee, K. H., Zon, L., Hammerschmidt, M. and Schulte-Merker, S.** (1997). The molecular nature of zebrafish swirl: BMP2 function is essential during early dorsoventral patterning. *Development* **124**, 4457-66.
- Klein, T. J. and Mlodzik, M.** (2005). Planar cell polarization: an emerging model points in the right direction. *Annu Rev Cell Dev Biol* **21**, 155-76.
- Koshida, S., Kishimoto, Y., Ustumi, H., Shimizu, T., Furutani-Seiki, M., Kondoh, H. and Takada, S.** (2005). Integrin α 5-dependent fibronectin accumulation for maintenance of somite boundaries in zebrafish embryos. *Dev Cell* **8**, 587-98.
- Kragtorp, K. A. and Miller, J. R.** (2006). Regulation of somitogenesis by Ena/VASP proteins and FAK during *Xenopus* development. *Development* **133**, 685-95.
- Krauss, S., Concordet, J. P. and Ingham, P. W.** (1993). A functionally conserved homolog of the *Drosophila* segment polarity gene *hh* is expressed in tissues with polarizing activity in zebrafish embryos. *Cell* **75**, 1431-44.
- Kudoh, T., Tsang, M., Hukriede, N. A., Chen, X., Dedekian, M., Clarke, C. J., Kiang, A., Schultz, S., Epstein, J. A., Toyama, R. et al.** (2001). A gene expression screen in zebrafish embryogenesis. *Genome Res* **11**, 1979-87.
- Kuhlman, J. and Eisen, J. S.** (2006). Genetic screen for mutations affecting development and function of the enteric nervous system. *Dev Dyn*.
- Kwan, K. M. and Kirschner, M. W.** (2003). *Xbra* functions as a switch between cell migration and convergent extension in the *Xenopus* gastrula. *Development* **130**, 1961-72.

Leptin, M. (2005). Gastrulation movements: the logic and the nuts and bolts. *Dev Cell* **8**, 305-20.

Lin, F., Sepich, D. S., Chen, S., Topczewski, J., Yin, C., Solnica-Krezel, L. and Hamm, H. (2005). Essential roles of G α _{12/13} signaling in distinct cell behaviors driving zebrafish convergence and extension gastrulation movements. *J Cell Biol* **169**, 777-87.

Linney, E. and Udvadia, A. J. (2004). Construction and detection of fluorescent, germline transgenic zebrafish. *Methods Mol Biol* **254**, 271-88.

Linsenmayer, T. F., Gibney, E. and Schmid, T. M. (1986). Segmental appearance of type X collagen in the developing avian notochord. *Dev Biol* **113**, 467-73.

Lutsenko, S. and Petris, M. J. (2003). Function and regulation of the mammalian copper-transporting ATPases: insights from biochemical and cell biological approaches. *J Membr Biol* **191**, 1-12.

Mahadevan, L. C., Willis, A. C. and Barratt, M. J. (1991). Rapid histone H3 phosphorylation in response to growth factors, phorbol esters, okadaic acid, and protein synthesis inhibitors. *Cell* **65**, 775-83.

Makita, R., Mizuno, T., Koshida, S., Kuroiwa, A. and Takeda, H. (1998). Zebrafish wnt11: pattern and regulation of the expression by the yolk cell and No tail activity. *Mech Dev* **71**, 165-76.

Marlow, F., Gonzalez, E. M., Yin, C., Rojo, C. and Solnica-Krezel, L. (2004). No tail co-operates with non-canonical Wnt signaling to regulate posterior body morphogenesis in zebrafish. *Development* **131**, 203-16.

Marlow, F., Topczewski, J., Sepich, D. and Solnica-Krezel, L. (2002). Zebrafish Rho kinase 2 acts downstream of Wnt11 to mediate cell polarity and effective convergence and extension movements. *Curr Biol* **12**, 876-84.

Marlow, F., Zwartkruis, F., Malicki, J., Neuhauss, S. C., Abbas, L., Weaver, M., Driever, W. and Solnica-Krezel, L. (1998). Functional interactions of genes mediating convergent extension, knypek and trilobite, during the partitioning of the eye primordium in zebrafish. *Dev Biol* **203**, 382-99.

- Matakatsu, H. and Blair, S. S.** (2004). Interactions between Fat and Dachshous and the regulation of planar cell polarity in the Drosophila wing. *Development* **131**, 3785-94.
- McCaig, C. D.** (1986). Myoblasts and notochord influence the orientation of somitic myoblasts from *Xenopus laevis*. *J Embryol Exp Morphol* **93**, 121-31.
- McCawley, L. J. and Matrisian, L. M.** (2001). Matrix metalloproteinases: they're not just for matrix anymore! *Curr Opin Cell Biol* **13**, 534-40.
- Mercer, J. F. and Llanos, R. M.** (2003). Molecular and cellular aspects of copper transport in developing mammals. *J Nutr* **133**, 1481S-4S.
- Miyagi, C., Yamashita, S., Ohba, Y., Yoshizaki, H., Matsuda, M. and Hirano, T.** (2004). STAT3 noncell-autonomously controls planar cell polarity during zebrafish convergence and extension. *J Cell Biol* **166**, 975-81.
- Miyamoto, S., Katz, B. Z., Lafrenie, R. M. and Yamada, K. M.** (1998). Fibronectin and integrins in cell adhesion, signaling, and morphogenesis. *Ann N Y Acad Sci* **857**, 119-29.
- Mlodzik, M.** (2002). Planar cell polarization: do the same mechanisms regulate Drosophila tissue polarity and vertebrate gastrulation? *Trends Genet* **18**, 564-71.
- Moeller, H., Jenny, A., Schaeffer, H. J., Schwarz-Romond, T., Mlodzik, M., Hammerschmidt, M. and Birchmeier, W.** (2006). Diversin regulates heart formation and gastrulation movements in development. *Proc Natl Acad Sci U S A* **103**, 15900-5.
- Morin-Kensicki, E. M. and Eisen, J. S.** (1997). Sclerotome development and peripheral nervous system segmentation in embryonic zebrafish. *Development* **124**, 159-67.
- Motoike, T., Loughna, S., Perens, E., Roman, B. L., Liao, W., Chau, T. C., Richardson, C. D., Kawate, T., Kuno, J., Weinstein, B. M. et al.** (2000). Universal GFP reporter for the study of vascular development. *Genesis* **28**, 75-81.
- Mullins, M. C., Hammerschmidt, M., Haffter, P. and Nusslein-Volhard, C.** (1994). Large-scale mutagenesis in the zebrafish: in search of genes controlling development in a vertebrate. *Curr Biol* **4**, 189-202.

Mullins, M. C., Hammerschmidt, M., Kane, D. A., Odenthal, J., Brand, M., van Eeden, F. J., Furutani-Seiki, M., Granato, M., Haffter, P., Heisenberg, C. P. et al. (1996). Genes establishing dorsoventral pattern formation in the zebrafish embryo: the ventral specifying genes. *Development* **123**, 81-93.

Myers, D. C., Sepich, D. S. and Solnica-Krezel, L. (2002a). Bmp activity gradient regulates convergent extension during zebrafish gastrulation. *Dev Biol* **243**, 81-98.

Myers, D. C., Sepich, D. S. and Solnica-Krezel, L. (2002b). Convergence and extension in vertebrate gastrulae: cell movements according to or in search of identity? *Trends Genet* **18**, 447-55.

Nakano, Y., Kim, H. R., Kawakami, A., Roy, S., Schier, A. F. and Ingham, P. W. (2004). Inactivation of dispatched 1 by the chameleon mutation disrupts Hedgehog signalling in the zebrafish embryo. *Dev Biol* **269**, 381-92.

Nasevicius, A. and Ekker, S. C. (2000). Effective targeted gene 'knockdown' in zebrafish. *Nat Genet* **26**, 216-20.

Neave, B., Holder, N. and Patient, R. (1997). A graded response to BMP-4 spatially coordinates patterning of the mesoderm and ectoderm in the zebrafish. *Mech Dev* **62**, 183-95.

Nikaido, M., Kawakami, A., Sawada, A., Furutani-Seiki, M., Takeda, H. and Araki, K. (2002). Tbx24, encoding a T-box protein, is mutated in the zebrafish somite-segmentation mutant fused somites. *Nat Genet* **31**, 195-9.

Ninomiya, H., Elinson, R. P. and Winklbauer, R. (2004). Antero-posterior tissue polarity links mesoderm convergent extension to axial patterning. *Nature* **430**, 364-7.

Nobes, C. D. and Hall, A. (1999). Rho GTPases control polarity, protrusion, and adhesion during cell movement. *J Cell Biol* **144**, 1235-44.

O'Halloran, T. V. and Culotta, V. C. (2000). Metallochaperones, an intracellular shuttle service for metal ions. *J Biol Chem* **275**, 25057-60.

Ochi, H., Pearson, B. J., Chuang, P. T., Hammerschmidt, M. and Westerfield, M. (2006). Hhip regulates zebrafish muscle development by both sequestering Hedgehog and modulating localization of Smoothed. *Dev Biol* **297**, 127-40.

Ohkawara, B., Yamamoto, T. S., Tada, M. and Ueno, N. (2003). Role of glypican 4 in the regulation of convergent extension movements during gastrulation in *Xenopus laevis*. *Development* **130**, 2129-38.

Orlow, S. J., Lamoreux, M. L., Pifko-Hirst, S. and Zhou, B. K. (1993). Pathogenesis of the platinum (cp) mutation, a model for oculocutaneous albinism. *J Invest Dermatol* **101**, 137-40.

Park, M. and Moon, R. T. (2002). The planar cell-polarity gene *stbm* regulates cell behaviour and cell fate in vertebrate embryos. *Nat Cell Biol* **4**, 20-5.

Park, T. J., Haigo, S. L. and Wallingford, J. B. (2006). Ciliogenesis defects in embryos lacking *inturned* or *fuzzy* function are associated with failure of planar cell polarity and Hedgehog signaling. *Nat Genet* **38**, 303-11.

Parsons, M. J., Pollard, S. M., Saude, L., Feldman, B., Coutinho, P., Hirst, E. M. and Stemple, D. L. (2002). Zebrafish mutants identify an essential role for laminins in notochord formation. *Development* **129**, 3137-46.

Pena, M. M. O., Lee, J. and Thiele, D. J. (1999). A Delicate Balance: Homeostatic Control of Copper Uptake and Distribution. *J. Nutr.* **129**, 1251-1260.

Penzo-Mendez, A., Umbhauer, M., Djiane, A., Boucaut, J. C. and Riou, J. F. (2003). Activation of Gbetagamma signaling downstream of Wnt-11/Xfz7 regulates Cdc42 activity during *Xenopus* gastrulation. *Dev Biol* **257**, 302-14.

Peterson, R. T., Link, B. A., Dowling, J. E. and Schreiber, S. L. (2000a). Small molecule developmental screens reveal the logic and timing of vertebrate development. *Proc Natl Acad Sci U S A* **97**, 12965-9.

Peterson, R. T., Link, B. A., Dowling, J. E. and Schreiber, S. L. (2000b). Small molecule developmental screens reveal the logic and timing of vertebrate development 10.1073/pnas.97.24.12965. *PNAS* **97**, 12965-12969.

Peterson, R. T., Shaw, S. Y., Peterson, T. A., Milan, D. J., Zhong, T. P., Schreiber, S. L., MacRae, C. A. and Fishman, M. C. (2004). Chemical suppression of a genetic mutation in a zebrafish model of aortic coarctation. *Nat Biotechnol* **22**, 595-9.

Pourquie, O. (2001). Vertebrate somitogenesis. *Annu Rev Cell Dev Biol* **17**, 311-50.

Raffel, M., Willert, C., Kompenhans, J. (1998). Particle Image Velocimetry: A Practical Guide: Springer, Berlin.

Rauch, G. J., Hammerschmidt, M., Blader, P., Schauerte, H. E., Strahle, U., Ingham, P. W., McMahon, A. P. and Haffter, P. (1997). Wnt5 is required for tail formation in the zebrafish embryo. *Cold Spring Harb Symp Quant Biol* **62**, 227-34.

Rawls, J. F., Mellgren, E. M. and Johnson, S. L. (2001). How the Zebrafish Gets Its Stripes. *Developmental Biology* **240**, 301-314.

Riggio, M., Filosa, S., Parisi, E. and Scudiero, R. (2003). Changes in zinc, copper and metallothionein contents during oocyte growth and early development of the teleost *Danio rerio* (zebrafish). *Comp Biochem Physiol C Toxicol Pharmacol* **135**, 191-6.

Rosenzweig, A. C. (2002). Metallochaperones: bind and deliver. *Chem Biol* **9**, 673-7.

Rothbacher, U., Laurent, M. N., Deardorff, M. A., Klein, P. S., Cho, K. W. and Fraser, S. E. (2000). Dishevelled phosphorylation, subcellular localization and multimerization regulate its role in early embryogenesis. *Embo J* **19**, 1010-22.

Roy, S., Wolff, C. and Ingham, P. W. (2001). The u-boot mutation identifies a Hedgehog-regulated myogenic switch for fiber-type diversification in the zebrafish embryo. *Genes Dev* **15**, 1563-76.

Rudnicki, M. A., Schnegelsberg, P. N., Stead, R. H., Braun, T., Arnold, H. H. and Jaenisch, R. (1993). MyoD or Myf-5 is required for the formation of skeletal muscle. *Cell* **75**, 1351-9.

Saude, L., Woolley, K., Martin, P., Driever, W. and Stemple, D. L. (2000). Axis-inducing activities and cell fates of the zebrafish organizer. *Development* **127**, 3407-17.

Schier, A. F. and Talbot, W. S. (2005). Molecular genetics of axis formation in zebrafish. *Annu Rev Genet* **39**, 561-613.

Schneider, S., Steinbeisser, H., Warga, R. M. and Hausen, P. (1996). Beta-catenin translocation into nuclei demarcates the dorsalizing centers in frog and fish embryos. *Mech Dev* **57**, 191-8.

Schoenwolf, G. C. and Smith, J. L. (2000). Gastrulation and early mesodermal patterning in vertebrates. *Methods Mol Biol* **135**, 113-25.

Schulte-Merker, S., Ho, R. K., Herrmann, B. G. and Nusslein-Volhard, C. (1992). The protein product of the zebrafish homologue of the mouse T gene is expressed in nuclei of the germ ring and the notochord of the early embryo. *Development* **116**, 1021-32.

Schulte-Merker, S., Lee, K. J., McMahon, A. P. and Hammerschmidt, M. (1997). The zebrafish organizer requires chordino. *Nature* **387**, 862-3.

Schulte-Merker, S., van Eeden, F. J., Halpern, M. E., Kimmel, C. B. and Nusslein-Volhard, C. (1994). no tail (ntl) is the zebrafish homologue of the mouse T (Brachyury) gene. *Development* **120**, 1009-15.

Scott, A. and Stemple, D. L. (2005). Zebrafish notochordal basement membrane: signaling and structure. *Curr Top Dev Biol* **65**, 229-53.

Sepich, D. S., Calmelet, C., Kiskowski, M. and Solnica-Krezel, L. (2005). Initiation of convergence and extension movements of lateral mesoderm during zebrafish gastrulation. *Dev Dyn* **234**, 279-92.

Sepich, D. S., Myers, D. C., Short, R., Topczewski, J., Marlow, F. and Solnica-Krezel, L. (2000). Role of the zebrafish trilobite locus in gastrulation movements of convergence and extension. *Genesis* **27**, 159-73.

Shih, J. and Fraser, S. E. (1996). Characterizing the zebrafish organizer: microsurgical analysis at the early-shield stage. *Development* **122**, 1313-22.

Shih, J. and Keller, R. (1992a). Cell motility driving mediolateral intercalation in explants of *Xenopus laevis*. *Development* **116**, 901-14.

Shih, J. and Keller, R. (1992b). Patterns of cell motility in the organizer and dorsal mesoderm of *Xenopus laevis*. *Development* **116**, 915-30.

Shim, H. and Harris, Z. L. (2003). Genetic defects in copper metabolism. *J Nutr* **133**, 1527S-31S.

Shimizu, T., Yabe, T., Muraoka, O., Yonemura, S., Aramaki, S., Hatta, K., Bae, Y. K., Nojima, H. and Hibi, M. (2005). E-cadherin is required for gastrulation cell movements in zebrafish. *Mech Dev* **122**, 747-63.

Simon, M. A. (2004). Planar cell polarity in the Drosophila eye is directed by graded Four-jointed and Dachshous expression. *Development* **131**, 6175-84.

Sokol, S. Y. (1996). Analysis of Dishevelled signalling pathways during Xenopus development. *Curr Biol* **6**, 1456-67.

Solnica-Krezel, L. (1999). Pattern formation in zebrafish--fruitful liaisons between embryology and genetics. *Curr Top Dev Biol* **41**, 1-35.

Solnica-Krezel, L. (2005). Conserved patterns of cell movements during vertebrate gastrulation. *Curr Biol* **15**, R213-28.

Solnica-Krezel, L. (2006). Gastrulation in zebrafish -- all just about adhesion? *Curr Opin Genet Dev* **16**, 433-41.

Solnica-Krezel, L. and Driever, W. (2001). The role of the homeodomain protein Bozozok in zebrafish axis formation. *Int J Dev Biol* **45**, 299-310.

Solnica-Krezel, L., Schier, A. F. and Driever, W. (1994a). Efficient recovery of ENU-induced mutations from the zebrafish germline. *Genetics* **136**, 1401-20.

Solnica-Krezel, L., Schier, A. F. and Driever, W. (1994b). Efficient Recovery of ENU-Induced Mutations From the Zebrafish Germline
. *Genetics* **136**, 1401-1420.

Solnica-Krezel, L., Stemple, D. L. and Driever, W. (1995). Transparent things: cell fates and cell movements during early embryogenesis of zebrafish. *Bioessays* **17**, 931-9.

Solnica-Krezel, L., Stemple, D. L., Mountcastle-Shah, E., Rangini, Z., Neuhauss, S. C., Malicki, J., Schier, A. F., Stainier, D. Y., Zwartkruis, F., Abdelilah, S. et al.

(1996). Mutations affecting cell fates and cellular rearrangements during gastrulation in zebrafish. *Development* **123**, 67-80.

Spemann, H. (1938). Embryonic Development and Induction. New Haven, CT: Yale University Press.

Stemple, D. L. (2005). Structure and function of the notochord: an essential organ for chordate development. *Development* **132**, 2503-12.

Stern, C. D. (2004). Gastrulation.

Stern, H., Murphey, R., Shepard, J., Amatruda, J., Straub, C., Pfaff, K., Weber, G., Tallarico, J., King, R. and Zon, L. (2005). Small molecules that delay S phase suppress a zebrafish bmyb mutant. *Nature Chemical Biology* **1**, 366-70.

Stickney, H. L., Barresi, M. J. and Devoto, S. H. (2000). Somite development in zebrafish. *Dev Dyn* **219**, 287-303.

Stone, D. M., Hynes, M., Armanini, M., Swanson, T. A., Gu, Q., Johnson, R. L., Scott, M. P., Pennica, D., Goddard, A., Phillips, H. et al. (1996). The tumour-suppressor gene patched encodes a candidate receptor for Sonic hedgehog. *Nature* **384**, 129-34.

Strutt, D. I. (2002). The asymmetric subcellular localisation of components of the planar polarity pathway. *Semin Cell Dev Biol* **13**, 225-31.

Supatto, W., Debarre, D., Moulia, B., Brouzes, E., Martin, J. L., Farge, E. and Beaurepaire, E. (2005). In vivo modulation of morphogenetic movements in Drosophila embryos with femtosecond laser pulses. *Proc Natl Acad Sci U S A* **102**, 1047-52.

Tada, M., Concha, M. L. and Heisenberg, C. P. (2002). Non-canonical Wnt signalling and regulation of gastrulation movements. *Semin Cell Dev Biol* **13**, 251-60.

Tajbakhsh, S., Borello, U., Vivarelli, E., Kelly, R., Papkoff, J., Duprez, D., Buckingham, M. and Cossu, G. (1998). Differential activation of Myf5 and MyoD by different Wnts in explants of mouse paraxial mesoderm and the later activation of myogenesis in the absence of Myf5. *Development* **125**, 4155-62.

Talbot, W. S., Trevarrow, B., Halpern, M. E., Melby, A. E., Farr, G., Postlethwait, J. H., Jowett, T., Kimmel, C. B. and Kimelman, D. (1995). A homeobox gene essential for zebrafish notochord development. *Nature* **378**, 150-7.

Thisse, B., Heyer, V., Lux, A., Alunni, V., Degraeve, A., Seiliez, I., Kirchner, J., Parkhill, J. P. and Thisse, C. (2004). Spatial and temporal expression of the zebrafish genome by large-scale in situ hybridization screening. *Methods Cell Biol* **77**, 505-19.

Thisse, C., Thisse, B., Schilling, T. F. and Postlethwait, J. H. (1993). Structure of the zebrafish *snail1* gene and its expression in wild-type, spadetail and no tail mutant embryos. *Development* **119**, 1203-15.

Thompson, J. D., Higgins, D. G. and Gibson, T. J. (1994). CLUSTAL W: improving the sensitivity of progressive multiple sequence alignment through sequence weighting, position-specific gap penalties and weight matrix choice. *Nucleic Acids Res* **22**, 4673-80.

Topczewska, J. M., Topczewski, J., Shostak, A., Kume, T., Solnica-Krezel, L. and Hogan, B. L. (2001). The winged helix transcription factor *Foxc1a* is essential for somitogenesis in zebrafish. *Genes Dev* **15**, 2483-93.

Topczewski, J., Sepich, D. S., Myers, D. C., Walker, C., Amores, A., Lele, Z., Hammerschmidt, M., Postlethwait, J. and Solnica-Krezel, L. (2001). The zebrafish glypican *knypek* controls cell polarity during gastrulation movements of convergent extension. *Dev Cell* **1**, 251-64.

Torres, M. A., Yang-Snyder, J. A., Purcell, S. M., DeMarais, A. A., McGrew, L. L. and Moon, R. T. (1996). Activities of the Wnt-1 class of secreted signaling factors are antagonized by the Wnt-5A class and by a dominant negative cadherin in early *Xenopus* development. *J Cell Biol* **133**, 1123-37.

Tree, D. R., Shulman, J. M., Rousset, R., Scott, M. P., Gubb, D. and Axelrod, J. D. (2002). Prickle mediates feedback amplification to generate asymmetric planar cell polarity signaling. *Cell* **109**, 371-81.

Trinh, L. A. and Stainier, D. Y. (2004). Fibronectin regulates epithelial organization during myocardial migration in zebrafish. *Dev Cell* **6**, 371-82.

Udvardia, A. J. and Linney, E. (2003). Windows into development: historic, current, and future perspectives on transgenic zebrafish. *Dev Biol* **256**, 1-17.

Ulrich, F., Concha, M. L., Heid, P. J., Voss, E., Witzel, S., Roehl, H., Tada, M., Wilson, S. W., Adams, R. J., Soll, D. R. et al. (2003). Slb/Wnt11 controls hypoblast cell migration and morphogenesis at the onset of zebrafish gastrulation. *Development* **130**, 5375-84.

Ulrich, F., Krieg, M., Schotz, E. M., Link, V., Castanon, I., Schnabel, V., Taubenberger, A., Mueller, D., Puech, P. H. and Heisenberg, C. P. (2005). Wnt11 functions in gastrulation by controlling cell cohesion through Rab5c and E-cadherin. *Dev Cell* **9**, 555-64.

Ungar, A. R., Kelly, G. M. and Moon, R. T. (1995). Wnt4 affects morphogenesis when misexpressed in the zebrafish embryo. *Mech Dev* **52**, 153-64.

van Eeden, F. J., Granato, M., Schach, U., Brand, M., Furutani-Seiki, M., Haffter, P., Hammerschmidt, M., Heisenberg, C. P., Jiang, Y. J., Kane, D. A. et al. (1996). Mutations affecting somite formation and patterning in the zebrafish, *Danio rerio*. *Development* **123**, 153-64.

Veeman, M. T., Axelrod, J. D. and Moon, R. T. (2003a). A second canon. Functions and mechanisms of beta-catenin-independent Wnt signaling. *Dev Cell* **5**, 367-77.

Veeman, M. T., Slusarski, D. C., Kaykas, A., Louie, S. H. and Moon, R. T. (2003b). Zebrafish prickles, a modulator of noncanonical Wnt/Fz signaling, regulates gastrulation movements. *Curr Biol* **13**, 680-5.

Voskoboinik, I. and Camakaris, J. (2002). Menkes copper-translocating P-type ATPase (ATP7A): biochemical and cell biology properties, and role in Menkes disease. *J Bioenerg Biomembr* **34**, 363-71.

Wallingford, J. B. and Habas, R. (2005). The developmental biology of Dishevelled: an enigmatic protein governing cell fate and cell polarity. *Development* **132**, 4421-36.

Wallingford, J. B., Rowning, B. A., Vogeli, K. M., Rothbacher, U., Fraser, S. E. and Harland, R. M. (2000). Dishevelled controls cell polarity during *Xenopus* gastrulation. *Nature* **405**, 81-5.

Warga, R. M. and Kimmel, C. B. (1990). Cell movements during epiboly and gastrulation in zebrafish. *Development* **108**, 569-80.

- Weidinger, G., Wolke, U., Kopranner, M., Klinger, M. and Raz, E.** (1999). Identification of tissues and patterning events required for distinct steps in early migration of zebrafish primordial germ cells. *Development* **126**, 5295-307.
- Weinberg, E. S., Allende, M. L., Kelly, C. S., Abdelhamid, A., Murakami, T., Andermann, P., Doerre, O. G., Grunwald, D. J. and Riggleman, B.** (1996). Developmental regulation of zebrafish MyoD in wild-type, no tail and spadetail embryos. *Development* **122**, 271-80.
- Westerfield, M.** (2000). The zebrafish book. A guide for the laboratory use of zebrafish (*Danio rerio*). Eugene: University of Oregon Press.
- Westfall, T. A., Brimeyer, R., Twedt, J., Gladon, J., Olberding, A., Furutani-Seiki, M. and Slusarski, D. C.** (2003). Wnt-5/pipetail functions in vertebrate axis formation as a negative regulator of Wnt/beta-catenin activity. *J Cell Biol* **162**, 889-98.
- Wilson, P. and Keller, R.** (1991). Cell rearrangement during gastrulation of *Xenopus*: direct observation of cultured explants. *Development* **112**, 289-300.
- Wilson, P. A., Oster, G. and Keller, R.** (1989). Cell rearrangement and segmentation in *Xenopus*: direct observation of cultured explants. *Development* **105**, 155-66.
- Winter, C. G., Wang, B., Ballew, A., Royou, A., Karess, R., Axelrod, J. D. and Luo, L.** (2001). Drosophila Rho-associated kinase (Drok) links Frizzled-mediated planar cell polarity signaling to the actin cytoskeleton. *Cell* **105**, 81-91.
- Witzel, S., Zimyanin, V., Carreira-Barbosa, F., Tada, M. and Heisenberg, C. P.** (2006). Wnt11 controls cell contact persistence by local accumulation of Frizzled 7 at the plasma membrane. *J Cell Biol*.
- Wolff, C., Roy, S. and Ingham, P. W.** (2003). Multiple muscle cell identities induced by distinct levels and timing of hedgehog activity in the zebrafish embryo. *Curr Biol* **13**, 1169-81.
- Wong, L. L. and Adler, P. N.** (1993). Tissue polarity genes of *Drosophila* regulate the subcellular location for prehair initiation in pupal wing cells. *J Cell Biol* **123**, 209-21.

- Wood, A. and Thorogood, P.** (1994). Patterns of cell behaviour underlying somitogenesis and notochord formation in intact vertebrate embryos. *Dev Dyn* **201**, 151-67.
- Xu, Y., He, J., Wang, X., Lim, T. M. and Gong, Z.** (2000). Asynchronous activation of 10 muscle-specific protein (MSP) genes during zebrafish somitogenesis. *Dev Dyn* **219**, 201-15.
- Yamashita, S., Miyagi, C., Carmany-Rampey, A., Shimizu, T., Fujii, R., Schier, A. F. and Hirano, T.** (2002). Stat3 Controls Cell Movements during Zebrafish Gastrulation. *Dev Cell* **2**, 363-75.
- Yamashita, S., Miyagi, C., Fukada, T., Kagara, N., Che, Y. S. and Hirano, T.** (2004). Zinc transporter LIV1 controls epithelial-mesenchymal transition in zebrafish gastrula organizer. *Nature* **429**, 298-302.
- Yang, C. H., Axelrod, J. D. and Simon, M. A.** (2002a). Regulation of Frizzled by fat-like cadherins during planar polarity signaling in the Drosophila compound eye. *Cell* **108**, 675-88.
- Yang, X., Dormann, D., Munsterberg, A. E. and Weijer, C. J.** (2002b). Cell movement patterns during gastrulation in the chick are controlled by positive and negative chemotaxis mediated by FGF4 and FGF8. *Dev Cell* **3**, 425-37.
- Yin, C. and Solnica-Krezel, L.** (2006). Convergence and extension movements mediate the specification and fate maintenance of zebrafish slow muscle precursors. *Dev Biol* **in press**.
- Yoong, S., O'Connell, B., Soanes, A., Crowhurst, M. O., Lieschke, G. J. and Ward, A. C.** (2007). Characterization of the zebrafish matrix metalloproteinase 9 gene and its developmental expression pattern. *Gene Expr Patterns* **7**, 39-46.
- Youn, B. W. and Malacinski, G. M.** (1981). Axial structure development in ultraviolet-irradiated (notochord-defective) amphibian embryos. *Dev Biol* **83**, 339-52.
- Zallen, J. A. and Wieschaus, E.** (2004). Patterned gene expression directs bipolar planar polarity in Drosophila. *Dev Cell* **6**, 343-55.

Zhou, X., Sasaki, H., Lowe, L., Hogan, B. L. and Kuehn, M. R. (1993). Nodal is a novel TGF-beta-like gene expressed in the mouse node during gastrulation. *Nature* **361**, 543-7.

Zon, L. and Peterson, R. (2005). In vivo drug discovery in the zebrafish. *Nature Reviews Drug Discovery* **4**, 34-44.